DURBAN UNIVERSITY OF TECHNOLOGY

INYUVESI YASETHEKWINI YEZOBUCHWEPHESHE

Evaluation of the effects of dye-mediated irradiation on metabolite production in *Chlamydomonas reinhardtii*

Submitted in fulfilment of the requirements of the degree of Doctor of Philosophy of Applied Science in Biotechnology in the Faculty of Applied Sciences at the Durban University of Technology

Luveshan Ramanna

Supervisor: Professor Faizal Bux

2022

Declaration

Evaluation of the effects of dye-mediated irradiation on metabolite production in *Chlamydomonas reinhardtii*

Luveshan Ramanna

I hereby declare that the dissertation represents my work. It has not been submitted before for any diploma/degree or examination at any other University.

2022

Reference declaration in respect of a doctoral thesis

I, Mr Luveshan Ramanna and Prof. Faizal Bux do hereby declare that in respect of the following dissertation:

Evaluation of the effects of dye-mediated irradiation on metabolite production in *Chlamydomonas reinhardtii*

As far as we know and can ascertain: no other similar thesis exists: all references as detailed in the thesis are complete in terms of all personal communications engaged in and published works consulted.

21st February 2022

Signature of Student **Date**

21st February 2022

Signature of Supervisor **Date**

Approval

I hereby approve the final submission of the following thesis:

Evaluation of the effects of dye-mediated irradiation on metabolite production in *Chlamydomonas reinhardtii*

On this 21st day of February 2022, at the Durban University of Technology.

Professor Faizal Bux

Supervisor

Doctoral Degree in Technology: Biotechnology

Durban University of Technology (DUT)

Dedication

This work is dedicated to the betterment of science and can be regarded as yet another steppingstone in science's inexorable quest for renewable and sustainable solutions. May future generations be inspired and strive to fulfil this endeavour.

Table of contents

List of figures

List of tables

List of equations

List of abbreviations

Abbreviation	Full Term
€	Euro
1Chl*	Singlet chlorophyll
$^1O_2$*	Singlet oxygen
3Car*	Triple-state carotenoids
3Chl*	Triplet chlorophyll
$^3O_2$	Ground-state molecular oxygen
3PGA	3-phosphoglyceric acid
$\Delta\psi$	Membrane potential across the thylakoid membrane
ΔpH	Proton gradient component
Acetyl-CoA	Acetyl coenzyme A
AFI	Areal fluorescence intensities
AGPase	ADP-glucose pyrophosphorylase
AKG	α-ketoglutarate
ANOVA	Analysis of Variance
ATP	Adenosine triphosphate
Bp	Base pairs
Car	Carotenoids, in Figure 4 and Equation 9
CBB	Calvin-Benson Bassham
cDNA	Complementary DNA
CEF	Cyclic electron flow
Chl	Chlorophyll, in Figure 4 and Equations 8-11
CIT	Citrate
CO_2	Carbon dioxide
Cont.	Control in Figures
Cyt b_6f	Cytochrome b_6f complex
CL	Continuous light
DCW	Dry cell weight
dH_2O	Distilled water
DMSO	Dimethylsulfoxide
DNA	Deoxyribonucleic acid
dNTPs	Deoxynucleoside triphosphates
DPA	Diphenylanthracene
DPO	Diphenyloxazole
EA	Energy absorption
ETC	Electron transport chain
ETR	Electron transport rate
F	Forward primer
F6P	Fructose 6-phosphate
FAS	Fatty acid synthesis
FDX	Ferredoxin
FNR	ferredoxin-$NADP^+$ reductase
FITC	Fluorescein isothiocyanate
FL	Flashing light
FUM	Fumarate

Abbreviations	Full Term
G1P	Glucose 1-phosphate
G3P	Glyceraldehyde-3-phosphate
G6P	Glucose 6-phosphate
GAPDH	Glyceraldehyde-3-phosphate dehydrogenase
GOX	Glyoxylate
HPLC	High-performance liquid chromatography
IR	Infrared
ISO	Isocitrate
ISC	Intersystem crossing
LEDs	Light-emitting diodes
LEF	Linear electron flow
LHC	Light-harvesting complex
lhcsr	Light-harvesting complex stress-related
LR	Lumogen Red
LSPR	Localised surface plasmon resonances
LY	Lumogen Yellow
MAL	Malate
MJ	Methanol jacket
MSDS	Material Safety Data Sheets
NADPH	Nicotinamide adenine dinucleotide phosphate
NDA2	NADPH oxidoreductase
NPQ	Non-photochemical quenching
NJ	No liquid jacket
NRT	No RT control
NTC	No template control
O_2	Oxygen
OAA	Oxaloacetate
OEC	Oxygen evolving complex
P680	chlorophyll *a* molecule in PSII core
PAM	Pulse amplitude modulated
PAR	Photosynthetically active radiation
PC	Plastocyanin
PCR	Polymerase chain reaction
PBR	Photo-bioreactor
PE	Photosynthetic efficiency
PFDs	Photon flux densities
PGM	Phosphoglucomutase
pgr5	proton gradient regulation 5 proteins
pgrl1	*pgr5*-like photosynthetic phenotype 1 proteins
PMF	Proton motive force
PPFDs	Photosynthetic photon flux densities
PQ	Plastoquinone
PS	Photosystem
qE	Energy-dependent component
qI	Photo-inhibitory/xanthophyll quenching
qPCR	Quantitative PCR
qT	State transitions

Abbreviation	Full Term
Q_A and Q_B	Primary and secondary Quinone acceptors, respectively
QY	Quantum yield
R	Reverse primer
R101	Rhodamine 101
R110	Rhodamine 110
R800	Rhodamine 800
R8G	Rhodamine 8G
rbcL	RuBisCo large subunit
rbcS	RuBisCo small subunit
RCs	Reaction centres
ROS	Reactive oxygen species
RLC	Rapid light curves
RNA	Ribonucleic acid
rRNA	Ribosomal RNA
RT	Reverse transcription
RuBisCo	Ribulose-1, 5-bisphosphate carboxylase/oxygenase
SA	South Africa
SDG	Sustainable development goal
SOQ	Singlet oxygen quenching
SP	Saturation pulse
SUC	Succinate
TAP media	Tris-acetate-phosphate media
TCA	Tricarboxylic acid cycle
T_m	Temperature of melt peak
TSEQ	Triple-state energy quenching
UK	United Kingdom
USA	United States of America
UV	Ultraviolet light
WJ	Water jacket

List of mathematical symbols

Symbol	Full Term	Measurement
%	Percentage	Mathematics/Statistics
λ	Wavelengths in meters (m)	Electromagnetic Spectrum
±	Approximately	Mathematics/Statistics
Δ	Delta	Mathematics/Statistics
Δ*Ct*	Delta *Ct*	Relative fold gene expression
ΔΔ*Ct*	Delta-delta *Ct*	Relative fold gene expression
A	Absorbance	Spectrometry
a. u	Arbitrary unit	Energy (fluorescence)
Avg.	Average	Statistics
ANOVA	Analysis of variance	Statistics
bp	Base pair	DNA size
C	Speed of light (3.00×10^{8} ms^{-1})	Mathematics/Distance
°C	Degrees Celsius	Temperature
cm	Centimetre	Length
cells mL^{-1}	Cells per millilitre	Concentration (*cells/v*)
Ct	Cycle threshold	Relative fold gene expression
d^{-1}	Per day	Time
DCW	Dry cell weight	Biomass
f	Frequency	Frequency
EJ	Exajoule	Energy
F′	Dark fluorescence yield	Photosynthesis parameter
F_0	Minimum fluorescence	Photosynthesis parameter
F_m	Maximal fluorescence yield	Photosynthesis parameter
F'_m	Maximum fluorescence	Photosynthesis parameter
F_v	Variable fluorescence	Photosynthesis parameter
F_v/F_m	Quantum efficiency of PSII	Photosynthesis parameter
g	Gram	Weight
$gm^{-2}d^{-1}$	Gram per meter per day	Productivity (*wt./v/t*)
gL^{-1}	Gram per litre	Concentration (*wt./v*)
h	Plank constant (6.63×10^{-34} Js^{-1})	Energy
hr	Hour	Time
J	Joules	Energy
Js^{-1}	Joules per second	Energy
kDa	Kilo Dalton	Weight (molecular mass)
kg	Kilogram	Weight
kJ	Kilojoule	Energy

Symbol	Full Term	Measurement
L	Litre	Volume
Lhr^{-1}	Litre per hour	Flowrate
ln	Natural log	Mathematics
M	Molar	Concentration
mM	Millimolar	Concentration
m	Meter	Length
mg	Milligram	Weight
mgg^{-1}	Milligram per gram	Concentration (*wt./wt.*)
mgL^{-1}	Milligram per litre	Concentration (*wt./v*)
$mgL^{-1}d^{-1}$	Milligram per litre per day	Productivity (*wt./v/t*)
min	Minutes	Time
MJ	Mega joule	Energy
mL	Millilitre	Volume
mLL^{-1}	Millilitre per litre	Concentration (*v/v*)
mm	Millimetre	Volume
ms	Millisecond	Time
$m^{-2}\ s^{-1}$	Meters square per second	Speed
mole	Molecule	Chemistry
n	Number of samples	Statistics
ng	Nanogram	Weight
nm	Nanometre	Length
OD	Optical density	Spectrometry
p	Alpha value (significance)	Statistics
psi	Pounds per square inch	Pressure
qL	coefficient of photochemical quenching	Photosynthesis parameter
QY	Quantum yield	Photosynthesis parameter
R^2	Regression constant	Statistics
rpm	Rotations per minute	Speed
S0	Ground electron state	Fluorescence parameter
S1	Singlet electron state	Fluorescence parameter
s	Seconds	Time
S	Svedberg unit	Sedimentation coefficient
s^{-1}	Per second	Time
SD	Standard deviation	Statistics
SEM	Standard error of the mean	Statistics
t	Time	Time
$t_1/_0$	Biomass at $time_1/_0$	Concentration
μ	Average growth rate	Growth rate
μgmL^{-1}	Microgram per millilitre	Concentration (*wt./v*)
µL	Microliter	Volume
µM	Micromolar	Concentration

Symbol	Full Term	Measurement
µmol photons·m^{-2}·s^{-1}	Micromole photons per meter per second	Electromagnetic Spectrum
V	Volt	Energy
v	Volume	Volume
W	Watts	Energy
wt.	Weight	Weight
Wm^2	Watts per meter squared	Energy
$X_{1/0}$	DCW at $time_{1/0}$	Concentration
Y(II)	Photochemical energy utilisation	Photosynthesis parameter
Y(NO)	Non-regulated energy dissipation	Photosynthesis parameter
Y(NPQ)	Regulated energy dissipation	Photosynthesis parameter

List of appendices

Acknowledgements

Firstly, I would like to thank the omnipresent for giving me the strength, determination, ability, faith, health, patience, and opportunity to accomplish this goal. I would like to express sheer gratitude to my family for their love and support throughout my life. To my dad, mum, and sister, thank you for inspiring and motivating me, encouraging me to pursue my research, tolerating me through the demanding times, and counselling me whenever I needed it. I hope your lives stay abundantly fruitful and I will always be indebted to you. Thank you to my wonderful aunts, uncles, and cousins for encouraging me through this endeavour. I would also like to acknowledge the loved ones who are no longer with me. Thank you for realising my capabilities long before I could!

A Ph.D. is not achieved by a single person, rather it is an entire team effort. As such, I would like to sincerely thank my supervisor, Prof. F. Bux, for believing in my potential and allowing me to conduct my research under your guidance and support. I believe your hard-natured personality has moulded me into being a better scientist. I would like to express my special thanks of gratitude to Dr I. Rawat for your technical assistance with my research. My heartfelt appreciation goes to my friends and colleagues at the Institute for Water and Wastewater Technology for their invaluable help, and companionship. My specific thanks go to Mr K. Pillay, Mr J. Gokal, Dr T. Mogany, Dr N. Deepnarain, Dr V. K Bhola, Dr A. S Guldhe, Dr F. A. Ansari, Dr P. Singh, Dr N. Renuka, Dr S.K. Ratha, and Prof. S. K. S. Pillay. The positive and constant criticism of my science showed me how much you care about my well-being. To the Durban University of Technology and the National Research Foundation of South Africa for funding and providing the facilities to make this study possible (UID: 111046). I would also like to thank all the staff members at the Department of Biotechnology and Food Science and the Faculty of Applied Sciences for all their help and continued support of me.

Finally, to all those who have given me advice, showed interest, encouraged, or in some way contributed to the completion of my Ph.D., I give my eternal thanks!

Preface

The outputs of this Doctor of Philosophy qualification are listed below.

Publications

Ramanna, L., Rawat, I. and Bux, F. 2017. Light enhancement strategies improve microalgal biomass productivity. *Renewable and Sustainable Energy Reviews*, 80: 765 – 773.

Ramanna, L., Rawat, I., Zerrouki, D. and Bux, F. 2018. A novel organic dye-based approach to increase photon flux density for enhanced microalgal pigment production. *Journal of Cleaner Production*, 198: 187 – 194.

Mogany, T., Bhola, V.K., **Ramanna, L**., and Bux, F. 2021. Evaluation of pigments and photosynthetic performance of *Chlamydomonas reinhardtii* under different cultivation conditions. *Bioprocess and Biosystems Engineering*, 45: 187 – 201.

Ramanna, L., Nasr, M., Rawat, I. and Bux, F. 2022. UV-mediated photosynthesis – A potential method to enhance incident light availability in *C. reinhardtii* for metabolites production and sustainable development. *Biomass and Bioenergy*, (submitted).

Conferences

Ramanna, L., Rawat, I. and Bux, F. 2017. Dye-based light manipulation for enhancement of microalgal pigment production. *The 7th International Conference on Algal Biomass, Biofuels and Bioproducts*. 18 – 21 June 2017, Miami, FL, USA.

Ramanna, L., Mogany, T., Rawat, I. and Bux, F. 2017. Dye-based light manipulation for the enhancement of microalgal biomass and pigments. *Algae Biomass Summit*. 29 October – 1 November 2017. Salt Lake City, Utah, USA.

Ramanna, L., Rawat, I. and Bux, F. 2019. A novel dye-based light manipulation strategy to increase photosynthetic active radiation for the enhancement of microalgal metabolites. *The 27th European Biomass Conference and Exhibition*. 27 – 30 May 2019, Lisbon, Portugal.

Abstract

Microalgae have emerged as one of the most promising feedstocks for the production of high-value metabolites and bioactive compounds. However, the commercial success of large-scale microalgal cultivation systems has been restricted due to the limited productivity of biomass and metabolites, which has been largely due to limited light availability. Light is one of the main factors that influence microalgal photosynthetic efficiency, carbon fixation capacity, cellular metabolism, and biomass production. Solar radiation is composed of a wide range of wavelengths such as ultraviolet (UV) (290 – 400 nm), visible (450 – 700 nm), and infrared rays (700 nm – 30 µm). Green microalgae only use the blue (400 – 500 nm) and red (600 – 700 nm) bands of the light spectrum for photosynthesis, referred to as photosynthetically active radiation (PAR). Spectral wavelengths that do not contribute to photosynthetically-driven energy conversion pass through the microalgal cells and remain unused. Hence, the conversion of photons from the unused to the usable wavelengths can produce/supplement a spectrum amenable to potentially increase metabolite production in microalgae.

This study aimed to enhance light availability to *Chlamydomonas reinhardtii* using organic dyes as incident light converters, thereby potentially improving photosynthetic efficiency and metabolite production. The first objective of this study dealt with determining the optimal solvent and dye concentration. Diphenylanthracene [DPA], Diphenyloxazole [DPO], Rhodamine 6G [R6G], Rhodamine 8G [R8G], Rhodamine 800 [R800], Fluorescein Isothiocyanate [FITC], Lumogen Yellow [LY], and Lumogen Red, [LR], were evaluated for their ability to absorb, convert, and emit photon flux densities (PFDs) in the PAR region. The DPA and DPO dyes absorbed light in the UV range (280 – 350 nm) and emitted in the violet/blue wavelengths (390 – 500 nm). Rhodamine 8G absorbed and emitted light between

200 – 300 and 450 – 500 nm, respectively, suggesting a blue-green region that could stimulate pigment and/or lipid production in algae. The fluorescent dye LY showed several sharp peaks at the green and blue light spectra (400 – 525 nm). The fluorescence intensity also extended to more than 600 nm, representing the green to yellow and red PAR portions. The LR dye demonstrated an excitation and emission range between 320 – 400 nm and 590 – 660 nm, respectively, while R6G, R800, and FITC did not exhibit irradiations in the PAR wavelengths. Most of the dyes displayed higher fluorescent intensities in methanol (10 mgL^{-1}) when compared to dyes dissolved in ethanol and acetone at higher concentrations. Lumogen Yellow, R8G, and LR emitted the highest emissions in the PAR regions which were 161873, 113138, and 61824 a.u, respectively.

The next objective focused on determining the effects of increased LY and R8G-mediated irradiance on the physiological responses in *C. reinhardtii*. Experiments were conducted in double-jacketed cylindrical photo-bioreactors. Outer jackets contained dye solutions while inner jackets contained microalgae. The dyes were dissolved in methanol (10 and 100 mgL^{-1}) and were stimulated using daylight tubes. The initial increase in irradiance from LY and R8G induced light stress in *Chlamydomonas*, which was characterised by non-photochemical quenching (NPQ). Increased NPQ from ~ 0.05 to 0.5 signified damage to the microalgal photosystem (PS). Accordingly, the quantum efficiencies of PSII decreased from approximately 0.6 to 0.2, resulting in transient growth until day 8, and low biomass production. The cultures grown under R8G irradiations showed increased carotenoid production in response to the light stress (~ 37%), while the LY-irradiated cultures showed the highest carotenoids throughout the experimental period (12 mgg^{-1}). After the 4^{th} day of experimentation, there was an inactivation in the NPQ process which was accompanied by a simultaneous increase in the quantum efficiencies in cultures grown under R8G and LY dye-

irradiance (47 and 34% respectively). The findings indicated that the alga required an initial dye-acclimation period, after which it was able to regulate the excess energy. Toward the end of the growth cycle, decreases in biomass were ascribed to light attenuation in the culture medium. Moreover, the effects of increased dye-irradiance may have manifested indirectly through the production of stress relief metabolites (protein, carbohydrate, and lipid).

The final objectives dealt with evaluating the dye spectral conversion ability and assessing light utilisation and metabolite production in *C. reinhardtii*. The emission intensities of the fluorescent dyes were increased using UV fluorescent tubes. The R8G dye pattern showed a sharp peak at about 498 nm. The LY dye demonstrated several sharp peaks at the green and blue light spectra; however, there was a drastic reduction in emissions indicative of photo-degradation. The LR dye exhibited an emission spectrum peak in the orange-red light region, providing effective light energy for microalgal growth. Cultures grown under LR irradiance exhibited increased photochemical energy utilisation [Y(II)] and decreased regulated heat dissipation [Y(NPQ)]. Additionally, the LR-irradiated cultures showed a 1.6- and 2.9-fold up-regulation in RuBisCo gene expression, verifying the increase in the photosynthetic process under increased red-light wavelengths. Carbohydrate and lipids were produced early in the growth phase, while biomass and protein concentrations were accumulated toward in later stages. Dye irradiations (LR and/or R8G) was associated with increased biomass productivity and metabolic content compared with the control (with no dye addition). The findings showed that R8G and LR can be applied to microalgal cultivation systems to improve light availability and enhance photosynthetic output. Hence, this study demonstrated the potential applicability of organic dyes as effective spectral converters of incident irradiation, supporting photosynthetic energy utilisation, and increasing metabolite yields with less input of energy in the algal systems.

Chapter 1 : Introduction

Ramanna, L., Rawat, I. and Bux, F. 2017. Light enhancement strategies improve microalgal biomass productivity. *Renewable and Sustainable Energy Reviews*, 80: 765 – 773.

The increasing demand for energy, food, and valuable high-value metabolites has prompted the development of novel and sustainable resources (Nwoba *et al.* 2019; Xu *et al.* 2019; Levasseur *et al.* 2020). Microalgae have attracted considerable interest worldwide, due to their extensive potential application in many business sectors. These photosynthetic organisms produce a wide range of high-valuable metabolites including polyunsaturated fatty acids, pigments, phycobiliproteins, polysaccharides, and phyco-hormones that can be utilised extensively in industries such as the food and feed, fuels, nutraceutical, pharmaceutical *etc.* (Nwoba *et al.* 2019; Sathasivam *et al.* 2019). Thus, algae represent a potentially viable source of sustainable high-value metabolites. Biomass is composed of between 7 – 23% lipid, 6 – 52% protein, and 5 – 23% carbohydrate (Chandra *et al.* 2019). Currently, 25% of the lipids produced are offered to food and chemical industries for 2 €/kg, while the rest are sold to produce biodiesel (0.50 €/kg), 20% of the soluble proteins are sold for food (5 €/kg), while the remaining portion is used for feed (80%, at 0.75 €/kg), (Sathasivam *et al.* 2019; Levasseur *et al.* 2020). Consequently, for human consumption algal biomass costs between 100 €/kg, animal and fish feed ranges between 5 – 20 €/kg, bulk chemicals range between 1 – 5 €/kg, and 0.40 €/kg for biofuel (Sathasivam *et al.* 2019).

Despite the potential technical and/or economic viability of microalgal high-value metabolite production, the commercial and environmental viability of the technology still requires improvement (Abu-Ghosh *et al.* 2016; Levasseur *et al.* 2020). Some of the challenges that hinder the production of microalgae technologies include but are not limited to: (*i*) optimal species selection in terms of metabolite productivity; (*ii*) the availability of incident light spectrum and distribution characterised by its photon flux densities (PFDs); (*iii*) the availability of various nutrients affecting growth (carbon, nitrogen, sulphur, phosphorus, magnesium, calcium, manganese, iron, *etc.*); (*iv*) varying culture conditions (pH, temperature, dissolved oxygen [O_2]); and (*v*) possible biological contamination (de Mooij *et al.* 2016; Gomes *et al.* 2017; Ajayan *et al.* 2019). A few strategies have been undertaken to increase microalgal productivity. These include culture condition optimisation (pH, temperature, light), design and construction of photo-bioreactors (PBRs) (contamination control), genetic modification for optimal species performance (in terms of light utilisation), and nutrient optimisation (replete/deplete) (Berteotti *et al.* 2016; Gomez *et al.* 2016; Goncalves *et al.* 2016; Wobbe *et al.* 2016; Levasseur *et al.* 2020).

Once these cultivation conditions are optimised and adequate amounts of nutrients are provided, light availability remains the only limiting factor (Nama *et al.* 2018; Nawrocki *et al.* 2019a). Light is a critical factor as it affects microalgal physiology thus affecting photosynthesis. Light irradiance level (quantity) and spectral composition (quality) influences microalgal photosynthetic efficiency (PE) which is defined as the portion of available incident radiation within the solar spectrum that can be converted/stored as chemical energy in biomass. Light irradiance also affects carbon fixation capacity, cell growth, and metabolism (Ma *et al.* 2019). Irradiance levels that are too low or are in excess can limit or inhibit the photosynthetic process (Nwoba *et al.* 2019). Photo-limitation results from the rapid light attenuation in

concentrated microalgal cultures and the large energy requirement of photosynthesis. In contrast, photo-inhibition results from an overexposure to light which damages microalgal photosystems (PSs). Consequently, these phenomena result in low areal microalgal biomass and metabolite productivity Microalgal growth and metabolite productivity correlate with light quality and quantity, *i.e.*, that changes in production yields respond to incremental or decremented changes in PFDs in specific wavelengths (Benavente-Valdes *et al.* 2016; Metsoviti *et al.* 2019).

Scientists have also assessed the impact/effects of multi-chromatic and monochromatic wavelength illuminations on the growth and metabolite productivity of microalgae (Ra *et al.* 2016; Kendirlioglu and Cetin 2017). Other studies have aimed to enhance PE by improving light conversion efficiencies using plasmonic waveguides, wireless light emitters, insulated glazing, *etc.* that sought to emit specific wavelengths to microalgae (Eroglu *et al.* 2013; Vadiveloo *et al.* 2015; Nwoba *et al.* 2019; Raeisossadati *et al.* 2019). These approaches filter PAR and reduce undesirable wavelengths, however, these systems are; (*i*) costly to implement at a large scale; and (*ii*) increase equipment, maintenance, and energy costs which ultimately limit their practical applicability (Eroglu *et al.* 2013; Nwoba *et al.* 2019; Raeisossadati *et al.* 2019). Nevertheless, these innovations have paved a path for the development and expansion of cost-effective, grid-independent, low carbon footprint microalgae-based metabolite production.

Findings from previous studies have shown that increased PFDs improve high-value metabolite content in microalgae (Gao *et al.* 2021; Sanchez-Tarre and Kiparissides 2021). Hence, adjusting light intensity and wavelength can be regarded as an effective strategy to regulate cellular metabolites and reroute the carbon flux between the algal metabolites. This

concept has not been widely adopted in large-scale algal cultivations due to the costs associated with artificial lighting systems (Benavente-Valdes *et al.* 2016). Artificial lighting can increase productivity by increasing light intensity and providing specific wavelengths, however, their use also increases production costs of the system which renders the process unfeasible to implement and/or sustain (Sung *et al.* 2018; Nwoba *et al.* 2019). Therefore, the application of increasing light intensity and wavelength will depend on the natural irradiance of sunlight (Benavente-Valdes *et al.* 2016; Nwoba *et al.* 2019).

Green microalgae can only use thin bands from the light spectrum because photosynthesis occurs within the 400 – 500 nm and 600 – 700 nm range. Large amounts of the incoming light energy (such as ultraviolet [UV] and infrared (IR) rays fall outside this region and are not absorbed. They are instead transmitted through the culture medium and remain unused resulting in a loss of photons (Sung *et al.* 2018; Nwoba *et al.* 2019). High-energy UV photons and IR radiations from sunlight are known to negatively affect microalgae causing photo-oxidation and overheating, respectively. Technologies such as spectral filtration reduce the transmission of wavelengths to the cultures resulting in less algal cellular damage. Consequently, the filtered wavelengths remain unused. Accordingly, an appropriate light management strategy should be provided to (*i*) avoid further energy wastage that might negatively influence the algal photosynthetic activity; and (*ii*) minimise the passage of spectral wavelengths having no photosynthetic value through the cells (Sung *et al.* 2018; Nwoba *et al.* 2019).

Spectral conversion of UV and IR wavelengths to photosynthetically active radiation (PAR) will reduce and also lead to higher PFDs in the PAR spectrum. Thus, to potentially enhance the economic efficiency of metabolite production, exploiting the spectral conversion

of UV and IR wavelengths represents a promising option for increasing light availability to microalgae. A wide array of dyes (*e.g*. Rhodamine and Lumogen) has shown promising results as light wavelength shifters, such as converting incident irradiation to PAR wavelengths, thereby improving biomass and algal metabolite productivity (Jang *et al.* 2018; Sung *et al.* 2018; Khoobkar and Delavari Amrei 2020). The organic and inorganic dyes demonstrate high quantum efficiency, wide absorption with narrow emission wavelengths, high absorption coefficients, and show good separation between the absorption and emission bands (Jang *et al.* 2018; Khoobkar and Delavari Amrei 2020).

Organic dyes represent promising candidates for converting incident radiation with no photosynthetic potential into PAR. Evaluating the potential of this approach for its application to microalgal cultivation systems can be highly beneficial (Seo *et al.* 2015; Ooms *et al.* 2016; Sung *et al.* 2018). Consequently, this study focused primarily on increasing light availability to *Chlamydomonas reinhardtii* by utilising organic dyes as spectral convertors of UV light, thereby enhancing the quantum of intensity in specific PAR wavelengths.

1. 1. Aim and Objectives

The study aimed to increase light availability to *Chlamydomonas reinhardtii* by employing organic dyes as light converters and to determine their effects on microalgal metabolite production.

To achieve the aim, the following objectives were undertaken:

i. Selection of solvent and optimisation of organic dye concentration to increase the photon flux densities of incident light in the photosynthetically active range,

ii. Determination of the effects of increased dye-mediated photon flux densities on the *C. reinhardtii* physiological responses,

iii. Investigation of the effects of dye-mediated photosynthetic photon flux densities on the expression pattern of the RuBisCo enzyme,

iv. Evaluation of dye spectral conversion ability and assessment of the light utilisation and metabolite production in *C. reinhardtii* in response to increased photosynthetic photon flux densities.

Chapter 2 : Literature Review

Ramanna, L., Rawat, I. and Bux, F. 2017. Light enhancement strategies improve microalgal biomass productivity. *Renewable and Sustainable Energy Reviews*, 80: 765 – 773.

2. 1. Microalgae

The increasing population, declining fossil fuel reserves, rising energy demands, and climate change have initiated the development of feedstocks for energy, chemical, and materials production from renewable sources, that is produced and processed in an eco-friendly way (Nwoba *et al.* 2019; Xu *et al.* 2019; Levasseur *et al.* 2020). The initial efforts were based around using conventional land-based crops, however, these practices are not sustainable due to: (*i*) competition with food production; (*ii*) the vast quantities of arable land and freshwater required; and (*iii*) the deleterious climate effects on crop-based practices (Sathasivam *et al.* 2019; Levasseur *et al.* 2020). Consequently, the mass cultivation of microalgae has emerged as a potential source for the sustainable production of commodities such as biofuels (biodiesel, bioethanol, biogas, biohydrogen, and bio-crude oil), and high-value metabolites that can be utilised as human and animal supplements for nutrition (Figure 2. 1) (Nwoba *et al.* 2019; Xu *et al.* 2019; Levasseur *et al.* 2020).

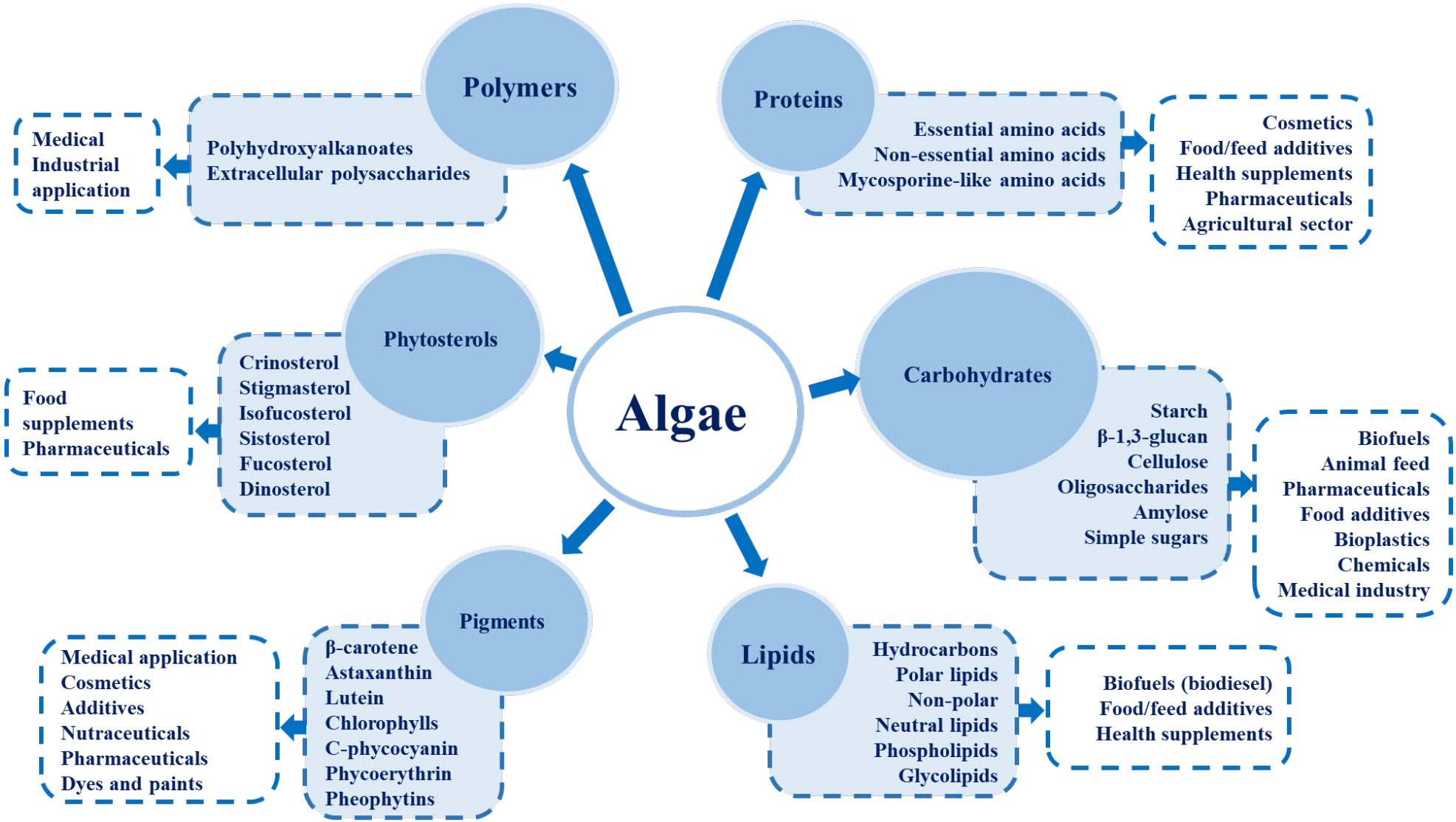

Figure 2.1: Potential applications of microalgal metabolites, adapted from Nwoba *et al.* (2019).

Algae are considered as clean renewable energy bioresources as they occur naturally and can be constantly replenished due to their rapid growth rates and doubling time (as little as 24 hr) (Nwoba *et al.* 2019; Xu *et al.* 2019; Levasseur *et al.* 2020). These organisms can be found in almost every habitat. Most species are found in marine environments, while other species grow in environments such as deserts, frozen soils, volcanic waters, *etc*. These organisms are the basic components of food chains and are responsible for approximately 40% of the global photosynthesis as they are the main producers of O_2 (Sathasivam *et al.* 2019; Levasseur *et al.* 2020). When compared to terrestrial crops, the cultivation of microalgae for the generation of renewable feedstocks is more beneficial due to: (*i*) their higher photosynthetic efficiencies leading to; (*ii*) faster growth rates (algae multiply in a few hours); (*iii*) algae can sequester 10 – 50 times more carbon dioxide (CO_2) than agricultural plants; (*iv*) robust environmental adaptability (algae can be cultivated on non-arable lands such as coastal beaches, saline-alkali lands, and deserts); (*v*) the ability to grow and recycle nutrients from saline and wastewater (industrial, domestic, and agricultural); and (*vi*) the ability to simultaneously produce multiple biologically active metabolites (Nwoba *et al.* 2019; Xu *et al.* 2019; Levasseur *et al.* 2020).

Algal species such as *Chlorella*, *Dunaliella salina*, and prokaryotic cyanobacteria such as *Arthrospira* (*Spirulina*) are widely used as human food, supplements, or feed supplements in aquacultural sectors because they are rich in proteins (50 – 70 *wt.* %). Photosynthetic organisms are also made up of a wide range of amino acids with aspartate and glutamate being the most abundantly produced. Proteins, essential, and non-essential amino acids are responsible for many biological functions in these organisms. These can be applied to the nutritional, nutraceuticals, and pharmaceuticals industries (Figure 2.1), (Nwoba *et al.* 2019; Sathasivam *et al.* 2019; Levasseur *et al.* 2020). When compared to crops like corn and soybeans, microalgae have demonstrated higher compositions of essential amino acids and

protein thereby increasing the health profile of livestock animals (Li-Beisson *et al.* 2019; Nawrocki *et al.* 2019a).

2. 2. Sustainability of microalgal systems

Emerging microalgal biotechnological applications have established the potential for algae to mitigate some of the global challenges, for example by providing a source of sustainably produced feedstocks for product development (Gifuni *et al.* 2018), (Figure 2.1). Subsequently, by improving the algal biomass and the associated value-added metabolite yield, microalgal biotechnology can assist in the accomplishment of the sustainable development goals (SDGs) including "*Zero Hunger*", "*Good Health and Well-being*", "*Affordable and Clean Energy*", "*Climate action*" *etc.*, (Figure 2.2), (Ansari *et al.* 2021; Sutherland *et al.* 2021).

Figure 2.2: Sustainable development goals describing environmental, economic, and industrial benefits obtained from microalgal systems (Ansari *et al.* 2021; Sutherland *et al.* 2021).

Granted, microalgae have been thoroughly studied in both the laboratory and in the field, its usefulness has been impeded by the difficulty experienced in large-scale cultivation. Large-scale algal cultivation systems, globally, have been hampered primarily by limited biomass and/or metabolite yields. The demand for algal biomass continues to increase, hence, producers require technological developments that reduce cost while retaining and elevating the quality of the biomass and/or high-value metabolites. Assuming that temperatures are optimal, there are suitable nutrients, and enough water, then limitations to the rate of photosynthesis and metabolite productivity can be attributed to the supply and/or utilisation of light (Ma *et al.* 2019). Thus, to optimise and ensure sustainable biomass and/or metabolite productivity, light energy must be utilised with the highest possible efficiency (Ma *et al.* 2019; Nwoba *et al.* 2019; Nzayisenga *et al.* 2020).

2. 3. The intrinsic nature of light

Each year the Earth receives approximately 3.9×10^6 MJ of energy in the form of solar radiation, which consists of a wide range of wavelengths (Figure 2. 2). The UV (10 – 390 nm), visible (390 – 750 nm), and IR (0.7 – 300 mm) spectrum accounts for 6, 52, and 42% of solar energy, respectively (Raeisossadati *et al.* 2019). The spectrum used by microalgae corresponds closely to the visible spectrum (400 – 700 nm) (Figure 2.3), however, photosynthetic organisms have different intracellular light-harvesting pigments, which enable them to utilise certain wavelengths within the spectrum (Eroglu *et al.* 2013; Liu *et al.* 2017).

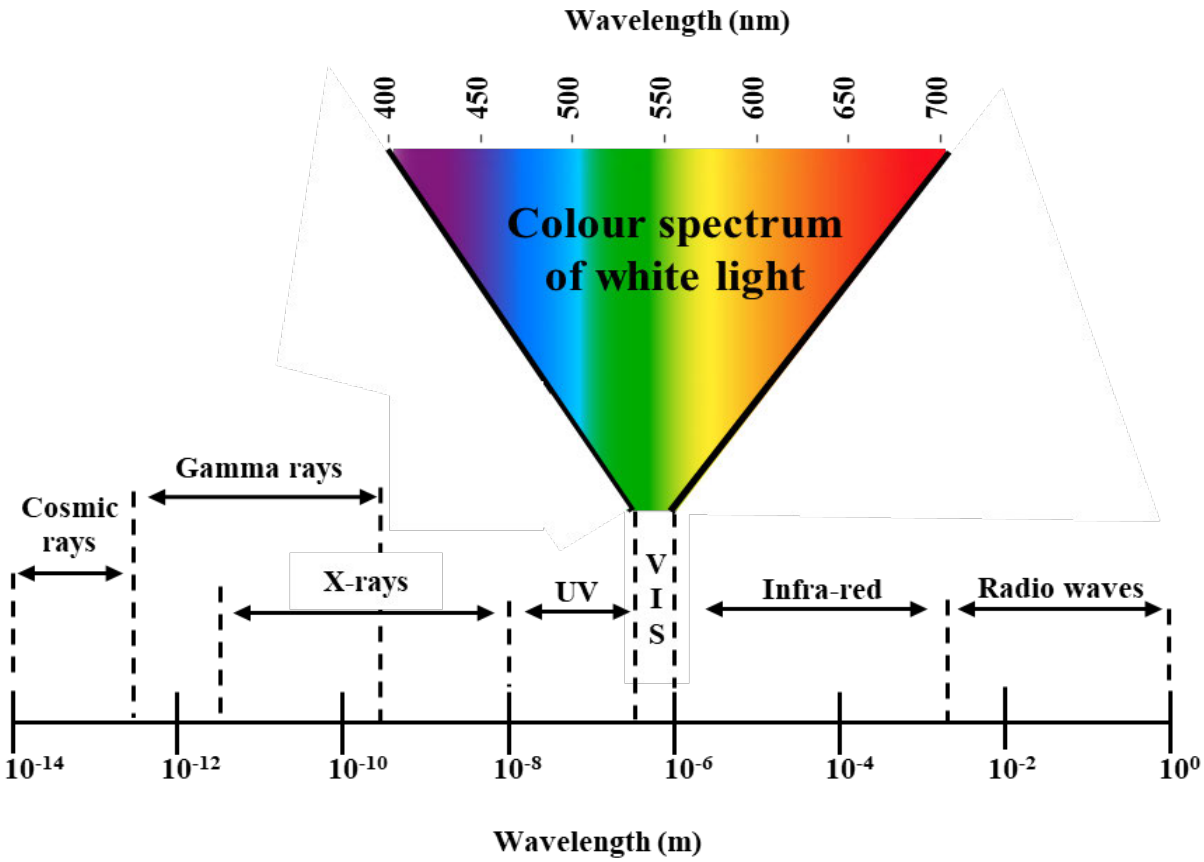

Figure 2.3: The electromagnetic radiation showing the visible light spectrum. Wavelength represented in meters (m) and nanometres (nm), adapted from Masojídek *et al.* (2013).

Photosynthesis in green algae occurs within the 400 – 500 nm and 600 – 700 nm spectral range, whilst green-yellow light (500 – 600 nm) and far-red (700 – 800 nm) are transmitted through the culture medium or are reflected (Baer *et al.* 2016; Liu *et al.* 2017). A large amount of light energy falls outside the PAR region and thus remains unused. The theoretical maximum value of oxygenic photosynthesis by microalgae to convert sunlight to biomass is approximately 13%. However, less than half of the theoretical value is achieved at a maximum using conventional microalgal culture conditions (Raeisossadati *et al.* 2019). The light-related variables known to affect microalgal growth and physiological responses include irradiance

level (PFDs) and spectral distribution (wavelength) (Vadiveloo *et al.* 2015; Danaee *et al.* 2018; Sung *et al.* 2018).

2. 4. Microalgal growth

There are three basic growth modes for microalgal cultivation: photo-autotrophic; heterotrophic; and mixotrophic cultivations. When grown photo-autotrophically, microalgae use sunlight as a source of energy to sequester inorganic carbon in the form of CO_2 from the environment (Patel *et al.* 2019; Choix *et al.* 2021). The photo-autotrophic growth regime is widely used to cultivate microalgae; however, it governs microalgal productivity and is limited to the availability of light. With regards to light availability, heterotrophic cultivation has been proposed as an alternative method for microalgal biomass production. Under heterotrophic cultivations, algae do not require light for growth because energy is solely derived from exogenous organic carbon such as acetate, glycerol, glucose *etc*. (Cecchin *et al.* 2018; Sim *et al.* 2019). During mixotrophic cultivations, algae simultaneously assimilate inorganic and organic carbon that is used for photosynthesis and respiration mediated carbon capture (*via* ATP generation) (Cecchin *et al.* 2018; Sim *et al.* 2019). Consequently, mixotrophic growth is more advantageous as it concurrently improves physiological performance and nutrient uptake increasing growth rates and biomass yields, and further boosting high-value metabolite accumulation (Pang *et al.* 2019; Choix *et al.* 2021). This type of growth involves both photosynthesis and respiration.

2. 4. 1. Photosynthesis

Microalgae use light energy as fuel for their metabolism. Photosynthesis is the process by which photosynthetic organisms convert light energy to chemical energy. This chemical energy is stored as carbohydrate molecules, which are produced by carbon fixation accompanied by water splitting (Choi *et al.* 2015; Derks *et al.* 2015; Liu *et al.* 2017; Pang *et al.* 2019). The overall reaction in which carbohydrates are formed during photosynthesis can be indicated by Equation 2.1 below:

$$CO_2 + 2H_2O \rightarrow (CH_2O) + O_2 + H_2O$$

Equation 2.1: Photosynthesis reaction

This reaction illustrates that microalgae convert carbon dioxide (CO_2) and water (H_2O) into organic products (CH_2O) and produce O_2. The equation is merely a summary statement as the process of photosynthesis involves numerous reactions catalysed by different enzymes depending on the type of photosynthesis performed.

2. 4. 1. 1. Oxygenic and anoxygenic photosynthesis

Photosynthesis can be divided into two categories, *i.e.* oxygenic and anoxygenic photosynthesis. Oxygenic photosynthesis is characterised by the generation molecular O_2 during the synthesis of glucose from CO_2 and H_2O while anoxygenic photosynthesis does not generate O_2. Also, oxygenic photosynthesis is performed by eukaryotic algae and prokaryotic cyanobacteria using chlorophyll and phycobilins, while photosynthetic prokaryotes such as the

filamentous green non-sulphur bacteria employ anoxygenic photosynthesis using bacteriochlorophylls (Xiong 2006; Chandaravithoon *et al.* 2020; Sandmann 2021).

Cyanobacteria are regarded as the evolutionary progenitors of chlorophyll *a* as they gave rise to chloroplasts in eukaryotic algae. However, the chlorophyll *a* pigments contained in the PSs of the photosynthetic bacteria differ structurally from cyanobacteria and algae. Prokaryotes such as heliobacteria have bacteriochlorophyll *g* while proteobacteria and sulphur bacteria synthesise various bacteriochlorophylls from *a* to *e*. These pigments absorb light at different frequencies and thus have slightly different colours (Xiong 2006; Chandaravithoon *et al.* 2020; Sandmann 2021). Consequently, the utilisation of the light by photosynthetic organisms is determined by the chemical nature of their native pigments.

2. 4. 1. 2. Pigments used in oxygenic photosynthesis

In green algae, photosynthesis can be defined as a chemical process mediated by a series of biological redox mechanisms that are initiated when light is captured by light-harvesting complexes (LHCs). The complexes are made up of light-capturing chromophores, *i.e.*, pigments attached to proteins. Chromophores vary based on the photosynthetic species. The most abundant chromophore in oxygenic photosynthesis is chlorophyll (Wobbe *et al.* 2016; Liu *et al.* 2017). Chlorophyll *a* is the main reaction pigment in green microalgae and absorbs violet-blue and red-light quanta at 410 – 430 nm and 660 nm wavelengths, respectively (Table 2.1), (Baer *et al.* 2016; Chandra *et al.* 2019). Chlorophyll *b* is the second most abundant in plants and green microalgae and absorbs blue (450 nm) and orange wavelengths (640 nm) (Eroglu *et al.* 2013; Nwoba *et al.* 2019). Chlorophyll *c* absorbs light between 447 – 452 nm

and is found in haptophytes, heterokonts, dinoflagellates, and cryptophytes; while chlorophyll *d* absorbs far-red light (~ 710 nm) and has been identified in Rhodophyta. Chlorophyll *f* absorbs longer wavelengths (> 800 nm) and has been identified in cyanobacteria (Table 2.1), (Eroglu *et al.* 2013; da Silva Ferreira and Sant'Anna 2016; Nwoba *et al.* 2019). Chlorophyll *c*, *d*, and *f* are considered to be accessory pigments that broaden the range of light absorption and transfer energy to the photosynthetic reaction centres (RCs). These molecules do not participate in electron transport by the photosynthetic electron transport chain (ETC).

Apart from light-harvesting, chromophores are also crucial as they ensure energy transfer of the absorbed photons. Carotenoids aid in microalgal chromatic adaptation by facilitating the harvesting of light. These pigments transfer the harvested energy to the chlorophyll *a* pigment. Carotenoids also function as free-radical scavenging metabolites, and thus, mitigate cellular oxidative damage by dissipating excess energy as heat (Hashimoto *et al.* 2015; Varela *et al.* 2015; Nwoba *et al.* 2019). Like carotenoids, phycobilins assist algae under low irradiance conditions by increasing the absorption spectrum for the cells to absorb light. Both carotenoids and phycobilins are accessory light-harvesting pigments that absorb wavelengths between 400 - 500 nm and 500 - 650 nm, respectively (Baer *et al.* 2016; Liu *et al.* 2017). All these pigments are involved in the light reactions of photosynthesis.

Table 2.1: Various light-harvesting pigments found in microalgae and their photonic characteristics (Eroglu et al. 2013; Nwoba et al. 2019).

Pigment class	Pigment constituent	Absorption spectrum (nm)	Pigment colour	Algal divisions
Chlorophylls	*a*, *b*, *c*1, *c*2, *d*, *f*	410 – 430 450 – 475 630 – 680 700 – 750	Green	*Chlorophyta*, *Cryptophyta*, *Cyanophyta*, *Chlorarachniophyta*, *Dinophyta*, *Euglenophyta*, *Glaucophyta*, *Heterokontophyta*, *Haptophyta*, *Prochlorophyta*, *Rhodophyta*
Carotenoids	α-, β- & ε-carotene, Lutein, Astaxanthin, Fucoxanthin, Violaxanthin, Zeaxanthin	400 – 550	Red, yellow, orange	*Cryptophyta*, *Cyanophyta*, *Glaucophyta*, *Prochlorophyta*, *Rhodophyta* *Chlorophyta*, *Chlorarachniophyta*, *Dinophyta*, *Euglenophyta*, *Heterokontophyta*, *Haptophyta*
Phycobilins	C-phycocyanin, Allophycocyanin, Phycoerythrin	500 – 650	Red, blue	*Cryptophyta*, *Cyanophyta*, *Glaucophyta*, *Rhodophyta*

2. 4. 1. 3. Light reactions of oxygenic photosynthesis

The light reactions occur in the chloroplast in the thylakoid membranes (Figure 2.4). In the first phase, the pigment antenna complexes absorb and transfer photon energy to the RCs of PSII. This excites the state electrons from a special pair of chlorophyll *a* molecules, *i.e.*, P680 (pigment absorbing light at 680 nm). The P680 chlorophylls have exceptionally strong

oxidising powers and consequently, drive the extraction of electrons from water within the oxygen-evolving complex (OEC) (Choi *et al.* 2015; Derks *et al.* 2015; Liu *et al.* 2017; Pang *et al.* 2019). This initiates the translocation of electrons through the thylakoid membrane forming an ETC. Throughout the light reactions, O_2 is produced *via* the photolysis of water (*e.g.*, water to protons/electrons/oxygen with involvement of manganese), while hydrogen provides the necessary electrons resulting in the formation of H^+ ions (Sekar and Ramasamy 2015; Liu *et al.* 2017). The light reactions can be summarised by Equation 2.2 below.

$$2H_2O + \text{Light} \rightarrow 4H^+ + 4e + O_2$$

Equation 2.2: Light reactions of photosynthesis

The electrons are transferred to the plastoquinone (PQ) pool (primary [Q_A] and secondary [Q_B] quinone acceptors). The PQs gain protons from the stroma and are then reduced by electrons which promote the releasing protons into the lumen. Next, electrons are funnelled to the cytochrome b_6f complex (Cyt b_6f), oxidising PQs before they collect more protons from the stroma. Electrons are transferred to plastocyanin (PC) and then reduced to the chlorophyll centre in PSI (P700) (Burlacot *et al.* 2019; Pang *et al.* 2019; Saroussi *et al.* 2019). The PSI complex has a maximum absorption at 700 nm. The difference in the peak absorption between the PSs is important as it decreases the overlap of the absorption bands and reduces competition for the same photons. This allows a balanced rate of energy absorption between the two PSs. Ultimately, electrons are transferred to PSI and the photosynthetic electron flux to stromal ferredoxin (FDX). Reduced FDX supplies electrons to the ferredoxin-$NADP^+$ reductase (FNR) which in turn supplies electrons to NADPH oxidoreductase (NDA2). The enzyme NDA2 moves electrons into the PQ pool for NADPH synthesis (Burlacot *et al.* 2019; Pang *et al.* 2019;

Saroussi *et al.* 2019). This transfer of electrons is called linear electron flow (LEF), denoted by the dashed red arrows in Figure 2.4.

Protons that are released from the splitting of water molecules and the PQ system (LEF) are highly concentrated in the thylakoid lumen. This results in the build-up of electrochemical potential commonly referred to as the proton motive force (PMF), (Sun *et al.* 2018; Zavrel *et al.* 2018). The PMF causes a proton gradient component (ΔpH) and a membrane potential component across the thylakoid membrane (Δψ). The subsequent proton flow governs the production of phosphorylating power (adenosine triphosphate [ATP]), *via* the chloroplastic ATP synthase, while electron flow controls the production of NADPH. Both pathways regulate cellular energetic balance (ATP/NADPH ratio) and need to be maintained at sufficient levels (Pang *et al.* 2019; Saroussi *et al.* 2019). The efficient use of NADPH generated by the LEF is crucial for cell survival and fitness. Furthermore, the over-reducing pressure in the algal chloroplast promotes the production of reactive oxygen species (ROS) which are harmful as they cause cellular photo-oxidative damage (Zavrel *et al.* 2018).

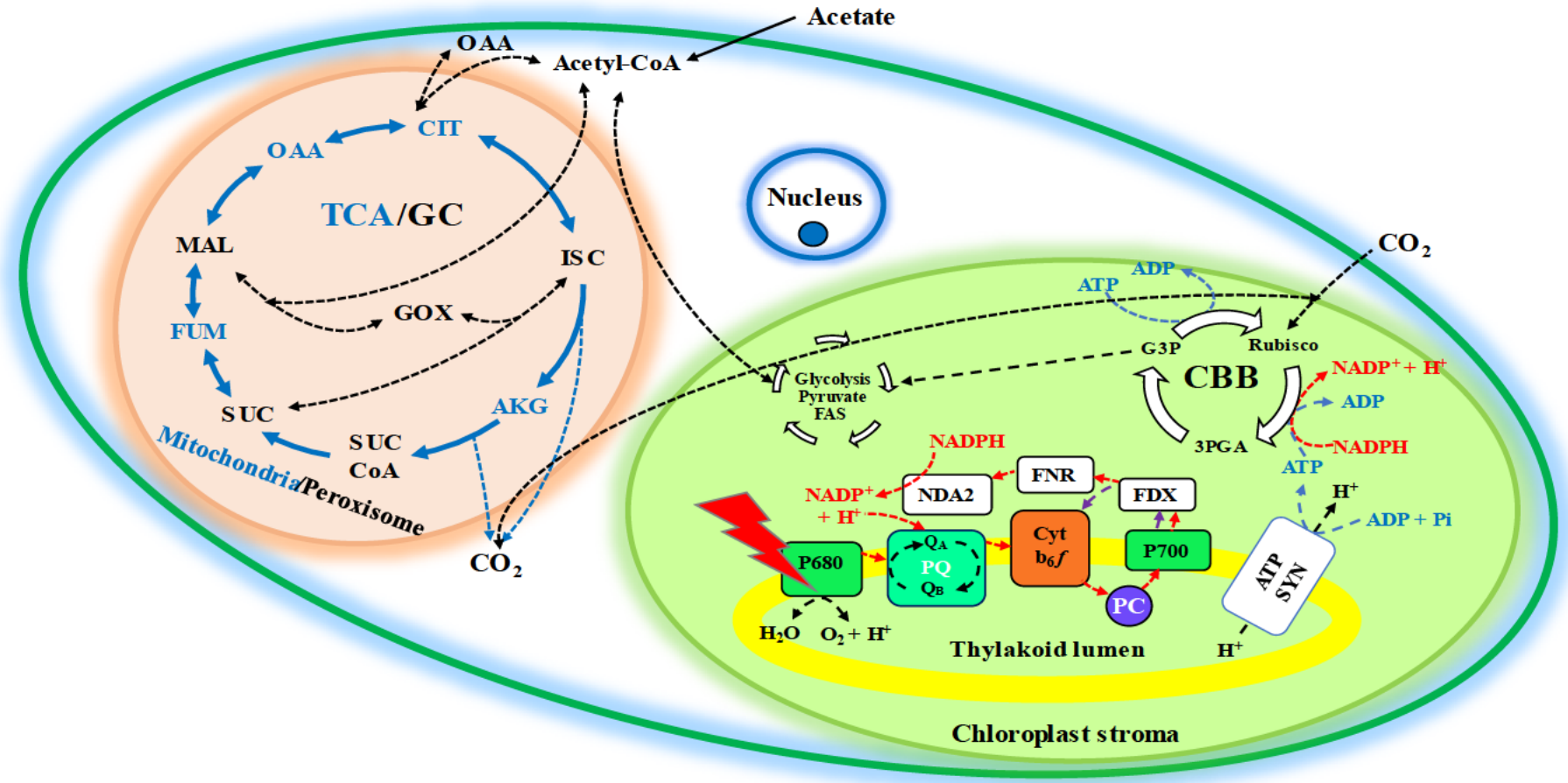

Figure 2.4: Simplified electron transfer pathways and carbon assimilation in *Chlamydomonas reinhardtii* and the interaction with mitochondrion and peroxisome. Photons are absorbed and transferred to the reaction centres of PSII (P680), which gains the energy to split water molecules. The reaction releases

electrons and protons. The red arrows denote linear electron flow through PSII and involve plastoquinone ([PQ], Q_A and Q_B), cytochrome b_6f (Cyt b_6f), plastocyanin (PC), PSI (P700), ferredoxin (FDX), ferredoxin-$NADP^+$ reductase (FNR), NADPH oxidoreductase (NDA2) and ATP synthase (ATP SYN). The purple dashed arrows denote cyclic electron flow in the chloroplast. The products of photosynthesis are used in the Calvin-Benson Bassham (CBB) where ribulose-1, 5-bisphosphate (RuBisCo) binds CO_2 to convert to 3-phosphoglyceric acid (3PGA) and then to glyceraldehyde-3-phosphate (G3P) The G3P is then used in other biosynthetic pathways such as glycolysis, fatty acid synthesis (FAS), the tricarboxylic acid cycle (TCA), or the glyoxylate cycle. Acetate is converted to acetyl-coenzyme A (Acetyl-CoA) and fed to the TCA or FAS. In the mitochondrion (blue wring), citrate (CIT) is converted to isocitrate (ISO), α-ketoglutarate (AKG), succinate (SUC), fumarate (FUM), malate (MAL), and oxaloacetate (OAA), whereas in the peroxisome (black text) ISC and acetyl-CoA are converted directly to SUC and then MAL *via* glyoxylate (GOX) and Acetyl-CoA, adapted from Saroussi *et al.* (2019) and Smith and Gilmour (2018).

Linear electron flow transfer chains contribute to the electrochemical proton gradient and subsequently to ATP production and luminal pH. However, LEF is only able to generate an ATP/NADPH ratio of 2.57/2, and therefore, other mechanisms are required to supply additional ATP to enhance this ratio. Hence, in addition to LEF, ferredoxin-mediated cyclic electron flow (CEF) occurring around PSI is used to provide additional energy (this process is shown with the purple dashed arrows in Figure 2.4), (Zavrel *et al.* 2018; Burlacot *et al.* 2019). Cyclic electron flow is defined as the return of reducing equivalents from the PSI pool of acceptors to its pool of donors. It involves the re-oxidation of NADPH and/or FDX through PQ, the Cyt b_6f complex, and PSI. This electron flow allows for the translocation of two protons for one light quantum converted by PSI. The pathway generates the transmembrane proton gradient used for ATP synthesis (Nawrocki *et al.* 2019a; Yadav *et al.* 2020). The CEF around PSI involves the proton gradient regulation 5 (*pgr5*) and *pgr5*-like photosynthetic phenotype 1 (*pgrl1*) proteins, that generate a component of the proton gradient crucial for the initiation of both NPQ and photosynthetic control (Nawrocki *et al.* 2019a; Yadav *et al.* 2020).

Excessive light regimes increase excess excitation energy which overexcites the photosynthetic pigments and the ETC, and thus induces the production of toxic ROS leading to photo-oxidative damage (Hashimoto *et al.* 2015; Katiyar *et al.* 2017). This photo-inhibition decreases microalgal productivity by damaging the essential proteins required for electron transfer during photosynthesis (Natali and Croce 2015; Quaas *et al.* 2015; Meagher *et al.* 2021). The risk of photo-inhibition is contingent on the redox state of the Q_A in PSII. When Q_A is oxidised and ready to accept electrons, light is absorbed, leading to the electron transport from water to PQ (Nikolaou *et al.* 2015; Baer *et al.* 2016). The electrons go through the ETC, and the energy is quenched. However, if Q_A is reduced, the ETC will be altered, and the excess irradiance directly leads to protein damage (Hashimoto *et al.* 2015; Katiyar *et al.* 2017).

Another possibility is that the excess electrons from PSI may lead to the formation of excited O_2 molecules which damage cell structures and lead to cell death (Quaas *et al.* 2015; Wobbe *et al.* 2016; Meagher *et al.* 2021). Nevertheless, photo-protective mechanisms have evolved to lessen the damage on the PSII. Redox alterations within the photosynthetic ETC occur when there are changes in light quality and quantity. Research has shown that an un-optimised PAR intensity (either too low or excessive) may become a stress attribute to photosynthesis, leading to photo-inhibition, and altering the photosynthetic functionality (Nikolaou *et al.* 2015; Baer *et al.* 2016). Certainly, stress attributes can be controlled by providing irradiance in specific wavelengths (Nwoba et al. 2019). In this way, manipulating the quantity and quality of light received by the algae can be used as a strategy to increase metabolites and/or biomass.

2. 4. 1. 4. Dark reactions of oxygenic photosynthesis

The chemical energies generated (*i.e.*, the products of photosynthetic electron transport NADPH and ATP) from the light-dependent reactions are used to drive CO_2 assimilation *via* the Calvin-Benson Bassham (CBB) cycle (Burlacot *et al.* 2019; Xu *et al.* 2019). Dark reactions do not require light and occur concurrently with light-dependent reactions (Hashimoto *et al.* 2015; Liu *et al.* 2017). The dark reaction, the reduction of CO_2 CBB cycle), can be described by Equation 2.3 below.

$$CO_2 + 4H^+ + 4e^- \rightarrow CH_2O + H_2O$$

Equation 2.3: Dark reactions of photosynthesis

The CBB cycle involves three phases *i.e.*, CO_2 fixation, reduction, and regeneration (Figure 2.4). One enzyme is critical for this pathway *i.e.*, ribulose-1, 5-bisphosphate

carboxylase/oxygenase (RuBisCo) as it is involved in carbon fixation (Sekar and Ramasamy 2015; Woodworth *et al.* 2015; Liu *et al.* 2017). The first step: (*i*) Carboxylation stage, 3-phosphoglyceric acid is produced by catalysing the condensation of CO_2 and the C5 body (ribose-1,5-biphosphate) by the enzyme RuBisCo; (*ii*) Reduction stage, where 3-phosphoglyceric acid is acidified by ATP into 1,3-diphosphate glyceric acid by the enzyme 3-phosphoglyceric acid kinase, and then reduced into glyceraldehyde-3-phosphoric acid by NADPH by the enzyme phosphoglyceraldehyde dehydrogenase; and (*iii*) Regeneration stage, involves the regeneration of ribulose-1,5-biphosphate. The glyceraldehyde-3-phosphate (G3P) molecule is acidified to ribonuclease-1,5-biphosphate under the action of ATP. At this point, the cycle is complete and ready to accept more carbon (Minagawa and Tokutsu 2015; Zavrel *et al.* 2018; Xu *et al.* 2019). The products of the photosynthetic reactions are transported to other organelles, including the mitochondria, where they are broken down to produce energy carrier molecules to satisfy the cellular metabolic demands.

2. 4. 2. Respiration

Respiration in algae can occur under both heterotrophic and mixotrophic cultivation modes. Based on the cytosol, chloroplasts, and mitochondrial interactions, respiratory O_2 uptake is enhanced after irradiation (light-enhanced respiration) which is likely stimulated by the increase in respiratory substrates produced during photosynthetic carbon assimilation. This function is in keeping with the metabolic and redox homeostasis of algal cells in the light. At a fundamental level, photosynthesis provides the sugars/polysaccharides that are catabolised *via* glycolysis and the TCA cycle. This is used to produce ATP *via* substrate-level phosphorylation and reducing equivalents that are used for respiratory electron transport and ATP synthesis by oxidative phosphorylation. Algae utilise organic carbon sources such as

acetate, glucose, or glycerol for energy generation as it requires less energy to assimilate (Cecchin *et al.* 2018; Pang *et al.* 2019; Patel *et al.* 2019). In the context of this research, acetate metabolism will be discussed. The majority of the acetate taken up by the cell is first converted to acetyl coenzyme A (acetyl-CoA) by acetyl-CoA synthetase before being transported across the mitochondrial membrane and assimilated *via* tricarboxylic acid (TCA) cycle (blue text, Figure 2.4). In the mitochondrion, the TCA cycle starts when: (*i*) acetyl-CoA reacts with the compound oxaloacetate to form citrate; (*ii*) citrate is reorganised to form isocitrate enzymatically *via* aconitase; (*iii*) isocitrate releases CO_2 and undergoes oxidation to form alpha-ketoglutarate *via* isocitrate dehydrogenase; (*iv*) alpha-ketoglutarate releases CO_2 and is oxidised to form succinyl CoA; (*v*) succinyl CoA is converted to succinate *via* succinic semialdehyde; (*vi*) succinate is oxidised to fumarate *via* succinate dehydrogenase; (*vii*) fumarate is hydrated to produce malate *via* fumarase; (*viii*) malate is oxidised to oxaloacetate *via* malate dehydrogenase. Each turn of the cycle enables the regeneration of oxaloacetate and the formation of two molecules of CO_2 (Zhang and Bryant 2015; Cecchin *et al.* 2018; Liang *et al.* 2018; Pang *et al.* 2019).

Under mixotrophic growth mode, the organic carbon provides auxiliary energy in the form of Acetyl-CoA, nicotinamide adenine dinucleotide phosphate (NADPH), and other intermediates for cellular biosynthesis while the CO_2 provided by cellular respiration is utilised for photosynthesis under the light conditions (Cecchin *et al.* 2018; Sim *et al.* 2019). The utilisation of both light and organic carbons reduces the microalgal dependency for a sole energy source. Depending on the circumstances, the organic carbon can be used for growth while the light energy can be used for energy generation and/or induce metabolites such as lipids, polyunsaturated fatty acids, carotenoids, tocopherol, and chlorophyll production (Pang *et al.* 2019). Past reports using *Haematococcus pluvialis*, *Chlorella regularis*, and *C. vulgaris*

have shown that oxidative carbon metabolism and photosynthesis function in synchronisation and independently (Pang *et al.* 2019; Choix *et al.* 2021). Hence, by providing adequate carbon and irradiance in specific wavelengths, microalgal growth can be substantially improved under mixotrophic growth, as compared to photo-autotrophic and/or heterotrophic growth mode systems (Cecchin *et al.* 2018; Pang *et al.* 2019).

Additionally, acetyl-CoA can be assimilated *via* the glyoxylate cycle in the peroxisome (black text, Figure 2.4), (Smith and Gilmour 2018). The glyoxylate cycle (photo-respiration) shares the activities of several enzymes with the TCA cycle including aconitase, citrate synthase, and malate dehydrogenase. The two major enzymes used in the glyoxylate cycle namely isocitrate lyase and malate synthase that convert isocitrate and acetyl-CoA into succinate and malate, are absent in the TCA cycle (Zhang and Bryant 2015; Liang *et al.* 2018). The net reaction of the glyoxylate shunt is used to supplement the production of precursors for carbohydrate or amino acid biosynthesis. This enables the cells to convert two acetyl-CoA units into succinate and avoid carbon loss as the CO_2-releasing steps of the TCA cycle. Hence, the glyoxylate cycle enables microalgal cells to photo-assimilate acetate and utilise acetyl-CoA more efficiently for fuelling gluconeogenesis and other anabolic pathways thereby generating biomass production (Cecchin *et al.* 2018; Pang *et al.* 2019).

Alternatively, acetyl-CoA is used for *de novo* production of fatty acids in the chloroplast (Zhang and Bryant 2015; Liang *et al.* 2018). Respiration encompasses an extensive glycolytic and oxidative pentose phosphate pathway, the tricarboxylic acid and glyoxylate cycle, and oxidative phosphorylation (ATP generation). These interactions are necessary as they regulate cellular homeostasis, however, mitochondrial respiration is also associated with the generation of ROS (Cecchin *et al.* 2018; Liang *et al.* 2018; Pang *et al.* 2019). This occurs due to the leakage

of electrons from the ETC during oxidative phosphorylation leading to a reduction of oxygen to form superoxide. The superoxide is then reduced to hydrogen peroxide. Both the superoxide and hydrogen peroxide produced during this process is considered mitochondrial ROS. Consequentially, algae have developed acclimation strategies to cope with such stressful situations in both open ponds systems and closed PBR systems (Vuppaladadiyam *et al.* 2018; Nwoba *et al.* 2019).

2. 5. Microalgal cultivation

2. 5. 1. Open pond systems

Open pond systems are the most feasible method for large-scale microalgae cultivation, primarily, as they utilise freely available sunlight for algal cultivation and can be cheaply constructed. These systems are usually shallow (0.25 – 0.5 m) to ensure the microalgal cultures receive sufficient exposure to sunlight. Open ponds consist of an oval-shaped closed-loop recirculation channel in which mixing is provided by paddle wheels (channel length: 25 m; width: 2 m; total surface area: 100 m^2) (Michael *et al.* 2015; Nwoba *et al.* 2019). These systems are relatively low-cost when compared to closed systems as they require minimal energy input to operate. Hydrodynamics and CO_2 supply are key drivers of the microalgal growth efficiency in these systems (Michael *et al.* 2015; Nwoba *et al.* 2019; Raeisossadati *et al.* 2019).

A significant challenge with open pond systems is the cost-effective delivery of light within the required wavelengths to the cultivation system. As light penetrates the algal culture, the irradiance is dispersed heterogeneously which is mainly due to light attenuation. Light attenuation can be defined as the absorption of light by algal pigments and the scattering of

light by the algal cells and other suspended particles. Additionally, the inhomogeneous distribution of the light results in a self-shading effect between the algal cells which further exponentially reduces the light distribution. Light attenuation is influenced by many factors including algal density, cell size, light path, and the variation of pigments (Wang *et al.* 2014; de Mooij *et al.* 2017). Apart from wavelengths selection, low or high irradiance levels negatively impact the photosynthetic process. Excess irradiance above the absorption limit for algal cells will cause damage to the PSII complex leading to photo-inhibition and a decrease in microalgal bio-productivity (Seo *et al.* 2015; Vadiveloo *et al.* 2015; Abu-Ghosh *et al.* 2016).

Contrastingly, low light levels hinder microalgal growth and the accumulation of metabolites *i.e.*, photo-limitation. Fortunately, microalgae can adapt to fluctuating irradiance conditions and optimise the use of available light *via* strategical acclimation mechanisms (Wang *et al.* 2014; de Mooij *et al.* 2017). At steady irradiance levels (50 – 100 µmol photons·m^{-2}·s^{-1}) cell density, cell size, distribution, and biochemical composition remain constant (Zhao *et al.* 2013; Sforza *et al.* 2015; Abu-Ghosh *et al.* 2016). Apart from the lower operating costs, the mass transfer between open systems and the environment leads to pollution and contamination, which increases the risk of culture collapse. Open pond systems have low reproducibility, low biomass concentration, and higher harvesting costs (Michael *et al.* 2015; Nwoba *et al.* 2019; Raeisossadati *et al.* 2019).

2. 5. 2. Closed photo-bioreactors

Photo-bioreactor cultivations offer several benefits when compared to open pond systems including, low contamination risk, high gas-liquid mass transfer rate, low water loss, high volumetric and areal productivity, better control of operational conditions (such as irradiance

levels, mixing, pH, and temperature), and low harvesting cost. However, like pond systems, one of the main variables affecting PBR technology is the provision of irradiance which is characterised by its PFD with a given distribution and spectrum (Gomez *et al.* 2016; Danaee *et al.* 2018). The quantity of direct and diffused incident irradiance has been found to significantly affect microalgal productivities and PE. The light limitation is one of the main problems associated with outdoor PBRs as it leads to decreased PE (Pawar 2016; Pruvost *et al.* 2016).

Maximising the light availability for microalgal utilisation is a critical factor. Even under optimal nutrition, poor light conditions (photo-limitation/inhibition) lead to losses in biomass and lowered metabolite concentrations. One option to achieve increases in metabolite productivity is through continuous microalgal cultivation in PBRs exposed to constant artificial lighting (Pruvost *et al.* 2016). Various types of artificial light including light emitting diodes (LEDs) have been widely used as alternatives to conventional fluorescent and halogen lamps (Wang *et al.* 2014; Wobbe *et al.* 2016). They can emit narrow bands of monochromatic light. Microalgae grown under blue or red monochromatic light exhibit enhanced growth when compared to multi-chromatic white light, which leads to increased metabolite production (Baer *et al.* 2016; Liu *et al.* 2017). As mentioned, the supply of artificial light for microalgal cultivation is extremely expensive and energy-intensive. This leads to increased production costs which limit their use in large-scale microalgal cultivation (Dogaris *et al.* 2015; Pruvost *et al.* 2016). Solar-powered LED arrays with low energy consumption are now available which could mitigate some of the operational costs but with an increase in set-up costs.

2. 6. Photo-regulation mechanisms in microalgae

Photo-regulatory responses are aimed at protecting against photo damage and attempt to balance light-harvesting and energy utilisation. Acclimation refers to the organism's ability to adapt to the cultivation conditions, in this case, photo-acclimation refers to the microalgal capacity to alter the photosynthetic apparatus structure and function in response to changes in irradiance. This process is comprised of a myriad of biochemical changes that are divided into two components: short-term and long-term stress responses (Girolomoni *et al.* 2019; Nawrocki *et al.* 2020). Short-term responses are typically reversible and the responses occur in the order of seconds to minutes under increased light irradiation (Meagher *et al.* 2021). Exact timeframes are variable due to the diversity between photosynthetic organisms and the type of physiological response initiated. However, these processes usually occur in a few seconds to hours. Excessive PFDs lead to the over-excitation of the LHCs, increasing the accumulation of chlorophyll triplets (Figure 2.5).

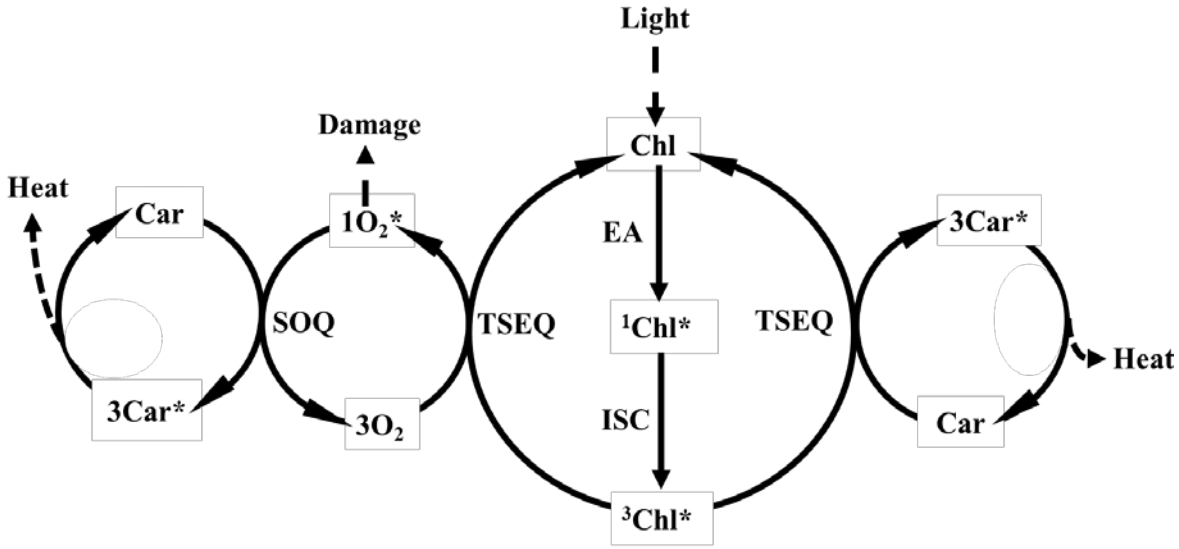

Figure 2.5: Chlorophyll based quenching mechanisms in microalgae. From the illustration, singlet chlorophylls (1Chl*) give rise to triplet chlorophylls (3Chl*) *via* intersystem crossing (ISC). Triple-state energy quenching (TSEQ) of 3Chl* by ground-state

molecular oxygen ($3O_2$) generates singlet oxygen ($1O_2$*). Carotenoids (Car) prevent cell damage by singlet oxygen quenching (SOQ) and TSEQ. These processes create triple-state carotenoids (3Car*) which dissipate excess heat. Adapted from Varela *et al.* (2015).

Upon irradiation, chlorophylls are excited to a state known as singlet chlorophylls (1Chl*) by direct energy absorption (EA). Sequentially, 1Chl* give rise to triplet chlorophylls (3Chl*) *via* an energy-less inter-conversion process referred to as intersystem crossing (ISC) (Wobbe *et al.* 2016; Girolomoni *et al.* 2019). Under increased PFDs, molecular O_2 is abundantly produced from water-splitting. Triple-state energy quenching (TSEQ) of 3Chl* by ground-state molecular oxygen ($3O_2$) generates singlet oxygen ($1O_2$*), the most ROS, (Varela *et al.* 2015; Wobbe *et al.* 2016). These ROS rapidly photo-oxidise PSII components which hinder photosynthesis by reversibly inhibiting the P680 chlorophyll RCs leading to cell damage. Carotenoids (Car, in the diagram) prevent cell damage by (*i*) singlet oxygen quenching (SOQ), and (*ii*) by deactivating 3Chl* *via* TSEQ. Both processes create triple-state carotenoids (3Car*), which return to the ground state by dissipating excess heat (Quaas *et al.* 2015; Girolomoni *et al.* 2019).

To lessen the risk of ROS damage, excess light is thermally dissipated by the microalgae. This is typically achieved *via* a key photo-regulative response strategy known as non-photochemical quenching (NPQ) of chlorophyll fluorescence (Moejes *et al.* 2017; Meagher *et al.* 2021). The NPQ is comprised of three components characterised by a particular type of kinetic behaviour: pH energy-dependent quenching (qE), state transitions (qT), and photo-inhibitory quenching (qI). Non-photochemical quenching mechanisms depopulate the excited states within the PSII pigment array (Girolomoni *et al.* 2019; Nawrocki *et al.* 2020).

2. 6. 1. Energy-dependent quenching, qE

Energy-dependent quenching referred to as qE, is rapidly induced by acidification of the thylakoid lumen upon light stress, which results in the protonation of the light-harvesting complex stress-related (*lhcsr*) proteins (*lhcsr*3 and *lhcsr*1). This immediately activates a signal for the feedback regulation of light-harvesting (Nawrocki *et al.* 2019a; Roach *et al.* 2020). In green algae such as *Chlamydomonas, lhcsr*3 is not constitutively expressed, it accumulates under blue light and activates a low-pH-dependent NPQ of PSII, whereas *lhcsr*1 is triggered by UV and visible light in the presence of high CO_2 (Nawrocki *et al.* 2019a; Roach *et al.* 2020). Contrastingly in *C. reinhardtii*, *lhcsr*3 is completely repressed by CO_2 in the presence of light. When the luminal pH drops to below 6, algae activate specialised enzymes that can reversibly convert oxygenated carotenoids (called xanthophylls) into de-epoxidised forms. This process known is known as the xanthophyll cycle (Goss and Lepetit 2015; Quaas *et al.* 2015).

Energy-dependent quenching also depends on the existence of the special xanthophyll molecules which are bound to the PS antenna proteins (Moejes *et al.* 2017; Meagher *et al.* 2021). The reaction is catalysed by the enzyme zeaxanthin epoxidase, is O_2 dependent, and requires NADPH and FDX as cofactors (Varela *et al.* 2015). Under excessive light, violaxanthin is de-epoxidated to zeaxanthin *via* the enzyme violaxanthin de-epoxidase. The reversible interconversion of violaxanthin into antheraxanthin and then zeaxanthin is essential for NPQ, and thus, both pigments are viewed as photo-protective rather than light-harvesting pigments (Quaas *et al.* 2015; Varela *et al.* 2015).

2. 6. 2. State transitions, qT

State transitions involve the relocation of the antenna amongst PSII and PSI. The mechanism redistributes excitation energy from the LHCII between PSII and PSI. This strategy is used by algae under low light adaptation for electron flow regulation. In green microalgae, the physical separation of PSII and PSI necessitates the existence of different antenna systems, which excite both PSs independently. State transitions regulate the reversible activation of specific proteins thereby optimising the relative absorption capacity of the PSs (Girolomoni *et al.* 2019; Nawrocki *et al.* 2020). The activation of the protein kinase STN7 enzyme, which is triggered by the reduced state of the PQ pool and Cyt b_6f complex, phosphorylates the subunits of the LHC complex of PSII. Some of these LHC complexes migrate laterally towards PSI. This migration modifies the relative cross-sections towards PSI, thereby balancing the light excitation of both PSs. It occurs due to the different absorption spectra of chlorophyll *a*/*b* and is termed as state 1 to state 2 transitions. The protein phosphatase 1/thylakoid associated phosphatase 38 (PPH1/TAP38) drives the reverse reaction. This enzyme dephosphorylates the LHCII linked with PSI which permits the reallocation to PSII. This process is referred to as the state 2 to state 1 transition (Moejes *et al.* 2017; Meagher *et al.* 2021).

In plants, state transitions are ascribed to optimising light absorption in low light. In the green alga *C. reinhardtii*, this mechanism represents a large component of the NPQ. Under excess irradiation, the alga reallocates a large fraction of its antenna between PSs, thereby contributing to photo-protection (Moejes *et al.* 2017; Nowicka 2020). With rapid NPQ processes prevailing over the phosphorylation-dependent regulation, qT may be reduced in algae adapted to physiologically relevant conditions (Girolomoni *et al.* 2019; Nawrocki *et al.* 2020). Consequently, CEF around PSI alleviates excess pressure on PSII.

2. 6. 3. Photo-inhibition, qI

Photo-inhibition (qI) contributes to the slowest component of NPQ and results from the continued over-excitation of the photosynthetic apparatus. This process mainly constitutes the degradation and disassembly of the D1 protein, the core subunit of PSII. The D1 protein is a multicomponent pigment-protein complex that is characterised by a rapid, photon-flux-dependent turn-over directly mediating photosynthetic electron transport and oxygen evolution. Generally, the extent of qI is a direct balance between the repair rate and the damaged PSII (Girolomoni *et al.* 2019; Nawrocki *et al.* 2020). Regardless of the fast turnover of the D1 proteins, high amounts of ROS increase D1 degradation leading to a decrease in the PE (Moejes *et al.* 2017; Meagher *et al.* 2021). Photo-inhibition is considered a photo-protective mechanism as the damaged PSII itself acts as a non-photochemical quencher, preventing over-reduction of the photosynthetic ETC (Girolomoni *et al.* 2019; Nawrocki *et al.* 2020).

The NPQ mechanisms described can be considered as dynamic (reversible) photo-inhibition and occur as a short-term strategy (Davis *et al.* 2013; Roach *et al.* 2020). In contrast, the long-term responses in algae imply ultrastructural changes to the cell, which in most cases involves the de-novo synthesis or breakdown of proteins, pigments, and redox cofactors (Girolomoni *et al.* 2019; Nawrocki *et al.* 2020).

2. 6. 4. Long-term stress responses of the photosynthetic apparatus

High irradiances (≥ 200 µmol photons·m^{-2}·s^{-1}) and extreme conditions lead to chronic photo-inhibition. Algae initiate long-term acclimation strategies that usually consist of alterations in the gene expression which eventually reduces the organism’s light-harvesting

capacity (Moejes *et al.* 2017; Meagher *et al.* 2021). The responses may last several hours or days and include responses that reduce the total number of RCs and LHC antennae, reduce the LHC antennae sizes, and the PSI to PSII ratio. These result from the transcriptional and translational regulation of specific proteins that make up these complexes (Davis *et al.* 2013; Moejes *et al.* 2017). Long-term responses are typically related to the increase and accumulation in antioxidant metabolism products, such as the lipid-soluble antioxidant *a*-tocopherol (vitamin E). Additionally, the rapid changes in the fluxes of the carbon and nitrogen metabolic pathways affect the redox state of cells. Collectively, these mechanisms ultimately attempt to prevent the production of ROS (Davis *et al.* 2013; Girolomoni *et al.* 2019; Nawrocki *et al.* 2020).

2. 7. Effects of light intensity on photosynthesis

Considerable changes may occur in the microalgae photosynthetic activity, pigment content, or lipid profile under various light intensities (Ra *et al.* 2016; Nwoba *et al.* 2019). The appropriate light irradiance level varies from 60 to 120 μmol photons·m^{-2}·s^{-1} depending on photo-period and species-specific characteristics. Researchers, however, have employed a light stress strategy to maximise the metabolite and/or biomass production (Benavente-Valdes *et al.* 2016; Metsoviti *et al.* 2019). Rayati *et al.* (2020), investigated the effect of five different light intensities (50, 100, 200, 400, and 800 μmol photons·m^{-2}·s^{-1}) on the growth and lipid accumulation of *Chlorococcum oleofaciens* KF584224. The algal cultures displayed the fastest growth rate and maximum biomass productivity (367.82 ± 21.63 mgL^{-1} d^{-1}) under 200 μmol photons·m^{-2}·s^{-1} light irradiance. The longest exponential growth, the highest lipid content (59.18%), and lipid productivity (126.72 mgL^{-1} d^{-1}) were achieved in cultures irradiated with 400 μmol photons·m^{-2}·s^{-1}. An increase in the irradiation to 800 μmol photons·m^{-2}·s^{-1} resulted

in a drastic decrease in the microalga cell density, implying the light energy was excessive and could not be utilised for biomass production through photosynthesis.

Ra *et al.* (2016), demonstrated the effects of increased light intensities on the growth and lipid accumulation in *Nannochloropsis oculata*, *Nannochloropsis salina*, and *Nannochloropsis oceanica*. The algae were grown at a 12:12 hr light/dark cycle under 40, 70, 100, and 130 μmol photons·m^{-2}·s^{-1} for 21 days. The authors showed that in all three species the biomass production was increased when the light intensity was increased from 40 to 100 μmol photons·m^{-2}·s^{-1} using blue LEDs. The highest biomass production of 0.68 gL^{-1} was obtained with *N. oculata*, while *N. oceanica* produced 0.60 gL^{-1} and *N. salina* produced 0.58 gL^{-1} at 100 μmol photons·m^{-2}·s^{-1}. A further increase in blue light intensity over 100 μmol photons·m^{-2}·s^{-1} resulted in a decreased specific growth rate from 0.030 h^{-1} to 0.011 h^{-1} for *N. salina* and 0.018 h^{-1} for *N. oceanica* and *N. oculata*. The increased intensity of blue light led to photo-inhibition of the cultures. The microalgal lipid content increased as the green light wavelength increased up to 100 μmol photons·m^{-2}·s^{-1}, which then decreased with a further increase in the light intensity. The lipid content achieved by *N. oculata*, *N. salina*, and *N. oceanica* was 41, 38, and 36% (*w*/*w*), respectively. These were the highest produced in the study. Consequently, the increased green wavelengths were absorbed by the carotenoid pigments leading to lipid production due to increased photo-inhibition. The literature indicated that increases in light intensities in specific wavelengths could drive growth and metabolite accumulation in algae, however, excessive intensities hinder productivity.

2. 8. Effects of wavelength on photosynthesis

2. 8. 1. Visible light spectra

The spectral composition of available light significantly affects microalgal growth and thus metabolism. Blue light is known to increase carotenoid production while red irradiance increases algal chlorophyll and protein composition (da Fontoura Prates *et al.* 2020). Algae utilise specific wavelengths of the light spectrum, thus there exists a direct correlation between pigment accumulation and irradiance. Accordingly, the most appropriate light wavelengths for microalgal cultivation should be sufficiently and selectively delivered to ensure optimal absorption by microalgal pigments for photosynthesis (Zhao and Su 2014; Choi et al. 2015). The optimal light wavelengths for the growth of different microalgal species are shown in Table 2.2.

Table 2.2: The optimal light wavelengths for the growth of algae and cyanobacteria.

Species	Optimal wavelength	References
Spirulina platensis	Red > white > yellow > green > blue	(Wang *et al.* 2014; Raeisossadati *et al.* 2019)
Chlorella sp.	Red > white > yellow > blue	(Wang *et al.* 2014)
C. vulgaris	Red > white > yellow > purple > blue	(Wang *et al.* 2014; Kendirlioglu and Cetin (2017))
Microcystis aeruginosa	Red > blue > white > green > yellow	(Wang *et al.* 2014)
A. platensis	Orange > white > blue-red > green > red > blue	(Kumar *et al.* 2021)
Nannochloropsis sp. (MUR266)	White > pink > red > blue > blue-green	(Vadiveloo *et al.* 2015)
N. salina *N. oceanica* *N. oculata*	Blue > red > white > purple > yellow > green	(Ra *et al.* 2016)
Botryococcus braunii	Red > blue > green	(Wang *et al.* 2014)
C. reinhardtii	Yellow > green > red > blue	(de Mooij *et al.* 2016)
Scenedesmus bijuga	Yellow > green > blue > red	(Mattos *et al.* 2015)

Kendirlioglu and Cetin (2017), tested the effects of blue, green, red, and white wavelengths of light on the growth, pigment, and protein content in *C. vulgaris*. The highest growth and protein content was observed in cultures illuminated with red light while chlorophyll *a* and *b* and astaxanthin was observed under green and blue irradiations, respectively. The red-light wavelength is optimal for the growth of most algal species. It is known that the microalgal PSI is enhanced by blue light wavelengths, while PSII is enhanced by longer wavelengths such as red light (Baer et al. 2016). This is primarily due to the

abundance of chlorophyll pigments in most algal which efficiently absorbs red light when compared to other light wavelengths. However, the lower energy of red light restricts its ability to penetrate highly dense microalgal cultures. It has also been reported that lipid and pigment accumulation can be increased by using blue and far-red wavelengths (Vadiveloo et al. 2015; Yang and Weathers 2015). Shorter wavelengths such as blue light have a higher possibility of causing photo-inhibition by striking the LHC at its peak electrical energy due to its high energy (Wang *et al.* 2014; Wobbe *et al.* 2016). To avoid photo-oxidative damage, microalgal cells convert excess light energy to chemical energy in the form of lipids.

Vadiveloo *et al.* (2015), integrated a photovoltaic cell with a microalgal cultivation system to provide filtered light spectra to the culture. Biomass productivity increased in the order of white (132.4 $mgL^{-1}\,d^{-1}$), pink (101 $mgL^{-1}\,d^{-1}$), red (86.2 $mgL^{-1}\,d^{-1}$), blue (28.9 $mgL^{-1}\,d^{-1}$), and blue-green light (12.9 $mgL^{-1}\,d^{-1}$) while blue light yielded the highest biomass productivity per photons and energy supplied (1.93 $mgL^{-1}\,d^{-1}$ [µmol photons$\cdot m^{-2}\cdot s^{-1}$]) $^{-1}$ for *Nannochloropsis* sp. (MUR266). The highest chlorophyll *a* content was observed when using blue and blue-green light (~ 1.3 pg/cell) while lipid content was ~ 60% higher under blue light. The authors surmised that this approach could allow for the full exploitation of sunlight and reduce dependence on artificial lighting. Similarly, Ra *et al.* (2016) found that blue light produced the highest biomass in *N. salina, N. oceanica,* and *N. oculata*. This ranged between 0.40 – 0.43 gL^{-1}, followed by the red LED (0.34 – 0.36 gL^{-1}), fluorescent light (0.19 – 0.29 gL^{-1}), purple LED (0.16 – 0.26 gL^{-1}), yellow LED (0.15 – 0.21 gL^{-1}), and green LED (0.05 – 0.07 gL^{-1}).

As much as the red and blue wavelengths are preferred, the absorbed action spectra of microalgae vary considerably (Table 2.2). Kumar *et al.* (2021), assessed the effects of filtered

light spectra on the growth and pigment content in *A. platensis*. Six different transparent PVC sheets were used to cover the lab-scale open raceway pond setup. Fluorescent white and yellow tubes were used to provide the lighting conditions. The alga was grown under white light (control, 350 – 750 nm); blue light (400 – 580 nm); blue-red light (390 – 700 nm); red (580 – 720 nm); orange (480 – 665 nm); and green light (430 – 520 nm) conditions. The algae that were grown under orange filtered light produced 3.3 gL^{-1} biomass (DCW). This was 61% higher when compared with the control condition. This was attributed to the enhanced absorption of the filtered orange light spectra by the light-harvesting pigment-protein complex (phycobilisome) in *A. platensis*. Moreover, cells cultivated under the filtered orange light spectra exhibited 62.7 and 23.5 mgL^{-1} chlorophyll *a*nd carotenoid content respectively, which were 40 and 29% higher than the control cultures. Moreover, the chlorophyll *a* content following exposure to the orange light spectra was 58% higher than the blue-red spectra (26 mgL^{-1}).

In addition, strains such as *C. reinhardtii* and *S. bijuga* have been known to exhibit higher biomass productivities under poorly absorbed yellow and green wavelengths. de Mooij *et al.* (2016), found that the biomass productivity of *C. reinhardtii* was 1.86 times higher under yellow light (3.78 $mgL^{-1}d^{-1}$) than under the strongly absorbed red and blue spectra (2.24 and 2.03 $mgL^{-1}d^{-1}$). Mattos *et al.* (2015), found that weakly absorbed green light was more photosynthetically effective for the cultivation of *S. bijuga*. The highest biomass productivity was found to be 30 $mgL^{-1}d^{-1}$ when compared to the blue and red spectra (6.67 and 15 $mgL^{-1}d^{-1}$, respectively). The authors surmised that in dense cultures, poorly absorbed wavelengths can penetrate more and can be utilised for photosynthesis (Mattos *et al.* 2015; de Mooij *et al.* 2016). Similar findings have been reported (Mohsenpour *et al.* 2012).

Due to the diversity in the algal species, there is no general all-purpose monochromatic wavelength that will be optimal for growth. Algae alter the composition of their photosynthetic apparatus to optimise their light-harvesting properties. This requires additional energy turnover, which is counterproductive when aiming to increase biomass and/or metabolite production. Hence, it would be more practical to tailor the wavelength of light to match pigment spectral absorbance during microalgal culture periods (Vadiveloo *et al.* 2015; Yang and Weathers 2015). Additionally, tailoring specific wavelengths such as the IR and UV will substantially increase the quantity of PAR delivered to the algal culture.

2. 8. 2. UV and infrared light spectra

Microalgae reside in the upper layers of many aquatic surfaces, and hence, are prone to high UV exposure which causes photo-bleaching coupled with the reduced upwelling of nutrients (Rastogi *et al.* 2014; Raeisossadati *et al.* 2019). Harmful UV wavelengths are absorbed by nucleic acids and proteins and cause oxidative damage and conformational changes to key metabolic components. This results in an inhibition in photosynthesis, damaging the CO_2 fixation and biological pumps thereby reducing their efficacy and subsequent conversion into organic matter (Sharma *et al.* 2015; Sun *et al.* 2021). Singh *et al.* (2019), found that UV-*b* fluxes reduced the photosynthetic performance of PSII by altering the photosynthetic performance index (reducing the electron transport system), decreasing the maximal quantum yield (F_v/F_m), altering the net closing rate of the RCs, and reducing the trapping flux and effective antenna sizes in both *Chlorococcum humicola* and *C. vulgaris*.

Infrared radiation is known to increase culture temperatures (thermal effects that overheat the culture); subsequently, disturbing the vital biochemical pathways/functions in algae and

requiring costly cooling equipment (Nwoba *et al.* 2019). Temperature is one of the main factors governing the rate of chemical reactions and the structure of the microalgal cellular components. It also influences membrane fluidity, enzymatic activity, and PE by reducing the ETC and other metabolic mechanisms which increases the occurrence of photo-respiration effects (da Silva Ferreira and Sant'Anna 2016). Photo-respiration changes the carboxylation step in the Calvin–Benson cycle to oxygenation, thus dissipating photonic energy. This accounts for approximately a 25% reduction in photosynthesis (Liu *et al.* 2017; Singh *et al.* 2019). Thus, wavelength conversion would eliminate issues such as UV induced cell damage and temperature-related IR stress on cultures.

2. 9. Effects of diurnal cycles and self-shading on microalgae

2. 9. 1. Diurnal cycles

Sunlight is the most cost-effective energy source for microalgae cultivation. However, its implementation has certain challenges which include day and night cycles, changes in weather, and seasonal changes which affect light intensity and spectrum (Abu-Ghosh *et al.* 2015; Abu-Ghosh *et al.* 2016). The light/dark cycle is a crucial factor as it influences microalgal growth. More importantly, changes in the light/dark cycles lead to variations in the biochemical composition of algae. Varying frequencies of the light/dark cycles can significantly enhance microalgal PE. *Nannochloropsis* sp. was found to grow better at 100 µmol photons·m^{-2}·s^{-1} at an 18:6 light/dark cycle in the batch cultivation, while a 12:12 light/dark cycle was best at high light intensities (200 µmol photons·m^{-2}·s^{-1}) (Wahidin *et al.* 2013). At the initial growth stages, constant or high PFD will lead to photo-inhibition owing to the relatively low cell concentrations (Wahidin *et al.* 2013; Abu-Ghosh *et al.* 2015). At later stages of cultivation, low

PFDs are insufficient for cell growth owing to the self-shading effect at high cell densities (6.5 × 10^7 cell mL^{-1}). Moderate light/dark cycles led to maximum lipid concentrations while longer or shorter light cycles (12:12) resulted in lower lipid content in *Nannochloropsis* sp. (Wahidin *et al.* 2013). Microalgae are capable of changing their chemical composition, pigment content and photosynthetic activity when cultivated under varying light and dark cycles. Decreases in the light irradiance levels will lead to increases in cellular content chlorophyll and carotenoid content to ensure efficient light-harvesting (Wahidin *et al.* 2013; Abu-Ghosh *et al.* 2015).

2. 9. 2. Self-shading

Microalgae cultivation systems become limited due to the decrease in PE of the culture possibly due to light attenuation of algal biomass (*i.e*., self-shading effects). The self-shading effect reduces algal productivity and the net energy balance of the entire process. Self-shading becomes a significant growth-limiting factor, in large-scale systems, as it limits light penetration through the algal cultivation. In open raceway ponds, mixing is of particular importance as it circulates microalgae in and out of shaded areas in the water column maintaining the distribution of cells, so they are equally exposed to nutrients, CO_2, and light. Mixing is accomplished by the use of a paddle wheel. As much as this is more energy efficient when compared to mechanical aeration, this increases the energy requirement needed to run the system (Sforza *et al.* 2012; Abu-Ghosh *et al.* 2015). Selecting the optimal water depth in Open pond cultivations are shallow to relieve the effects of self-shading (Michael *et al.* 2015; Nwoba *et al.* 2019).

Owing to the turbulent flow in PBRs, microalgal cells are continuously cycled between the irradiated and dark zones in the reactor. This constant cycling between zones creates a

flashing light (FL) effect that improves photosynthetic performance as it provides an optimal balance of light-harvesting and photo-protection (Sforza *et al.* 2012; Abu-Ghosh *et al.* 2016). Additionally, the PE of microalgal cells remains constant under FL. This is because flashes, and the dark periods succeeding the flashes, facilitate the efficient utilisation of the photochemical energy absorbed by microalgae, whereas continuous light (CL) significantly reduces, degrades and alters chloroplast ultra-structures (Wang *et al.* 2014; Abu-Ghosh *et al.* 2016).

2. 10. Metabolites produced in response to light

Microalgal growth and metabolite production are affected by different growth conditions such as light quality and quantity, temperature, pH, or media composition (carbon, nitrogen, phosphorous, iron, or sulphur). Consequently, the microalgal biochemical make-up is correlated to the systematic use of light energy (pathways), and energy storage products. Electrons produced by photosynthesis can have several allocations: to produce functional biomass (mainly proteins), storage molecules (carbohydrates and lipids), maintenance and respiration (Vuppaladadiyam *et al.* 2018). Table 2.3 shows the chemical composition of the primary metabolites in several microalgal species.

Sánchez-Saavedra *et al.* (2020), grew *C. vulgaris* under white, blue, yellow, and green light at a constant irradiation level (50 µmol photons$\cdot m^{-2} \cdot s^{-1}$). Algal growth and metabolite production was evaluated at exponential and stationary phase. It was found that: (*i*) under white light growth rates were higher; (*ii*) in the exponential phase cell sizes increased using yellow light; (*iii*) during exponential growth there was higher dry weight observed with green light;

(*iv*) under white and green light protein content was significantly increased in the exponential phase; (*v*) during stationary phase carbohydrate levels were significantly increased using yellow light; (*vi*) lipid content was significantly increased during the exponential phase using blue light; (*vii*) biomass productivity was the highest under blue light in the exponential growth phase, while, in a stationary growth phase it was higher with yellow light; (*viii*) chlorophyll and carotenoid levels were significantly increased during exponential growth under yellow and green light (Sánchez-Saavedra *et al.* 2020).

In *N. gaditana*, red light photons accelerated the cell cycle. Under red light illumination, photosynthetic reducing equivalents were accumulated as lipids and carbohydrates, enhancing microalgal lipid content. Blue light stimulated the growth which increased biomass, chlorophyll, and carotenoid content (Patelou *et al.* 2020). The cited literature emphasizes that the response to light is species-specific and is also dependent on cultivation conditions.

2. 10. 1. Proteins

Depending on the cultivation conditions, studies have reported both increases and decrease in protein content with an increase in light irradiance (Li-Beisson *et al.* 2019; Nawrocki *et al.* 2019a). Metsoviti *et al.* (2019), studied the effects of white and red LED irradiance at 520, 390, 260, and 130 µmol photons·m^{-2}·s^{-1} on the growth rate and metabolite composition of *C. vulgaris* (12:12 hr light/dark periods). The researchers found that during the exponential growth phase, an increase from 130 to 260, to 390, and 520 µmol photons·m^{-2}·s^{-1} led to consequent increases in the growth rate and protein concentration in *C. vulgaris*. The increased protein productivities were attributed to increases in biomass productivity.

Table 2.3: Primary metabolite content in microalgae and cyanobacteria (dry *wt.* %).

Microalgae	Protein (%)	Carbohydrate (%)	Lipid (%)	References
C. reinhardtii	45 – 48	17 – 57	9 – 21	(Park *et al.* 2015; Chia *et al.* 2018)
C. vulgaris	51 – 58	9 – 51	14 – 26	(Metsoviti *et al.* 2019; Nzayisenga *et al.* 2020; Sánchez-Saavedra *et al.* 2020)
C. sorokiniana	35 – 53	30 – 40	10 – 30	(Gifuni *et al.* 2018)
Dunaliella salina	22 – 57	21 – 32	6 – 70	(Chia *et al.* 2018; Vuppaladadiyam *et al.* 2018)
Scenedesmus obliquus	50 – 56	10 – 47	12 – 14	(Chia *et al.* 2018; Vuppaladadiyam *et al.* 2018)
Nannochloropsis sp.	20 – 25	18 – 30	15 – 60	(Vadiveloo *et al.* 2015; Chia *et al.* 2018)
Arthrospira maxima (*Spirulina*)	60 – 71	13 – 16	7 – 10	(Markou and Nerantzis 2013; Vadiveloo *et al.* 2015)

Note: the metabolite ranges for the species have been combined from the referenced studies.

The microalgal protein content is regulated by nitrogen concentrations in the culture medium. During exponential growth, nitrogen is required for biomass production and protein biosynthesis, while in the stationary phase, nitrogen is depleted resulting in lipid accumulation

(Metsoviti *et al.* 2019). As proteins are important structural and metabolic components of microalgal cells; their production is also dependent on light intensity. Higher light intensities result in increased lipid as an energy storage product, however, this also occurs at higher nitrogen levels depending on the actual intensity used. He *et al.* (2015), showed that under high light irradiances protein content decreased with increased lipid production in *Chlorella* sp. It should be mentioned that the alga was subjected to continuous illumination at varying light irradiances (40, 200, and 400 µmol photons·m^{-2}·s^{-1}), (He *et al.* 2015). Nitrogen is used to provide provisions for carbon skeletons for amino acid and protein synthesis. Under increasing light irradiances, the cellular protein is degraded to provide carbon and energy for lipid biosynthesis (da Fontoura Prates *et al.* 2020; Nzayisenga *et al.* 2020).

Also of equal importance is the effects of the spectral composition of light on protein production concerning the algal species and cultivation conditions (da Fontoura Prates *et al.* 2020). Kendirlioglu and Cetin (2017), showed that *C. vulgaris* produced the highest protein content when irradiated with red, white, and blue light. The study by Asuthkar *et al.* (2016) found that the protein content of *Chlorella pyrenoidosa* was increased under blue, red, and white light, respectively. The results of these studies demonstrate the diverse response by different species to increases in light intensity. Proteins produced by microalgae vary significantly (6 to 70% of their dry cell weight [DCW]) depending on the species and environmental factors, although the majority of them have a total soluble protein level that reaches around 50% (Table 2.3).

2. 10. 2. Carbohydrates

Carbohydrates are compounds that are mostly derived from photosynthesis. Certain microalgae species can accumulate up to 50% of their dry weight as carbohydrates (Table 2.3). In carbohydrate accumulating microalgae, light intensity and carbon concentration determine the PE of the strain. *Chlorella* sp. can accumulate between 18 – 57%, while *Nannochloropsis* sp. produces up to 30% in carbohydrate content (Chia *et al.* 2018). Green microalgae have rigid cell walls, consisting of structural polysaccharides like cellulose and/or other biopolymers (Li-Beisson *et al.* 2019; Nawrocki *et al.* 2019a). Apart from structural polysaccharides, algae also accumulate considerable amounts of energy storage and cell communication carbohydrates, *e.g.*, starch and exopolysaccharides in *Chlamydomonas.* Carbohydrate metabolism in microalgae varies widely depending on their structural and biological activities and species (Sathasivam *et al.* 2019; Levasseur *et al.* 2020). These metabolites serve a variety of functions in algal cells.

Carbohydrates represent a form of energy and carbon storage products. They are responsible for permitting imbalances between the rate of reduced carbon production and consumption in photosynthesis and growth, respectively (Seo *et al.* 2015; Nwoba *et al.* 2019; Sathasivam *et al.* 2019). Furthermore, carbohydrates function as free radical scavengers and are important in containing turgor pressure in microalgal cell walls (structural polysaccharides) thereby permitting multicellularity. Research has shown that the conversion of carbohydrates to lipids occurs when cells are exposed to excess irradiations at varying wavelengths (Seo *et al.* 2015; Nwoba *et al.* 2019; Sathasivam *et al.* 2019).

The composition of energy reserve compounds is not the same in all microalgae and can be manipulated through growth conditions. Generally, high light intensities (> 150 µmol photons·m^{-2}·s^{-1}) increase the carbohydrate content. In *Porphyridium* species, there was a 3-fold increase in carbohydrate content, while the cyanobacterium *Arthrospira maxima* increased its carbohydrate content to 34% from about 7 – 10% under increased irradiance (Markou and Nerantzis 2013). Depending on growth conditions, *C. vulgaris* produces between 9 and 41% carbohydrate (*w*/*w*) of its DCW while *Scenedesmus obliquus* accumulates between 10 – 47% (Table 2.3), (Sathasivam *et al.* 2019; Levasseur *et al.* 2020). These organisms have been used for biofuels production due to their high-density carbohydrate and lipid content (≥ 50% dry-weight) (Nwoba *et al.* 2019; Sathasivam *et al.* 2019; Levasseur *et al.* 2020). Highly fluctuating carbohydrate levels have been previously reported (Chia *et al.* 2015), yet under natural irradiation, light is not regarded as the major factor influencing carbohydrate synthesis due to the strong variation of the weather conditions. Accordingly, carbohydrate content and biomass levels will be higher on sunny days when compared to cloudy days. This is because increased light irradiance increases the rate of photosynthesis (Markou and Nerantzis 2013).

2. 10. 3. Lipids

Lipids are mainly responsible for maintaining cellular structure (polar lipids), and function as energy storage molecules within the microalgae cell (non-polar lipids), (Li-Beisson *et al.* 2019; Sathasivam *et al.* 2019). Polar lipids such as glycerophospholipids aid in the separation of the different intracellular organelles and are also responsible for providing a selectively permeable membrane that shields the cell from the outside (Li-Beisson *et al.* 2019; Sathasivam *et al.* 2019). As previously mentioned, both low and saturating lighting conditions are unfavourable for microalgal growth and may induce undesirable responses in cells (Alishah

Aratboni *et al.* 2019; Li-Beisson *et al.* 2019). When the light irradiance is low, *e.g.*, below the compensation point, microalgal growth is compromised leading to reduced biomass concentrations which negatively impacts lipid accumulation. As the light irradiance increases, microalgal growth is increased and maximum PE occurs. The positive effect of light increases lipid accumulation functions up to a point (Li-Beisson *et al.* 2019). Above the compensation point (saturation point), causes photo-inhibition, microalgal PSs are damaged, and photo-oxidation reduces lipid accumulation (Alishah Aratboni *et al.* 2019).

Nzayisenga *et al.* (2020), studied the effects of increasing light intensities (50, 150, and 300 µmol photons·m^{-2}·s^{-1}) on the growth and lipid production in *C. vulgaris*, *S. obliquus*, *Desmodesmus* sp., and *Ettlia pseudoalveolaris*, (Table 2.3). When grown at 300 µmol photons·m^{-2}·s^{-1}, *Desmodesmus* sp. displayed the highest increase in fatty acids content (6.2%), while *S. obliquus* showed a 5.8% increase. The lipid contents of the algae were positively correlated to the light irradiance. The researchers concluded that under high irradiance, algae convert excess photo-assimilates into lipids thereby counteracting photo-oxidative processes. Additionally, Krzeminska *et al.* (2015) found that the total lipid content in *C. protothecoides* was increased by 24.8, 16.8, and 37.5% when grown under 35, 130, and 420 µmol photons·m^{-2}·s^{-1}, respectively. Contrastingly, *E. pseudoalveolaris* and *C. vulgaris* exhibited decreased lipid content when grown under a light irradiance of 300 µmol photons·m^{-2}·s^{-1} than when compared to 50 and 150 µmol photons·m^{-2}·s^{-1}, despite their increased biomass production. Hence, there exist differences in species' mechanisms in response to light intensity, which could result in either higher or lower lipid contents.

2. 10. 4. Secondary metabolites

Microalgae also produce a wide range of secondary metabolites including pigments, phytosterols, biopolymers, hydrocarbons, and waxes (Nwoba *et al.* 2019; Sathasivam *et al.* 2019; Levasseur *et al.* 2020). These compounds exhibit beneficial health properties such as vitamin precursors, antioxidant properties, anti-inflammatory agents, and immune activators (Figure 2.1), (Nwoba *et al.* 2019; Sathasivam *et al.* 2019). Consequently, they can be used as food or feed supplements, as a source of bioactive molecules, or can be applied to pharmaceutical or cosmetic applications as natural colours. The chlorophyll content in microalgal cells varies from 0.5 to 4% of their dry weight, according to environmental conditions and the strain (da Silva Ferreira and Sant'Anna 2016). On average, carotenoids represent between 0.1 – 0.2% of the DCW.

Another avenue of interest in microalgal biotechnology is the production and exploitation of phytosterols, (Figure 2.1). Sterols are essential components of microalgae. They are involved in regulating various membrane-associated metabolic processes such as signal transduction and also control membrane fluidity and permeability (Goff *et al.* 2019; Hannan *et al.* 2020; Randhir *et al.* 2020). Light has been identified as a major stress factor known to affect sterol composition and content in various microalgal species. Increasing light intensities stimulate photosynthesis and the production of sterols (Wang *et al.* 2014; Goff *et al.* 2019). These compounds provide inherent benefits to human beings and have been used as animal nutrition, cosmetic components, and food colorants (Figure 2.1). They promote anti-inflammatory activity, cholesterol reduction, and have anti-cancer properties. Phytosterols of commercial importance include crinosterol, sitosterol, stigmasterol, isofucosterol, and dinosterol, which

have been applied to the pharmaceutical sectors (Goff *et al.* 2019; Hannan *et al.* 2020; Randhir *et al.* 2020).

2. 11. Strategies for enhancing spectral availability in microalgae

Sunlight is generally used when cultivating microalgae as it is free and abundant, however, its penetration is restricted to a limited area below the surface of the cultivation system (Teo *et al.* 2014; Baer *et al.* 2016). This is mostly due to the density of the algal culture. For this reason, outdoor cultivation usually requires large surface areas with shallow depths to ensure sufficient biomass productivity. Furthermore, intensities of natural light in outdoor cultivation systems vary with day/night cycles, shifting weather conditions, and seasonal changes (Darko *et al.* 2014; Hashimoto *et al.* 2015; Baer *et al.* 2016). Most importantly, sunlight is more intense than artificial light with the various wavelengths being distributed equally. The way in which sunlight is delivered to algae is of paramount importance. This determines the economic viability of large-scale mass microalgal cultivation. Therefore, tailor-made light delivery techniques will be beneficial especially when biomass and/or metabolite production is desired. Approaches such as optically filtering light to supply specific wavelengths to algal cultures have been proposed (Table 2.4) (Patelou *et al.* 2020), yet have not been successfully implemented at a large scale due to the insufficient quantities of light delivered (Duarte and Costa 2018).

Table 2.4: Approaches toward improving the light availability in microalgae.

Alga/(e)	Products	Process	Wavelengths	References
C. fusca LEB 111 *S. nidulans* LEB 115	Biomass, pigments, lipids	LEDs	420 – 470 nm	(Duarte and Costa 2018)
A. obliquus	Biomass, pigments, lipids	FL-LEDs	460 – 700 nm	(Choi *et al.* 2015)
N. gaditana	Biomass, metabolites	Colour filters	350 – 900 nm	(Patelou *et al.* 2020)
C. vulgaris (UTEX #236)	Biomass, carbohydrate	Optical membrane filters	100 nm – 1 mm (solar)	(Michael *et al.* 2015)
Chlorella sp.	Biomass, chlorophyll *a*, and total carotene	Wavelength shifter sheets	300 – 800 nm (full spectrum)	(Delavari Amrei *et al.* 2014)
C. vulgaris	Biomass	Nanoparticle light filtration	642, 662 and 710 nm	(Eroglu *et al.* 2013)
Scenedesmus dimorphus, *C. reinhardtii*, *C. vulgaris*	Biomass	Phosphorescent paints	425 – 600 nm	(Danaee *et al.* 2018)
Chlorella sp.	Biomass, lipid	Fluorescent paints	300 – 800 nm (full spectrum)	(Seo *et al.* 2014)
N. gaditana	Biomass, lipid	Organic dyes	400 – 700 nm	(Sung *et al.* 2018)
C. vulgaris	Biomass, lipid	Organic dyes	300 – 800 nm (full spectrum)	(Seo *et al.* 2015)
Chlorella sp.	Biomass, lipid	Organic dyes	600 – 700 nm	(Khoobkar and Delavari Amrei 2020)

Most often, artificial lighting systems are implemented for the production of high-value-added metabolites (Duarte and Costa 2018). Fluorescent lamps and LEDs have been used due to their high-intensity and narrow emission spectra (Darko *et al.* 2014; Nwoba *et al.* 2019). Other common types of artificial light sources used for microalgal cultivations include halogen lamps, high-intensity discharge lamps, and incandescent bulbs. The appropriateness of a particular light source will depend largely on the light quality (which include the PAR spectrum and distribution), power consumption, cost, and conversion efficiency. Furthermore, a combination of specific spectral regions will likely be needed to optimise production outcomes (Choi *et al.* 2015).

2. 11. 1. Artificial illuminators

Energy absorption by microalgae is dependent on their chemical make-up. To increase production capacities, cultivation systems using artificial lighting are now being considered (Teo *et al.* 2014; Baer *et al.* 2016; Wobbe *et al.* 2016). Fluorescent lamps can provide and sustain the photosynthetic photon fluency required for high productivity. Cool-white fluorescent lamps (*i.e.*, enhanced blue and red spectra) are common, however, the emitted spectrum and intensity cannot be sustained over prolonged periods (> 6 months). High-intensity discharge lamps such as metal halide lamps and high-pressure sodium have high fluency (max. 200 lumens per watt) and high PAR efficiencies (max. 40%). However some drawbacks include: (*i*) elevated arc to fire energy requirements; (*ii*) high operational temperatures that prevent their placement close to canopies; (*iii*) uneven spectral distributions *i.e.* high proportions of green-yellow regions; (*iv*) significant UV radiations; and (*v*) altered red to far-red ratios which shift according to the input power, strongly limiting their use and novelty (Darko *et al.* 2014; Nwoba *et al.* 2019).

To ensure a sufficient amount of PAR to reach the cells, artificial incident light needs to be delivered homogeneously over the irradiated surface of culture vessels (Teo *et al.* 2014; Baer *et al.* 2016). As culture densities increase, light becomes the limiting factor to obtain a cost-effective operation. Although dense suspensions are preferred to maximise production, too concentrated cultures may increase light reduction to the culture. The light availability is in excess at a short path length, and it is further decreased with an increase in the light path length. For this reason, higher incident irradiation is required to allow more illumination at the section with a longer light path length. A possible downside is that this may result in photo-inhibition and photo-oxidation for the algal cells at the short light path length. Artificial lamps are commonly used in algal cultivation because they have high light intensities, have emission peaks that overlap the cell absorption spectra, and provide the optimal quantum yield and excitation balance between PSII and I. In addition, the incident light intensity should integrate with the specific light path length (Wang *et al.* 2014; Hashimoto *et al.* 2015; Baer *et al.* 2016; Wobbe *et al.* 2016).

Microalgal light utilisation efficiencies and biomass productivities are said to be greater under artificial light when compared to sunlight. This is because artificial illumination provides a constant source of lighting which permits the cultivation of microalgae in any location. Furthermore, these light sources can be tuned to produce a spectrum with either one or more wavelengths with varying spectral intensities. Incandescent light bulbs mostly produce yellow, orange, or red light. Standard “cool white” fluorescent bulbs emit mostly yellow-green light (Wang *et al.* 2014; Hashimoto *et al.* 2015; Baer *et al.* 2016; Wobbe *et al.* 2016). When choosing a light source, a balance between economics and the requirement of the final products needs to be considered. Duarte and Costa (2018), evaluated blue LEDs as an alternative energy source for the cultivation of *Chlorella fusca* LEB 111 and *Synechococcus nidulans* LEB 115 (Table

2.4). Cultures were grown under constant illumination at varying intensities (50, 100, and 150 μmol photons·m^{-2}·s^{-1}). Growth was increased by 80% in *S. nidulans* LEB 115 using blue LEDs which was approximately 3.3-fold higher than *C. fusca* LEB 111. The difference in growth between the strains was related to the difference in pigment composition. *Synechococcus nidulans* LEB 115 possessed phycobiliproteins which increased the absorption band (420 – 470 nm). The blue light was found to induce > 19% (*w/w*) lipid accumulation in *C. fusca* LEB 111 (Duarte and Costa 2018). Despite the potential of this strategy, its large-scale application is challenging bearing in mind the high cost of artificial illumination infrastructure and operation. Hence this technology is not recommended (Baer *et al.* 2016; Wobbe *et al.* 2016).

2. 11. 2. Spectral selection and filtration

2. 11. 2. 1. Wave guides

It has been demonstrated that wavelength filtration represents an economically feasible and practical method of supplying specific light spectra to large-scale microalgal cultivations (Michael *et al.* 2015; Nwoba *et al.* 2019). Patelou *et al.* (2020), used an integrated omics approach to detect changes in the growth and metabolism of *N. gaditana* during environmental light alteration (Table 2.4). The authors used several colour filters to obtain different wavelengths (no filter, red, blue, and green). The transmittance wavelength was measured between 350 – 900 nm. The red filtered light induced the overall production of both transcripts and metabolites involved in amino acid metabolism in *N. gaditana*. Blue filtered light triggered a decrease in carbohydrate concentration with an increase in polyunsaturated fatty acids content. The lowest induced responses in metabolite and gene transcript levels were observed under green filtered light. The authors concluded that light filtering of solar irradiance

represented a cost-effective method that can be applied to large-scale PBR microalgal systems (Patelou *et al.* 2020).

Michael *et al.* (2015), used a unique filter made from a nanoscale coating that selectively transmitted specific wavelengths from natural sunlight (Table 2.4). The researchers applied the coating to plastic sheeting. Plastic was used as opposed to glass due to its thickness, flexibility, and versatility. The material was found to effectively transmit visible spectra, thus, allowing specific light bands to be more prominent than others. The filters reflected UV and IR rays which would otherwise cause photo-oxidation and photo-inhibition in the microalgal cells. Two variations of the light filters were used in their work. The membrane consisted of optically clear Type D Mylar substrates. The substrates were subsequently coated with layers of nano-scale width metal oxides to create the filters. Both the red and blue filters allowed the transmission of light in the 620 – 710 nm and 450 – 495 nm wavelength spectrum, respectively. Both wavelength filters, however, allowed variable amounts of the remaining visible spectrum to transmit.

The researchers found that the light filters were unable to improve the growth of *C. vulgaris* when cultured in glass flasks. This was attributed to the additional reflection of light by the glass wall culture flasks. They did, however, improve the biomass yields in plastic PBR systems. It should be noted that plastic PBR systems filter out UV light without the aid of a filtering agent (Michael *et al.* 2015). Biomass productivity increased by 34% in flat panel reactors and by 100% in rotating algal biofilm systems. Additionally, the red-light filter increased carbohydrate production by 22 and 13% when compared to the control and blue filter, respectively. The authors concluded that the light filters provided an efficient method for improving microalgal growth. This was due to their specific selectivity of desirable

wavelengths from sunlight. The light filters enhanced biomass yield in different PBRs, however, high operational and construction costs associated with specific reactor design have prevented the widespread installation of these systems. The researchers concluded that further studies are needed to estimate the manufacturing costs for this technology at a large scale (Michael *et al.* 2015).

Delavari Amrei *et al.* (2014) investigated the spectral shifting of UV-*a* radiation by utilising fluorescent material as a tool for improving the growth rate of *Chlorella* sp. Solutions of fluorescent dye Uvitex OB were mixed with thermoplastic acrylic resin and air sprayed onto polycarbonate sheets which contained UV absorber additives. These were then integrated into the walls of PBRs. The research found that these wavelength shifting sheets increased biomass productivity, chlorophyll *a*, and total carotene content by 10, 21, and 28%, respectively, when compared to the uncoated PBRs. This was attributed to the reduction of UV-*a* radiation.

Mohsenpour *et al.* (2012), investigated the influence of light source on the growth of *C. vulgaris* by adapting light wavelength using luminescent sheets. The researchers immobilised the Lumogen F dyes (violet, green, yellow, orange, and red) series on thermoplastic polymethyl methacrylate. They found that the light emission by violet light (400 – 450 nm) produced the most efficient wavelength bands essential for the growth of microalgae cells. The highest biomass (43.29×10^6 cells mL^{-1}) was achieved using violet dyes followed by green, orange, and red dyes. It was concluded that by modifying illumination strategies microalgal cultivation was enhanced under natural light (Mohsenpour *et al.* 2012). The studies by Mohsenpour *et al.* (2012) and Delavari Amrei *et al.* (2014) differ from the current study in that the dyes used were immobilised onto solid media as compared to the liquid dye solutions. Solid-state dye immobilisations negate the problems associated with toxicity, flammability, compactness,

versatility, ease to operate and maintain, and have high photo-stability properties. However, selected polymers should allow light transmission and lessen light absorbance by the material itself.

2. 11. 2. 2. Plasmonic light scattering

Localised surface plasmon resonances (LSPR) of metal nanoparticles are utilised as wavelength-specific backscattering light filters (Torkamani *et al.* 2010; Eroglu *et al.* 2013; Ahmed *et al.* 2017), (Table 2.4). Inserting silver nanoparticles and gold nanorods around microalgal culture flasks were shown to increase the formation of chlorophyll pigments in *C. vulgaris* cells, thereby, increasing biomass yields (Eroglu *et al.* 2013). This occurred due to the backscattering in the spectral regions that favour microalgal growth. Localised surface plasmon resonances focus on the interaction between electrical light field components and conduction band electrons of the metal nanoparticles. This leads to an oscillation of the surface electrons at a resonant frequency. This frequency generates a dipole oscillation that may be used as an estimation of the spectrum produced by separated nanoparticles and, therefore, describes scattering as a result of the LSPR. This generates a moderately thin scattering peak that may be adjusted to specific wavelength regions by the geometry and composition of metal nanoparticles (Eroglu *et al.* 2013; Ahmed *et al.* 2017). Torkamani *et al.* (2010), found that silver nanoparticles were able to enhance the overall growth of *C. reinhardtii* and *Cyanothece* 51142 by 30%. It was found that wavelength-specific backscattering in the blue region of the spectrum was achievable by using silver nanoparticles with cultures exposed to the full spectrum of light. As much as spectral filtration represents an effective strategy for microalgal cultivation, the portions of the spectrum that pass through the cultures remain unused. This is wasteful, and thus, light conversion seems to be a more practical approach.

2. 11. 3. Spectral conversion

2. 11. 3. 1. Fluorescent paints

Commercial fluorescent paints have been evaluated for their ability to convert UV to visible light thereby controlling the solar intensity. These paints are fairly inexpensive and readily available. Aqueous paint solutions have high quantum yields (QYs) and low toxicity (Seo *et al.* 2014). Danaee *et al.* (2018), studied the effects of luminescent paint afterglow illumination on the growth of *S. dimorphus*, *C. reinhardtii*, and *C. vulgaris* (Table 2.4). The phosphorescent pigments in the paint absorbed the fraction of light that was not used by the algae, resulting in an afterglow that acted as a complementary light source. The algae were grown in glass bowls that were partially painted with the blue and green phosphorescent paints. The authors found no significant change in growth under the green treatment, however, the blue afterglow increased growth. The biomass recorded under the blue paint treatment was 42, 23, and 17% higher than the control for *Chlamydomonas*, *Scenedesmus*, and *Chlorella*, respectively. Additionally, blue phosphorescence led to ~ 40% increase in chlorophyll *a* and *b* content. The treatments imposed no additional energy costs for illumination and promote the application of phosphorescent material as supplementary light sources in microalgal growth and pigment production (Danaee *et al.* 2018).

Seo *et al.* (2014), also found that fluorescent paints could not only block excess solar energy but also convert unusable UV wavelengths to usable visible ones. The enhancement of growth and lipid content was successfully achieved by varying different colour paints. Maximum growth of 1.7 gL^{-1} was obtained with red paint, whereas the best lipid content (30%) was achieved with blue paint. Some of the presumed challenges associated with using paints would include (*i*) paint insolubility (insoluble materials have to be mixed with

binders/compounds that attach them to a substrate); (*ii*) increases in costs associated with paint dilutions due to high viscosity; and (*iii*) transparency (host matrices should have good optical transparency in the absorption and emission region of the dissolvent paint) (Al-Aqmar *et al.* 2015). Although there is not an abundance of literature in this field, the concept certainly warrants further investigation.

2. 11. 3. 2. Fluorescent dyes

Organic fluorescent dyes can be utilised as incident light converters as they can concentrate, direct, and scatter light. Using these dyes to concentrate incident light for microalgal production could greatly reduce the need for artificial lighting systems (Seo *et al.* 2015; Sung *et al.* 2018). As incident radiation passes through an organic dye, it is absorbed by the luminescent species. These incoming photons excite dye molecules from the ground electronic state, S0, to the vibrational levels of the first excited electronic state, S1. This is a higher state, one of being ready to emit radiation (the singlet state) (Maillard *et al.* 2020). It then decays non-radiatively by internal conversion to the lowest vibrational level of S1. Photons are fluorescently emitted because of molecule decay from the excited to the ground state, *i.e.*, to one of the vibrational levels in S0. Within this state, dye molecules emit light *via* fluorescence. Transitions between the different vibrational states of the dye molecule give rise to peaks in the absorption and emission spectra (Al-Aqmar *et al.* 2015; Ooms *et al.* 2016; Langhals 2020). The emitted fluorescence is wavelength-specific depending on the dye (Zehentbauer *et al.* 2014; Abu-Ghosh *et al.* 2015; Langhals 2020). As microalgae absorb in specific wavelengths, fluorescent dyes could be used to enhance microalgal biomass and specific intracellular metabolites, as demonstrated by (Sung *et al.* 2018; Khoobkar and Delavari Amrei 2020).

Organic dyes are now being utilised in numerous fluorescent applications including dye lasers, tracers for laser-induced fluorescence, deoxyribonucleic acid (DNA) or protein labelling *etc.*, This is due to their excellent fluorescence and other photo-physical properties (Zhang *et al.* 2014; Kang *et al.* 2019). A major advantage of these dyes is their broad spectral emission characteristics that allow wavelength tuning (Abou-Kana 2012; Zehentbauer *et al.* 2014). This phenomenon could have a significant impact on future microalgal applications (Zehentbauer *et al.* 2014; Cyprych *et al.* 2015). There are many well-known functional dyes, such as porphyrin, coumarin, rylene, cyanine, boron-dipyrrin (Bodipy), *etc*. The basic fluorescence properties of some well-known dyes can be seen in Table 2.5. Lumogen dyes excite between 420 – 550 nm and have a broad emission between 350 – 700 nm (Mohsenpour *et al.* 2012) while DPA dyes show narrower emission spectra between 400 – 500 nm (Sung *et al.* 2018). The fluorescence integrity and wavelength of organic dyes is dependent on the dye concentrations. Zhang *et al.* (2014), measured the fluorescence lifespan, QY, and emission maxima of twenty fluorescein-based dyes dissolved in ethanol and phosphate-buffered saline under constant conditions. Based on their results, it was established that fluorescence properties are strongly dependent on the molecular structures of the dye (Abou-Kana 2012; Zhang *et al.* 2014).

Table 2.5: Excitation and emission maxima of several fluorescent dyes.

Dye/ Trade names	Excitation (nm)	Emission (nm)	References
Alexa fluorophore 350	346	442	(Thermo.Fisher.Scientific 2015)
Alexa fluorophore 405	401	421	
Alexa fluorophore 568	578	603	
Alexa fluorophore 594	590	617	
Alexa fluorophore 647	650	665	
Alexa fluorophore 680	679	702	
Coumarin	387	470	
Cyanine 3B	558	572 – 620	
Cyanine 3.5	581	594 – 640	
Cyanine 5	649	666	
Rhodamine	500 – 600	600 – 700	(Abou-Kana 2012; Zehentbauer *et al.* 2014)
Diphenylanthracene (DPA)	300 – 400	400 – 500	
Lumogen dyes	200 – 300	350 – 700	(Mohsenpour *et al.* 2012)
DPA	300 – 400	400 – 500	(Sung *et al.* 2018)
Rhodamine 110	420 – 550	500 – 620	
Rhodamine 101 (R101)	460 – 620	550 – 700	
DPA	300 – 400	400 – 500	(Seo *et al.* 2015)
R101	500 – 600	550 – 700	
Rhodamine 6G	497 and 534	615	(Khoobkar and Delavari Amrei 2020)

For the successful application of fluorescent dyes in microalgal technology, adequate knowledge of their effects is a prerequisite. The absorption and emission spectra of the dyes and the influence of the solvent and solvent polarity. The increase in polarity leads to a hypsochromic shift both in absorption and fluorescence spectra, and quantum yield decreasing. The variation of the substituents may lead to Stokes shift change and fluorescence maxima shift to longer wavelengths (Hassan *et al.* 2014). Furthermore, changing of the dissolution solvent may lead to fluorescence enhancement/quenching. This is a valuable characteristic of the dyes as their emissions can be tuned to mirror microalgal photosynthetic regions. Organic solvents such as ethanol and methanol have been commonly used for dye dissolution. This is due to the excellent dye dispersion properties which increase fluorescent efficiency (Abou-Kana 2012; Zehentbauer *et al.* 2014; Zhang *et al.* 2014). However, organic solvents cannot be used with longer wavelength absorbing dyes (near-IR and IR). This is due to the presence of hydroxyl group overtones in this spectral range that causes vibrational overtones that interfere with the dye absorption process. Inorganic solvents such as water are hardly used as dissolving solvents because certain dyes such as Lumogen Yellow (LY) and Lumogen Red (LR) are highly hydrophobic molecules due to their chemical structure. A possible solution to overcoming the problems associated with this would be to incorporate the dye molecule onto a solid medium. However, this is labour intensive, economically challenging, and time-consuming (Kang *et al.* 2019).

When choosing an appropriate solvent for organic dyes the following criteria should be met: (*i*) the solvent must be transparent at both the excitation and emission wavelengths of the dye; (*ii*) the dye should be soluble in the solvent under consideration; (*iii*) the solvent must be photochemically stable when exposed to the exciting radiation, (Brackmann 2000; Zehentbauer *et al.* 2014; Maillard *et al.* 2020). In addition, dye lifespans should be determined in advance

and, must match lifespans similar to the algal cultures being used. The light-induced degradation of fluorescent dyes (photo-bleaching) is known to limit the lifespan of dyes by reducing their fluorescence longevity and visual appearance over time. Hence, efficient solvents that limit the rates of photo-bleaching in dyes need to be utilised (Abou-Kana 2012; Ali *et al.* 2012; Zehentbauer *et al.* 2014; Al-Aqmar *et al.* 2015). Suppressing this phenomenon is crucial when cultivating microalgae under wavelength manipulation (Guha and Basu 2014).

Due to their valuable traits, organic dyes have been exploited in chemistry, but only to a limited extent in microalgal biotechnology (Seo *et al.* 2015; Sung *et al.* 2018). Khoobkar and Delavari Amrei (2020), employed Rhodamine 6G (R6G) to increase the growth, lipid, and chlorophyll content in *Chlorella* sp. grown in a double-layer flat panel PBR (Table 2.4). The researchers dissolved the dye in water because ethanol or methanol corroded the Plexiglas PBR. When compared to the control, biomass productivity rate and the maximum specific growth rate were increased by 60 and 23%, respectively, when the light passed through R6G before reaching the algae. It was concluded that R6G was an effective spectral converter for the conversion of green light to longer wavelengths. Sung *et al.* (2018), used fluorescent dyes to improve the sunlight utilisation efficiency in *N. gaditana* (Table 2.4). The researchers used Diphenylanthracene (DPA), Rhodamine 110 (R110), and Rhodamine 101 (R101) dissolved in ethanol (10^{-5} M). It was shown that DPA increased the proportion of blue light whilst decreasing the UV range (300 – 400 nm). Rhodamine 110 absorbed and emitted light between 420 – 550 nm and 500 – 620 nm, respectively while R101 was used to modify green light and substantially increase the proportion of red irradiance. The authors found that when DPA and R101 were used to supplement blue and red spectra, the biomass productivity of *N. gaditana* was increased by 35.1 and 40.3%, respectively. It was further stated that all cultures showed high QY values implying that most of the irradiations were being used. This stimulation of

photosynthetic activity was found to correlate with rapid growth under DPA and R101 mediated irradiations. Consequently, after day 10, lipid productivity increased by 26.9 and 39.4% under DPA and R101, respectively.

Seo *et al.* (2015), attempted to utilise organic dyes to enhance microalgal growth (Table 2.4). The researchers also tested DPA and R101 dissolved in ethanol, but grew the alga C. *vulgaris*, under a light intensity of 50 Wm^2 (~ 105 μmol photons$\cdot m^{-2}\cdot s^{-1}$). They found that maximum cell growth (1.5 gL^{-1}) was obtained with R101, and the highest lipid concentration (30%) was reached with DPA. They concluded that increased biomass and lipid content could be achieved simultaneously by combining the dyes. This study displayed the advantage of utilising certain organic dyes to convert unusable radiation to usable wavelengths, thus, increasing the productivity of microalgal biomass and lipids (Seo *et al.* 2015). The researchers measured dye QY and found that DPA and R101 showed 90 and 100% fluorescence efficiencies, respectively. This showed that the dye solutions were capable of converting and emitting almost 100% of the absorbed light. The QY of organic dyes is one of the key photo-physical properties when selecting efficient dye concentrators for microalgal cultivation (Abou-Kana 2012; Ali *et al.* 2012; Hassan *et al.* 2014). However high QYs can be associated with excess light emission. High light irradiance will inevitably result in photo-inhibition of microalgal growth (Kim *et al.* 2014). For optimal light utilisation and high microalgal metabolite productivities, the emitted light needs to be complementary to the microalgal absorption spectra. Over a broad range, a good correlation is achieved between microalgal biomass and PE productivity. The research cited demonstrated that both light quantity and quality has a major influence on biomass and metabolite production. By designing and constructing PBRs using such dyes and materials, photosynthetic productivity of microalgae

can be enhanced and available resources, including sunlight and land, judiciously utilised (Nwoba *et al.* 2019).

2. 11. 4. Challenges associated with dye spectral conversion

Fluorescent dyes such as DPA, Lumogen, and Rhodamine (Table 2.5), have been developed and applied to several industries, *e.g*. the medical industry as fluorescent probes (Seo *et al.* 2015; Raeisossadati *et al.* 2019). Recently, the dyes have been applied to microalgal systems using specialised PBRs (Seo *et al.* 2015; Khoobkar and Delavari Amrei 2020). Apart from the benefits described above (section 2.5.2), these PBR systems increase microalgal costs due to the high energy use (mixing, cooling, and embodied energy), and capital cost. Systems that facilitate spectral modification (selection, filtration, or conversion) often add cost and complexity to standard cultivation systems such as open raceway ponds, for example, however, spectral conversion allows control of the proportion of solar energy that is converted into chemical energy as biomass. At the same time, the wavelength bands delivered by each dye can be optimised to maximise the total conversion efficiency of the algae (Stanley *et al.* 2016).

Achieving high biomass density is critical for process economics. One way to reduce capital and operating costs associated with spectral conversion would be to construct specialised PBRs with the dye molecules immobilised on inexpensive polymer-based spectrally selective films (Dogaris *et al.* 2015). Consideration should be given to polymers that transmit visible light, allowing efficient dye excitation. Furthermore, dyes absorbing and converting near-IR or IR to usable wavelengths can effectively suppress heat generation and provide temperature control, reducing the need for extraneous cooling of reactors (Nwoba *et*

al. 2019). Alternatively, the successful commercial-scale manufacture of cost-effective energy harvesting spectrally selective glass provides a feasible way to construct high-efficiency PBRs, such as double-jacketed cylindrical PBRs. These reactors hold the organic dye/solvent solution in the outer jacket and the algae in the inner jacket. Light is absorbed by the dyes and emitted to the algae. A PBR made from the energy-harvesting spectrally-selective glass panels would selectively allow > 70% of the visible spectrum of sunlight to the microalgae culture, while simultaneously absorbing and converting > 90% of the UV and IR radiation (Nwoba *et al.* 2019). The glass panels have an expected lifetime exceeding 30 years. This approach would make full use of sunlight, decreasing the lighting cost in algal production systems. Consequently, the motivation behind the implementation of dye spectral conversion technologies will be to reduce the cost of microalgal biomass production and hence help advance the current status of the microalgal bio-products industry. The benefits of such systems in terms of microalgal/metabolite productivity will outweigh the cost of production (Nwoba *et al.* 2019).

Before scale-up, many considerations must be addressed. For instance, the fluorophores mentioned above could be toxic, difficult to store, unstable due to oxidative photo-bleaching, and are expensive. In most cases, the exact toxicity of the fluorescent dyes is not well known, but they should, like all chemicals, be considered dangerous/hazardous until proven otherwise. Accordingly, careful consideration should be given to the chemical and physical properties of the substance/s (Brackmann 2000). In many instances, the dyes may be required as dye solutions (Sung *et al.* 2018). The solvent in which the dyes are dissolved is also considered a hazard as they may be highly toxic, irritants, narcotics, and/or anaesthetics. Also, solvents such as dimethylsulfoxide (DMSO), methanol, dioxane, and benzyl alcohol can carry their solutes through the skin and into the body. When dissolved, upon decomposition some dye solutions

form hazardous compounds while others could be highly reactive. Therefore, when upscaling the technology, these hazards must be addressed, and cautious handling of dye solutions is required (Brackmann 2000).

Due to the novelty of dye spectral conversion, there is limited availability of detailed and up-to-date large-scale microalgal production feasibility data in the literature, and high variability in costs are reported for similar conversion technologies. It should be noted that the dye spectral conversion, although promising for reducing microalgal production costs, is still at a small-scale (proof of concept phase). Ongoing design improvements and scale-up studies will allow a detailed techno-economic analysis of dye spectral conversion for microalgal biomass/metabolite production.

2. 12. Motivation for the study

Several key issues need to be addressed before a commercial algal production process can be developed. These include, but are not limited to, the ability to produce high amounts of high-value metabolites, the ability to efficiently convert raw algal biomass to end products, and ultimately to lower the cost of operations (Michael *et al.* 2015; Pruvost *et al.* 2016). Low biomass and metabolite productivities negatively affect the economics of their commercial production, which is in part, owing to limited light availability ultimately leading to inefficient energy utilisation. Light-specific variables such as spectral quality (wavelength) and quantity (irradiance level) are known to affect microalgal photosynthesis and metabolite production (Nwoba *et al.* 2019).

As much as sunlight can present itself as an economically viable source of light, controlling the beneficial components of the spectrum is currently not achievable. Artificial light can overcome some of the hurdles of sunlight utilisation by controlling light emissions, however, the cost and energy limitations need to be overcome (Nwoba *et al.* 2019). Section 2.11., conceptualised the potential of manipulating light as an enhancement strategy to increase the amount of light available for microalgal cultivations. Customising the incident light spectrum received by algal cultures could ensure the provision of light for the production of microalgal metabolites (Raeisossadati *et al.* 2019).

Many approaches included the applications of insulated glazing, plasmonic waveguides, switchable glass, and wireless light emitters aimed to improve microalgal light-harvesting and transformation. However, these technologies might be costly at the large-scale implementation, especially in integrated microalgae-based biorefineries for high-value metabolite production. The technologies filter or reflect excessive UV radiation while fluorescent materials convert UV to visible light, thus increasing the light intensity by the addition of photons. This could potentially increase the light-to-biomass conversion efficiency, mitigating a major constraint and filling the gap between theoretical and industrial productivity. However, the realisation of this concept requires further innovations in microalgal cultivation techniques, physiology, and metabolic network. From this standpoint, improving the PAR irradiance levels (*i.e.*, photosynthetic PFDs [PPFDs]) using organic dyes has comparatively the largest potential for a successful application (Seo *et al.* 2014). Beneficially, the spectral conversion will allow both qualitative and quantitative light delivery as it will reduce the amount of harmful radiation (such as UV and IR), simultaneously enhancing PAR and further improving light distribution. This will maximise the efficiency of solar energy can be conversion into biomass and bio-products.

Therefore, this research focused primarily on increasing light availability to *Chlamydomonas reinhardtii* by using organic dyes to absorb and concentrate UV light, thereby enhancing the quantum of intensity in specific PAR wavelengths. Accordingly, to assess the viability of this concept, several criteria needed to be evaluated. These included the selection of optimal dye, dissolution solvent, and concentration to increase PAR emission to promote microalgal growth and/or metabolite production. Understanding the dye and solvent interactions and the effect of concentration on emission intensity will allow the ability to tune the photo-physical properties of the dyes to match photosynthetic pigment absorption for future application. In *C. reinhardtii* the optimal growth can be established when an additional carbon source is applied in the presence of light, which simultaneously increases metabolite production (Moejes *et al.* 2017; Nama *et al.* 2018). Consequently, the effects of increased dye-mediated PPFDs was investigated to evaluate its influence on microalgal metabolite production without compromising biomass concentration. By understanding the metabolic responses of *C. reinhardtii* to the dye-mediated irradiations, a strategy can be developed to tailor the dye-mediated emissions toward specific metabolite production. The light utilisation efficiency of the alga was determined using physiological analyses, of which RuBisCo gene expression studies were conducted to verify these findings. To date the novel concept has not been thoroughly investigated (in terms of dye spectra, emission potential, and photo-stability), hence this serves as preliminary research in the area of spectral conversion using organic dyes. The application of UV dye-mediated conversion as a tool in microalgal production systems will allow for the economic/efficient usage of solar energy thereby improving feasibility in the process. This new concept could be potentially applied in next-generation microalgal cultivation systems, which may potentially contribute toward the SDGs.

2. 13. Hypotheses

i. Organic dyes can absorb, convert, and concentrate unusable wavelengths into specific beneficial wavelength bands thereby increasing PAR availability in *C. reinhardtii*.

ii. An increase in dye-mediated PPFDs will stimulate the production of photo-regulatory metabolites such as carotenoids, proteins, lipids and/or carbohydrates.

Chapter 3 : Selection of organic dye, solvent, and dye concentration

Ramanna, L., Rawat, I. and Bux, F. 2018. A novel organic dye-based approach to increase photon flux density for enhanced microalgal pigment production. *Journal of Cleaner Production*, 198: 187 – 194.

3. 1. Introduction

Fluorophores have been used extensively for the preparation of advanced molecular probes that have been applied to biological, biomedical, environmental, and toxicological research (Liu *et al.* 2013; Malfatti *et al.* 2018; Pilla *et al.* 2018). These fluorescent materials have also been used for optoelectronics and new light sources, luminescent solar concentrators, lasers, active optical waveguides, computer displays, LEDs, semiconductor quantum dots, and luminescent biosensors and bioassays (Cyprych *et al.* 2015; Reisfeld and Levchenko 2017; Malfatti *et al.* 2018).

More recently, fluorophores have also been deployed as incident light converters to increase light availability in microalgal cultures (Sung *et al.* 2018). This is due to their: (*i*) UV-VIS absorption and fluorescence spectra; (*ii*) high absorption coefficients which enable the capturing of sufficient quantities of photons; (*iii*) tuneable emission and absorption spectra; (*iv*) high quantum conversion efficiencies; (*v*) low-cost; and (*vi*) extended photo-stabilities (Seo *et al.* 2015; Durairaj *et al.* 2017; Gao *et al.* 2017; Delgado-Sanchez 2019). The ability to tune dye excitation and emission spectra to match chlorophyll absorption minimise background

absorption or scattering while maximising the penetration of the light signal in algal cultivation (Liu *et al.* 2013; Cyprych *et al.* 2015; Pilla *et al.* 2018).

The unique electron distribution of different dye entities affects the photo-physical properties and parameters like the quantum efficiency (yield), fluorescent lifetimes of the excited dye states, pH, polarity, and hydrogen bonding power of the chemical environment. Moreover, solvent-dependent photo-physical characterisation must be performed to establish spectra diverseness to suit the intended application/s (Malfatti *et al.* 2018; Pilla *et al.* 2018). Fundamentally understanding the relationship between the fluorophore and solvent interactions and the effect of fluorophore concentration on emission intensity allows the ability to tune the photo-physical properties of the dyes to match photosynthetic pigment absorption. The realisation of such vital knowledge will be helpful for the rational application of high-performing fluorophores to microalgal technology (Liu *et al.* 2013). Thus, this Chapter aimed to find the optimal dye, solvent, and concentration that could be used to enhance light availability to *C. reinhardtii*.

3. 2. Materials and Methods

3. 2. 1. Dye and solvent selection

The DPA, Diphenyloxazole (DPO), Rhodamine 8G (R8G), R6G, Rhodamine 800 (R800), Fluorescein Isothiocyanate (FITC), LY, LR dyes were evaluated for their ability to absorb and convert unusable wavelengths to PAR (Sigma-Aldrich, Germany). The dyes were dissolved in methanol (≥ 99.9%), ethanol (99%), and acetone (99.5%) at a constant concentration (100 mgL^{-1}) (Zehentbauer *et al.* 2014). Dye solutions were analysed using a Cary

Eclipse Fluorescence Spectrofluorometer equipped with a Xenon flash lamp (15 W, spectral distribution between 190 nm and 2000 nm) (Agilent, SA). Full-spectrum scans were generated to determine the optimal dye solvent. The bandwidth was set at 1 nm but the graphs were plotted every 10 nm to maintain clarity of data sets. The chemicals and solvents that were used in this study were purchased from Sigma Aldrich. The solvents were of high-performance liquid chromatography (HPLC) grade (Sigma Aldrich, Germany). The output power of fluorescent dye is strongly dependent on the purity of the solvent. Poor quality solvents may contain impurities and additives which strongly affect the upper state lifetime of the dye or may catalyse photochemical reactions (Brackmann 2000).

3. 2. 2. Dye concentration optimisation

A series of dye solutions (100, 10, 1, and 0.1 mgL^{-1}), for each of the dyes, stated in Section 3. 2. 1, were prepared gravimetrically in methanol, ethanol, and acetone (Zehentbauer *et al.* 2014). Full-spectrum scans were generated to determine the optimal dye concentration. Average fluorescent intensities were calculated from the mean dye intensities between the respective wavelength emission bands. Areal fluorescent intensities (area under the curve) were calculated using the Trapezoid rule. The curve was divided into a series of trapezoids. The trapezoid areas were calculated (height × width). The sum of the areas of the trapezoids (representing PAR wavelengths) was calculated.

$$y = f(\mathrm{x})$$

Equation 3.1: Trapezoid formula

Where *f*(x) was a continuous function on the interval between [x = 400 nm, x = 500 nm] and [x = 600 nm, x = 700 nm].

3. 2. 3. Statistical analyses

All experimentations were carried out in triplicate. Data were expressed as a mean ± standard deviation of the mean (SD). The results were subjected to a one-way Analysis of Variance (ANOVA) at a 95% confidence limit ($p = 0.05$). Student T-tests were used to locate the differences in significant results. Correlation analyses were used to investigate the relationship between the data sets. All statistical analyses were performed using Microsoft office 365 (excel) for Windows (Microsoft, USA). The conversions from Wm^2 to μmol photons·m^{-2}·s^{-1} was calculated using a calculation factor of 2.1 (Sager and McFarlane 1997). All graphs were drawn using Graph Pad Prism version 5.00 for Windows (Graph Pad Software, San Diego California, USA).

3. 3. Results and Discussion

3. 3. 1. Dye and solvent selection

Successful application of organic dyes in liquid medium requires adequate knowledge of their characteristics. Eight different fluorescent dyes were dissolved in methanol, ethanol, and acetone at a constant concentration (100 mgL^{-1}) and evaluated for their ability to convert the unused wavelengths of light to PAR (Figure 3.1 - Figure 3.3). The solvents used were selected from literature (Zehentbauer *et al.* 2014; Malfatti *et al.* 2018). The DPA dye absorbed light between 280 – 310 nm and emitted between 390 – 430 nm (Figure 3.1 A). The findings showed

the dye emitted light in the PAR region which were also comparable to previous studies. Sung *et al.* (2018), found that DPA in ethanol was capable of absorbing and emitting photons between the 300 – 400 nm and 400 – 500 nm wavelength range, respectively. Seo *et al.* (2015), showed that DPA demonstrated a 90% quantum yield in ethanol, though, the concentration of the dye solutions used was not stated. The current findings showed that the ideal solvent for DPA dissolution was methanol as it maintained higher fluorescent intensities (~ 1000 a.u).

The DPO dye showed absorption and emission ranges between 320 – 350 nm and 340 and 370 nm, respectively (Figure 3.1 B). The DPO dye displayed intense absorption spectra in all solvents (~ 1000 a.u), however, the dye emission signals were low. When dissolved in acetone, the DPO dye showed higher emissions (344 a.u) when compared to methanol and ethanol (246 and 74 a.u, respectively). This further demonstrated that by dissolving dyes in their appropriate solvents, it will be possible to tune and set the emission wavelength to a desired spectral value or PFD. In the current study, the higher DPO emissions in acetone may have resulted from the formation of molecular dye clusters/aggregates (Maillard *et al.* 2020). Aggregation of the fluorophore at high concentrations will result in either the enhancement of fluorescence intensity (aggregation-induced emission), the quenching of fluorescence intensity (aggregation caused quenching), or an unchanged state of fluorescence intensity (Kang *et al.* 2019; Maillard *et al.* 2020; Ramya *et al.* 2020). The behaviour observed indicated the possibility of forming some type of dye clusters/aggregates. The influence of the solvent on the dye is determined by the energy of the intermolecular interactions of the fluorophore and solvent molecules. This occurs frequently while the dyes are in the energised/excited state (Maillard *et al.* 2020). The higher energy of the solute-solvent interaction results in a lower rate of constant transition from the excited to the ground state. This increases the dye lifetime

in the excited state. Thus, the fluorophores energy formation contributes to the solubility variation with different solvents (Lukavenko *et al.* 2009; Maillard *et al.* 2020).

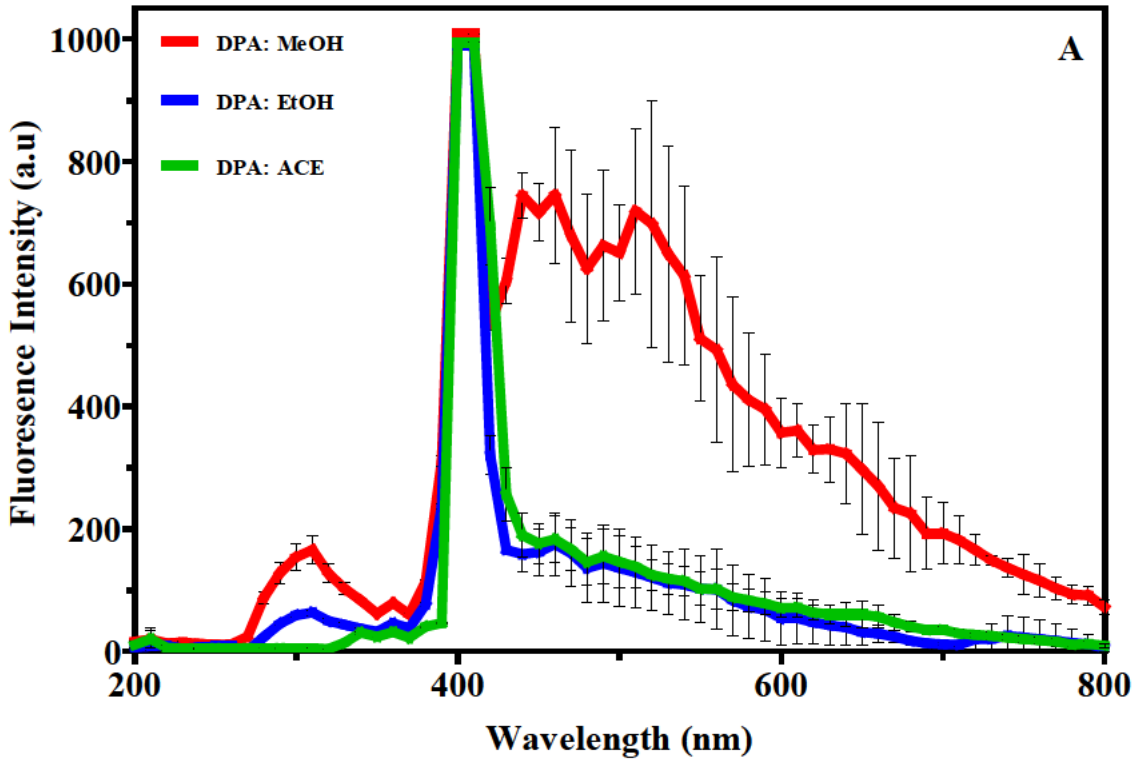

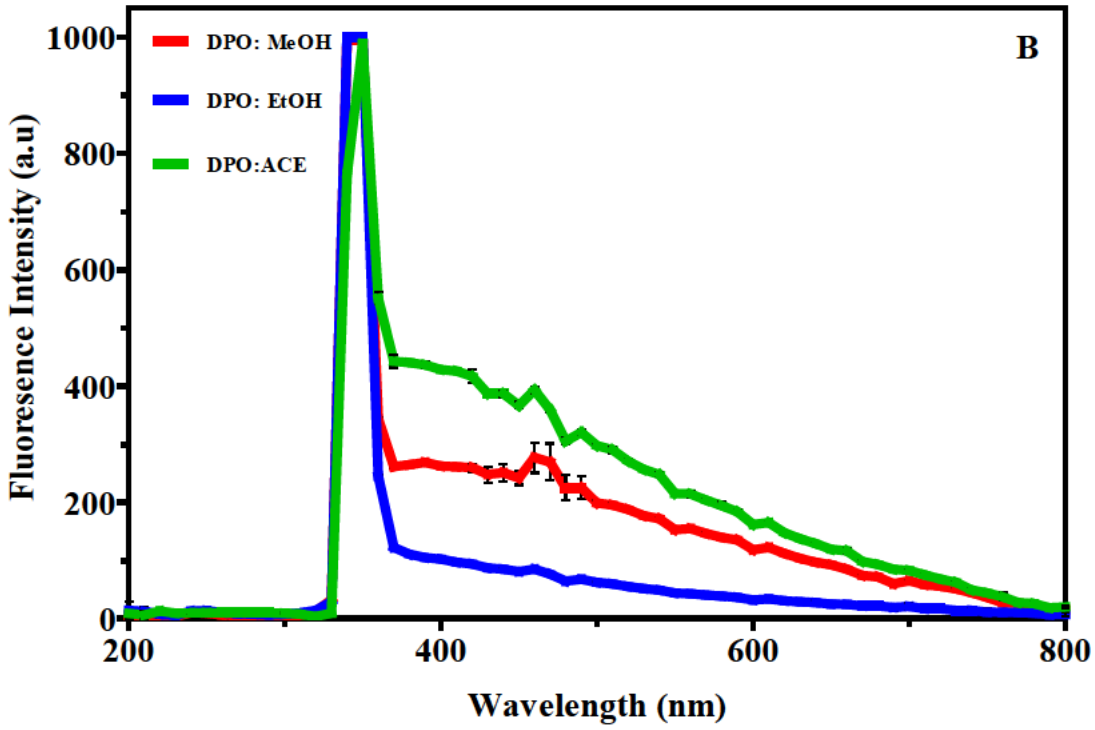

Figure 3.1: Fluorescence spectra of **(A)** Diphenylanthracene (DPA) and **(B)** Diphenyloxazole (DPO) dissolved in methanol (MeOH), ethanol (EtOH), and acetone (ACE) at 100 mgL^{-1}. The DPA and DPO dyes excitation wavelengths were between 280 – 310 and 320 – 350 nm, respectively. Data are expressed as a mean ± SD (n = 3) and plotted at every 10 nm.

The findings showed that R8G absorbed light between 200 – 300 nm (Figure 3.2 A). When dissolved in acetone, the R8G dye exhibited an emission peak between 460 – 520 nm and demonstrated the highest average fluorescent intensity (713 a.u). However, acetone was not chosen as the desired solvent as there was only a slight overlap of dye emission in the PAR, (± 20 nm). When dissolved in the alcohol solvents the emission peak was extended (460 to 800 nm), (Figure 3.2 A). Rhodamine 8G displayed the same fluorescent intensities in methanol and ethanol (653 a.u), and therefore, either solvent could be used to dissolve the dye ($p > 0.05$). Rhodamine dyes are known for their down-conversion of light (blue to green), (Stanley *et al.*

2016). Sung *et al.* (2018) found that R110 absorbed light between 420 – 550 nm and emitted light between 500 – 620 nm while R101 showed peak absorption and emission at 565 and 586 nm respectively (green to red conversion), (Table 2.4). These wavelength emissions could be beneficial when cultivating algal species such as *C. reinhardtii* and *S. bijuga*. These strains have shown a preference for the yellow, green, red, and blue wavelengths, (Table 2.2), (Mattos *et al.* 2015; de Mooij *et al.* 2016).

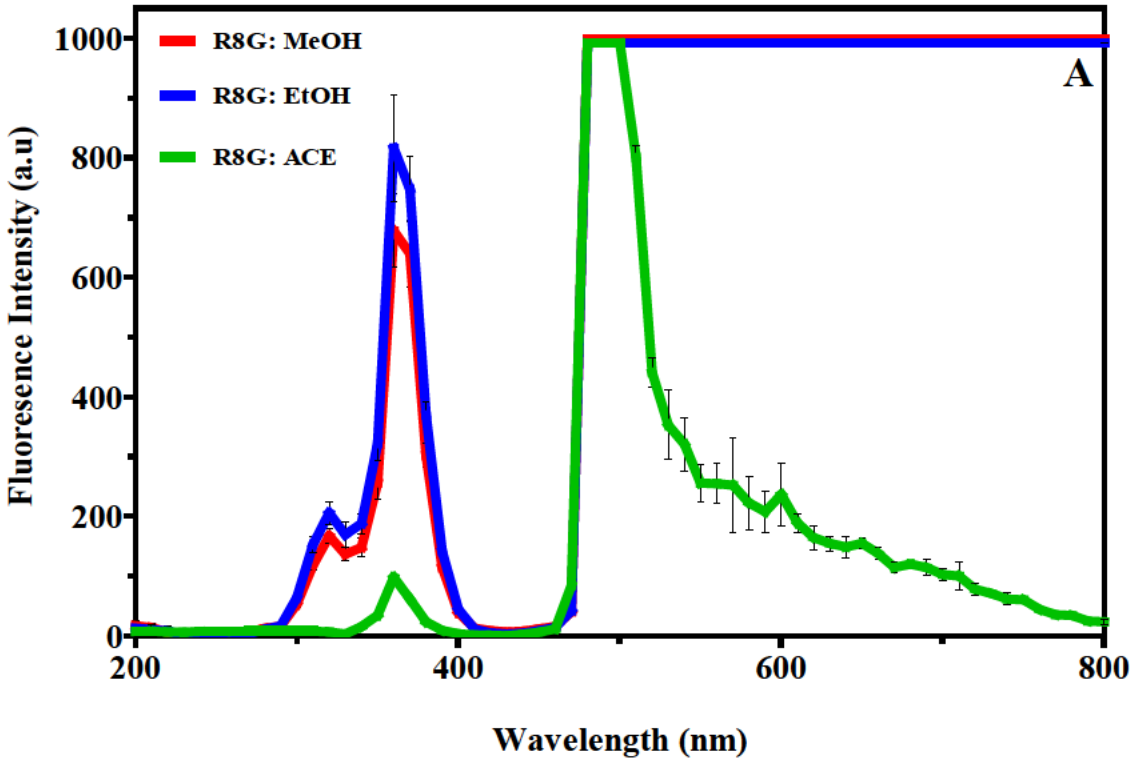

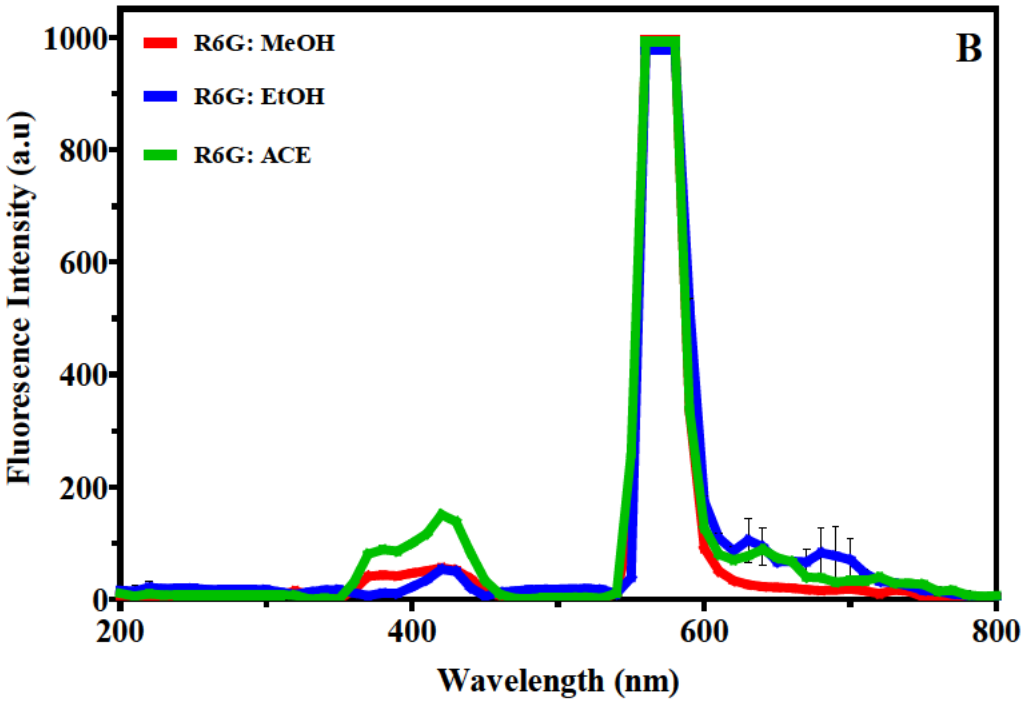

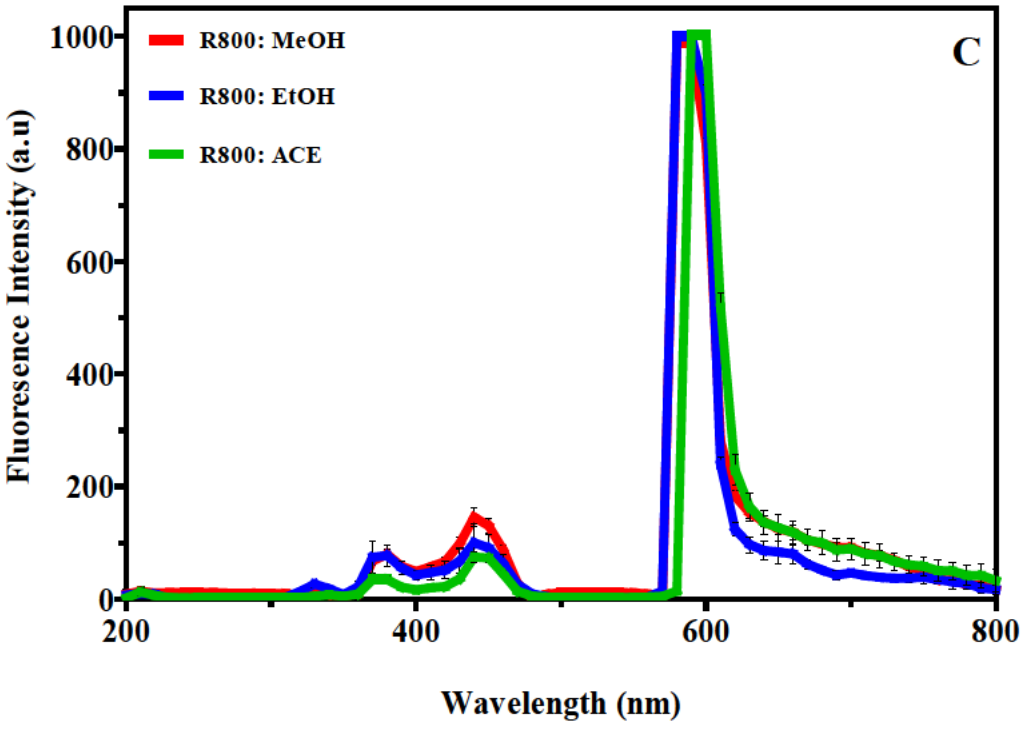

Figure 3.2: Fluorescence spectra of **(A)** Rhodamine 8G (R8G), **(B)** Rhodamine 6G, and **(C)** Rhodamine 800 (R800) dissolved in methanol (MeOH), ethanol (EtOH), and acetone (ACE) at 100 mgL^{-1}. The R8G dye excitation wavelength was between 200 – 300 nm, while

R6G and R800 showed similar excitation between 350 – 480 nm. Data are expressed as a mean ± SD (n = 3) and plotted at every 10 nm.

Rhodamine 6G and R800 showed similar excitation spectra (350 – 480 nm), yet, differed in emission ranges (Figure 3.2 B and C). The R6G dye exhibited an emission range between 540 – 590 nm, while the R800 dye emitted light between 570 – 630 nm. The R6G dye spectra showed comparability with a previous study. Khoobkar and Delavari Amrei (2020), found that R6G had two absorption peaks in the green light spectrum (497 and 534 nm) and emitted light in the orange-red wavelengths (615 nm). The average fluorescent intensities for R6G, when dissolved in acetone (705 a.u.), were higher when compared to methanol (688 a.u.) and ethanol (667 a.u.) ($p < 0.05$) (Figure 3.2 B), whereas R800 demonstrated the opposite trend. Literature shows that the intensity of the R6G emissions is strongly dependent on the pH. By contrast, R800 is almost insensitive to this parameter and the intensity of its spectral emissions remain almost invariable for all pH values. The difference in behaviour suggests that the molecular cations in the dyes interact differently with the solvents and that, particularly for the R800, the state of charge does not significantly affect the adsorption of this molecule (Zehentbauer *et al.* 2014; Malfatti *et al.* 2018). Fluorescent intensities of R800 decreased when dissolved in methanol, ethanol, and acetone giving 513, 488, and 443 a.u. respectively (Figure 3.2 C). From the findings, R800 could potentially be considered for algal cultivation as it emitted in the PAR region. These emission ranges agreed with previous studies (Gao *et al.* 2017; Malfatti *et al.* 2018). Rhodamine dyes show affinity for several organic and inorganic solvents (Zehentbauer *et al.* 2014; Malfatti *et al.* 2018). In the current study, there was a significant difference between R800 dissolved in methanol and acetone ($p < 0.05$). Fluorescence in methanol was higher and therefore, methanol can be regarded as the optimal solvent for this dye.

Zehentbauer *et al.* (2014), investigated the fluorescence spectral pattern of R6G dissolved in ethanol, methanol, acetone, dimethyl sulfoxide (DMSO) n-propanol, iso-propanol, n-butanol, and n-pentanol at constant dye concentration. The researchers found minor differences in the dye spectral emissions between the different solvents. The highest fluorescence intensity and shortest peak wavelength were observed for methanol (568 nm) while the lowest fluorescence intensity and the longest peak was observed in DMSO (579 nm). Rhodamine 6G exhibited similar wavelength emission ranges, however, the dye demonstrated higher intensities in acetone (Figure 3.2 B). Differences in fluorescent intensities between the current investigation and the study conducted by Zehentbauer *et al.* (2014) may be due to; (*i*) the differences in dye solvation, (*ii*) absorption of light in the individual solvents may have been different at the excitation wavelengths, or (*iii*) temperature or pH variations of the dye solutions (Zehentbauer *et al.* 2014; Malfatti *et al.* 2018). Therefore, depending on the application, future research focussing on R6G should also test dye emissions in various classes of solvents to ensure dye fluorescent integrity (wavelength and intensity) as individual accounts and circumstances may vary. It should be noted that organic dye quantum yield is usually higher in solvents such as methanol, and forms aggregates which do not mix homogenously in solvents like acetone or water (Maillard *et al.* 2020; Ramya *et al.* 2020).

Fluorescein Isothiocyanate dissolved in acetone exhibited very low fluorescent intensities when compared with dyes dissolved in ethanol and methanol (< 400 a.u) (Figure 3.3 A). Furthermore, dyes in ethanol and methanol showed no significant difference in the fluorescent intensities ($p > 0.05$), and therefore either solvent can be considered optimal for dye dissolution. Dye excitation ranged between 300 – 400 nm while emission ranged between 500 – 580 nm. Consequently, this dye was not considered for further evaluation as it exhibited an emission range not corresponding to the PAR region. The LY and LR dyes demonstrated a

similar excitation range between 320 – 350 nm and 320 – 400 nm, respectively (Figure 3.3 B and C). The LY dye emitted light from 420 nm to well over 800 nm in all three solvents while the LR dye exhibited an emission range between 590 – 660 nm in methanol. Both LY and LR dyes demonstrated broader emission peaks and emitted in the PAR region. The findings indicated that both LY and LR dyes would be suitable for microalgal cultivation.

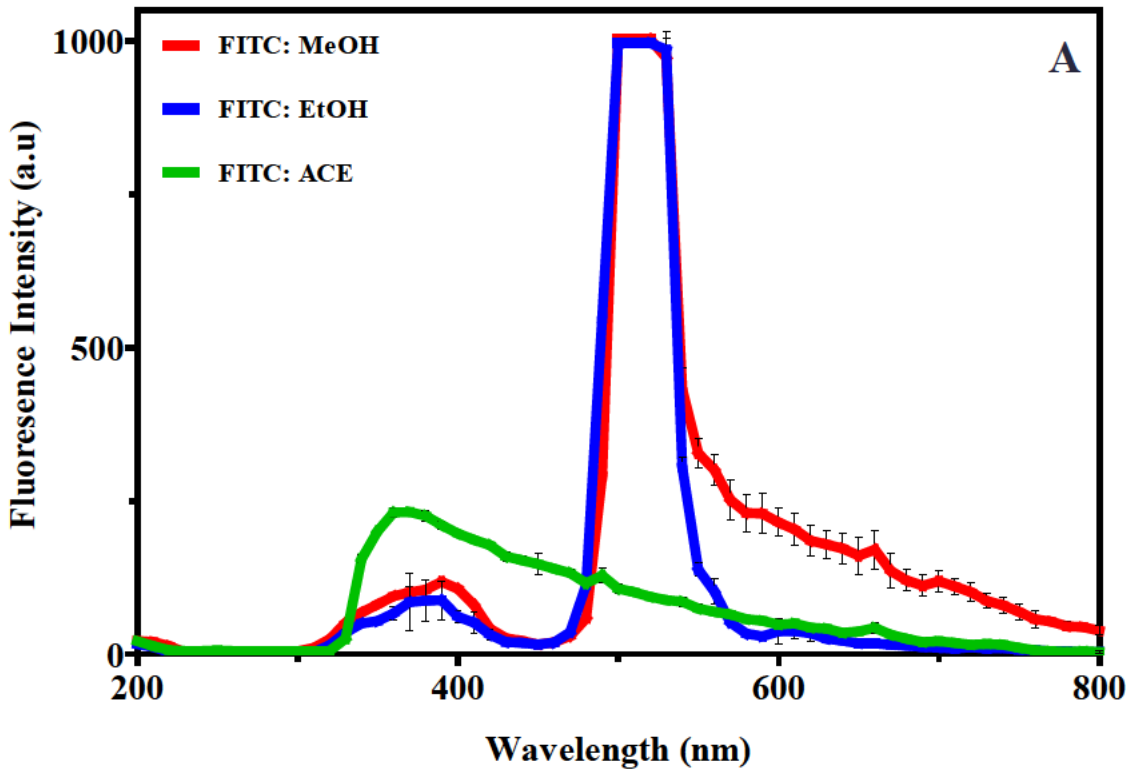

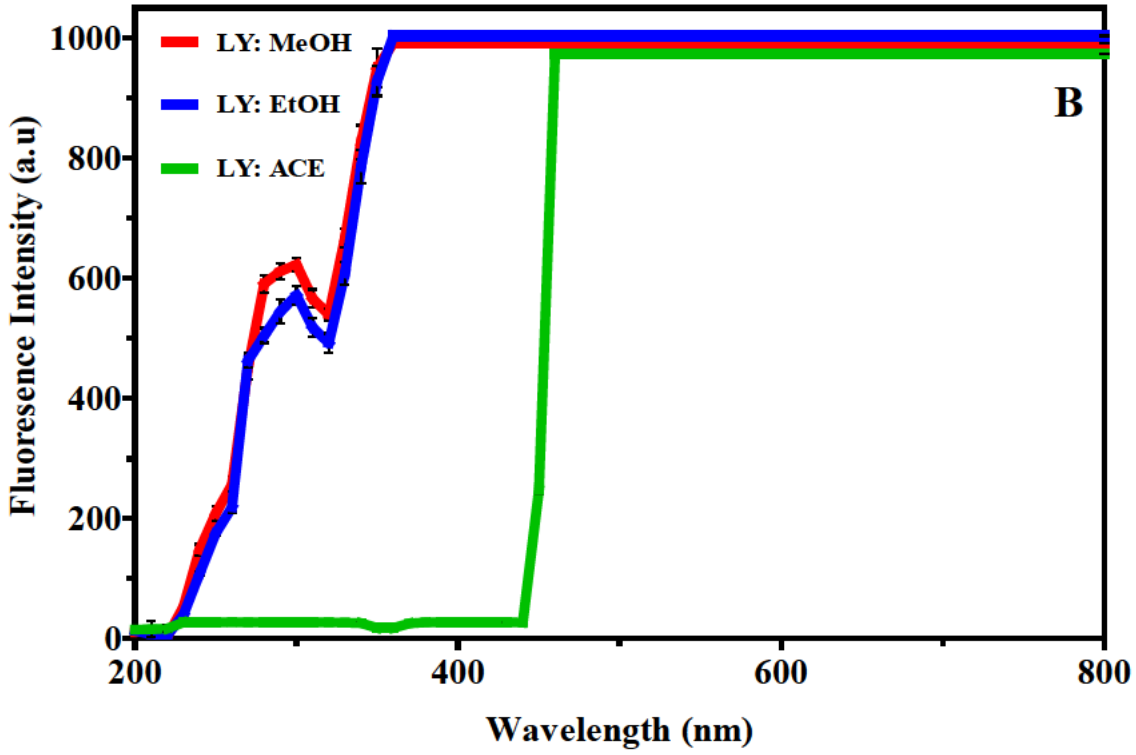

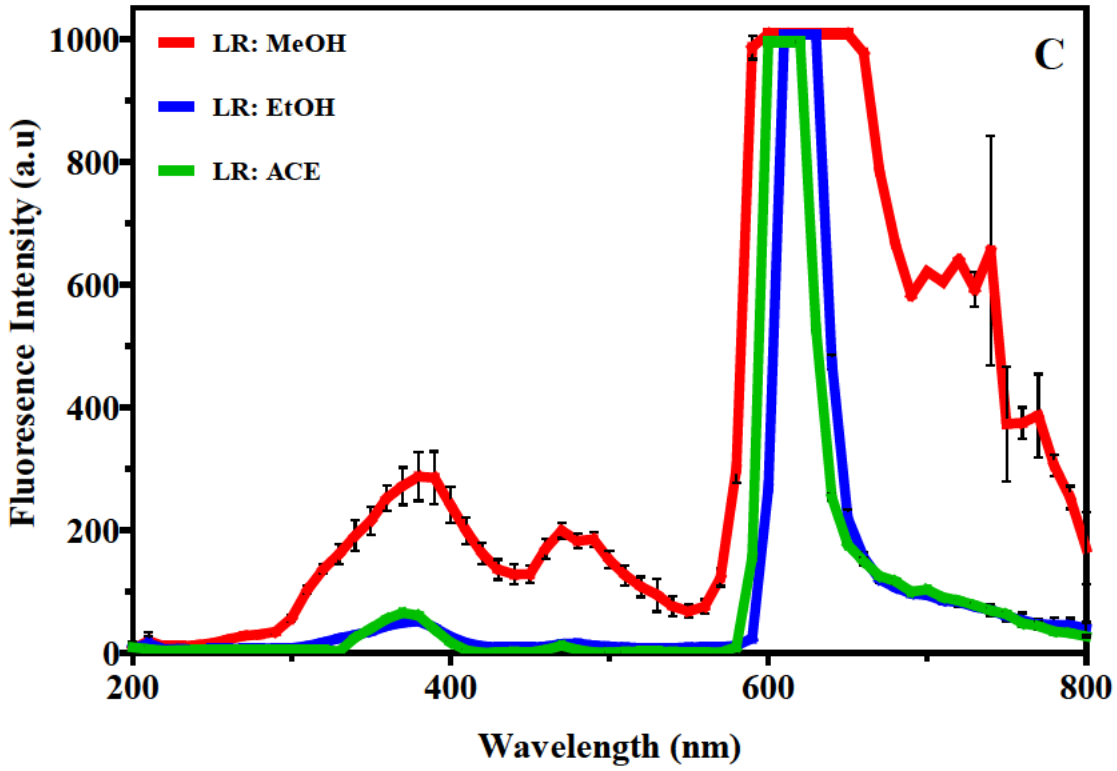

Figure 3.3: Fluorescence spectra of **(A)** Fluorescein Isothiocyanate (FITC), **(B)** Lumogen Yellow (LY), and **(C)** Lumogen Red (LR) dissolved in methanol (MeOH), ethanol (EtOH), and acetone (ACE) at 100 mgL^{-1}. The FITC dye excitation wavelength was between

300 – 400 nm, while LY and LR showed excitation between 320 – 350 and 320 – 400 nm, respectively. Data are expressed as a mean ± SD (n = 3) and plotted at every 10 nm.

The results showed that the dye spectra varied in terms of peak wavelength and intensity (Figure 3.1 – Figure 3.3). Different dyes demonstrate different spectral conversion efficiencies (Zehentbauer *et al.* 2014; Zhang *et al.* 2014). This is highly dependent on the chemical structure of the dye and the interaction between the dye molecule and the solvent. Dyes dissolved in both alcohols exhibited higher emission peak intensities when compared to acetone. These fluctuations were attributed to, firstly, the slight differences in the solvation of the dye molecules in the individual solvents (Zehentbauer *et al.* 2014; Zhang *et al.* 2014), and secondly, to the absorption of UV radiation by acetone (Shen *et al.* 2015).

Acetone has low proton affinity, relatively low boiling point, and is miscible in most organic solvents. Absorption of a quantum of light energy from a photon leads to its photo-dissociation (also known as photolysis or photochemical decomposition) (Lukavenko *et al.* 2009; Speight 2018). Photolysis is not limited to the effects of visible light but any photon with sufficient energy can cause the chemical transformation of the inorganic bonds of the chemical. Since the energy of a photon is inversely proportional to the wavelength, electromagnetic waves with the energy of visible light or higher, such as UV light, X-rays, and gamma rays can also initiate photolysis reactions (Speight 2018). Hence, the absorption of UV radiation initiated the photochemical decomposition of acetone resulting in the production of acetyl and methyl radicals that oxidised dye molecules. Consequently, solvents should not absorb light in the same region as the dye. Hence, methanol and ethanol are preferred as they absorb light with a molar absorption coefficient in the 700 – 900 nm range (Maillard *et al.* 2020). For these reasons, acetone was not chosen as an appropriate solvent for dye solutions.

From the findings, the LY and LR dyes demonstrated higher fluorescent intensities in methanol and ethanol (Figure 3.3 B and C). These solvents demonstrate good solubility, optical transparency, and proper absorption and emission of the dissolvent dye (Maillard *et al.* 2020). Organic solvents like methanol and ethanol have been evaluated by previous researchers due to their excellent dispersion properties, thus increasing dye fluorescent efficiency (Abou-Kana 2012; Zehentbauer *et al.* 2014; Zhang *et al.* 2014). The fluorescence spectra in both the alcohols were relatively constant, though, methanol exhibited slightly higher emission intensities. This indicated that the solvation in methanol was different when compared with ethanol and can be explained by the molecular properties of the solvent. Methanol is more protic allowing more efficient dye dissolution, has a higher dielectric constant and is a stronger nucleophile compared to the other alcohols. Additionally, the interactions of the methanol molecule with the environment are governed due to its small molecular size. This behaviour is strongly dominated by the polar group while in other alcohols the polar and non-polar contributions are more balanced (Maillard *et al.* 2020). Furthermore, the use of methanol as a solvent may be preferred due to its wide availability (as denatured alcohol), or its lower cost as opposed to acetone or ethanol (Zehentbauer *et al.* 2014; Maillard *et al.* 2020). Therefore, based on the current findings, methanol was considered an appropriate solvent for dye dissolution. The dyes considered for further experimentation can be seen in Table 3.1.

Table 3.1: Dye emission spectra of Diphenylanthracene (DPA), Rhodamine 8G (R8G), Rhodamine 800 (R800), Lumogen Yellow (LY), and Lumogen Red (LR) dissolved in methanol at 100 mgL^{-1}.

Dye	Excitation (nm)	Emission (nm)
DPA	280 – 310	390 – 430
R8G	200 – 300	460 – 800
LY	320 – 350	420 – 800
LR	320 – 400	590 – 660

The dyes were selected based on their emission spectra and fluorescence intensities. Only DPA, R8G, LY, and LR demonstrated emission ranges in the PAR. Although R800 emitted light 570 – 630 nm, the dye exhibited a broad absorption range in the PAR (350 – 480 nm). This dye would absorb beneficial PAR irradiations; hence, it was not considered for further evaluation. The LY dye showed the broadest emission range (420 – 800) when compared while the DPA dye showed the narrowest emission bandwidth (30 nm). The LR dye exhibited an emission bandwidth of 60 nm in the red wavelength.

3. 3. 2. Dye concentration optimisation

From the analyses of the fluorescence spectra, when dissolved at 100 mgL^{-1}, DPA, R8G, LY, and LR dyes displayed high fluorescent intensities (> 1000 a. u) and broader emission ranges (Figure 3.4 A – D). At 100 mgL^{-1}, the DPA dye exhibited the narrowest emission range in the PAR (390 – 430 nm), (Table 3.1 and Figure 3.4 A). As the dye concentration decreased (< 10 mgL^{-1}), fluorescent intensities decreased (< 600 a.u). In the case of R8G, the dye emitted

light between, 460 – 800 nm. As dye concentrations were lowered there was a shift in the peak emissions (± 30 nm). Dye concentrations of 100 mgL^{-1} displayed emission ranges at 480 nm, whereas at 10 mgL^{-1} or lower, emission ranges started at 450 nm (Figure 3.4 B). This potentially resulted in higher emissions at lower dye concentrations and hence, 10 mgL^{-1} was considered an optimal concentration for this dye. The emission spectrum of less concentrated molecules typically induces a hypsochromic shift. This is a shift of the peak to shorter wavelengths with higher energy (Delgado-Sanchez 2019). Larger spectral shifts result in diminished re-absorption effects resulting in narrower wavelength bands.

Dyes with tuneable frequencies can be used to increase the light availability in specific spectral ranges for algae to produce specific metabolites. Under high/low dye-irradiance, conformation changes in chlorophyll, carotenoid, or phycobiliprotein biosynthesis may occur which could be beneficially applied to industries such as pharma- and nutraceutical (Table 2.1), (Sung *et al.* 2018; Khoobkar and Delavari Amrei 2020). Research has evaluated the efficacy of organic dyes in a liquid medium to enhance light availability to microalgae (Sung *et al.* 2018; Khoobkar and Delavari Amrei 2020), however, the studies have focussed primarily on biomass and metabolite production rather than the physiological responses.

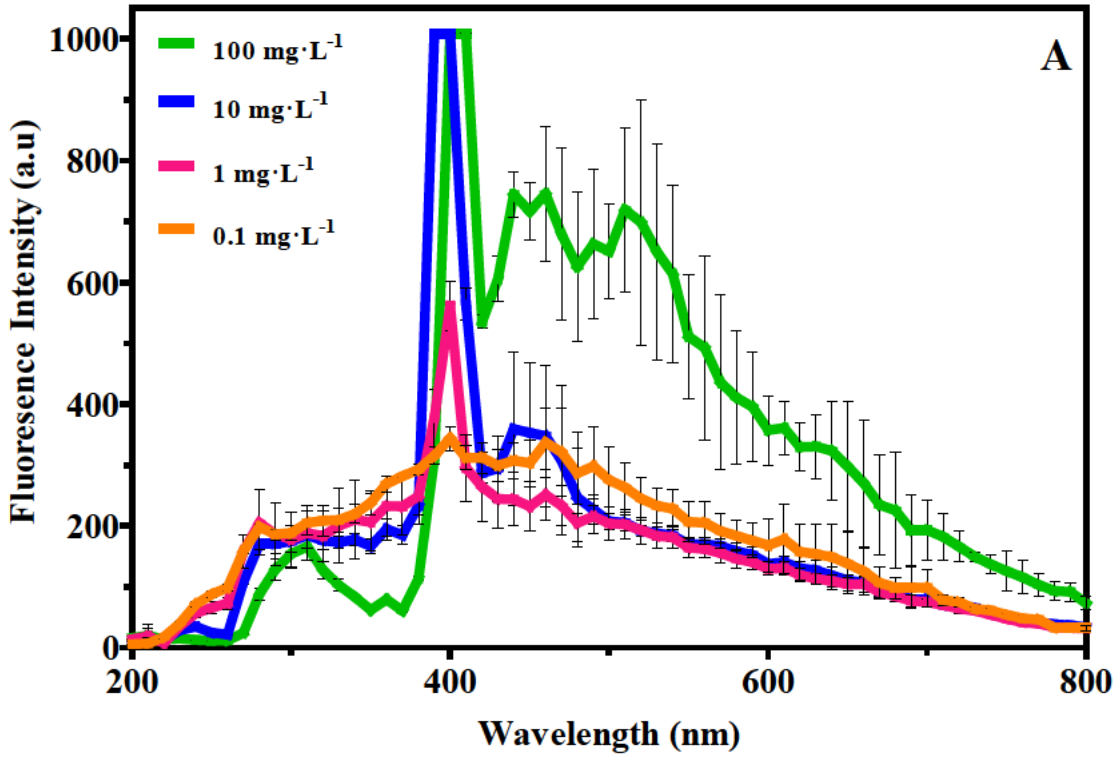
A
100 mg·L-1
10 mg·L-1
1 mg·L-1
0.1 mg·L-1
Fluoresence Intensity (a.u)
Wavelength (nm)
0
200
400
600
800
1000
200
400
600
800

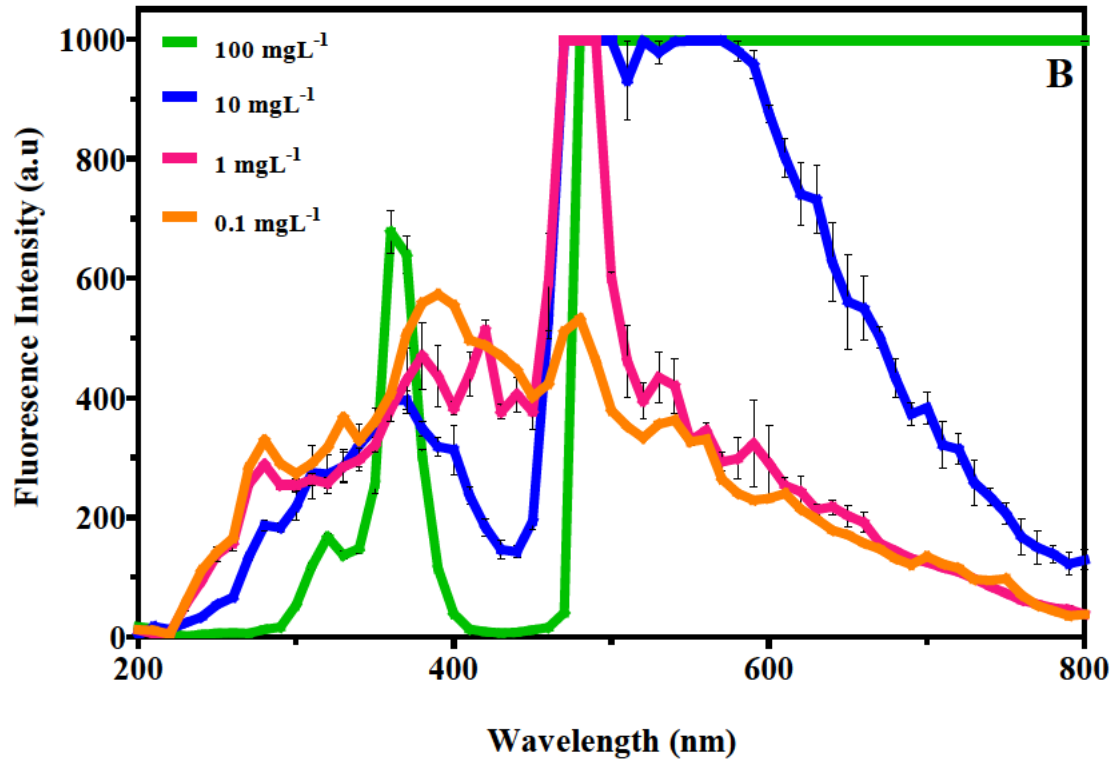
B
100 mgL-1
10 mgL-1
1 mgL-1
0.1 mgL-1
Fluoresence Intensity (a.u)
Wavelength (nm)
0
200
400
600
800
1000
200
400
600
800

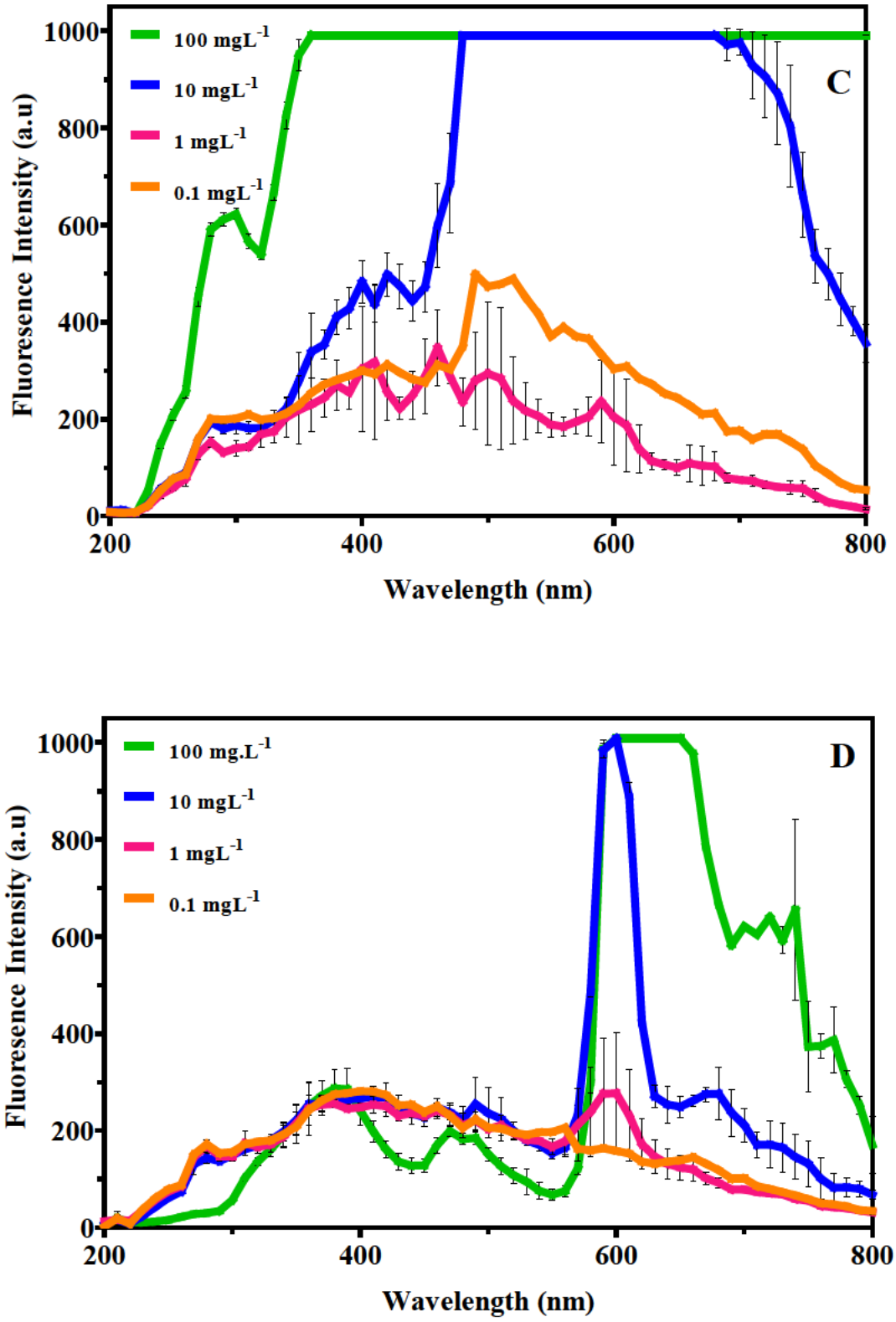

Figure 3.4: Fluorescence spectra of **(A)** Diphenylanthracene, **(B)** Rhodamine 8G (R8G), **(C)** Lumogen Yellow (LY), and **(D)** Lumogen Red (LR) dissolved in methanol at 100, 10, 1, and 0.1 mgL^{-1}. Data are expressed as a mean ± SD (n = 3) and plotted at every 10 nm.

The appearance of smaller secondary spectral peaks indicated the formation of molecular dimers (Zehentbauer *et al.* 2014), making interpretation of the optical spectra more challenging. Dimer formation facilitates wavelength tunability, however, its occurrence promotes the re-absorption/re-emission effect. An increased number of dye molecules in solution results in the unexcited dye molecules absorbing the radiation emitted by the excited dye molecules (Al-Aqmar *et al.* 2015; Reisfeld and Levchenko 2017). The possibility of exciting molecules by absorption of a photon previously emitted by another molecule in the medium (self-absorption) is increased at high dye concentrations (Al-Aqmar *et al.* 2015).

Dye molecule self-absorption poses a problem as it results in broad emission bands (Zehentbauer *et al.* 2014). This effect can be seen with LY (Figure 3.4 C). The dye showed an emission range between 420 – 800 nm. The thermal broadening in the emission ranges (> 700 nm) will increase the quantity of IR rays, further increasing the culture temperatures. This may not be conducive to microalgal growth and metabolite production (Vuppaladadiyam *et al.* 2018; Alishah Aratboni *et al.* 2019). Hence, 100 mgL^{-1} was not selected as the optimal concentration for LY. At 10 mgL^{-1}, the dye showed an optimal emission range (450 – 700 nm) with high intensities (> 1000 a. u), which can be considered suitable for microalgal cultivation. The optimal concentration for the LR dye was 100 mgL^{-1}. The dye emitted light between 590 – 660 nm. At lower concentrations (10 mgL^{-1}), the dye emission range decreased (by ~ 70 nm), (Figure 3.4 D).

Lowered dye concentration (10 mgL^{-1}) promoted the absorption of minimal light which resulted in higher or maximal fluorescent emissions. Similar observations have been previously reported (Khoobkar and Delavari Amrei 2020). As the dye concentrations decreased there was

a steady decrease in the fluorescent output energy which occurred due to the gradual photo-degradation of the dyes. Similar occurrences have been reported by Al-Aqmar *et al.* (2015), while the same effect was observed between all the dyes in all three solvents (Appendix A). Only the DPO and R6G dyes retained a high emission spectrum (Appendix A, Figures A2 and A4, respectively). These emissions were, however, not in the PAR region. Dyes dissolved at 1 mgL^{-1} or below exhibited erratic spectral emission curves, particularly in the case of the LY (Figure 3.4 C). With decreases in the dye concentration, its optical spectra undergo noticeable transformations, most notable are the decreases in fluorescence intensities and high levels of error in the results. At lower concentrations, there was less dye in the solution which could have resulted in uneven absorption and/or emission of light (Al-Aqmar *et al.* 2015). Light waves passing through diluted dye solutions are not continuously absorbed but bring about individual molecular electronic transitions which cause lowered fluorescence emissions (Langhals 2020). This was reflected in the areal fluorescence intensities (AFI) of the dyes at 10 and 1 mgL^{-1}, which can be seen in Table 3.2.

Table 3.2: Areal fluorescence intensities in the PAR regions of the various dyes evaluated in methanol at optimal concentrations. Fluorescence measured in arbitrary units (a.u). Data are expressed as a mean (n = 3).

Dye	**10 mgL^{-1}**		**AFI**	**1 mgL^{-1}**		**AFI**
	400 – 500 nm	**600 – 700 nm**		**400 – 500 nm**	**600 – 700 nm**	
DPA	36651	10897	47548	25363	10277	35639
R8G	51405	61733	113138	62266	19366	81632
LY	63121	98752	161873	27871	11566	39437
LR	24667	37157	61824	23388	13649	37037

When compared to the DPA and LR dyes, R8G and LY emitted the highest areal fluorescent intensities in the PAR region. These were 113138 a.u and 161873 a.u, respectively. Furthermore, the yellow and green wavelengths have been shown to stimulate growth and high-value-added product biosynthesis in *C. reinhardtii* (de Mooij *et al.* 2016), hence, LY and R8G were selected for further evaluation on the effects of increased light availability on algal growth and metabolite production.

3. 4. Conclusion

The dyes evaluated showed higher affinities for methanol. Dyes maintained higher fluorescent intensities in methanol than ethanol, while acetone was found to absorb UV radiation leading to lower dye excitation. From the eight dyes evaluated only DPA, LR, R8G, and LY demonstrated potential as spectral converters for application in microalgal cultivations as the dye emission spectra corresponded with the PAR wavelengths. Dye concentrations of 100 mgL^{-1} lead to dye self-absorption resulting in broad emission bands falling out of the PAR. The optimal dye concentration was 10 mgL^{-1} while lower concentrations ($\leq$ 1 mgL^{-1}) exhibited uneven absorption and/or emission of light and gradual decreases in dye output energy. Both LY and R8G exhibited the highest fluorescence emissions in the PAR and were taken to the next phase of experimentation.

Chapter 4 : Effects of increased dye-mediated photon flux densities on the microalgal physiological responses

Ramanna, L., Rawat, I. and Bux, F. 2018. A novel organic dye-based approach to increase photon flux density for enhanced microalgal pigment production. *Journal of Cleaner Production*, 198: 187-194.

4. 1. Introduction

Abiotic stress such as excessive irradiation is known to affect algae at the physiological and biochemical levels (Eroglu *et al.* 2013; Raeisossadati *et al.* 2019). Increased levels of solar radiation compromise the performance, growth, photosynthesis, and reproduction of microalgae, inherently affecting the biomass and pigment content. In microalgal cultivation, the low spectral conversion efficiency can be attributed to a loss of photons by reflection, photo-saturation, and photo-inhibition (Ma *et al.* 2019; Nwoba *et al.* 2019). This limits algal PE and productivity. Depending on species, microalgae show different levels of sensitivity to stress. Under excessive irradiance algae reduce their chlorophyll content thus decreasing the quantum yield of photosynthesis, which is correlated with the reduction of growth (Eroglu *et al.* 2013; Raeisossadati *et al.* 2019). The physiological acclimation of algae to irradiation is largely dependent on; (*i*) the balance between the photo-protective mechanisms; (*ii*) the activation and accumulation of antioxidants and antioxidant enzymes; and (*iii*) the accumulation of light-screening photo-protective metabolites such as carotenoids. By regulating these processes/metabolites, algae can maintain their PE (Eroglu *et al.* 2013; Nwoba *et al.* 2019; Raeisossadati *et al.* 2019).

The physiological status of microalgae is usually assessed by monitoring the changes in the total chlorophyll concentration and cell densities (spectrophotometrically or by DCW) (Ma *et al.* 2019; Nwoba *et al.* 2019). The physiological responses of microalgae can be qualitatively or semi-quantitatively assessed using growth, pigment analyses, and pulse amplitude modulated (PAM) fluorometry. Hence, this chapter aimed to evaluate the effect of LY and R8G irradiance on the physiological responses of *C. reinhardtii*.

4. 2. Materials and Methods

4. 2. 1. Strain identification

4. 2. 1. 1. Morphological identification

An isolated microalgal strain from the Institute for Water and Wastewater culture collection was used in this study. The microalgal sample was morphologically identified using a phase-contrast Primo Star Microscope (Carl Zeiss, USA). Cultures were thoroughly homogenised using a vortex mixer and viewed at 1000X. Micrographs were taken using a camera attached to the microscope, the Zen 2 Lite software was then used to create image files (Carl Zeiss, USA).

4. 2. 1. 2. Molecular identification

Deoxyribonucleic acid (DNA) extraction was done by using ZR Fungal/Bacterial DNA Kit™ (Zymo Research) according to the manufacturer's instruction. Amplification using primers 18S-AB1 (5´GGAGGATTAGGGTCCGATTCC3´) and 18S-TW4 (5´CTTCCGTCAATTCCTTTAAG3´) that targeted the conserved regions of the 18S rRNA

genes was performed according to Altschul *et al.* (1997). The polymerase chain reaction (PCR) products were sequenced by Inqaba Biotechnical Industries (Pty) Ltd. (RSA). The Basic Local Alignment Search Tool (BLAST) was used to find closely related nucleotides sequences that were obtained from GenBank. The sequences were edited and aligned using BioEdit. Thereafter, a phylogenetic tree was constructed using the Maximum Likelihood method in MEGA 7 software (Tamura *et al.* 2011).

4. 2. 2. Effects of irradiance and solvent polarity on the growth of *C. reinhardtii*

4. 2. 2. 1. Photo-bioreactor operation and culture conditions

Experiments were conducted in borosilicate glass double-jacketed cylindrical PBRs (Figure 4.1). The PBRs had an outer jacket for the organic dye/solvent solution and an inner jacket for microalgal cultivation. The path length between the layers was 1 cm and the reactor had a working volume of 3.5 L. The PBRs were housed in an incubator equipped with 220 V electric fans to regulate air to prevent heating (Appendix B). To ensure equal light distribution and adequate dye excitation, the PBRs were centralised along with the light source in the incubator. Pre-acclimatised microalgae (four days) were inoculated into the PBRs at inoculum sizes approximately ± 0.3 gL^{-1} (± 10%). Submersible pumps (SP-600, 220V-5W, 260 Lhr^{-1} flow rates [Resun, China]), were used to provide adequate mixing in the PBRs. *Chlamydomonas reinhardtii* was grown on Tris Acetate Phosphate (TAP) medium (Appendix C) (Natali and Croce 2015). To establish a baseline for growth, algae were grown in PBRs using no liquid jacket (NJ), a water jacket (WJ), and a methanol jacket (MJ) under 16:08 hr light/dark periods. The PBRs received approximately 75 µmol photons·m^{-2}·s^{-1} irradiance which was provided by T8 standard tubes (F18W/daylight) (Tungsram, Hungary). Photosynthetic

irradiance levels were measured using a PAR Vernier probe (PAR-BTA SQ-110 20772) and recorded using a LabQuest 2 data capturing unit, (Vernier, USA).

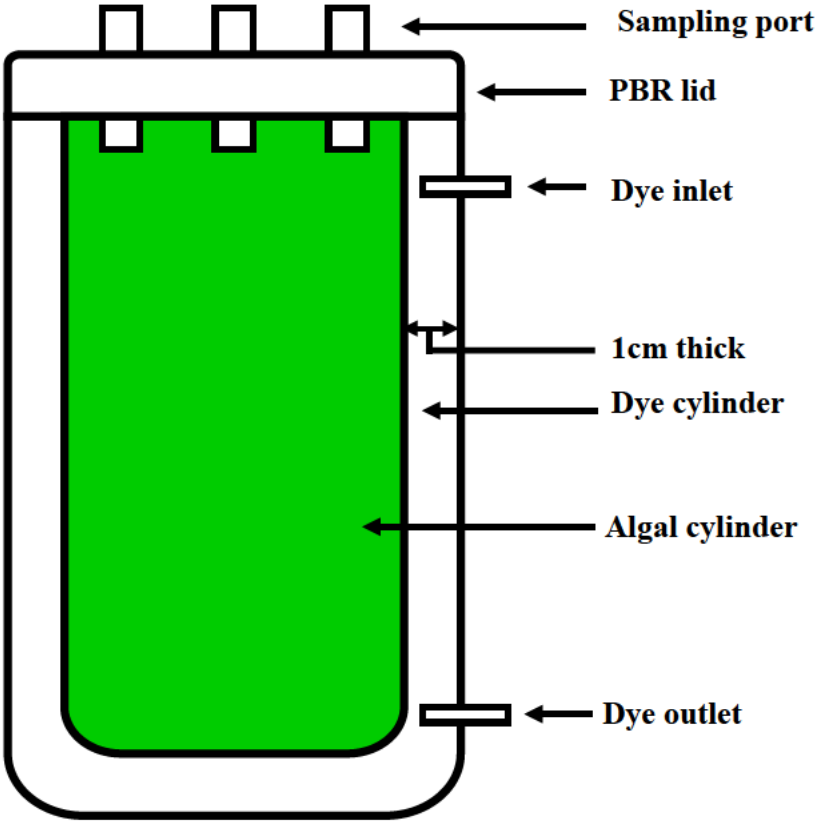

Figure 4.1: Schematic of glass double-jacketed cylindrical photo-bioreactor.

4. 2. 3. Growth of *C. reinhardtii* under dye-mediated irradiance

Chlamydomonas reinhardtii was grown in PBRs as per section 4. 2. 2. 1. The R8G and LY dyes were used in this phase of experimentation. The dyes were dissolved in methanol at 10 mgL^{-1}. Control experiments were set up where the microalgal cells were grown in a reactor that received light passing through a methanol blank. Culture pH and temperatures were measured using a Hanna pH/mV 211 bench meter equipped with a HI 1131B pH probe and a HI 7669/2W temperature probe (Hanna Instruments, USA). Temperatures fluctuated between

24 – 27 °C while pH ranged between 7.6 and 9.5 throughout the study (Appendix D). Ampicillin was added to the culture medium to prevent bacterial contamination (50 μgmL^{-1}).

4. 2. 3. 1. Measurement of growth and biomass

The growth of microalgal cultures was determined gravimetrically as DCW (gL^{-1}). Briefly, 10 mL algal samples were centrifuged for 10 min at 2.091 × g. Supernatants were discarded, and pellets were washed with distilled water (dH_2O), and re-centrifuged. Thereafter, the pellets were harvested and dried at 50 ºC for 24 h on dried and pre-weighed watch glasses. After drying, the watch glasses were cooled in a desiccator and then the weight was recorded. The DCW was determined as the difference between the pre-weighed watch glasses and the weights of those containing the dried samples. Final weights were interpolated to gL^{-1} and used to establish growth rates (μ) as per Kim *et al.* (2014).

$$\mu = \frac{(\ln X_1 - \ln X_0)}{t_1 - t_0}$$

Equation 4.1: Microalgal growth rate

Where X_1 and X_0 were the DCW at time t_1 and t_0, respectively.

4. 2. 3. 2. Pigment analyses

Total chlorophyll and carotenoid contents were determined to evaluate the biochemical responses of microalgae subjected to increased dye-mediated irradiance. Three 10 mL algal

samples were centrifuged for 10 min at 2.091 × g. Supernatants were discarded, and pellets were washed with dH_2O and re-centrifuged. Pellets were harvested and re-suspended in 10 mL of 100% acetone. These were vortexed for 1 min and left for 24 hr in the dark on ice for extraction at 4 ºC. The extraction time was strictly adhered to maintain accuracy and precision within the results. The samples were centrifuged, and the supernatant was collected. Supernatant absorbance levels were read at 470, 645, and 662 nm using a spectrophotometer (Agilent, USA), (García-Cañedo *et al.* 2016). Pigment concentrations were calculated as per the formulas (Lichtenthaler and Wellburn 1983; Almeida *et al.* 2017):

$$\text{Total Chlorophylls } (a+b) = 7.05(A645) + 18.09(A662)$$

Equation 4.2: Total chlorophyll concentration

$$\text{Total Carotenoids} = \frac{[1000(A470) - 2.27(Chl\ a) - 91.4\ (Chl\ b)]}{227}$$

Equation 4.3: Total carotenoid concentration

$$\text{Chlorophyll a } (Chl\ a) = 11.75(A662) - 2.35(A645)$$

Equation 4.4: Chlorophyll *a* concentration

$$\text{Chlorophyll b } (Chl\ b) = 18.61(A645) - 3.96(A662)$$

Equation 4.5: Chlorophyll *b* concentration

Where A was the absorbance reading at that wavelength and Chl *a*/*b* was the chlorophyll concentrations on that day. Pigment content was calculated by dividing the wet weight of the

pigment by the biomass (DCW) present in 10 mL on that given day. Values were interpolated to achieve mgg^{-1}.

4. 2. 4. Photo-physiological analyses

Non-invasive PAM fluorescence measurements were conducted to determine the overall photosynthetic performance of microalgae subjected to increased dye-specific wavelength irradiations. The Dual-PAM 100 Fluorometer (Heinz Walz Gmbh, Effeltrich, Germany) was used to detect changes in P680 (PSII) chlorophyll fluorescence (Grudzinski *et al.* 2016). Measurements were carried out using the Dual-PAM V1.19 software. Algal samples were diluted until constant turbidity was reached (0.1 at 750 nm). Microalgal samples dark-adapted for at least 15 min. Samples (~ 2 mL) were placed in a quartz cuvette and carefully positioned in the PAM fluorometer sample holder. Microalgal cells were analysed under actinic light and rapid light curves (RLCs) were generated by measuring the electron transport rates (ETRs) to eleven irradiance levels (PAR 0, 11, 18, 27, 42, 58, 100, 221, 344, 536, and 830 µmol photons$\cdot m^{-2}\cdot s^{-1}$) for 30 s. The F_v/F_m (quantum efficiency of PSII) was induced and detected by a Saturation Pulse (SP) (2000 µmol photons$\cdot m^{-2}\cdot s^{-1}$) that lasted 200 – 1000 ms. Fluorescence parameters were calculated automatically by the Dual-PAM software. The quantum efficiency was calculated as per the equation below:

$$F_v/F_m = \frac{(F_m - F_0)}{F_m}$$

Equation 4.6: Quantum efficiency of PSII

Where F_v, F_m, and F_0 represent variable, maximum, and minimum fluorescence after dark-adaptation, respectively. The F_m value was induced by the SP. This ensured multiple

turnovers with a transient closure of the RCs. Consequently, F_m is related to a state of fully closed PSII RCs (Nama *et al.* 2018; Yadav *et al.* 2020). The extent of photo-regulation was monitored through the NPQ index:

$$\mathrm{NPQ} = \frac{(F_m - \mathrm{F'}_m)}{\mathrm{F'}_m}$$

Equation 4.7: Non-photochemical quenching index.

Where F'_m referred to the maximum fluorescence level determined during actinic irradiation. The difference between F'_m and F_m represented the dissipation of energy due to photo-regulation (Nama *et al.* 2018; Yadav *et al.* 2020).

4. 2. 5. Statistical analyses

The statistical analyses were accomplished as per Chapter 3 (section 3. 2. 3). Briefly, experimentations were carried out in triplicate (three runs). Data were expressed as a mean ± standard deviation of the mean (SD). The data were subjected to one-way Analysis of Variance (ANOVA) at a 95% confidence limit and Student T-tests were used to locate the differences in significant results ($p = 0.05$).

4. 3. Results and Discussion

4. 3. 1. Strain identification

4. 3. 1. 1. Morphological identification

The algal cells had an approximate diameter of 5 – 10 µm and were oval, (Figure 4.2). The cells had a single large cup-shaped chloroplast housing one prominent pyrenoid and an eyespot. Based on these microscopic observations the alga was preliminarily identified to belong to the genus *Chlamydomonas*, previously described by Tran and Kaldenhoff (2020).

Figure 4.2: Light micrograph of *Chlamydomonas* under 1000X magnification.

Chlamydomonas spp. is known to be unicellular flagellated green algae having a proteinaceous cell wall and contractile vacuoles. The flagella, which are easily shed and regrown, gives the organism the ability to be motile and demonstrate phototaxis (Sasso *et al.*

2018). The micrograph in Figure 4.2. show the cells without flagella. Flagella loss may occur at different stages of the life cycle (resorption) or in response to stress (deflagellation). These two processes occur at different locations and by different mechanisms: resorption is a consequence of constitutive disassembly at the tip of the cell, while deflagellation involves active severing of the axoneme at the base of the flagellum. *Chlamydomonas* cells shed their flagella in anticipation of mitosis (cell division). The four key phases of the *Chlamydomonas* cell cycle are interphase, prophase, metaphase, and cytokinesis. Interphase cells are flagellated and the basal bodies are connected by a fiber that can be easily visualised. The image captured (Figure 4.2) may represent the prophase or metaphase, in which flagella have been resorbed into the cell, allowing the alga to actively divide (Tran and Kaldenhoff 2020).

Deflagellation often occurs under stressful conditions such as extremes in light intensity, temperature or pH shock, treatment with chemicals (*e.g*. dibucaine or alcian blue), mechanical shear (such as harsh homogenisation), and/or the presence of toxic agents in the medium (*e.g*. detergents or alcohols). Hence, deflagellation serves a protective function for cells under adverse conditions. Flagella shedding could have occurred to minimise exposure to environmental stress (Tran and Kaldenhoff 2020).

4. 3. 1. 2. Molecular identification

Chlamydomonas spp. can be found in stagnant, marine, freshwater, ice, and damp soil (Tran and Kaldenhoff 2020). Hence, due to the diversity of the *Chlamydomonas* species, molecular identification was conducted to confirm assignment to genus level. A phylogenetic tree was inferred from 18S rRNA gene sequences (Figure 4.3). The tree was constructed using the Maximum Likelihood method based on the Kimura 2-parameter model. The

Chlamydomonas isolate C1 had a sequence length of 741 base pairs (bps), the query coverage comparison to *Chlamydomonas reinhardtii* was 99% and the sequence similarity had a confirmed identification of 99.73%. The photosynthetic capabilities of *C. reinhardtii* coupled with the ability to produce a range of metabolites under various cultivation conditions make this alga suitable for a range of applications (Patel *et al.* 2019; Choix *et al.* 2021). Researchers have fully sequenced this alga, thus providing ample data on functional genes, making it extremely useful for studies regarding adaptive responses at the cellular, physiological, and biochemical levels (Natali and Croce 2015; Gomes *et al.* 2017). Furthermore, the relative simplicity of the metabolism and cell structure made this organism an ideal representative of the microalgal species to be used in this study (Cecchin *et al.* 2018; Sim *et al.* 2019).

Figure 4.3: The phylogenetic tree of *C. reinhardtii* isolate C1. The numbers indicated the percentages of 1,000 bootstrap replications.

4. 3. 2. Effects of irradiance and solvent on the growth of *C. reinhardtii*

To establish baseline growth, *C. reinhardtii* was grown in the PBRs using NJ, a WJ, and an MJ and under standard daylight tubes (Figure 4.4). Cultures grown using NJ and MJ showed a three-day exponential phase, followed by a four-day stationary phase, and then a death phase. The observations demonstrated the rapid growth in this strain of alga as previously described by Sasso *et al.* (2018), and Tran and Kaldenhoff (2020). The algae exhibited the highest biomass of 1.5 and 1.4 gL^{-1}, respectively (day 7). Microalgae cultivated in the PBR using the WJ showed maximum biomass (1.2 gL^{-1}) on day 5. This was significantly different when compared to MJ and NJ ($p < 0.05$). Moreover, the algae grown using the WJ had a shorter growth cycle (6 days) with lower biomass. This was reflected by the average growth rates; algae grown using NJ and the MJ were 0.70 d^{-1} and 0.20 d^{-1} (day 7), respectively, while the algae that were grown using the WJ was 0.26 d^{-1} (day 5). The algae grown using NJ showed a 34 and 11% increase in biomass when compared to the algae grown under the WJ and MJ, respectively, while cultures grown under the MJ exhibited a 26% increase in biomass when compared to the WJ, ($p < 0.05$) (day 7).

Water is known to absorb light between 600 – 800 nm, giving rise to a strong overlap of the fluorescence spectra (Maillard *et al.* 2020). The lower growth and biomass concentration in *C. reinhardtii* grown using the WJ was attributed to the absorption of red and the emission of blue light by water (Zehentbauer *et al.* 2014). After day 4 biomass densities were high, consequently, blue light penetration was limited/restricted. The resulting transient growth was attributed to a reduction of light penetration, causing the self-shading effect (WJ, Figure 4.4).

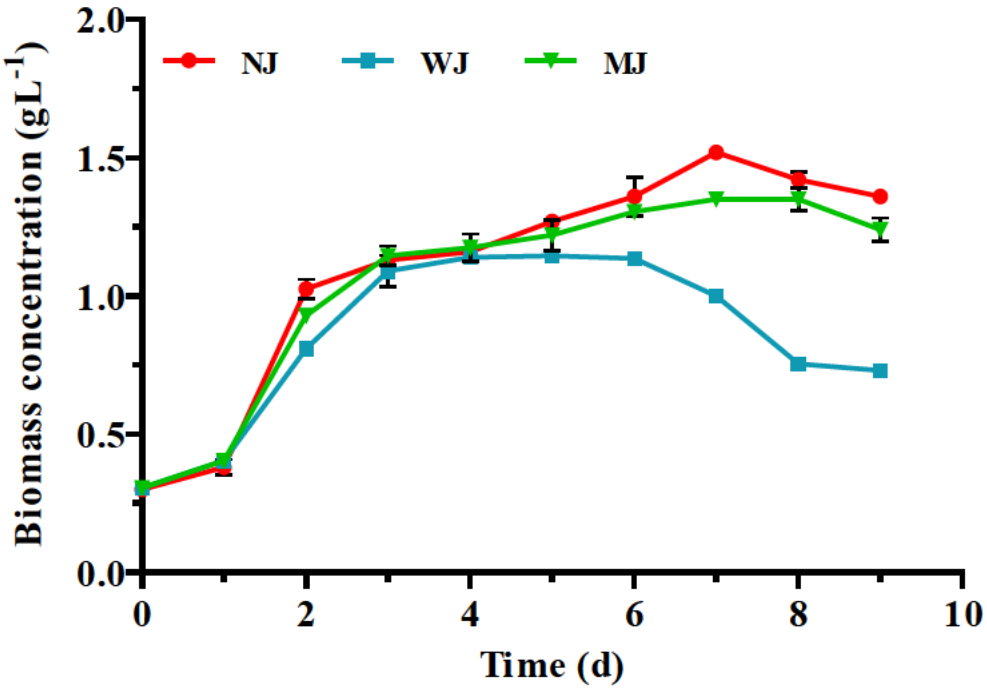

Figure 4.4: Growth curves of *C. reinhardtii* using no liquid jacket (NJ), a water jacket (WJ), and a methanol jacket (MJ). Data are expressed as a mean ± SD (n = 3).

Water has a higher polarity when compared to methanol. This is due to the two hydrogen atoms and the O_2 atom within the water molecule (H_2O) whereas methanol (CH_3OH) has four hydrogen atoms (Maillard *et al.* 2020). Methanol is influenced by the $^{+1}$ effect of the methyl group on the O_2 molecule. Also, O_2 is bonded to one carbon which is more electronegative than hydrogen, therefore, charge separation between the atoms is less. As the solvent polarity increases, light absorption increases. This is attributed primarily or exclusively to the non-resonant and resonant interactions of visible light with the electrons of the substance (*i.e.* water). Subsequently, light attenuation may have been increased in the cultures using the WJ, leading to a reduction of light penetration to the algal cells (WJ, Figure 4.4). Non-resonant processes include Rayleigh scattering, refraction, diffraction, or interference while resonant interactions contain those between photons and matter such as absorption, selective reflection,

or emission. Absorbed photons promote vibrational transitions within the molecule. This leads to high overtone and combination states of the nuclear motions of the molecule, *i.e.* to highly excited vibrations (Zehentbauer *et al.* 2014; Maillard *et al.* 2020). Water is a well-known fluorescence quencher and can compete with radiative and other non-radiative deactivation processes (Maillard *et al.* 2020). Subsequently, the LY and R8G dyes used in further experimentations were dissolved in methanol.

4. 3. 3. Effects of dye-mediated irradiance on the growth of *C. reinhardtii*

The quantity and quality of light are known to impact microalgal growth as it determines the effectiveness of light utilisation (Grudzinski *et al.* 2016; Patelou *et al.* 2020). Depending on the circumstances, increased irradiance is associated with increased or decreased microalgal growth (Vadiveloo *et al.* 2015; Sung *et al.* 2018). Between days 2 to 5, the cultures grown under R8G exhibited increased biomass (9 – 26%), when compared to LY (Figure 4.5). The results were similar to the findings achieved by Ajayan *et al.* (2019). The researchers grew *C. reinhardtii* under different light qualities (white, blue, red, green LEDs, and fluorescent lamps). The highest cell concentration and specific growth rate were obtained under blue light when compared to other light conditions. The authors attributed the higher biomass concentration to the larger cell size attained under blue illumination. It was concluded that blue light gave more photon energy which was favourable for cellular growth (Ajayan *et al.* 2019).

Comparison of the growth under dye-mediated irradiance showed that *C. reinhardtii* grew transiently until day 8, suggesting a reduction in the photosynthetic process (Figure 4.5), (Patel *et al.* 2019). The highest biomass concentrations for the control, LY, and R8G cultures were 1.4, 1.2, and 1.1 gL^{-1} (day 8), respectively. Average algal growth rates were 0.25, 0.17,

and 0.14 d^{-1} under the control, LY, and R8G irradiance (day 8), respectively. Algae receiving LY and R8G irradiations exhibited no significant difference in biomass concentrations when compared to the control ($p > 0.05$). The adaptability of *C. reinhardtii* to the increased light availability could perhaps explain why the wavelength conversion had no clear effect on biomass. As the density of the culture increased the overall biomass production increased up to day 8 but then decreased (between 0.88 – 1.16 gL^{-1}). This occurrence varies extensively depending on light irradiance and microalgal species, as previously observed (Duarte and Costa 2018; Ajayan *et al.* 2019). As biomass levels increased, light in the culture medium was attenuated, which led to the self-shading effect and the decrease in biomass (Sforza *et al.* 2012; Abu-Ghosh *et al.* 2015). The apparent re-growth after day 10 (Figure 4.5) could have been due to bacterial/fungal contamination resulting from frequent sampling.

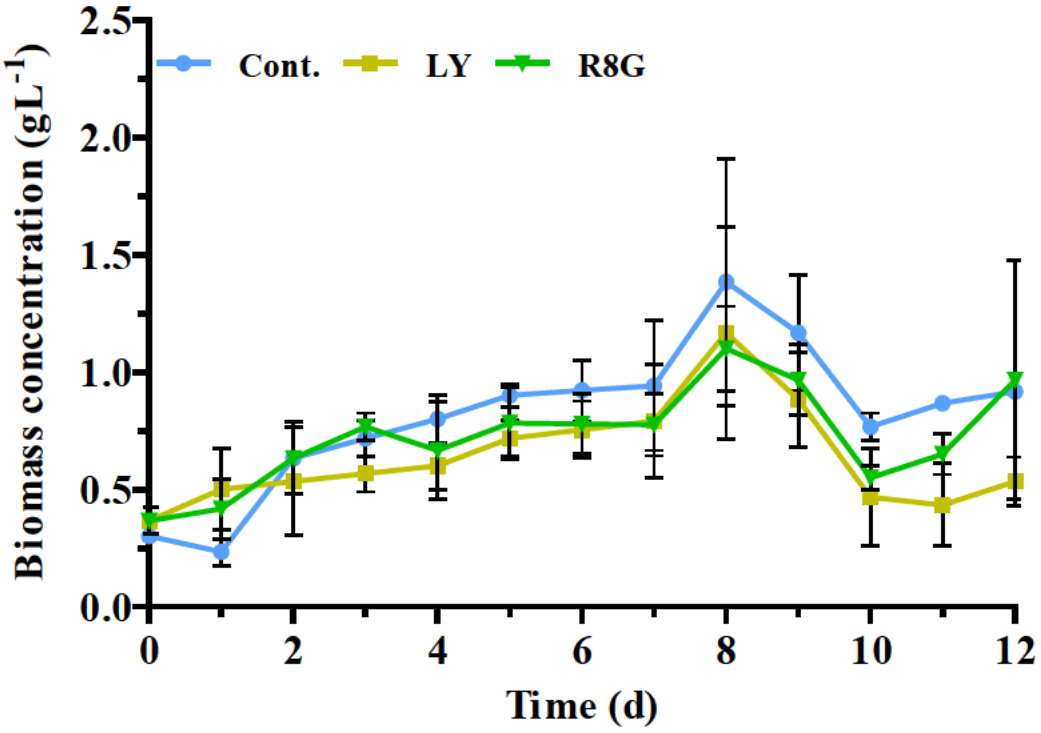

Figure 4.5: Growth curves of *C. reinhardtii* grown under control (Cont.), Lumogen Yellow (LY), and Rhodamine 8G (R8G) under artificial daylight tubes. Control reactors were

set up where the microalgal cells received light passing through a methanol blank. Data are expressed as a mean ± SD (n = 3).

Increased dye-irradiations from LY and R8G induced acclimation responses which imposed metabolic burdens that lowered biomass productivity. Similar results were obtained by Straka and Rittmann (2018). Baer *et al.* (2016), showed that biomass productivity increased with a decrease in the red wavelength, thus excessive red radiation was detrimental to the algae. Microalgae do not grow well under excess full red illumination as this decreases the rate of cell division due to metabolic shifts. Rapid shifts in light irradiance lead to photo-damage and a decrease in biomass production (Straka and Rittmann 2018). However, the cells can be repaired by low-intensity blue light exposure. This occurs because blue light promotes gene transcription thereby enhancing enzyme regulation (Seo *et al.* 2015).

Sung *et al.* (2018), attempted to improve the light utilisation efficiency in *N. gaditana* under batch cultivation mode employing DPA, R110, and R101 as spectral converters (Table 2.4). Results showed that there was substantially higher biomass produced under the enriched light of DPA and R101. *Nannochloropsis* growth was impaired under R110. The dye converted blue to green light. The reduction of blue light appeared to negatively affect growth at the early stage. Final biomass concentration under DPA, R101, R110 and control conditions reached 2.7, 2.8, 2.2, and 2.0 gL^{-1}, respectively. The study demonstrated the wide applicability of three organic dyes and the potential for spectral conversion in algal systems.

Similarly, Seo *et al.* (2015) found that DPA and R101 irradiations stimulated the growth accumulation of *C. vulgaris* (Table 2.4). Biomass concentrations reached 1.4 gL^{-1} when utilising DPA at a light intensity of 100 Wm^2 (~ 210 µmol photons$\cdot m^{-2} \cdot s^{-1}$). With R101 at 100

Wm^2, biomass concentrations reached 1.7 gL^{-1}, which was similar to the growth at 150 Wm^2 (~ 315 µmol photons·m^{-2}·s^{-1}) without using an organic dye. It was evident from the studies that the DPA dye was effective at promoting the growth and lipid production of both *N. gaditana* and *C. vulgaris* (Seo *et al.* 2015; Sung *et al.* 2018). In contrast to the cited literature, the current study showed no observable increase in biomass concentrations. However, it is important to note that in the reported studies (Seo *et al.* 2015; Sung *et al.* 2018), different algal species were studied using different light sources while employing varying light intensities. Hence the biomass concentrations and growth kinetics differed. Interestingly the study by Seo *et al.* (2015), did not elucidate the possible mechanisms behind the growth and the varied responses in connection with chlorophyll biosynthesis.

4. 3. 4. Effects of dye-mediated irradiance on pigment production in *C. reinhardtii*

Total chlorophyll content was analysed to validate the effects and influence of irradiation on the growth of *C. reinhardtii* (Figure 4.6). Initially, the chlorophyll content in *C. reinhardtii* was approximately 10 mgg^{-1}. Microalgae respond to changes in light irradiations by modulating the composition of their photosynthetic apparatus. Consequently, fluctuations in cellular pigment concentrations affect the light absorption capacity of microalgae (Baer *et al.* 2016; Yarnold *et al.* 2016). Cultures grown under R8G demonstrated higher chlorophyll concentrations on day 4 (~ 15 mgg^{-1}), with a 45 *wt.* % increase when compared to the control (8 mgg^{-1}). When compared to LY-irradiated cultures, R8G grown cultures exhibited higher chlorophyll content between days 2 to 8. Increased chlorophyll pigments resulted from the variation in light spectra between dyes and control.

Other studies regarding the effects of light pigment contents have come to similar conclusions (Kim *et al.* 2014; Baer *et al.* 2016). Vadiveloo *et al.* (2015), observed that the chlorophyll *a* content in *Nannochloropsis* sp. was three times higher when grown using blue-green (~ 60 *wt.* %) and blue lights (~ 60 *wt.* %) when compared to red (~ 10 *wt.* %), white (~ 10 *wt.* %), or pink (~ 20 *wt.* %), data extrapolated from Figure 4 in reference Vadiveloo *et al.* (2015). The higher production of chlorophyll *a* under blue light was attributed to complementary chromatic adaptation. This is a process where the major light-harvesting pigments are regulated to match the absorption spectra patterns of the incident light used for cultivation. Generally, changes in chlorophyll content are species-specific and vary depending on the growth condition, yet the responses to light spectra and exposure may have similar outcomes in terms of chlorophyll production in algae (Vadiveloo *et al.* 2015). Cultures grown under LY demonstrated the highest chlorophyll concentrations on day 10 (42 mgg^{-1}). The major *in vivo* chlorophyll absorption signature occurs in the blue and red regions of the PAR spectra (Vadiveloo *et al.* 2015). Hence, the increased pigment content could be due to the proportion of red to blue light emissions by the dyes (Table 4). The red light emitted was directly absorbed by chlorophyll molecules (Eroglu *et al.* 2013; Nwoba *et al.* 2019).

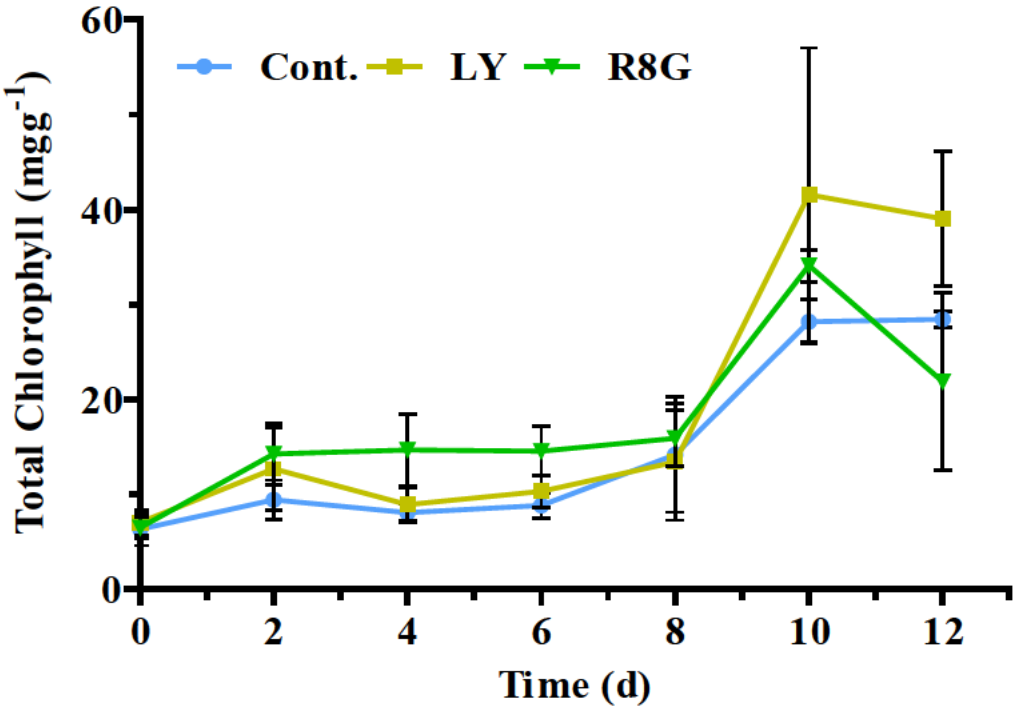

Figure 4.6: Total chlorophylls content of *C. reinhardtii* grown under control (Cont.), Lumogen Yellow (LY), and Rhodamine 8G (R8G) under artificial daylight tubes. Control reactors were set up where the microalgal cells received light passing through a methanol blank. Data are expressed as a mean ± SD (n = 3).

Initially, the carotenoid content in *C. reinhardtii* was low (~ 2 mgg^{-1}). Microalgae grown under the blue-green emissions of R8G exhibited increased carotenoid concentrations over control cultures between days 2 to 10 (Figure 4.7). On day 4 there was a 37% increase in carotenoids under R8G irradiance (5 mgg^{-1}). Photo-regulation of the cultures were initiated in the earlier stages of growth due to increased light irradiance (Figure 4.5), (Yarnold *et al.* 2016). As carotenoids make up the core complexes of both PSI and PSII and in the Cyt b_6f complex, they promote the stability and functionality of the photosynthetic apparatus (Gong and Bassi 2016). Ajayan *et al.* (2019) observed similar findings with regards to pigment production in *C. reinhardtii*. It was found that the maximum total chlorophyll and carotenoid content were observed under blue light. This was ascribed to the changes in the expression of chlorophyll-

binding proteins and genes at transcriptional and post-transcriptional levels. Blue light stimulated the up-regulation of phytoene synthase and desaturase *via* carotenoid biosynthesis. The researchers suggested that the increase in carotenoid/chlorophyll synthesis in *C. reinhardtii* may be a direct result of light stress. The pigments were produced as a mechanism to protect the cells from photo-inhibition.

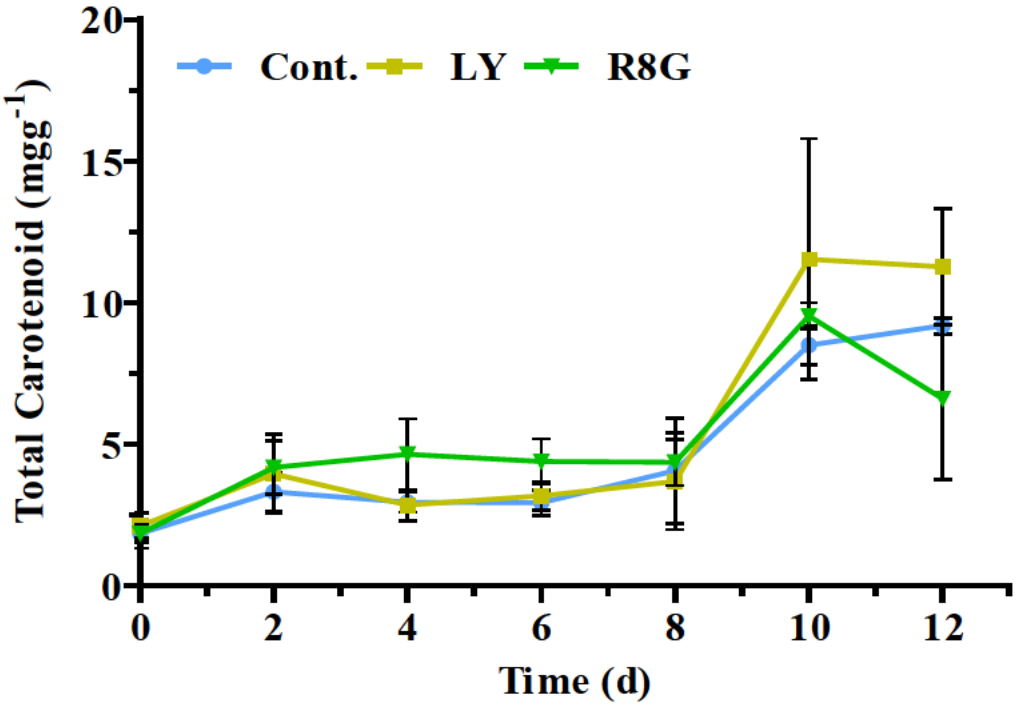

Figure 4.7: Total carotenoid content of *C. reinhardtii* grown under control (Cont.), Lumogen Yellow (LY), and Rhodamine 8G (R8G) under artificial daylight tubes. Control reactors were set up where the microalgal cells received light passing through a methanol blank. Data are expressed as a mean ± SD (n = 3).

The highest carotenoid yield was obtained on day 10 under LY-mediated irradiance (12 mgg^{-1}). This represented a significant increase of 33% as compared to the control ($p < 0.05$). The LY dye exhibited higher efficiency for the transfer of photons from the UV region to a wide range of visible wavelengths, (Figure 3.3 B). Consequently, LY emitted 31% more AFI

than R8G, (Table 3.2). This spectral property was advantageous for algal cultivation. Accordingly, cultures grown under LY received a 38 and 19% increase in red and blue irradiations. The simultaneous increase in both chlorophyll and carotenoid pigment contents in the cultures under dye irradiance on day 10 was attributed to the self-shading effect. Increased biomass levels led to attenuated light conditions in the PBRs which stimulated pigment biosynthesis for light capture (Sforza *et al.* 2012; Abu-Ghosh *et al.* 2015). Under reduced light availability algae increase their photosynthetic carotenoid content to aid in light-harvesting outside the range of chlorophyll pigments (Varela *et al.* 2015; Gong and Bassi 2016; Wobbe *et al.* 2016). The light energy that is captured is transferred to the P680 core complex, where it is trapped and used to drive electron flow through the rest of the photosynthetic process (Chapter 2, section 2. 4. 1).

4. 3. 5. Effects of dye-mediated irradiance on the physiological responses of *C. reinhardtii*

Cultures grown under increased irradiance demonstrated spiked NPQ values (Figure 4.8). Light stress was observed by the increased NPQ from 0.050 to 0.283 on day 2. This implied that the algal cells required an initial dye-acclimation stage that lasted approximately two days. Initial increases in PSII energy dissipation implied that dye-mediated irradiations were excessive, and photo-damage had occurred. Light stress is known to damage thylakoid membranes which are related to structural and functional changes of the PSII and PSI, thereby interrupting the CBB cycle (Nawrocki *et al.* 2019a; Nawrocki *et al.* 2020). Consequently, the electron flow and the reemission of energy as fluorescence light may have been disrupted, rather than directed to fuel the photochemical processes (Roach *et al.* 2020; Meagher *et al.* 2021). Interestingly, Nowicka (2020) showed that when grown under low light, *C. reinhardtii*

is not able to effectively induce NPQ, while cultivation under high light irradiances makes this microalga capable of efficient NPQ development. The researchers studied the practical aspects of the measurements of non-photochemical chlorophyll fluorescence quenching in *C. reinhardtii*. Hence, the increased irradiation from the dye emissions was in excess to significantly induce a higher NPQ level when compared to the low PFD control cultures. The NPQ was not active between days 4 and 6 (Figure 4.8), indicating that microalgae were able to regulate and utilise the dye-mediated irradiations. Excess light energy, not absorbed, may have been reflected or dissipated as heat *via* chlorophyll/carotenoid-based quenching mechanisms (Figure 2.5). Hence the reduction in NPQ on day 5 (Figure 4.8). The highest NPQ values were exhibited on day 12. This ranged between 0.5 – 0.9 in all cultures. The absorbed photons exceeded that which were utilised for photosynthesis which resulted in the re-activation of NPQ (Natali and Croce 2015; Quaas *et al.* 2015).

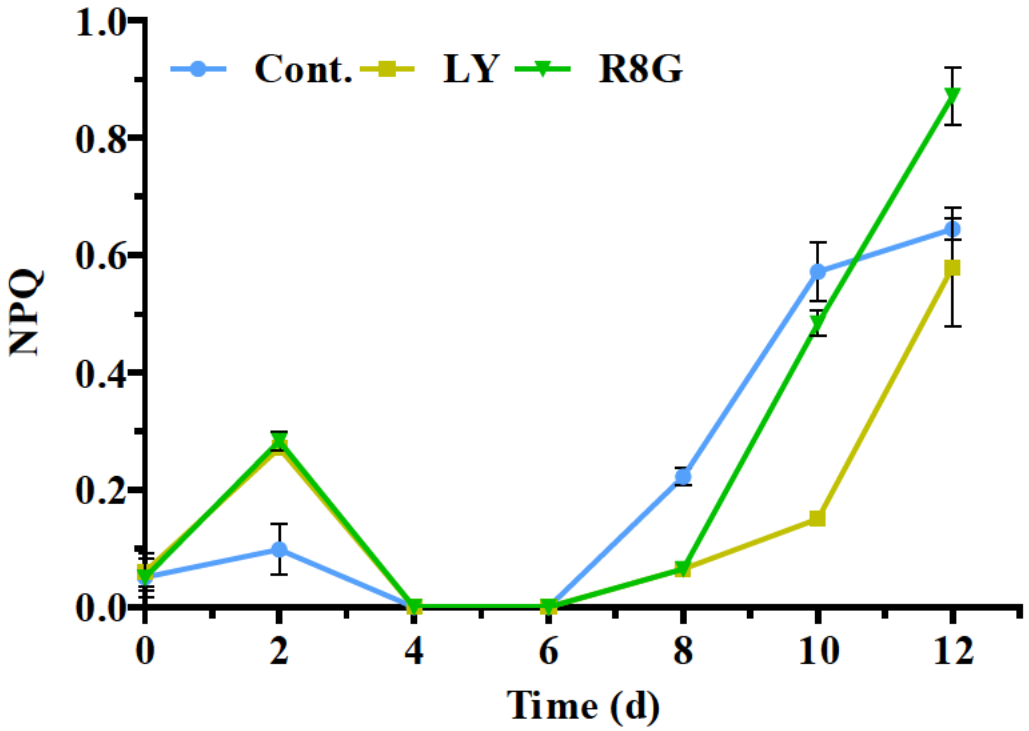

Figure 4.8: Non-photochemical quenching (NPQ) of *C. reinhardtii* grown under control (Cont.), Lumogen Yellow (LY), and Rhodamine 8G (R8G) under artificial daylight tubes, **(A)**

and **(B)** Quantum efficiency (F_v/F_m). Control reactors were set up where the microalgal cells received light passing through a methanol blank. Data are expressed as a mean ± SD (n = 3).

The NPQ capacity of microalgae can be regarded as one of the most sensitive factors when dealing with light irradiance (Natali and Croce 2015; Quaas *et al.* 2015). It reflects a conglomerate of different molecular processes encompassing: qE (energy-dependent quenching); qI (photo-inhibitory quenching); and qT (state transitioning) (Chapter 2, section 2. 6). Studies have shown that when grown under increased PFDs, *C. reinhardtii* xanthophyll production is less important for qE while the crucial role is played by the *lhcsr* proteins (Nowicka 2020; Roach *et al.* 2020; Meagher *et al.* 2021). In *C. reinhardtii*, exposure to increasing light results in a rapid quenching of the PSs antennae, which are associated with the presence of *lhcsr*3 and *lhcsr*1. These *lhcsr* proteins act as pH-sensitive switches between the light-harvesting and photo-protective state. Consequently, at later stages, this quenching can be correlated with the amount of de-epoxidised xanthophylls (Natali and Croce 2015; Quaas *et al.* 2015). The observations implied there was a low contribution of the cumulative xanthophyll cycle in NPQ (previously described in Chapter 2, section 2. 6. 1), however, the role of respiration cannot be excluded from the NPQ analyses. Also, the extent of qE is lowered by acetate in the growth medium. In the presence of acetate, the over-reduced state of the mitochondrial ETC causes the generation of ROS, thereby contributing to the establishment of photo-inhibition, as seen in previous studies (Esquivel *et al.* 2017; Meagher *et al.* 2021). However, a clearer insight into photochemical energy utilisation and the NPQ process is essential.

Chlamydomonas reinhardtii showed good physiological performance under increased dye-mediated irradiance, although with variable success, suggesting different degrees of

sensitivity and physiological strategies (qE or qT). The findings are similar to studies carried out by other researchers (Nawrocki *et al.* 2019b; Nowicka 2020; Meagher *et al.* 2021), indicating that state transitioning may be responsible for the major part of the NPQ process as it is predominant in *Chlamydomonas*. The variations in the NPQ parameter could be attributed to the differences in state transitions, in *Chlamydomonas* and the main contributor to the NPQ (Nowicka 2020). Upon changes in spectral quality and quantity, a reorganisation of the algal antennae occurs to ensure a balanced excitation of the two PSs and hence an optimal photosynthetic quantum yield. This process involves the reversible displacement of the PSII antenna to PSI under conditions in which PSII is overstimulated relative to PSI. The function of qT in *C. reinhardtii* is the regulation of the electron flow (Nowicka 2020; Roach *et al.* 2020; Meagher *et al.* 2021). Electrons were diverted to alternative pathways such as PSII-mediated cyclic processes. The ATP and reducing equivalents produced were used in metabolic processes including pigment formation, nutrient assimilation, and cellular repair (Quaas *et al.* 2015; Yarnold *et al.* 2016). This reduced PE resulted in declined growth in *C. reinhardtii*, hence, the amplitude of NPQ was consistent with the start of dye-acclimation (Figure 4.5). Consequently, changes in the carotenoid concentrations reflected the role of these pigments in modulating PS activities (Varela *et al.* 2015; García-Cañedo *et al.* 2016). These pigments may have been produced for light regulation to improve quantum efficiencies in the algae (Figure 4.9).

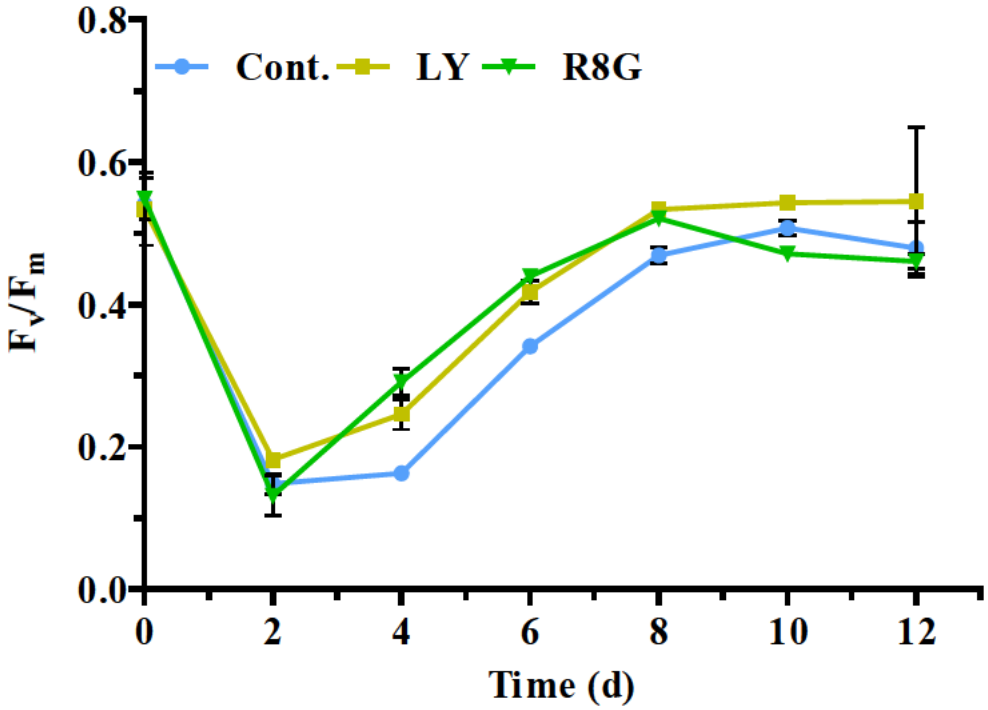

Figure 4.9: Quantum efficiency (F_v/F_m) of *C. reinhardtii* grown under control (Cont.), Lumogen Yellow (LY), and Rhodamine 8G (R8G) under artificial daylight tubes. Control reactors were set up where the microalgal cells received light passing through a methanol blank. Data are expressed as a mean ± SD (n = 3).

The F_v/F_m ratios of algae grown under dye-mediated irradiance and control cultures followed a similar trend (Figure 4.9). All cultures demonstrated high F_v/F_m values at the start of experimentation (~ 0.6). Decreased F_v/F_m values between days 0 to 2 (from approximately 0.6 to 0.2), indicated reduced PSII function which could be attributed to acclimation and/or adaptation to increased dye-mediated irradiance. Furthermore, acetate assimilation may result in the down-regulation of photosynthesis, stimulation of respiration and/or chloro-respiration, and the reduction of intersystem electron transfer. Growth during this time could also be attributed to respiration. During this period the cells were actively dividing to regulate the excess light. This may account for the gradual increase in the biomass levels between these days. Similarly, Sung *et al.* (2018) noticed that *N. gaditana* required a 2 – 3-day photo-adaption

period (acclimation), characterised by lower F_v/F_m values when grown under DPA and R101 irradiance. Correspondingly, *Chlamydomonas* PSs were under photo-oxidative stress from increased dye-mediated irradiance, evident by the increased NPQ (Figure 4.8). The rate of endogenous light decay was relatively more significant resulting in a net decrease in microalgal light utilisation efficiency (Figure 4.9). When microalgae are exposed to increased irradiations, PSII is repeatedly damaged and needs to be continually repaired *via* the re-synthesis of damaged components such as proteins (Yarnold *et al.* 2016; Meagher *et al.* 2021). The repair of damaged PSs along with the dissipation of thermal energy further reduced the overall efficiency of light utilisation by the algae. This has been previously described by researchers (Yarnold *et al.* 2016; Meagher *et al.* 2021), affirming that mechanisms that prevent photo-damage tend to cause a reduction in light utilisation efficiency. This was also reflected in the decreased rate of microalgal growth (Figure 4.5).

After the dye-acclimation phase, growth increased followed by a 47 and 34% increase in quantum efficiency under R8G, and LY when compared to the control (day 4). Increased F_v/F_m ratios are indicative of active photosynthesis and are correlated with increased cell densities and growth rates (Sung *et al.* 2018). The highest F_v/F_m ratios exhibited by the control, LY and R8G cultures were seen between days 8 to 10, (0.4 – 0.5). Quantum efficiency was higher in the cultures grown under dye-mediated irradiance. Likewise, Sung *et al.* (2018), noticed that the highest F_v/F_m ratios in *N. gaditana* were exhibited under DPA and R101 emissions than when compared to the control. Increased quantum efficiency was attributed to an increase in chlorophyll *a*. A similar observation was seen in the current study. With an increase in chlorophyll production (Figure 4.6), there was an increase in the F_v/F_m ratios (Figure 4.9), implying that the increased portion of chlorophyll was related to elevated photochemical efficiency. One possible limitation in the PAM fluorometry experiments was that negative

controls were not used to validate the photosynthetic performance in *C. reinhardtii*. These controls (using herbicides such as atrazine or diuron) block photosynthesis and show a significant impact on several chlorophyll fluorescence parameters (Gomes *et al.* 2017).

The effect of increased dye-mediated PFDs on the growth of *Chlamydomonas* was not pronounced, yet this manifested indirectly through increased production of metabolites (primary/secondary) that function as defences against excess irradiation. The light-harvesting ability of *Chlamydomonas* was significantly affected by increased PFDs. Toward the end of the growth cycle increases in carotenoid content was ascribed to light-harvesting, and therefore, is consistent with the hypothesis that increased dye-mediated PPFDs stimulated carotenoid production. Increased PFDs were indirectly responsible for carotenoid productivity as a means of photo-regulation (acclimation). From this standpoint, the photo-acclamatory response to increased dye-mediated irradiance can be used as a strategy to induce metabolite accumulation (carotenoid, protein, carbohydrate, and lipid). To stimulate photo-regulatory metabolites, dye-irradiance should exceed 75 µmol photons·m^{-2}·s^{-1}. This assumption can be validated by the current findings with increases in NPQ. Thus, a more realistic light source emitting higher UV irradiance was required to adequately excite dye molecules and achieve higher dye-mediated PFDs. Additionally, to ensure verifiable results and to further assess the emission potential of the dyes, the dye conversion abilities and fluorescence lifetimes needed to be determined. Hence, the continued focus of the research was to further the understanding of the dye properties under higher UV stimulation and study these effects on the microalgal photo-acclamatory response.

4. 4. Conclusion

A comparison between the basic growth characteristics obtained (*i.e*., growth rate, chlorophyll and carotenoid yield, and biomass production) showed that *Chlamydomonas* isolate C1 did not differ fundamentally against matching data in the literature. The change in PFDs from the dye-irradiance spiked the production of pigments in the cultures. Under LY and R8G irradiance, *C. reinhardtii* showed a 32 and 45% increase in chlorophyll and a 37% increase in carotenoids. The dye irradiance caused the cultures to enter photo-acclimation which was evident by the increased NPQ. In the earlier stages of growth, there was an increase in light availability which corresponded to a stressed condition. Photo-regulation (acclimation) was exhibited by decreased growth, increased pigment, increased NPQ (65%), and decreased quantum efficiencies of PSII (from ± 0.553 to ± 0.278), to expend excess irradiation. Additionally, to illicit a significant response on *C. reinhardtii* growth and/or metabolite production, there should be an increase in light intensity. Consequently, the fluorescent dyes need to be sufficiently excited using UV radiation. This response can be used as a strategy to induce metabolite production.

Chapter 5 : Evaluation of UV-mediated dye spectral conversion and assessment of the light utilisation and metabolite production in *C. reinhardtii*

Ramanna, L., Nasr, M., Rawat, I. and Bux, F. 2022. UV-mediated photosynthesis – An effective method to enhance incident light availability in *C. reinhardtii* for metabolites production and sustainable development. *Biomass and Bioenergy* (submitted).

5. 1. Introduction

It has been shown that abundant light provides energy for microalgal cell growth, whereas higher light exposures lead to photo-inhibition. The algal chloroplasts are most affected by excessive light conditions. In the microalgal PSII, the excess energy can generate a 3Chl* which passes excitation energy to O_2, producing $1O_2$* (Chapter 2, section 2. 6. 1), (Varela *et al.* 2015; Wobbe *et al.* 2016). Also, under abiotic stress, over-reduction of PSI leads to the generation of the O_2^- and subsequently H_2O_2 (Quaas *et al.* 2015; Girolomoni *et al.* 2019). When in excess, ROS breakdown nearby membrane lipids in the chloroplasts or structures in the cytosol affecting algal metabolism in two ways; (*i*) through the redox signalling pathways or, (*ii*) at an extremal ROS accumulation level, through less specific cytotoxic damage of cellular components (Varela *et al.* 2015; Wobbe *et al.* 2016).

Under increased PFDs, metabolites such as proteins, carbohydrates, and lipids play pivotal roles in the photo-protection (acclimation) of the algal photosynthetic apparatus. Due to their specific acclimation responses, microalgae are usually cultivated using stress-based

strategies to improve the production and conversion of process-compatible metabolites (Nama *et al.* 2018; Sun *et al.* 2018). Acclimation (photo-regulation) in response to stress can play a key role in metabolite biosynthesis (Nama *et al.* 2018; Sun *et al.* 2018). Hence, significant research efforts are needed to comprehend the relationship between essential factors (such as the spectral composition of light) and the productivity of photosynthetic microalgal cells (Kumar *et al.* 2021).

Dye fluorescent emissions were monitored and the spectral energy conversion capabilities of the R8G, LY, and LR dyes were evaluated under UV excitation. The algal growth and biochemical constituency were analysed in terms of protein, carbohydrate, lipid, and pigment content. The light utilisation efficiency of *C. reinhardtii* was determined using physiological analyses, of which gene expression studies were conducted to verify these findings. Additionally, multivariate analysis was used to describe the correlations between dye fluorescence, microalgal biomass, metabolite production, and physiological status. Thus, the goal of the research was to establish an efficient dye-based strategy for tailoring specific algal metabolite over-production. This chapter aimed to assess the effects of increased UV-mediated dye-irradiations on metabolite production in *C. reinhardtii*.

5. 2. Materials and Methods

5. 2. 1. Dyes and fluorescence spectra

Rhodamine 8G and LY dyes were dissolved in methanol at 10 mgL^{-1} while LR was dissolved at 100 mgL^{-1}. The dyes were stimulated using T8 terrarium fluorescent tubes containing 30% UV-*a* and 5% UV-*b* (Reptistar T8 [F18W/6500K]) (Sylvania, UK). Based on

the findings from the previous chapter, the UV radiation was hypothesised to sufficiently excite dye molecules. Specifically, UV *a* and *b* wavelengths were used as these occur between 320 – 400 and 280 – 315 nm, respectively. The PFDs before experimentations were measured to quantitatively determine the amount of additional PAR in the PBR that was provided by the fluorescent dyes compared to the control and to determine the amount of UV irradiation that was absorbed by the dyes. Irradiance measurements were taken for four hours outside and inside the PBRs (without algae) at constant height (20 cm). Reactors received ± 115 $m^{-2}s^{-1}$ PAR which was measured using a PAR Vernier probe while UV light was measured using UV-*a* and UV-*b* probes (UVA-BTA UVA1610R1, UVB-BTA UVB3515R2), (Vernier, USA). The Beer-Lamberts Law was used to calculate the amount of light absorbed by the dyes and transmitted into the PBRs:

$$A = -log10\ [\frac{I}{I0}]$$

Equation 5.1: Beer-Lamberts Law

$$T = [\frac{I}{I0}]$$

Equation 5.2: Light transmission

Where *A* and *T* represented the light absorbance and transmittance, respectively, both expressed as a percentage. *I* and I_0 represented the transmitted and incidental irradiance, respectively.

To gain insight into the lifespan and the energy converted and released by the dyes, fluorescent emissions were analysed every two days. These were accomplished using a

Spectrofluorometer as per section 3. 2. 1. The Planck relationship was used to calculate the energy of a photon as per Equation 5.3.

$$E = hf$$

Equation 5.3: Energy of a photon

Where *E* represents energy in Joules (J), *h* represents the Plank constant which is 6.63×10^{-34} Js^{-1}, and *f* represents the frequency. The relationship between wavelength and frequency is:

$$f = \frac{C}{\lambda}$$

Equation 5.4: Frequency and wavelength relationship

Where *f* is frequency, the speed of light [C] equals 3.00×10^{8} ms^{-1}, and λ is the specific emission wavelengths in meters (m) (Langhals 2020).

5. 2. 2. Growth of *C. reinhardtii* under UV-mediated irradiance

Chlamydomonas was grown in TAP medium and initially acclimated for 4 days under 16:08 hr light/dark periods to the 30% UV-*a* and 5% UV-*b* fluorescent tubes (Reptistar T8). The higher percentage of UV light from these tubes were expected to intensify dye excitation. Experiments were conducted in PBRs as per section 4. 2. 2. 1. Reactors received ±115 µmol photons·m^{-2}·s^{-1} of light. Inoculum sizes on day 0 were approximately 0.3 gL^{-1} (DCW). Ampicillin (50 µgmL^{-1}) was added to the culture medium to prevent bacterial contamination. Methanol without any dye was used as the positive control while *Chlamydomonas* was grown in the dark to achieve a negative control.

Due to the consistency of the results from the previous chapter, microalgal growth was monitored by changes in absorbance values at 750 nm using a spectrophotometer (Yarnold *et al.* 2016). Biomass concentrations were determined indirectly by correlating absorbance readings with DCW (Appendix E). Biomass concentrations were calculated using Equation 5.5.

$$y = 0.981x - 0.272, r^2 = 0.9993$$

Equation 5.5: Dry cell weight correlation

Biomass values were used to calculate average growth rates (μ), as per Equation 4.1.

5. 2. 3. Photo-physiological analyses

The vitality of the microalgal cellular photosynthetic apparatus was monitored as above using a PAM fluorometer. To gain an understanding of photosynthetic light utilisation, critical data was extrapolated from the RLCs that yielded information relating to the partitioning of the absorbed photons between photochemical and non-photochemical energy utilisation. These included the quantum yields of the three pathways of photosynthetic energy utilisation, (*i*) effective PSII quantum yield [Y(II)] (photochemical energy utilisation), (*ii*) regulated energy dissipation [Y(NPQ)], and (*iii*) non-regulated energy dissipation [Y(NO)]. Fluorescence parameters were calculated automatically by the Dual-PAM software based on the equations below:

$$\mathrm{Y(II)} = \frac{(\mathrm{F'_m} - \mathrm{F})}{\mathrm{F'_m}}$$

Equation 5.6: Yield of light utilisation

$$Y(NPQ) = \frac{1 - Y(II) - 1)}{(NPQ + 1 + qL\left(\frac{Fm}{F0} - 1\right))}$$

Equation 5.7: Yield of regulated energy dissipation

$$Y(NO) = \frac{1}{(NPQ + 1 + qL\left(\frac{Fm}{F0} - 1\right))}$$

Equation 5.8: Yield of non-regulated energy dissipation

Where the fluorescence yield, F, was assessed in conjunction with the application of the SP. The parameters F'_m, F_m, and F_0 have been described previously (Chapter 4 section 4. 2. 4), and qL represents the coefficient of photochemical quenching (Nama *et al.* 2018; Yadav *et al.* 2020). The NPQ represents the non-photochemical quenching index. Under all scenarios, the sum of all quantum yields amounts to 1 as shown by the equation below:

$$Y(II) + Y(NPQ) + Y(NO) = 1$$

Equation 5.9: Sum of quantum yields

5. 2. 4. Gene expression studies

5. 2. 4. 1. RNA extraction, cDNA synthesis, and PCR

Total ribonucleic acid (RNA) was extracted with the Qiagen RNeasy Plant Mini Kit following the manufacturer's protocols (Qiagen, Germany). Briefly, algal samples were collected using a pipette and centrifuged for 10 min at 2.091 × g. Supernatants were discarded, and pellets were washed with dH_2O, and re-centrifuged. Thereafter, the cells were washed with

2 mL RNA*later* solution for RNA stabilisation (Thermo Fischer Scientific, USA), and ~ 30 mg samples (fresh weight) were dissolved in lysis buffer and subjected to 10s bead beating using a bead mill homogeniser (Bead Ruptor 12) (Omni International, USA). Lysates were transferred to 2 mL shredder spin columns using a pipette and centrifuged for 2 min at full speed using a Sigma 1-14K centrifuge (≥ 8000 × g) (Sigma, Germany). The flow-through supernatants were transferred to 2 mL Eppendorf tubes. A half volume of ethanol (96 – 100%) was added to the cleared lysates and mixed by pipetting. Samples were transferred to RNeasy spin columns and centrifuged for 15 s at ≥ 8000 × g. Spin columns were retained while the flow-throughs were discarded. A series of buffers were added to the spin columns. These were used to wash and purify the RNA. Buffers were removed by centrifuging for 15 s at ≥ 8000 × g. The RNeasy spin columns were then placed in new Eppendorf tubes. To elute the RNA, 50 µL RNase-free water was added to the spin column membranes and centrifuged for 1 min at ≥ 8000 × g. Total RNA concentrations, integrity, and purity were measured at 260/280 nm with a nanophotometer (Implen, USA). The RNA transcript absorbance ratios at 260 and 280 nm were ~ 2.0, which generally indicates that the RNA was pure and not degraded.

Reverse transcription (RT) was carried out using the RevertAid First Strand complementary DNA (cDNA) synthesis kit as per the manufacturer's protocols (Thermo Fischer Scientific, USA). A positive control glyceraldehyde-3-phosphate dehydrogenase (GAPDH) mouse RNA template and gene-specific primers were supplied with the kit (Table 5.1). This was run with the samples and used to confirm cDNA synthesis. Briefly, reaction mixtures contained 50 ng RNA, 0.4 µM forward kit primer, 0.4 µM reverse kit primer, 4 µL 5X reaction buffer, 1 µL RNase inhibitor, 10 mM deoxynucleoside triphosphates (dNTPs), and 1 µL RT enzyme. Reaction volumes were made up to 20 µL using RNase-free water. The samples were thoroughly vortexed and incubated at 25 °C for 5 min, then at 42 °C for 60 min.

Reactions were terminated by heating to 70°C for 5 min. Total cDNA concentrations, integrity, and purity were measured with the nanophotometer used previously. The newly synthesised cDNA was used as a substrate for the PCR. The oligonucleotide sequences of primers used for the PCR can be seen in Table 5.1.

KAPA Taq ReadyMix PCR Kit was used for cDNA amplification (KAPA Biosystems, USA). The PCR assay was performed using a Veriti 96 well thermal cycler (Applied Biosystems, USA). Primers were selected to target a key functional gene involved in photosynthesis (RuBisCo large subunit [rbcL]) (Giridhar Babu *et al.* 2017). The expression level of the 18S ribosomal RNA (rRNA) gene was unaffected by different experimental factors throughout all experiments (control and dye-specific PFDs) and was, therefore, used as the reference gene in this study (Giridhar Babu *et al.* 2017). For quality assurance, GAPDH cDNA, no template control (NTC), and no RT (NRT) controls were run as positive and negative controls, respectively.

Table 5.1: Primers used for gene expression studies.

Gene	Primer Sequence	Amplicon size (bp)	Annealing Temp. (°C)	Reference
rbcL	(F) ATACCGTGTGGAGGACCTTG (R) AGCCAGTTCCAGGTGAAGAA	201	56	(Giridhar Babu *et al.* 2017)
18S	(F) CCTGCGGCTTAATTTGACTC (R) GCGAACCAACCGTGACTATT	192	55	
GAPDH	*	496	58	As per kit.

bp- Base pairs; F- Forward; R- Reverse, *- not supplied with kit instructions.

Briefly, reaction mixtures contained 50 ng cDNA, 1X KAPA Taq ReadyMix, 0.4 µM forward, and 0.4 µM reverse primers. Reaction volumes were made up to 25 µL using RNase-free water. The PCR protocol consisted of an initial denaturation for 3 min at 95°C, followed by 35 cycles of melting (30 s at 95 °C), gradient annealing (30 s at 53 – 65 °C), and extension (1 min at 72 °C). For product verification, gel electrophoresis was run using lithium acetate borate (LAB) gels and LAB buffer (Appendix F) (Brody *et al.* 2004). For referencing DNA size, the FastRuler low range DNA ladder was used (Thermo Fischer Scientific, USA). Gels were viewed on a ChemiDoc XRS+ molecular imager (Bio-Rad Laboratories, USA). The gels were subjected to 300V for 5 min (Appendix G).

5. 2. 4. 2. Real-Time qPCR

The PowerUp™ SYBR™ Green Master Mix was used for Real-Time qPCR (Applied Biosystems, USA). The qPCR assay was performed using the CFX96 Touch™ Real-Time PCR Detection System (Bio-Rad Laboratories, USA). Briefly, the reaction mixtures contained 50 ng cDNA, 1X SYBR Green qPCR Ready Mix, 0.4 µM forward, and 0.4 µM reverse primers. Reaction volumes were made up to 25 µL using RNase-free water. The qPCR amplification protocol consisted of a 95 °C for 3 min activation of the polymerase followed by 40 cycles of melting (10 s at 95 °C), gradient annealing (30 s at 55 – 65 °C), and extension (1 min at 72 °C). Fluorescence was monitored continuously to confirm amplification specificity. Gene expression studies were conducted in triplicate on days 4 and 8. For quality assurance, GAPDH cDNA, no template control (NTC), and no RT (NRT) controls were run as positive and negative controls, respectively.

A melt curve (65 – 95 °C at a rate of 0.5 °C s^{-1}) was performed at the end of the amplification reaction for product verification and to check for the possible primer-dimer formation. The control GAPDH, rbcL, and rRNA amplicons melted at 88, 76.6, and 82.5 °C, respectively (Appendix H). All primer sets showed efficiencies of 100 – 110%. The temperature of the melt peaks (T_m) was calculated based on the initial fluorescence curve by plotting the negative derivative of fluorescence versus temperature. Equation 5.10 was used to analyse the relative gene expression (Ma *et al.* 2019).

$$2^{-\Delta\Delta Ct}$$

Equation 5.10: Relative fold gene expression formula

Where *Ct* represented the cycle threshold of the sample. It is the cycle number where the fluorescence generated by the amplicon is distinguished from the background noise. Delta (Δ) is used to describe the difference between two numbers. Δ*Ct* is defined by Equation 5.11 as:

$$\Delta\Delta Ct = \Delta Ct_{(treated\ sample)} - \Delta Ct_{(untreated\ sample)}$$

Equation 5.11: Delta-delta *Ct* formula

Where Δ*Ct* represented the difference between the Δ*Ct* values of the treated sample (dye-irradiated) and the untreated sample (control). Δ*Ct* is defined by Equation 5.12 as:

$$\Delta Ct = Ct_{(target\ gene\ )} - Ct_{(housekeeping\ gene)}$$

Equation 5.12: Delta *Ct* formula

Where Δ*Ct* represented the difference in cycle threshold values for the gene of interest and the housekeeping gene for the given sample.

The data obtained represented the fold change (increase or decrease) of the target gene in dye-irradiated cultures relative to the control sample and was normalised to the expression of the endogenous 18S rRNA reference housekeeping gene. The CFX Manager ™ Software version 3 for Windows was used to analyse the qPCR data and draw melt curves (Bio-Rad Laboratories, USA).

5. 2. 5. Biochemical analyses

The influence of increased dye-mediated PFDs on the biochemical composition of *C. reinhardtii* was determined in terms of metabolite production *i.e.*, pigment, protein, carbohydrate, and lipid production. Pigments were extracted and determined as per Chapter 4 section 4. 2. 3. 2. All metabolite contents were calculated by dividing the wet weight of the metabolite present in 10 mL biomass (DCW) on that given day. Values were interpolated to achieve mgg^{-1}.

5. 2. 5. 1. Protein analyses

Microalgal protein concentrations were experimentally estimated using a modified Bradford method (Chia *et al.* 2015). For analyses, 10 mL samples were centrifuged for 10 min at 2.091 × g. Supernatants were discarded, pellets were washed with dH_2O, and re-centrifuged. The pellets were then re-suspended in 1.5 mL 0.5M sodium hydroxide. Extraction was carried out for 2 hr at 100 °C in a water bath (Memmert, Germany). The samples were centrifuged, and the extracted proteins were obtained by collecting the supernatant. To every millilitre of supernatant, 4 mL of Bradford reagent (0.01% Coomassie blue, 4.7% ethanol, and 8.5%

phosphoric acid) was added and allowed to stand for 5 min at 20 °C. Absorbance was read at 595 nm against a reagent blank using a spectrophotometer. Total protein concentrations were obtained *via* calibration curves made using bovine serum albumin (BSA) (10 – 160 µgmL^{-1}), (Appendix I). For quality control, 10 µgmL^{-1} BSA was used as the standard. Microalgal protein concentrations were determined by using the formula below:

$$y = 178.13x - 19.353, r^2 = 0.994$$

Equation 5.13: Protein correlation

5. 2. 5. 2. Carbohydrate analyses

The carbohydrate content was experimentally estimated using a modified phenol-sulphuric acid method (Chia *et al.* 2015). For analyses, 10 mL samples were centrifuged for 10 min at 2.091 × g. Supernatants were discarded, pellets were washed with dH_2O, and re-centrifuged. The pellets were then re-suspended in 1 mL of dH_2O, thereafter, 1 mL phenol solution (10% *w/v*) was added to it. This was vortexed and 5 mL of concentrated sulphuric acid was quickly added. The mixture was left to stand for 10 min at 20 °C. The supernatant was read at 485 nm against a reagent blank using a spectrophotometer. Carbohydrate concentrations were obtained from a calibration curve of glucose (10 – 160 µgmL^{-1}), (Appendix J). For quality control, 10 µgmL^{-1} glucose solution was used as the standard. Microalgal carbohydrate concentrations were determined by using the formula below.

$$y = 101.55x - 2.2026, r^2 = 0.9973$$

Equation 5.14: Carbohydrate correlation

5. 2. 5. 3. Lipid analyses

To analyse lipid content, 20 mL of chloroform-methanol (2:1 *v/v*) was added to the biomass pellets and vortexed (Seo *et al.* 2015). This was heated at 100 °C for 10 min in a START D microwave digester for cell disruption (Milestone S.r.l., Italy). The mixtures were centrifuged for 10 min at 2.091 × g and the biomass pellets were discarded. The supernatant was transferred to pre-weighed bijous bottles. The solvent was evaporated in an oven at 60 °C for 24 hr. After drying, the pre-weighed bijous bottles were cooled in a desiccator and then the weight was recorded. The total lipids were quantified gravimetrically as per the equation below. Metabolite content was calculated by dividing the weight of the metabolite by the microalgal DCW on that given day.

$$Lipid = postweight\ (mg) - preweight\ (mg)$$

Equation 5.15: Lipid concentration

5. 2. 6. Statistical analyses

Growth, pigment, and physiological analyses were conducted every two days. Due to the insignificance in the difference between the days, cell constituent results were expressed every four days. Prior experimental runs provided reliable estimates of the sample variability ($p > 0.05$) (Appendix K); therefore, experimentations were carried out in duplicate. One-way Analysis of Variance (ANOVA) was carried out, using a confidence limit of 95%, to locate the differences in significant results ($p = 0.05$). Multivariate analysis (principal component analyses [PCA]) was used to describe the correlations between dye fluorescence, microalgal biomass, metabolites production, and physiological status (Nasr and Zahran 2016; Deepnarain

et al. 2019; Colina *et al.* 2020). Statistical analyses were performed using the functions "anova2" and Statistics Toolboxes, and "pca" and "pca-cov" in MATLAB R2015a. For this purpose, the data sets were z-score transformed and condensed into three PCs.

5. 3. Results and Discussion

5. 3. 1. Dye fluorescence spectra

Figure 5.1 shows the UV-*a* and *b* irradiances, PAR quantities, and dye fluorescence intensities transmitted into the microalgal culture to illustrate the spectral conversion, emission capacities, and photo-stabilities of the dyes. The variation in results could assign to the dyes functionality to shift the wavelengths present in the spectrum, converting UV light to blue, green, or red light. The PBRs received approximately 500 $mW \cdot m^{-2}$ of UV-*a* irradiance (Figure 5.1 A), which could assist in stimulating microalgal photosynthesis and growth. Xu and Gao (2016), reported that 11 species of the green, red, and brown algae were able to utilise UV-*a* irradiance for triggering photosynthetic carbon fixation, especially in the absence of PAR. The amount of UV-*a* transmitted inside the PBRs under the control, LR, LY, and R8G conditions represented 74, 35, 43, and 41% of the total UV-*a* received, respectively (Figure 5.1 A).

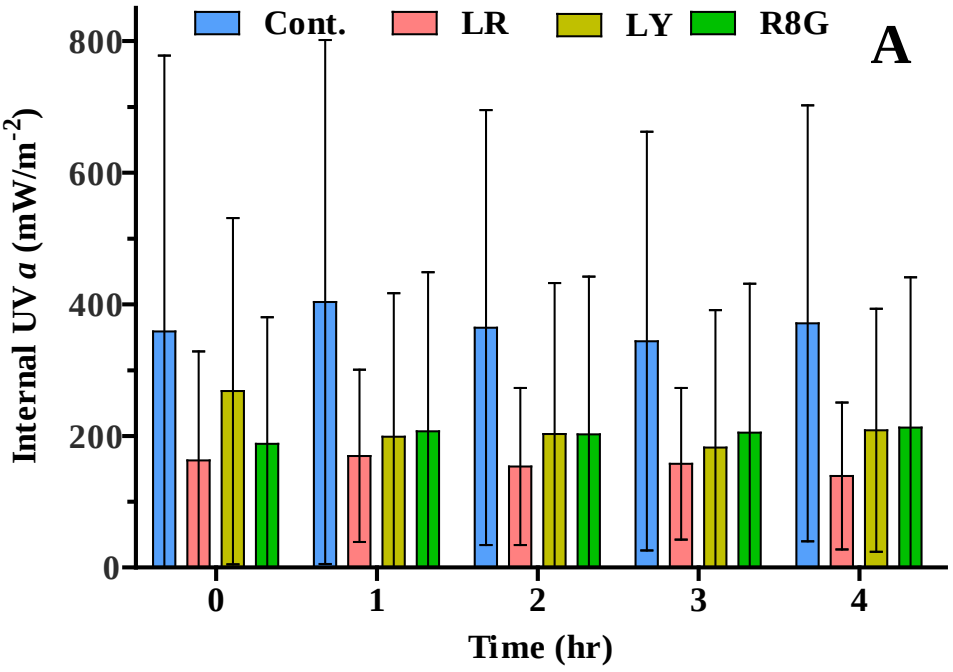
Cont.
LR
LY
R8G
A
800
600
400
200
0
Internal UV a (mW/m-2)
0
1
2
3
4
Time (hr)

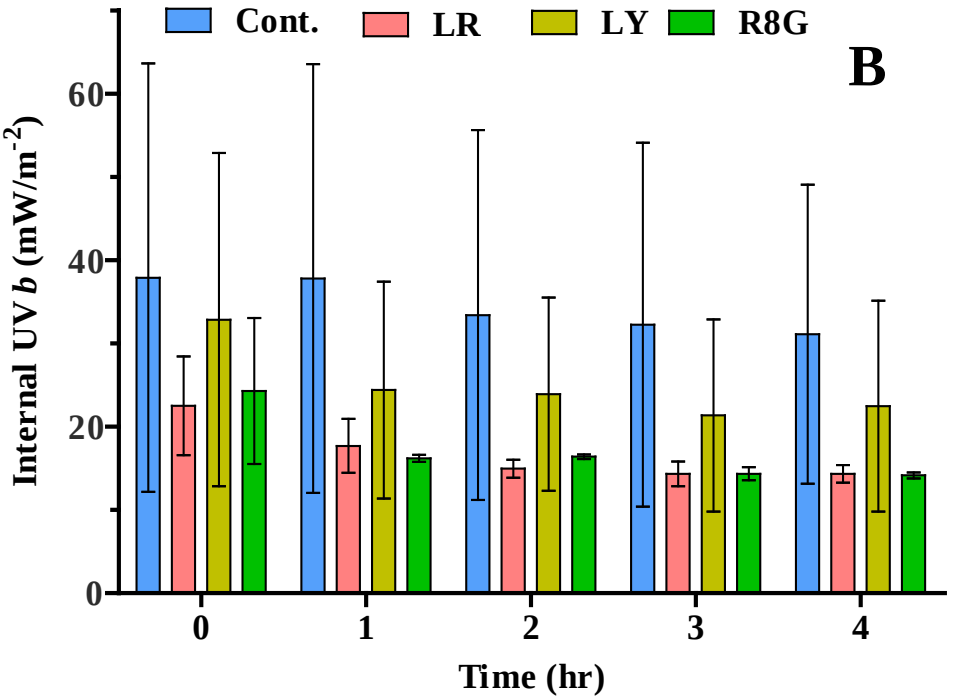
Cont.
LR
LY
R8G
B
60
40
20
0
Internal UV b (mW/m-2)
0
1
2
3
4
Time (hr)

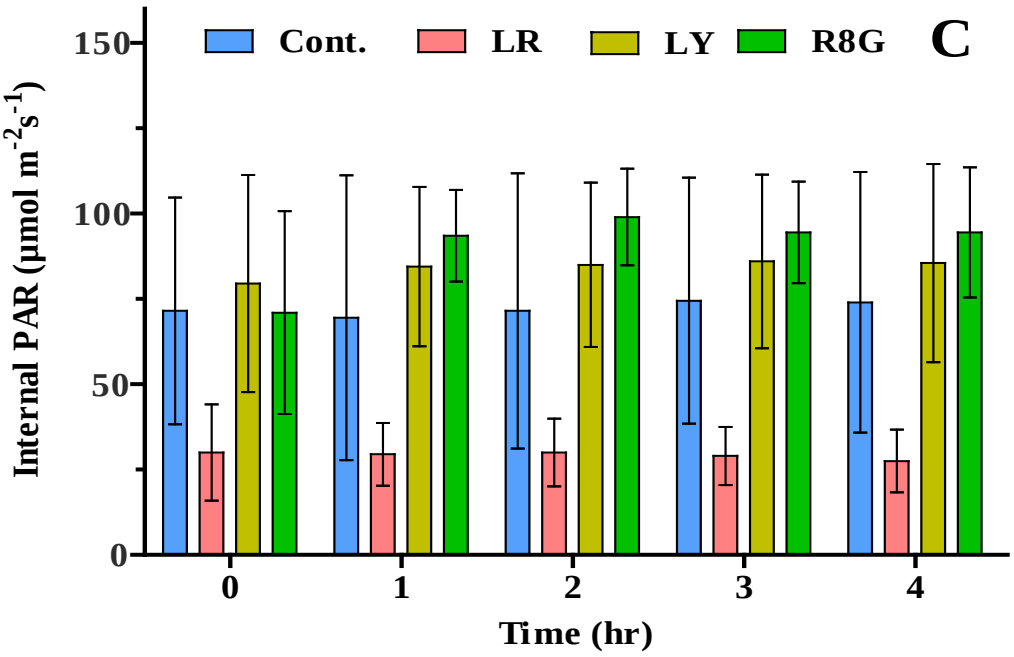

Figure 5.1: Spectral transmission of **(A)** UV-*a*, **(B)** UV-*b*, and **(C)** PAR of the control (Cont.), Rhodamine 8G (R8G), Lumogen Yellow, and Lumogen Red (LR) under 30% UV-*a* and UV-*b* fluorescent tubes. Data are expressed as a mean ± SD (n = 2).

The PBRs also received approximately 350 mW·m^{-2} UV-*b* irradiance, transmitting 9.7, 4.9, 7.1, and 4.8% into the culture media of control, LR, LY, and R8G, respectively (Figure 5.1 B). Transmittance measurements of the dyes in this study suggested that they altered the spectra of light inside the PBRs. In particular, the dyes reduced the amount of UV light that would otherwise be received by the algae (evident by the control). The effects of UV-*b* radiation on microalgae have been highlighted by Singh *et al.* (2019). Generally, UV-*b* radiation is known to decrease the rate of photosynthesis both directly (photo-oxidative effects on the PSs) and indirectly (by decreasing chlorophyll pigments), thus resulting in lowered growth (Chapter 2, section 2. 8. 2). Due to their broad spectral excitation, the dyes attenuated

55 – 77% of UV-*b* (Figure 5.1 B) and transmitted them into the PAR (Figure 5.1 C). This observation was confirmed by the increased PAR irradiance (*i.e.*, for LY and R8G).

The PBRs received 110 µmol photons·m^{-2}·s^{-1} of PAR *via* the UV fluorescent tubes. The quantities of PAR transmitted into the microalgal culture under control, LR, LY, and R8G were 72 ± 26, 29 ± 7, 84 ± 19, and 91 ± 13 µmol photons·m^{-2}·s^{-1}, respectively (Figure 5.1 C). Increased PAR under the control conditions was ascribed to the additional white light emitted from the fluorescent tubes. White light is known to promote PE and capacity, ETR, and growth rate of algae due to its more broad spectral distribution (400 – 700 nm) (Li *et al.* 2019; Sanchez-Tarre and Kiparissides 2021). The control allowed the passage of visible while the dyes absorbed or reflected the light. Lumogen yellow and R8G emitted the highest quantities of PAR, subsequently, these were ~ 16% and 26% higher than the control. Tentatively, this finding suggested that the photosynthetic performance of *C. reinhardtii* grown in the PBR-assisted R8G would be higher than that cultivated under control, LR, and LY by 1.3, 3.1, and 1.1 folds, respectively (theoretically calculated using the DCW and dye PFDs).

The R8G dye absorbed light at 287 nm, however, when compared to the previous finding (Figure 3.2 A), the dye demonstrated a slight shift in the peak emission wavelength (Figure 5.2 A). Under artificial daylight exposure the dye emitted at approximately 470 nm, while under UV exposure, the R8G dye pattern showed a sharp peak at about 498 nm, suggesting a blue-green region between 400 and 500 nm (Khoobkar and Delavari Amrei 2020). Furthermore, the energy converted and released by R8G was 3.97×10^{-19} J·$photon^{-1}$, suggesting that this dye could stimulate pigment and/or lipid production in algae (Seo *et al.* 2015; Sung *et al.* 2018). The emission spectra and the resulting energy value exhibited by R8G further established the conversion and concentrating effect of the dye. The resulting bandwidth shift was

approximately 20 nm. Typically, fluorophore dyes like rhodamine exhibit a shift pattern ≤ 70 nm, thus demonstrating the practicality (tunability) of the dye. The magnitude of the shift depends strongly on the molecule being excited and the nature of the solvent (Durairaj *et al.* 2017; Gao *et al.* 2017). Bandwidth shifts result from differences in solvent polarity, specific solute-solvent interactions, acid-base reactions, and charge-transfer interactions (Maillard *et al.* 2020).

The reorganisation of the methanol molecules around the newly formed excited dye molecules gave rise to the bathochromic shift in R8G. As opposed to the hypsochromic shift, previously mentioned, bathochromic shifts are characterised by the positional shift of the peak wavelength to a longer one with lower energy (Durairaj *et al.* 2017; Delgado-Sanchez 2019). Decreases in the energy gaps between excited and ground states (S1 and S0, respectively), resulted in the wavelength shift. Examples of these shifts have been reported previously (Stanley *et al.* 2016; Durairaj *et al.* 2017; Gao *et al.* 2017; Sung *et al.* 2018). The findings by these researchers establish the dye adaptability regarding specific wavelength tuning efficiency. Literature states that upon dye excitation, the electrons are moved from the negative to the positive end of the dye. This changes the dye polarity, causing the excited state to be less polar than the ground state which resulted in a blue-green shift in emissions (Abou-Kana 2012; Zehentbauer *et al.* 2014; Zhang *et al.* 2014). The shift in R8G emission possibly enabled higher transmission of irradiance to cells deeper in the culture suspension where they were used for photosynthesis (Mattos *et al.* 2015; de Mooij *et al.* 2016). The interactions between the methanol and dye molecules played a significant role in either dye stabilisation or destabilisation of the ground state more than the excited state electrons. For R8G, this phenomenon could be used to broaden PAR emissions while simultaneously increasing irradiance levels.

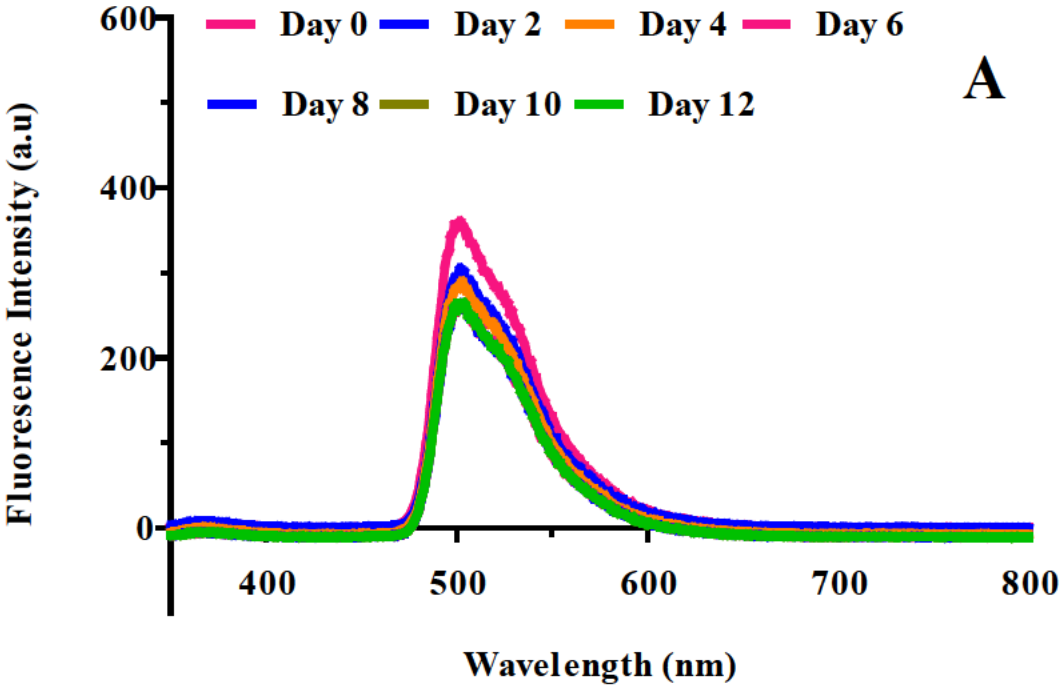
Day 0
Day 2
Day 4
Day 6
Day 8
Day 10
Day 12
A
Fluoresence Intensity (a.u)
600
400
200
0
400
500
600
700
800
Wavelength (nm)

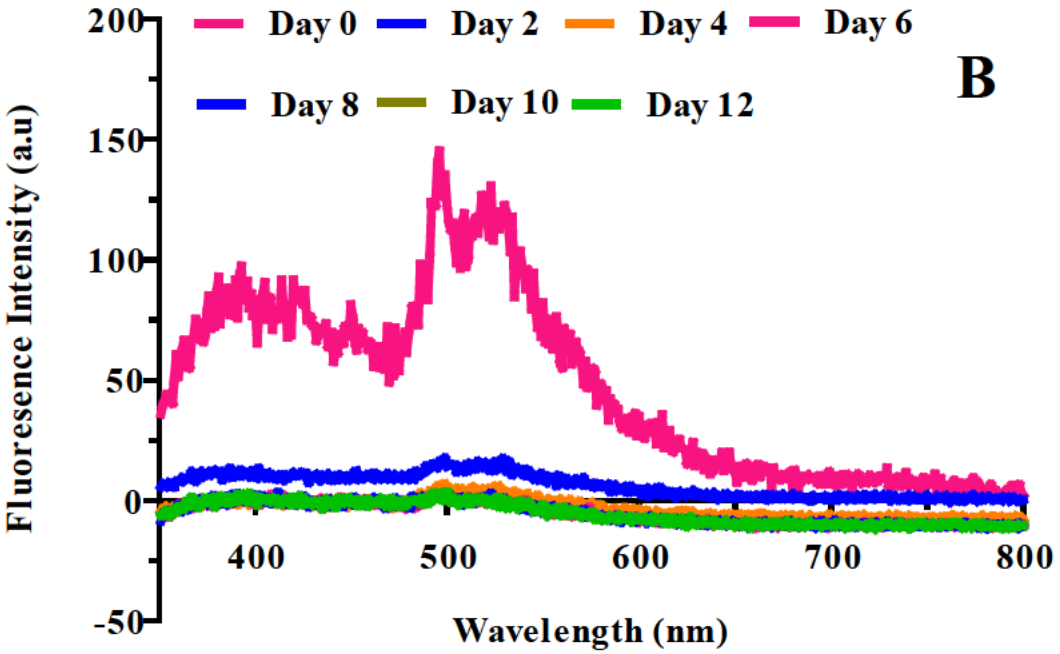
Day 0
Day 2
Day 4
Day 6
Day 8
Day 10
Day 12
B
Fluoresence Intensity (a.u)
200
150
100
50
0
-50
400
500
600
700
800
Wavelength (nm)

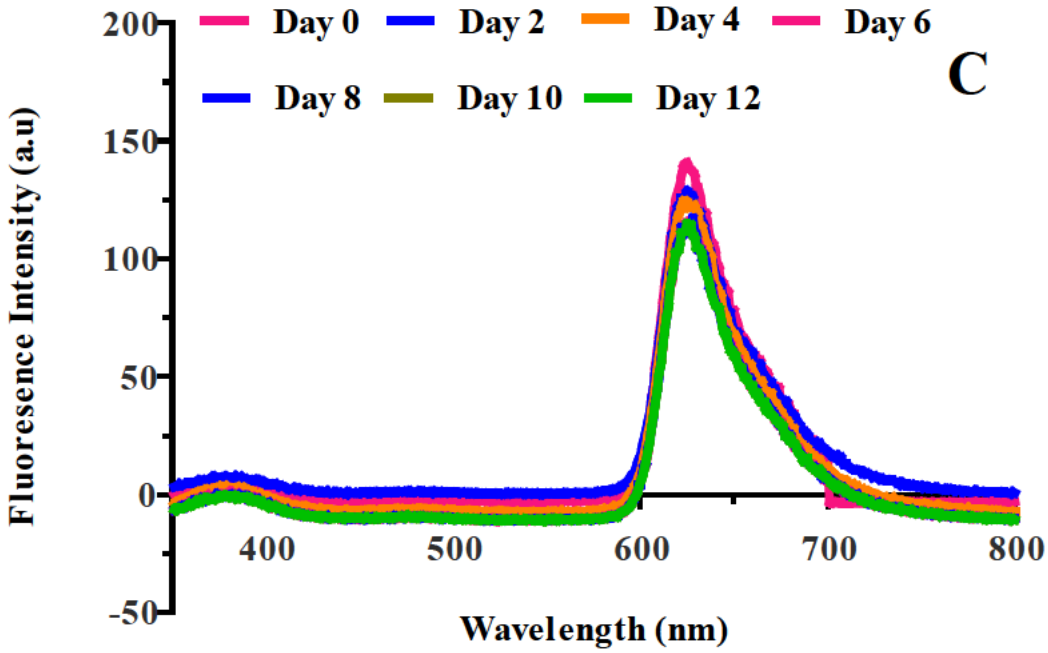

Figure 5.2: Fluorescent intensities of **(A)** Rhodamine 8G (R8G), **(B)** Lumogen Yellow (LY), and **(C)** Lumogen Red (LR) under 30% UV-*a* and UV-*b* fluorescent tubes. Data are expressed as a mean ± SD (n = 2) and plotted every 10 nm.

The LY fluorophore absorbed the light at 254 nm, which was then emitted at a wavelength = 499 nm (Figure 5.2 B), complying with the PAR wavelengths. The theoretical energy converted and released from LY was 3.99×10^{-19} J·photon^{-1}, demonstrating the ability of the dye to convert and concentrate energy in specific wavebands. The higher energy level and broad emission spectrum of LY suggested that the dye could stimulate growth and/or metabolite production in *Chlamydomonas*. However, the fluorescent dye LY was unstable and showed several sharp peaks at the green and blue light spectra (400 – 525 nm). This was due to uneven dye dissolution or dye aggregation as LY dyes show poor solubility at room temperatures (~ 24 °C), similarly described by Kang *et al.* (2019). In acetone, the dye exhibits

0.5 gL^{-1} solubility's while in methanol and ethanol the dye shows 0.1 gL^{-1} solubility's at 20 °C (Brackmann 2000). The fluorescence intensity also extended to more than 600 nm, representing the green to yellow and red PAR portions; however, there was a drastic reduction in emissions after day 0, (Figure 5.2 B). By visual inspection, the LY dye changed in colour from yellow to transparent, which was indicative of photo-degradation (also known as photo-bleaching) (Delgado-Sanchez 2019). Excess photon excitation may lead to the destruction of the dye and/or solvent molecules. Photo-bleaching occurs when a previously excited molecule absorbs additional photons (sequential absorption), or a molecule absorbs several photons at the same time. In these absorption processes, the molecule can absorb so much energy that the binding energy is surpassed, and the molecule dissociates, or at least changes, its structure. This process is more probable during excitation with UV light than with visible light. Hence, photo-degradation leading to reduced photo-stability in the LY dye was attributed to the UV light source (Brackmann 2000).

Lub *et al.* (2019), demonstrated a similar dye photo-bleaching phenomenon from Lumogen orange 240 (1), suggesting the deficient photochemical stability of the imposed dyes. Their study demonstrated that the ethoxy or propoxy derivative of Lumogen orange 240 obtained by irradiation in ethanol or propanol caused a shift of yellow/orange colour to pale red. Consequently, transformed dye intermediates have higher absorption coefficients and thus, absorb irradiation at the same wavelength of the dye (Delgado-Sanchez 2019). However, the dye photo-bleaching phenomenon is impractical when considering lighting applications in microalgae cultivation. Hence, these dyes are frequently immobilised in plastics that contain butadiene and plasticisers or that are partially crystalline and are employed in advertising and design as sign markers, plotters, *etc*.

The fluorescent dye LR absorbed light at the wavelength 290 nm and emitted it at 626 nm promoting the emission of PAR (Figure 5.2 C). Similar findings have been previously observed by Carbone *et al.* (2019). This emission spectrum had a peak in the orange-red light region (wavenumber between 600 and 700 nm), providing effective light energy for microalgal growth (calculated as 3.17×10^{-19} J·photon^{-1}). The red-light condition is preferable to either well-mixed or non-dense microalgae culture because it has the longest wavelength band and the lowest level of light energy in the PAR range (Jang *et al.* 2018; Khoobkar and Delavari Amrei 2020). The reduced level of PAR can be attributed to the characteristics of the dye (Figure 5.2 C). Red dyes reflect the red wavelength while absorbing UV and transmitting visible light (Jang *et al.* 2018). The converted spectra by the dyes were suitable for microalgae growth. These findings illustrate the spectral conversion and emission capacities of each dye. The variation in results could assign to the dyes functionality to shift the wavelengths present in the spectrum, converting UV light to blue, green, or red light. Additionally, the findings are consistent with the hypothesis that the dyes were able to absorb, convert, and concentrate incident light to usable bands thereby increasing PAR availability. Increased PAR would be beneficial and should result in increased algal growth.

5. 3. 2. Effects of UV-mediated dye irradiance on the growth of *C. reinhardtii*

When compared to previous results, the baseline cultures showed a one-day lag phase, a three-day exponential phase, followed by a four-day moderate stationary phase, and then the death phase (Figure 4.4). The highest growth was recorded on day 7 (1.0 – 1.5 gL^{-1}). Under artificial daylight exposure (Figure 4.5), cultures exhibited an initial two-day dye-acclimation period which was validated by the decreased F_v/F_m values and the corresponding increase in NPQ (Figure 4.7 A and B). Furthermore, the alga showed a growth rate of 0.20 d^{-1} (day 7) with

steady and higher growth up to day 8 (1.1 – 1.4 gL^{-1}). The balanced combination of long- and short-wavelengths in white light resulted in a moderate microalgae growth rate (Figure 4.5). Growth under UV-mediated dye-irradiations occurred in phases (Figure 5.3). Cultures demonstrated accelerated growth until day 3, followed by gradual growth until day 5, and then by slower/decreased growth (compared to the control). When compared to control cultures, dye irradiated algal growth were substantially increased in the first three days of growth. This was also confirmed by the growth rates which were 0.6, 0.67, 0.71, and 0.72 d^{-1} for the control, LR, LY, and R8G were, respectively. This was considerably faster than previous growth (Figure 4.5), thus initially, the increased dye-mediated irradiations were advantageous for algal growth and biomass production.

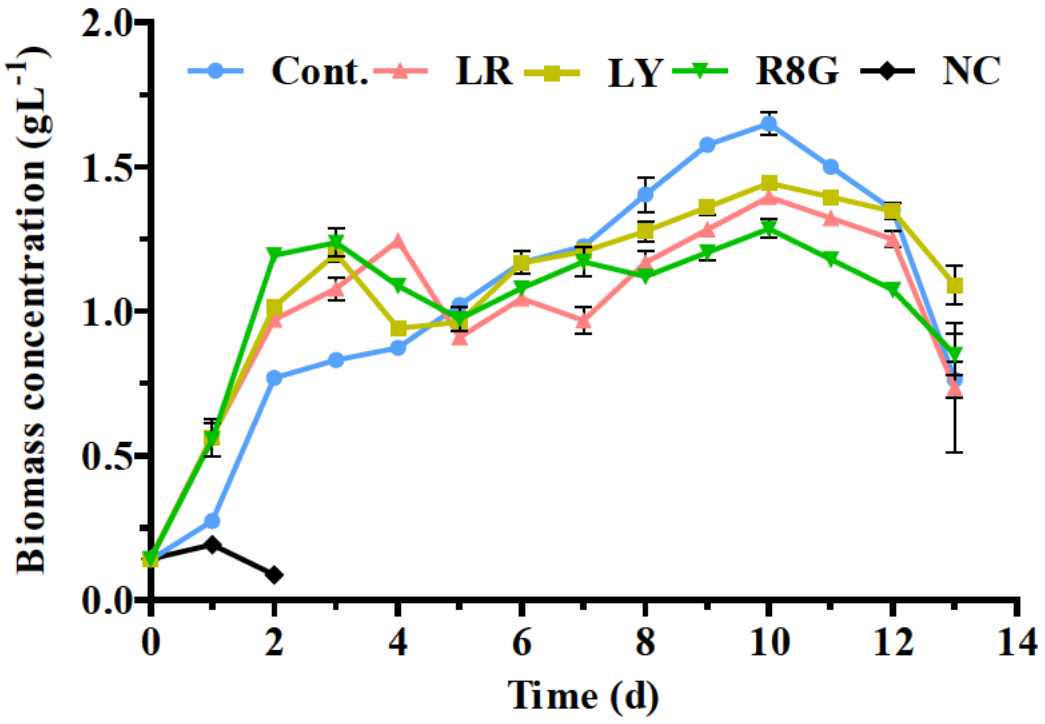

Figure 5.3: Growth profile of *C. reinhardtii* under control (Cont.), Lumogen Red (LR), Lumogen Yellow (LY), and Rhodamine 8G (R8G) using 30% UV-*a* and UV-*b* fluorescent tubes. Control reactors were set up where the microalgal cells received light passing through a

methanol blank. The negative control (NC) was left in the dark. Data are expressed as a mean ± SD (n = 2).

Under the UV-mediated dye irradiations (Figure 5.3), the biomass concentrations ranged between 0.82 – 0.83, 1.05 – 1.10, 1.18 – 1.22, and 1.20 – 1.27 gL^{-1} on day 3 for the control, LR, LY, and R8G, respectively. Consequently, the biomass productivity under dyes irradiance was between 27 – 39% higher than the control (on day 3). During the exponential phase of growth, algae increase their cellular division to reduce photosynthetic complexes in response to excess irradiations. This strategy is used to mitigate photo-inhibition within the cells (Nawrocki *et al.* 2019b; Nowicka 2020; Meagher *et al.* 2021). The control cultures required seven days to reach similar biomass yields as the dye-irradiated cultures (1.20 – 1.24 gL^{-1}), demonstrating the beneficial effect of increased light availability provided by the dyes. By the 5^{th} day-time point, there was an inhibition in cell division under dye-irradiations to match the irradiance level resulting in slower growth. The results implied that dye-irradiations were beneficial in the rapid growth phase (day 3) but were in excess by the 5^{th} day. This was also evident by the decreased growth rates which were 0.1, 0.09, 0.08, and 0.06 d^{-1} for the control, LR, LY, and R8G, respectively. Despite the transient arrest in growth on day 5, LR and R8G grown algae showed a significant difference in biomass from the control and LY irradiated cultures ($p < 0.05$). After the 5^{th} day, the growth concentrations increased by 89, 12, 54, and 18%, respectively, reaching their maximum values on day 10 ($p > 0.05$).

The cultures in the presence of LR grew faster than the control during the first 4 days (Figure 5.3). However, the emitted PAR with LR (29 μmol photons$\cdot m^{-2}\cdot s^{-1}$) was at least two times lower than the control (72 μmol$\cdot$photons$\cdot m^{-2}\cdot s^{-1}$), while R8G emissions (91 μmol$\cdot$photons$\cdot m^{-2}\cdot s^{-1}$) were higher than the control and three times that of LR irradiations

(Figure 5.1 C). A large portion of the red wavelength was reflected by LR which may explain the lower PFD. Cultures that were grown under LR-mediated irradiance acclimated to the lower energy level of light (3.17×10^{-19} J·photon^{-1}) and produced more biomass (~ 0.048 g·L^{-1}) per µmol photons·m^{-2}·s^{-1} available. The biomass/PAR observation under the LR-mediated irradiance was higher than the control, LY, and R8G conditions by 2.1, 2.8, and 3.4 folds, respectively. This finding could be because red light has the lowest light energy level with the longest wavelength (600 – 700 nm), which is close to the optimal level of chlorophyll in PSs, thus the red light was directly absorbed and utilised for photosynthesis, (Seo *et al.* 2015; Sun *et al.* 2018). Similarly, Khoobkar and Delavari Amrei (2020) found that under the red irradiations of Rhodamine 6G the biomass production rate and maximum specific growth rate of *Chlorella* sp. were increased up to 60 and 23%, respectively.

The R8G dye shifted UV to the green wavelengths rather than PAR, consequently, the algal cultures received light between 480 – 550 nm. Green irradiance, containing higher energy (3.97×10^{-19} J·photon^{-1}), is poorly absorbed yet has higher transmittance than white, red, or blue, and can penetrate dense cultures (Mattos *et al.* 2015). This is due to the complete absorption of PAR by the cells closer to the illuminated surface. In all likelihood, the transmitted green light increased culture growth. Similarly, de Mooij *et al.* (2016) also found that green-yellow light maximised biomass productivity in *C. reinhardtii* when compared to the control, blue, orange-red, and deep red light. It has been suggested that the blue and green wavelengths (between 390 – 580 nm) improve algal growth due to the light absorbance spectrum of secondary metabolites such as fucoxanthin (Gao *et al.* 2021). Increased growth/biomass under LY irradiations was attributed to (*i*) the initial additional PAR provided by the fluorescent tubes (Figure 5.1 A); and (*ii*) the absorption and consequent reduction of

UV-irradiations (Figure 5.1 B and C). The results suggested that the UV-mediated dye-irradiance increased growth, supporting previous findings (Seo *et al.* 2015; Sun *et al.* 2018).

The control cultures showed slow growth, in the early stages, which was attributed to the UV irradiation (evident by Figure 5.1 B and C). There was no observable evidence of control acclimation (Figure 5.3). During the second phase of growth (day 5 – 10), the growth rates in all cultures decreased, however, control cultures produced more biomass and exhibited higher growth rates when compared to dye-irradiated cultures. The white light could promote the microalgae PE due to its more varied spectral distribution (multi-chromatic at full PAR spectrum 400 – 700 nm) compared with monochromatic illumination (Sanchez-Tarre and Kiparissides 2021). Also, under lower PFDs microalgae achieve up to 80% of their theoretical maximum PE. This is due to the inherent nature of light.

Increased dye-mediated PFDs could have inflicted damage to algal PSs, which inhibited cell division and biomass productivity (de Mooij *et al.* 2016; Sung *et al.* 2018). Under high PFDs ($\geq$ 150 µmol photons$\cdot m^{-2} \cdot s^{-1}$), maximum light use efficiency by microalgae decreases (de Mooij *et al.* 2016). This is because cells are coerced into absorbing light energy. The observed limitation in biomass accumulation may have been due to photo-saturation of the algal PSs (Gifuni *et al.* 2018). Photosystems are incapable of processing a high number of photons. As this is in excess, it cannot be converted to biochemical energy (Ajayan *et al.* 2019). This leads to oversaturation, PS impairment, and consequently, a waste of light energy through heat dissipation. Both the adaptation and reparation mechanism of the PSs cannot be maintained under increased PFDs (Gifuni *et al.* 2018), evidenced by the previous PAM fluorometry findings (Figure 4.7). The results implied that the mechanisms for resistance were more essential than mechanisms of repair. Such mechanisms vary at the species level. The

extent of PS saturation and light use efficiency is dependent on the wavelength-specific absorption capacity of the alga (Stanley *et al.* 2016; Beecraft *et al.* 2017; Sun *et al.* 2018).

Under mixotrophic growth, the effects of increased dye-mediated PAR on algae could be partly masked due to the presence of acetate. Assumingly, acetate should promote heterotrophic growth in *C. reinhardtii*. On the contrary, the growth observed under the negative control confirmed that algal growth was influenced by dye-mediated irradiations (Figure 4.5). The cultures grew for two days; biomass levels on day 1 ranged between 1.83 – 1.99 $g \cdot L^{-1}$ which further decreased to between 0.08 – 0.09 $g \cdot L^{-1}$ on day 2. Under mixotrophic growth, algae utilise light energy to fix CO_2 *via* photosynthesis and assimilate organic carbon. Consequently, light has a beneficial effect on the mixotrophic algal growth and product yield (Cecchin *et al.* 2018; Sim *et al.* 2019).

Patel *et al.* (2019), evaluated the effect of different lighting conditions on the mixotrophic growth of *Chlorella protothecoides* UTEX-256 using glucose, glycerol, and acetic acid. The alga was grown under light-deficient (35 µmol photons$\cdot m^{-2} \cdot s^{-1}$ at 16:08 hr light/dark), light-sufficient (150 µmol photons$\cdot m^{-2} \cdot s^{-1}$ at 16:08 hr light/dark), and continuous lighting (35 and 150 µmol photons$\cdot m^{-2} \cdot s^{-1}$), maintaining photoheterotrophic conditions. Autotrophic growth was accomplished by using CO_2 while heterotrophic conditions were maintained in the dark. Cultures that were grown using glucose were achieved in completely dark conditions. There was similar mixotrophic growth under the continuous light-deficiency and light-sufficient conditions. Cultures that were grown using glycerol only exhibited autotrophic growth. Despite the light conditions, there was no growth in the heterotrophic and/or photoheterotrophic cultures using light. Cultures grown using acetic acid needed comparatively more irradiance for effective carbon assimilation. The results implied that light utilisation was regulated by the

carbon substrate utilised and that cultures using acetic acid required increased light intensities with increasing growth to avoid the self-shading effect. The observation that mixotrophic growth is supported by light irradiations has also been reinforced by previous researchers (Cecchin *et al.* 2018; Sim *et al.* 2019).

All cultures exhibited similar trends in the pH values (between 7 and 8), indicating that the algae were consuming carbon and growing in biomass. Furthermore, temperatures fluctuated between 23 – 26 ℃ (Appendix D, Figure D2 A and B, respectively), which is optimal for algal growth (Darko *et al.* 2014; Nwoba *et al.* 2019).

5. 3. 3. Effects of UV-mediated dye irradiance on photosynthesis

5. 3. 3. 1. Photosynthetic energy utilisation of *C. reinhardtii*

The F_v/F_m ratio represents a significant parameter in photosynthetic growth, however, to fully gauge and understand light utilisation in *C. reinhardtii* the Y(II), Y(NPQ), and Y(NO) values are more ideally suited. By elucidating these essential parameters, together with gene expression and metabolite synthesis, a fuller representation of energy utilisation in *C. reinhardtii* can be obtained. The Y(II) parameter represents the fraction of light energy that can be used photochemically in PSII, while the excess energy is non-radiatively dissipated as heat (Colina *et al.* 2020; Yadav *et al.* 2020).

Initially, all cultures exhibited low yields in photochemical energy utilisation (0.05) (Figure 5.4). The low photochemical energy utilisation in all cultures could assign to the initial

four-day UV-acclimation phase, which photo-damaged the cells. This was also observed by Colina *et al.* (2020) when studying the oxidative stress response of *C. reinhardtii* to UV-*c* stress. The UV-*c* radiation had an adverse effect on microalgal photosynthesis, resulting in a reduction of the quantum efficiency from approximately 0.6 to 0.52 in 5h (data extrapolated from graph), and a decrease in chlorophyll concentration that was attributed to the acclimation. Similarly, Yadav *et al.* (2020) found that under high light conditions (250 and 500 µmol photons·m^{-2}·s^{-1}), the quantum yield of *C. reinhardtii* wild type (137c and t222+) was reduced by 20 – 30% in both high salt media (photoautotrophic conditions) and TAP media (photoheterotrophic conditions). Despite the low energy utilisation and difference in the cultivation modes, the cells acclimated to the excess light by initiating adaptive and photo-protective stress alleviating mechanisms such as NPQ (Yadav *et al.* 2020).

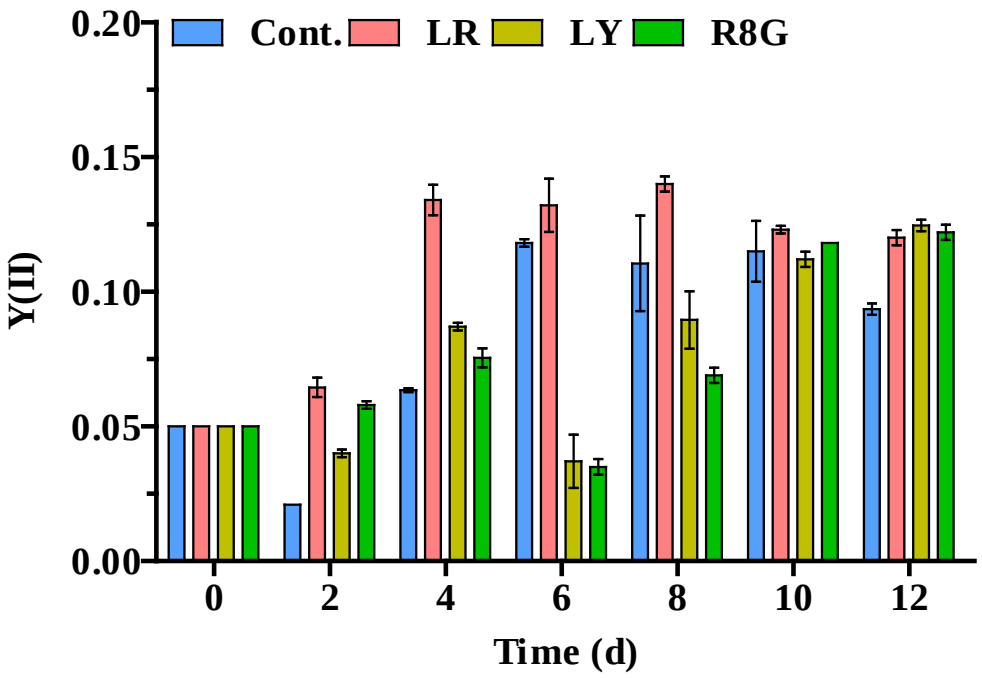

Figure 5.4: Photochemical energy utilisation [Y(II)] of *C. reinhardtii* grown under control (Cont.), Lumogen Red (LR), Lumogen Yellow (LY), and Rhodamine 8G (R8G) using

30% UV-*a* and UV-*b* fluorescent tubes. Control reactors were set up where the microalgal cells received light passing through a methanol blank. Data are expressed as a mean ± SD (n = 2).

When compared to dye-irradiations, Y(II) values under control conditions was extremely low (typically > 0.5 under normal conditions) and extended ($p < 0.05$), which was indicative of damage to PSII (Figure 5.4). Likewise, LY and R8G irradiated cultures displayed reduced Y(II) values (< 0.1, between days 2 – 4). This impairment of photosynthetic processes was further confirmed by the reduction in growth (Figure 5.3). After day 4 the yield of Y(II) increased, however, cultures consistently exhibited low light utilisation throughout the study (≤ 15%). Light stress is related to structural and functional changes of the PSII and PSI (Nawrocki *et al.* 2019a; Nawrocki *et al.* 2020), which disrupt electron flow to photochemical processes (Roach *et al.* 2020; Meagher *et al.* 2021). Cultures grown under LR received reduced light, however, the cultures showed consistently higher Y(II) values (≥ 70%). This confirmed that most of the red light was being photo-chemically utilised by the alga, similar to previous findings (Khoobkar and Delavari Amrei 2020). This implied that the LR dye could be applied to microalgal systems and could be useful in promoting biomass production. The effects of red light on the microalgal PSII have been discussed previously (see Section 2.8.1).

Initially, the regulated heat dissipation, Y(NPQ), values were low (approximately 0.05), signifying the initial heat dissipation was minimal (Figure 5.5). Increased Y(NPQ) was observed in all cultures up to day 4 followed by a decrease, whereas the yield of Y(NO), non-regulated heat dissipation, decreased gradually as the experiment progressed (Figure 5.6). Cultures under control, LY, and R8G irradiations showed the highest Y(NPQ) values on day 4. These ranged between 0.106 – 0.165, 0.124 – 0.197, and 0.120 – 0.138, respectively, ($p < 0.05$). When there is excessive excitation energy, the regulated heat dissipation is usually

associated with the stimulation of the xanthophyll cycle. For PSII this corresponds to decreased excitation which ultimately has a protective effect. In contrast, Y(NO) occurs due to the closure of the PSII centres, inhibiting electron transport which could result in possible damage caused by hazardous side reactions like the generation of ROS (Quaas *et al.* 2015; Girolomoni *et al.* 2019). Furthermore, the previous findings (Figure 4.5) indicated that dye-acclimation lasted approximately 2 days, verified by the increased NPQ up to day 2, which decreased to 0 between days 4 to 6 (Figure 4.7 B). The current findings suggested that the UV dye-mediated PFDs was still in excess by day 5, evidenced by the decreased growth from day 4 to 5 (Figure 5.3 and Figure 5.4).

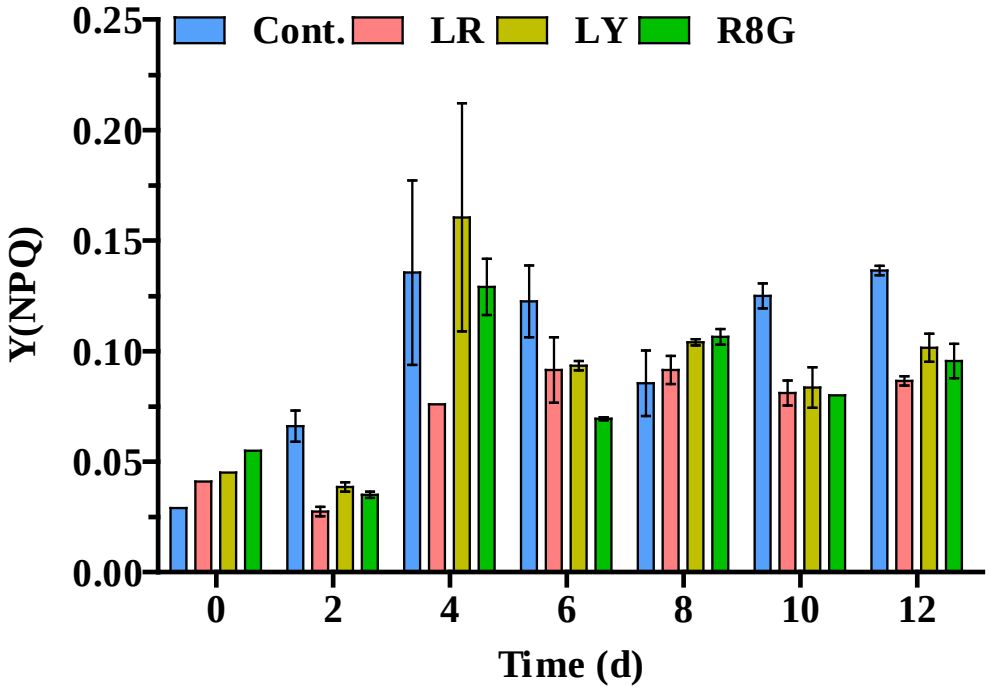

Figure 5.5: Regulated energy dissipation [Y(NPQ)] of *C. reinhardtii* grown under control (Cont.), Lumogen Red (LR), Lumogen Yellow (LY), and Rhodamine 8G (R8G) using 30% UV-*a* and UV-*b* fluorescent tubes. Control reactors were set up where the microalgal cells received light passing through a methanol blank. Data are expressed as a mean ± SD (n = 2).

Accelerated growth before day 5 was attributed to increased dye-mediated PFDs, which were more than the algal photosynthetic capacity. As mentioned, cultures grown under increased dye-mediated PFDs demonstrated active growth and division to reduce light penetration through the medium, thereby attempting to reduce photo-inhibition (Nawrocki *et al.* 2019b; Nowicka 2020; Meagher *et al.* 2021). The stabilisation of the Y(NPQ) values after day 6 could be ascribed to the influence of the light-limiting factor on the inhibition of algae photosynthesis (Li *et al.* 2020), indicating that *C. reinhardtii* retained the physiological means to utilise and regulate energy (Figure 5.5).

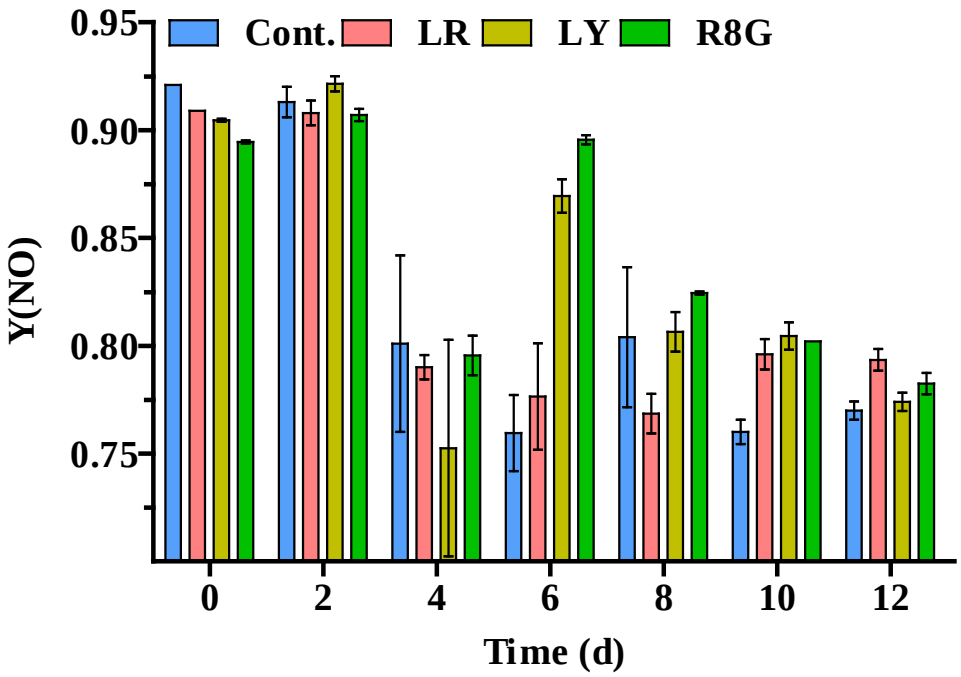

Figure 5.6: Non-regulated energy dissipation [Y(NO)] of *C. reinhardtii* grown under control (Cont.), Lumogen Red (LR), Lumogen Yellow (LY), and Rhodamine 8G (R8G) using 30% UV-*a* and UV-*b* fluorescent tubes. Control reactors were set up where the microalgal cells received light passing through a methanol blank. Data are expressed as a mean ± SD (n = 2).

Initially, energy dissipation *via* the non-regulated pathway in PSII was high (> 0.9) implying that photo-damage had occurred in the algal PSII (Figure 5.6). As previously described by Nama *et al.* (2018), this observation indicated that algal PSs were impaired due to photo-oxidation and unable to convert all of the received light into chemical energy. A substantial amount of energy is expended on strategies that aim to restore cellular homeostasis (Gifuni *et al.* 2018; Ma *et al.* 2019). This promoted the conclusion that the dyes were adequately excited by the UV light source (Reptistar tubes), absorbing more photons and emitting higher irradiances (Figure 5.1). The high Y(NO) values exhibited between days 0 – 2 also suggested the constitutive loss of energy due to excessive PFDs (> 90%). During the photo-adaptation phase, the excessive light energy is dissipated through the non-regulated pathway. However, on day 4, the increased yield of Y(II) and decreased Y(NO) signified the usage of light energy by the alga (Figure 5.4 and Figure 5.6, respectively). The increased Y(NO) and biomass values implied that *C. reinhardtii* retained the physiological means to regulate energy, (Figure 5.6 and Figure 5.3, respectively). Similar findings have stated that with an increase in light intensity, *C. reinhardtii* biomass increased to alleviate light usage by diluting it's PSs (Nama *et al.* 2018). Certainly, the dye-mediated strategy can be exploited to increase light availability to microalgae cultivated in areas receiving low/inadequate sunlight irradiance.

Interestingly, the Y(NO) yield gradually decreased as the experiment progressed, which suggested that the fraction of non-regulated energy dissipation played a role in dye-acclimation, agreeing with Yadav *et al.* (2020), in that the microalgae utilised the energy to mitigate the stress (dye-mediated) and acclimated to the increased irradiance. Under increased light irradiance heat dissipation is essential, however, it reduces photon conversion efficiency and biomass production rates (Gomes *et al.* 2017; Roach *et al.* 2020). Similarly, the decreased

growth and quantum utilisation in *C. reinhardtii* (Figure 5.3 and Figure 5.4), may provide evidence of this phenomenon. The concomitant decreases in Y(II) with an increase in Y(NO) and Y(NPQ) can be related to modifications within the ETC (Nama *et al.* 2018; Roach *et al.* 2020). The findings also confirmed the recovery ability of *C. reinhardtii*, previously demonstrated by other researchers (Yarnold *et al.* 2016; Roach *et al.* 2020).

5. 3. 3. 2. Photosynthetic gene expression

Ribulose bisphosphate carboxylase/oxygenase is the first enzyme in the CBB cycle able to fix CO_2 into organic molecules (3-phosphoglycerate), as well as catalysing the initial reaction of the photo-respiratory pathway (Figure 5.7), (Esquivel *et al.* 2017; Shene *et al.* 2018). The photosynthetic process is can be improved by increasing light irradiance (Esquivel *et al.* 2017), however, excess irradiance can lead to photo-inhibition. Under LY and R8G irradiations, the lowered gene expression and decreased biomass coincided with increased Y(NPQ), (Figure 5.5). The gene expression of RuBisCo in these cultures was significantly down-regulated by 1.2- and 1.4-fold on day 4 ($p < 0.05$), suggesting an inhibition in photosynthesis. The reduction in the expression of the rbcL gene on the 4^{th} day could suggest a stressful condition (dye-acclimation phase between days 0 – 5 [Figure 5.3]), (Colina *et al.* 2020). This is in agreement with the occurrences under mixotrophic cultivation mode *i.e.*, the downregulation of the transcripts coding for the RuBisCo large subunits (Figure 5.7), often followed by a decrease in chlorophyll content (Cecchin *et al.* 2018; Pang *et al.* 2019). The increased reducing power derived from acetate metabolism causes an over-reduction of PQs, likely inhibiting its reduction by CEF around PSI but increasing demand of PSI electron acceptors like FDX and FNR (Figure 2.3), (Cecchin *et al.* 2018; Pang *et al.* 2019).

Under LR-irradiance RuBisCo expression was up-regulated on days 4 and 8 (Figure 5.7), showing the potential to significantly improve microalgal growth (Figure 5.3). When compared with the control, rbcL expression under LR was significantly up-regulated by 1.6 and 2.9-fold on days 4 and 8, respectively ($p < 0.05$). Under LR-irradiations transcript levels increased by 47 and 15% when compared to LY (days 4 and 8, respectively), and 9% when compared with R8G irradiance (days 4 and 8). Accordingly, the LR-irradiated cultures displayed consistently higher Y(II) values (≥ 70%) ($p < 0.05$), (Figure 5.4). This further indicated that most of the red light was being photo-chemically utilised by the alga, hence the increased demand for RuBisCo and potential gene expression. As much as blue light stimulates RuBisCo, red light also induces RuBisCo expression to fulfil the increased need for energy generation required to operate shorter growth and cell cycles (Cecchin *et al.* 2018; Pang *et al.* 2019).

Sanchez-Tarre and Kiparissides (2021), studied the effects of illumination on the RuBisCo small subunit (rbcS) gene expression in mixotrophically-grown *Chlamydomonas reinhardtii* 11/32C. The alga was grown at 400 μmol photons·m^{-2}·s^{-1} under blue, red, and white LEDs. Cultures grown under red light showed significantly higher gene expression when compared to both blue and white light. In addition, the average rbcS expression in cultures grown under blue light was significantly higher than those grown under white light. Thus, the findings in the current investigation are in agreement with Sanchez-Tarre and Kiparissides (2021). The converted wavelengths emitted from LR, R8G, and/or LY had a statistically significant effect on the average rbcL gene expression ($p < 0.05$), (Figure 5.4). The level of rbcL expression under control cultures was much lower than those achieved under the dye irradiation. An explanation for this occurrence could be that under PAR/UV light (containing

both long- and short-wavelengths), the reduction in photosynthetic gene expression was caused by the imbalance of excitation energy distributed between PSII and PSI.

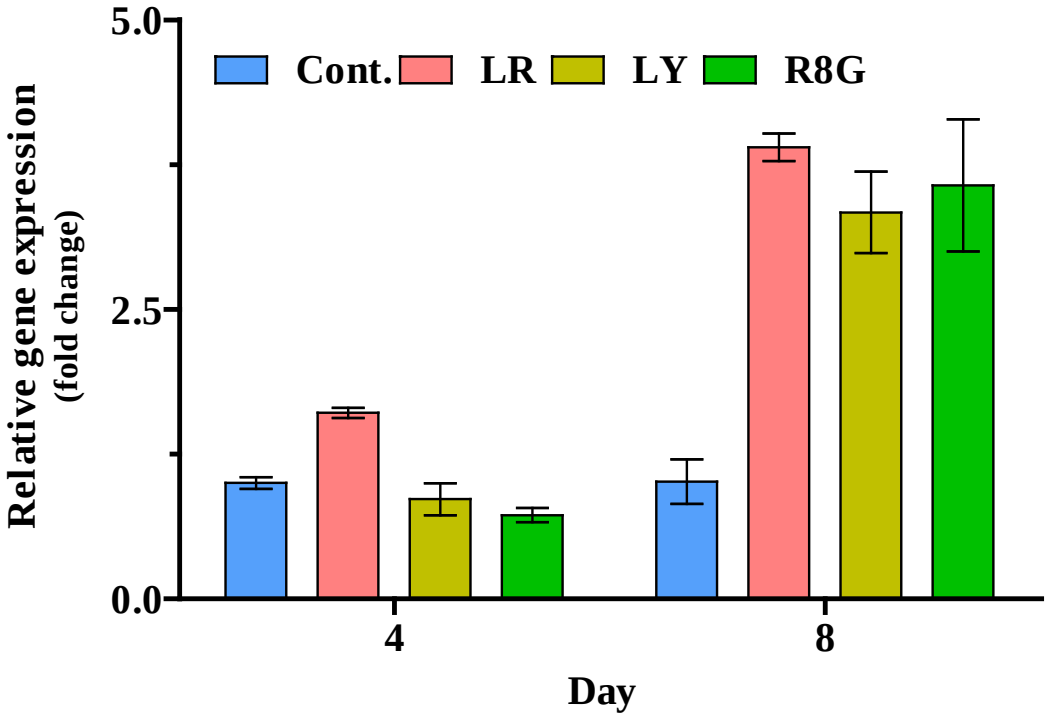

Figure 5.7: Relative gene expression (rbcL) of *C. reinhardtii* grown under control (Cont.), Lumogen Red (LR), Lumogen Yellow (LY), and Rhodamine 8G (R8G) using 30% UV-*a* and UV-*b* fluorescent tubes. Control reactors were set up where the microalgal cells received light passing through a methanol blank. Data are expressed as a mean ± SD (n = 3).

The cultivation of *C. reinhardtii* using both acetate and light as an energy source changed the energetics of PSII. This has been previously described (Sun *et al.* 2018; Sanchez-Tarre and Kiparissides 2021). In a mixotrophic mode, there is competition for carbohydrates between uptake of external organic carbon sources and the CBB cycle (*i.e.*, inorganic carbon uptake). In *C. reinhardtii* the majority of carbon flux was directed toward the glyoxylate cycle (Boyle *et al.* 2017; Tibocha-Bonilla *et al.* 2018). This is a known occurrence under mixotrophic growth

as there is a higher energetic demand for carbon upon acclimation (Boyle and Morgan 2009; Boyle *et al.* 2017). Briefly, acetate is metabolised to triose by the ATP-dependent entry into the glyoxylate shunt to produce reducing equivalents. These are used by the NAD(P)H dehydrogenase to reduce the PQ pool, consequently leading to interruptions in the balance between ATP and NADPH, and the subsequent losses in the ETC. This directly affects the energy regulation as the ETC is under governance by the redox state of the PQ pool (Nowicka 2020; Roach *et al.* 2020; Meagher *et al.* 2021). These interactions amongst the energy generating organelles have been previously implicated in stress responses (Davis *et al.* 2013; Boyle *et al.* 2017; Tibocha-Bonilla *et al.* 2018). In essence, mitochondrial metabolism was active and crucial for photosynthesis under UV-mediated dye conditions, thus establishing the importance of the interactions between the mitochondria and chloroplast (as described in Chapter 2). Alternative pathways specifically enhance/improve protection against oxidative stress by redirecting metabolites from the chloroplast to respiratory pathways. Hence, the oxidation of photosynthetic products by the mitochondria helped in maintaining the balance between reduced and oxidised products within the chloroplast (Davis *et al.* 2013).

On day 8, LY and R8G grown cultures were significantly up-regulated by 60 and 62%, respectively ($p < 0.05$), (Figure 5.7). By this time, *C. reinhardtii* had fully acclimated to the UV-mediated dye irradiations (evident by the increased growth, Figure 5.3). After dye-acclimation (day 0 – 4), cultures used light energy to direct electron flux through RuBisCo (Figure 5.7). Consequently, the cells produced NADPH through linear ETC to supply metabolism with NADH. In this case, increasing light flux was directed through the CBB cycle, the RuBisCo flux increased rapidly with the increase in irradiance while the glyoxylate shunt flux gradually decreased (Boyle and Morgan 2009; Boyle *et al.* 2017). The increase in growth

verified these explanations (Figure 5.3). This could explain the increased expression of rbcL on day 8 as compared to day 4.

Interestingly, Sanchez-Tarre and Kiparissides (2021) observed that the biomass and growth rate of *C. reinhardtii* 11/32C did not strongly correlate with rbcS gene expression levels. Although the red and blue light illuminated cultures displayed higher rbcS expression, cultures illuminated with white light showed more growth rate and higher biomass values. Hence, the current investigation is in agreement with the findings of Sanchez-Tarre and Kiparissides (2021). The control cultures exhibited higher biomass (Figure 5.3), yet displayed lower rbcL expression (day 8), (Figure 5.7). The balanced combination of long- and short-wavelengths making up control conditions resulted in the fastest biomass production. It has been shown that monochromatic red or blue light does not fully satisfy the microalgal growth requirements and the absence of one of the two light qualities creates photosynthetic inefficiencies. Various studies have found that mixed red and blue light accelerates photosynthesis and the growth of algae (Zhao and Su 2014; Choi *et al.* 2015; Baer *et al.* 2016). Perhaps the absence of one of these wavelengths under the dye-irradiation reduced *Chlamydomonas* growth. This could explain the contrasting impact of different dyes on gene expression.

In addition to transcriptional control *via* light-induced gene expression, rbcL expression is dependent on many factors such as light quantity and quality, temperature and pH, pigment biosynthesis, photosynthetic apparatus integrity, and substrate (carbon) utilisation (Boyle and Morgan 2009; Boyle *et al.* 2017). Furthermore, photo-inhibitory effects that arise from photosynthesis (photo-autotrophic growth) may not necessarily correspond to more traditional ecological mechanisms under mixotrophic cultivations. Quantum efficiencies may show

considerable decreases while growth and photosynthetic CO_2 fixation may remain relatively unimpaired (Beecraft *et al.* 2017). Given the quantum mechanical nature of photosynthesis, traditional considerations alone cannot be used to sufficiently explain many of the processes involved. Photosynthesis depends on the inputs, and therefore, process mechanics could change. This could explain some of the observed effects. A deeper understanding of the structure-function relationships in photosynthesis will prove useful for developing strategies aimed at either increasing/decreasing carboxylation (photosynthetic productivity) or oxygenation (photo-respiration). By doing so, a clear perspective on energy utilisation and metabolic activities can be drawn. Given this fact, any future gene expression studies related to light enhancement should focus on several enzymes involved in the photosynthetic and respiratory pathways. These include but are not limited to ATP synthase, FNR, NDA2, and acetyl CoA synthase (Figure 2.4). Additionally, transcript and protein levels (*e.g*., the pigment-binding *lhcsr* protein complex) need to be analysed to verify the protein levels follow the transcript levels.

5. 3. 4. Effects of UV-mediated dye irradiance on metabolite production in *C. reinhardtii*

5. 3. 4. 1. Pigment production

Initially, the chlorophyll contents of the cultures grown under the control, LR, LY, and R8G ranged between 43 – 57; 48 – 65; 58 – 76; and 62 – 75 $mg \cdot g^{-1}$, respectively (Figure 5.8), which was attributed to the acclimation in *C. reinhardtii* in response to the UV-light source (Reptistar bulbs). Within this period, the dye-irradiated cultures exhibited about 5 – 27 *wt.* % higher chlorophyll contents than the control. The chlorophyll molecules in microalgae are

responsible for absorbing and transferring light energy *via* photosynthesis (Gomaa *et al.* 2016; Sun *et al.* 2018). Similar observations have been reported by Khoobkar and Delavari Amrei (2020). The researchers found that spectral modification using R6G increased chlorophyll content in *Chlorella* sp. During the study, the algae that were grown under occurred under R6G irradiations produced higher chlorophyll. The highest chlorophyll under R6G (~ 0.8 *wt.* %) and the control (~ 0.2 *wt.* %) were achieved on day 8. It was concluded that chlorophyll was produced for light harvesting and was highly dependent on light quality and quantity (Khoobkar and Delavari Amrei 2020).

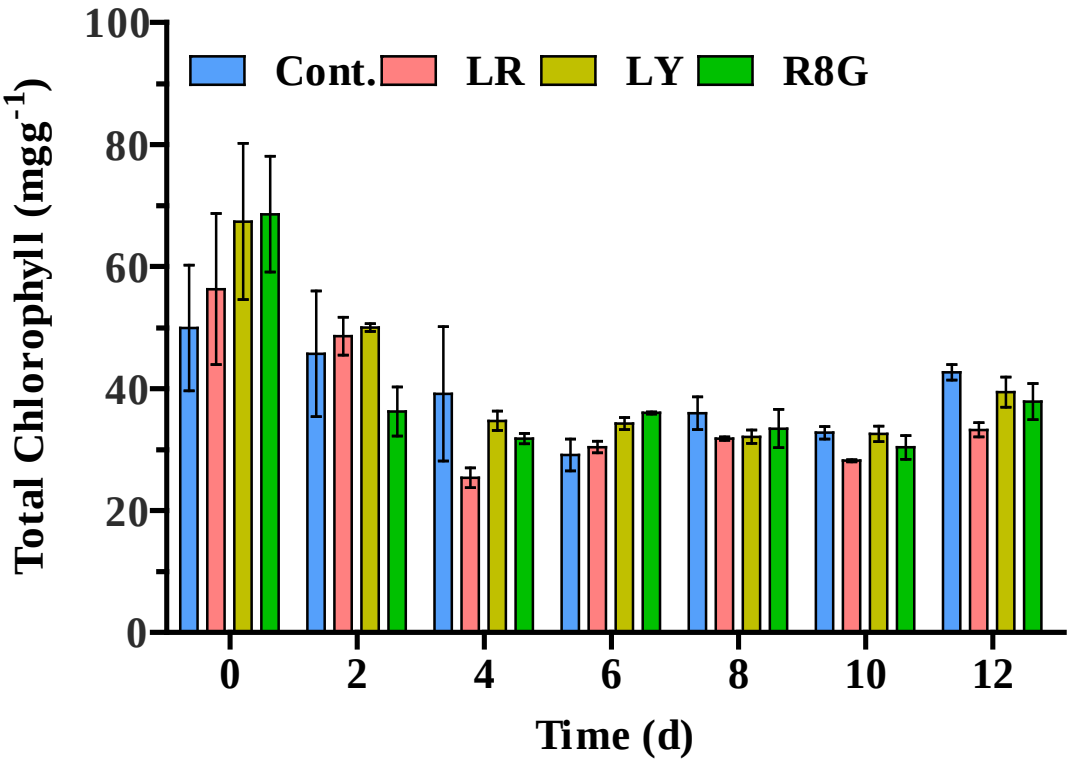

Figure 5.8: Total chlorophyll content of *C. reinhardtii* grown under control (Cont.), Lumogen Red (LR), Lumogen Yellow (LY), and Rhodamine 8G (R8G) using 30% UV-*a* and UV-*b* fluorescent tubes. Control reactors were set up where the microalgal cells received light passing through a methanol blank. Data are expressed as a mean ± SD (n = 2).

On day 4 the LY-grown cultures showed the highest chlorophyll content when compared to the other dyes (~ 34 mgg^{-1}), ($p < 0.05$) (Figure 5.8). On day 6 dye-irradiated cultures produced between 4 – 19 *wt.* % more chlorophyll than the control. This ranged between 27 – 31; 30 – 31; 33 – 35; and 35 – 36 mgg^{-1} for the control, LR, LY, and R8G grown cultures, respectively. Control cultures showed higher total chlorophyll on days 4 and 8 when compared to the dye-irradiated cultures. Under reduced usable irradiation the algae regulate chlorophyll pigments to harvest more of the available light. Low PFDs require increased efficiency in light-harvesting which is achieved *via de novo* synthesis of photosynthetic pigments (Derks *et al.* 2015; de Mooij *et al.* 2016; Nama *et al.* 2018). This was also seen previously (Figure 4.6), as increased thermal dissipation induced the production and distribution of pigments which was linked with changes in the light utilisation efficiency.

Despite the noticeable increases between the dye-irradiated samples and the control, the chlorophyll pigment content was reduced throughout the study (Figure 5.8). Photo-regulative processes (acclimation) involve the active degradation of pigment complexes to restrict the transfer of excitation energy to the PSs, thereby preventing their oversaturation and damage (de Mooij *et al.* 2017; Sung *et al.* 2018). Meagher *et al.* (2021), determined the effects of photo-acclimation strategies in *C. reinhardtii* strain CC125 during the exponential and stationary phases of growth. It was found that from the exponential phase, the algae transitioned into a declining growth phase where the cells sustained a slow rate of growth in both low (70 µmol photons$\cdot m^{-2}\cdot s^{-1}$) and extremely high-light (700 µmol photons$\cdot m^{-2}\cdot s^{-1}$). During this period, both cultures exhibited a conditional decline in chlorophyll levels which was associated with acclimation. In the current study, this phenomenon resulted in a reduction in growth, consequently leading to an intrinsic decrease in the energy conversion capacity of PSII (evidenced by the reduced Y(II), Figure 5.4), similar to the findings of Yadav *et al.* (2020).

More importantly, decreased energy conversion capacities are caused by the decreased availability of $NADP^+$, the terminal electron acceptor in the photosynthetic ETC, due to the lower activity of the CBB cycle (Nawrocki *et al.* 2019b; Meagher *et al.* 2021). Photosynthetic reactions lead to the generation of energy and reducing equivalents through the ETC (Chapter 2, section 2. 4. 1). Consequently, the CBB cycle remains the main consumer of the generated ATP and NADPH. Under decreased irradiance, the inadequate quantity of energy reduced the activity of the ATP and NADPH dependent reactions (in the CBB cycle). Subsequently, this resulted in the reduced regeneration rate of ribulose-1,5-biphosphate from ribulose-5-phosphate. The ATP independent reversible reactions are still active. Triose phosphates are continuously exchanged with free phosphate *via* the triose phosphate transporter export reactions. This results in the reduction of the CBB cycle intermediates and a concomitant increase of the orthophosphate pool (Matuszynska *et al.* 2019; Nawrocki *et al.* 2019b; Meagher *et al.* 2021).

The chlorophyll content started to increase until day 12, showing higher levels for the control culture. The chlorophyll contents ranged between 42 – 44, 32 – 34, 38 – 41, and 36 – 40 mgg^{-1} for the control, LR, LY, and R8G grown cultures, respectively (day 12). Increased chlorophyll content per cell was attributed to the reduction in light irradiance due to increasing biomass, thereby adapting the light/shade condition to enhance the light energy utilisation (Ferreira *et al.* 2016). Under decreased light regimes, algae synthesise accessory pigments like carotenoids to assist in light capture.

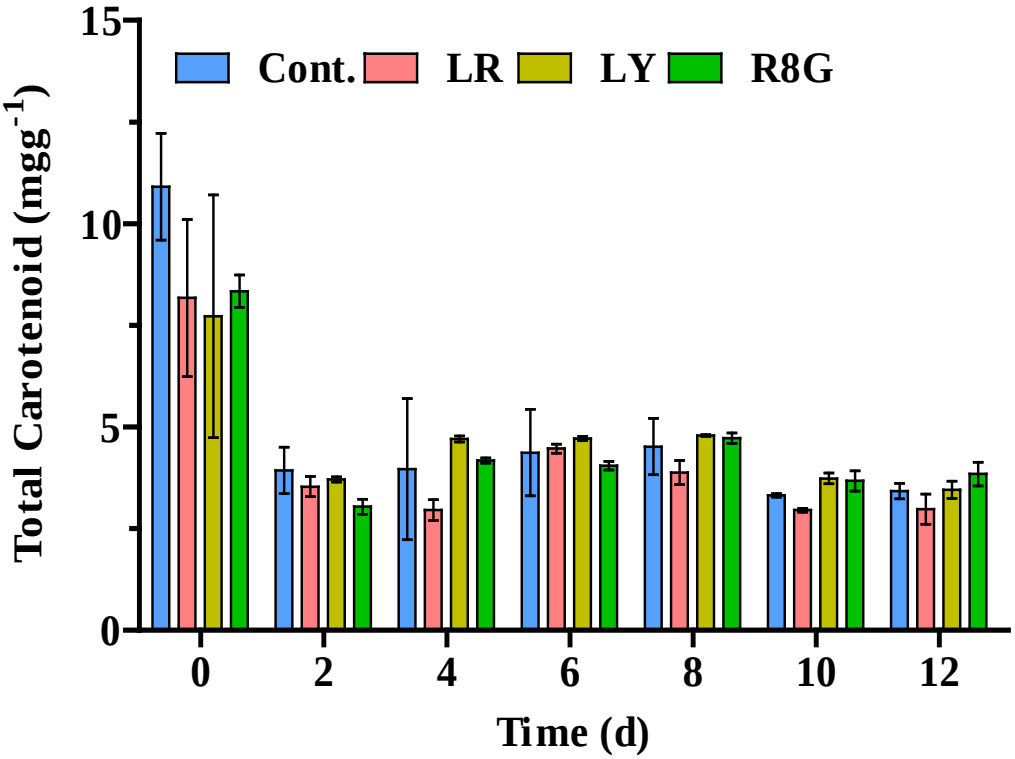

Figure 5.9: Total carotenoid content of *C. reinhardtii* grown under control (Cont.), Lumogen Red (LR), Lumogen Yellow (LY), and Rhodamine 8G (R8G) using 30% UV-*a* and UV-*b* fluorescent tubes. Control reactors were set up where the microalgal cells received light passing through a methanol blank. Data are expressed as a mean ± SD (n = 2).

The highest carotenoid content was noticed on day 0, recording between 10 – 12, 7 – 9, 6 – 10, and 8 – 9 mgg^{-1} for the control, LR, LY, and R8G grown cultures, respectively (Figure 5.9). The carotenoid accumulation in microalgae is essential to protect the photosynthetic apparatus against photo-oxidative damage (NPQ), (Nawrocki *et al.* 2020; Nowicka 2020). Photo-protection compounds in algae (pigments, protein, carbohydrate, and lipid) are produced in response to UV radiation exposure, (Chapter 2 section 2. 8. 2) (Singh *et al.* 2019; Colina *et al.* 2020). Hence, the initial increased carotenoid production as a protective (ROS) response was attributed to the initial acclimation to the UV light source. On day 4 the carotenoid content ranged between 3 – 4; 2 – 3; 4 – 5; and 4 – 5 mgg^{-1} for the control, LR, LY, and R8G grown

cultures, respectively. The LR profile exhibited the lowest carotenoid content compared with those grown under LY and R8G ($p < 0.05$), indicating that *Chlamydomonas reinhardtii* grown under LR was subjected to reduced light stress (Figure 5.9 and Figure 5.4). As mentioned, red photons emitted by LR at a lower irradiance level (29 μmol photons·m^{-2}·s^{-1}) were beneficially absorbed by the chlorophyll molecules and used for photosynthesis. On day 8 the carotenoid content was recorded between 4 – 5, 3 – 4, 4 – 5, and 4 – 5 mgg^{-1} for the control, LR, LY, and R8G grown cultures, respectively. The current findings support literature in that microalgal chlorophyll and carotenoid ranged between 0.5 – 4.0 and 0.1 – 0.2% of their DCW (Levasseur *et al.* 2020). The carotenoid content achieved by the algae grown under UV light was similar to those produced previously (Figure 4.6 B). In light of this evidence, the findings in Chapter 4 questioned the specific functionality of carotenoids in the NPQ process of *Chlamydomonas* in response to dye-irradiance. Both chlorophyll and carotenoid concentrations declined with the cultivation time. This was similar to other studies consistently reporting that excess irradiance levels negatively affect pigment biosynthesis, ultimately affecting photosynthesis (Ferreira *et al.* 2016; Li *et al.* 2019). Reductions in photosynthesis may lead to reductions in essential biomolecules like proteins.

5. 3. 4. 2. Protein production

Microalgal biomass comprises proteins, lipids, and carbohydrates, in which the fractions of these three biochemical components are modified by varying the light intensity. The initial protein content of *C. reinhardtii* grown under control, LR, LY, and R8G irradiations ranged between 210 – 258, 217 – 301, 196 – 263, and 226 – 245 mgg^{-1}, respectively. Apart from day 0, protein content in dye-irradiated cultures was significantly higher throughout the study when compared to the algae grown under control conditions ($p < 0.05$), (Figure 5.10). On day 4, the

protein content ranged between 183 – 188, 197 – 203, 293 – 308, and 233 – 285 mgg^{-1} under control, LR, LY, and R8G irradiations, respectively. Cultures that were grown under LY displayed between 38, 33, and 13 *wt.* % significant increase in protein content when compared to the algae grown under control, LR, and R8G irradiance ($p < 0.05$), (Figure 5.10). Proteins were produced in response to the potential oxidative stress (Gifuni *et al.* 2018), which was authenticated by the concomitant decreases in light utilisation, (Figure 5.4), and increases in light dissipation, Y(NPQ) and Y(NO) resulting from excess irradiance (Figure 5.5 and Figure 5.6, respectively). Oxidative damage was also associated with the increase in protein turnover (Figure 5.10). Previous studies have demonstrated similar findings (Colina *et al.* 2020; Meagher *et al.* 2021).

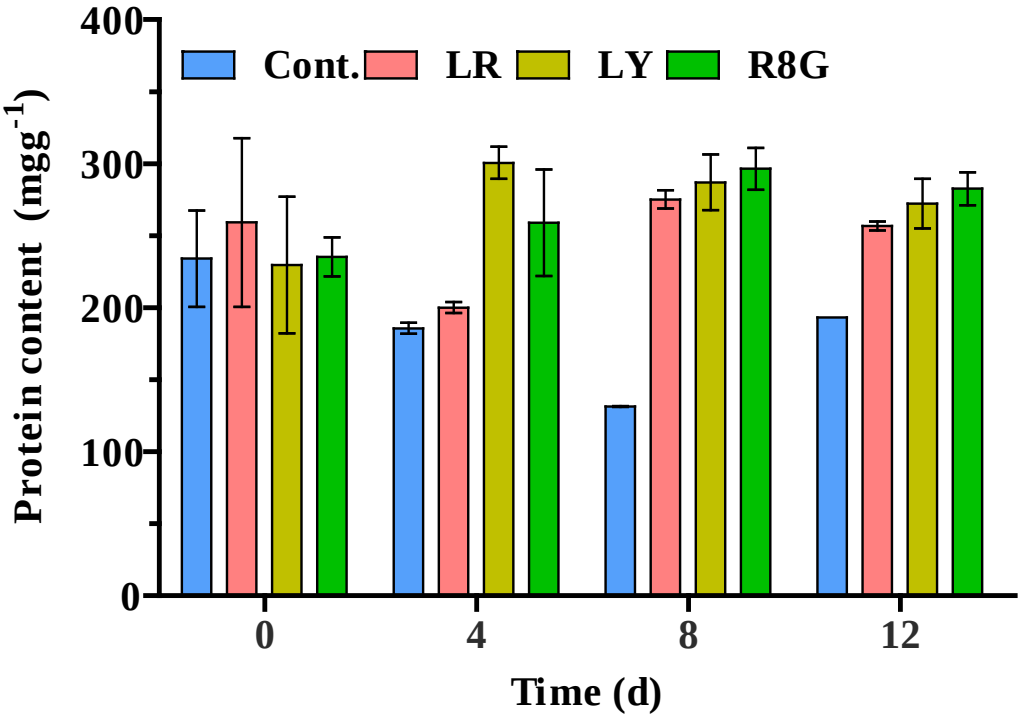

Figure 5.10: Protein content of *C. reinhardtii* grown under control (Cont.), Lumogen Red (LR), Lumogen Yellow (LY), and Rhodamine 8G (R8G) using 30% UV-*a* and UV-*b*

fluorescent tubes. Control reactors were set up where the microalgal cells received light passing through a methanol blank. Data are expressed as a mean ± SD (n = 2).

The physiological alteration of microalgae in response to acclimation entails: (*i*) *de novo* biosynthesis of protein complexes and the induction of oxidative stress-protective processes; (*ii*) transcriptional alterations with structural reorganisation and modifications to metabolic pathways; and (*iii*) modifications in the composition of the LHC which affect the photosynthetic apparatus and PE (de Mooij *et al.* 2017). The protein contents ranged between 130 – 131, 271 – 280, 273 – 301, and 286 – 307 mgg^{-1} for the control, LR, LY, and R8G irradiated cultures, respectively (day 8). This represented a 52, 54, and 56 *wt.* % increase in protein content under LR, LY, and R8G when compared to the control ($p < 0.05$). Protein after dye-acclimation was ascribed to the alteration of protein–pigment complexes used to promote microalgal growth and photosynthetic acclimation (Gifuni *et al.* 2018), further validated by increased chlorophyll and biomass (Figure 5.8 and Figure 5.3, respectively). The dye irradiance may have caused damage to the PSII central subunits triggering specific photo-protective responses based on its turnover. These involve the synthesis of new proteins with the degradation of old damaged ones, and the fast coordinated folding and integration into different PS complexes (Colina *et al.* 2020).

In green microalgae such as *C. reinhardtii*, excess light irradiance triggers and/or modifies the expression of many photosynthetic genes to adjust the concentration and abundance of the total protein (Meagher *et al.* 2021). Following the decline in growth, the production and accumulation of cellular proteins were directed toward cellular survival and not division (Figure 5.3). Increases in protein may be due to the induction of NPQ. The production of the *lhcsr* proteins triggers and assist the process of energy quenching by enhancing the

production of anti-oxidative stress compounds which are proteinaceous (Derks *et al.* 2015; Roach *et al.* 2020). The acclimated metabolic adaptation triggered by increased PFDs was used to expend excess energy that resulted in lowered biomass concentrations. Toward the end of the growth cycle, intracellular protein degradation occurred to provide energy in the form of carbon molecules. This led to attenuated photosynthetic capacity which ultimately caused growth retardation and cell death (Sun *et al.* 2018). This may explain the decrease in protein content on day 12. The protein fraction made up the biggest constituent in the microalgae biomass. Depending on the species of alga and the environmental conditions, protein content varies between 6 – 70% of their DCW (Bernaerts *et al.* 2019; Levasseur *et al.* 2020). In addition to environmental factors, interactions of the microalgae with the culture medium illicit continuous changes in the algal biochemical composition. These variations reflect on the cellular metabolism and consequently their carbohydrate makeup.

5. 3. 4. 3. Carbohydrate production

The initial carbohydrate content of *C. reinhardtii* grown under control, LR, LY, and R8G irradiated cultures ranged between 128 – 183, 178 – 181, 184 – 186, and 185 – 207 mgg^{-1}, respectively. This declined by ~ 33 *wt.* % on day 4 (Figure 5.11). Carbohydrates serve a wide range of biological functions in the microalgal cell. These include being produced as energy and carbon storage products, structural components, and cell communication molecules (Bernaerts *et al.* 2019; Levasseur *et al.* 2020). Hence, carbohydrate content was influenced by the rate of reduced carbon production and consumption in photosynthesis and growth, respectively (Sung *et al.* 2018; Vuppaladadiyam *et al.* 2018).

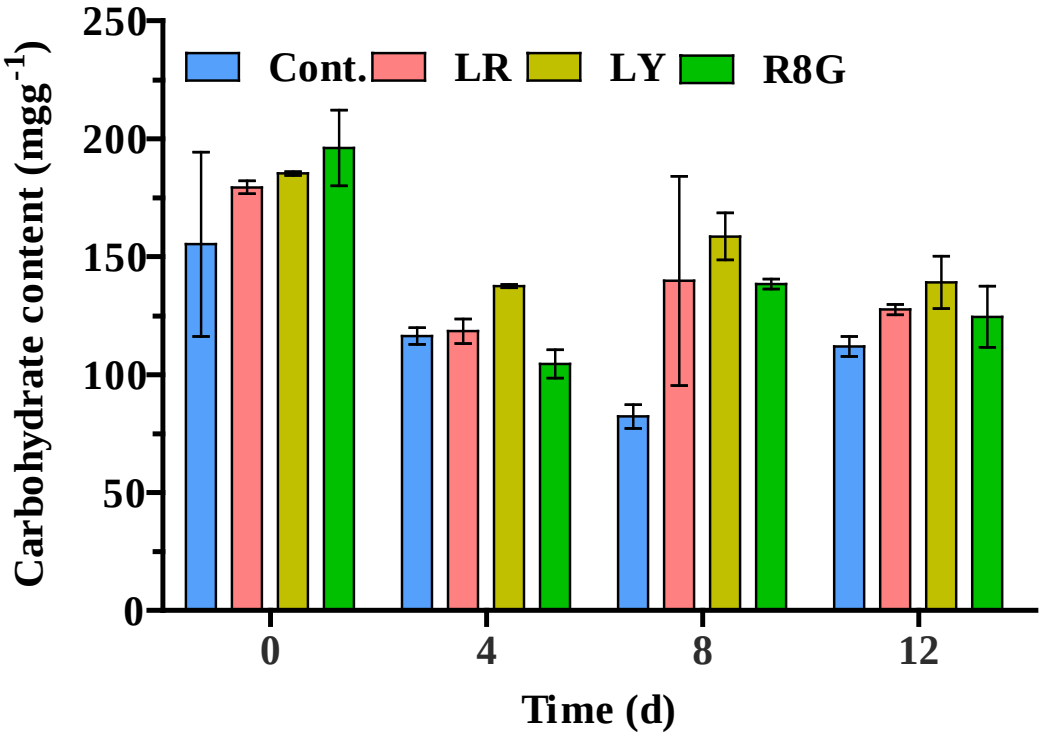

Figure 5.11: Carbohydrate content of *C. reinhardtii* grown under control (Cont.), Lumogen Red (LR), Lumogen Yellow (LY), and Rhodamine 8G (R8G) using 30% UV-*a* and UV-*b* fluorescent tubes. Control reactors were set up where the microalgal cells received light passing through a methanol blank. Data are expressed as a mean ± SD (n = 2).

When compared to the control, the LR, LY, and R8G irradiated cultures produced higher carbohydrate (between 1.7, 15, and 1.9 *wt.* %, respectively on day 4), ($p < 0.05$) (Figure 5.11). The decrease in carbohydrate content between days 0 to 4 was ascribed to the increase in light utilisation and heat dissipation (Figure 5.4 and Figure 5.5, respectively), energy flux through the CBB cycle (Figure 5.7), and growth (Figure 5.3). On day 8, the carbohydrate content ranged between 79 – 86; 108 – 171; 152 – 166; and 137 – 140 mgg^{-1} for the control, LR, LY, and R8G irradiated cultures, respectively. This represented 41, 48, and 40 *wt.* % increase in carbohydrate content under LR, LY, and R8G irradiated cultures, respectively.

Under dye-mediated irradiance, the cultures exhibited a significant increase in carbohydrate accumulation ($p < 0.05$) (Figure 5.11). Similar findings were achieved by Ajayan *et al.* (2019). The researchers found that *C. reinhardtii* exhibited a higher carbohydrate under blue illumination when compared to white, red, green LEDs, and fluorescent lamps. Furthermore, it was suggested that white and fluorescent lamp wavelengths negatively influenced carbohydrate accumulation, while the low carbohydrate content was attributed to the onset of nutrient depletion (Ajayan *et al.* 2019).

Spectral acclimation significantly affected the metabolic use of energy (substantiated by the increased Y(NPQ) values, Figure 5.5). Apart from their functions relating to algal photosynthesis, carbohydrates act as free radical scavengers and structural components regulating turgor and permitting multicellularity. Turgor pressure plays a significant role in the promotion of algal growth by influencing several processes including the import of nutrients/materials and cell volume expansion. Carbohydrates increase/decrease the solute concentration in the cell thereby regulating osmotic potential and turgor pressure, facilitating cell division and growth (Chia *et al.* 2015). Photochemical energy was funnelled toward the synthesis of carbohydrates (Sung *et al.* 2018; Vuppaladadiyam *et al.* 2018).

Visual inspection of the dye-irradiated cultures revealed evidence of culture foaming and aggregation and PBR culture wall adhesion. This occurrence was not previously seen in this study (Chapter 4) and coincided with an increase in carbohydrate content on and after day 8. Many species of microalgae (including *C. reinhardtii*, *C. mexicana*, *C. augustae*, *C. corrosa*) are known to produce extracellular polymeric substances commonly referred to as exopolysaccharides (EPS) (Kroen and Rayburn 1984; Allard and Tazi 1993; Zhu *et al.* 2012; Bafana 2013). In the current study, soluble EPS may have been fixed to the cell surface (cell-

bound polymers) and/or it is excreted into the growth medium, which facilitated the formation of aggregates by cell adhesion. Exopolysaccharides can be considered a high-value metabolite and more research should be undertaken to screen and characterise its production. Interestingly, EPS production may also be reflective of an adaptive response to environmental stresses (such as excessive PAR, UV, or salinity levels) (Davis *et al.* 2013; Delattre *et al.* 2016; Bernaerts *et al.* 2019). Typical responses to environmental stress involve the diminution of the protein and carbohydrates with the accumulation of cellular lipids.

5. 3. 4. 4. Lipid production

The lipid content ranged between 276 – 302, 285 – 322, 269 – 322, and 266 – 359 mgg^{-1} for the control, LR, LY, and R8G irradiations, respectively (day 0). Generally, algae cultivated under increased light irradiance tend to accumulate more lipids by altering excess photo-assimilates into fatty acids (Sun *et al.* 2018). Lipid content was high (Figure 5.12), which was associated with a triggered physiological synchronisation for the maintenance of cellular redox homeostasis in response to UV irradiance (Chia *et al.* 2015). The degradation of lipid between days 0 and day 4 may have been necessary to provide adequate energy required for the active growth and cellular division, (Figure 5.3). Apart from being structural components of the PSs, lipids provide sources of energy for growth as well as serve as electron sinks for excess energy (Sung *et al.* 2018; Vuppaladadiyam *et al.* 2018). This period was also highlighted by faster growth rates, low light utilisation efficiencies, and low chlorophyll content (Figure 5.4 and Figure 5.8, respectively). Additionally, mixotrophic algal growth using acetate may reorientate the carbon pool toward the production of lipid (Esquivel *et al.* 2017), (evident from the decrease in carbohydrate and increase in lipid, Figure 5.11 and Figure 5.12, respectively).

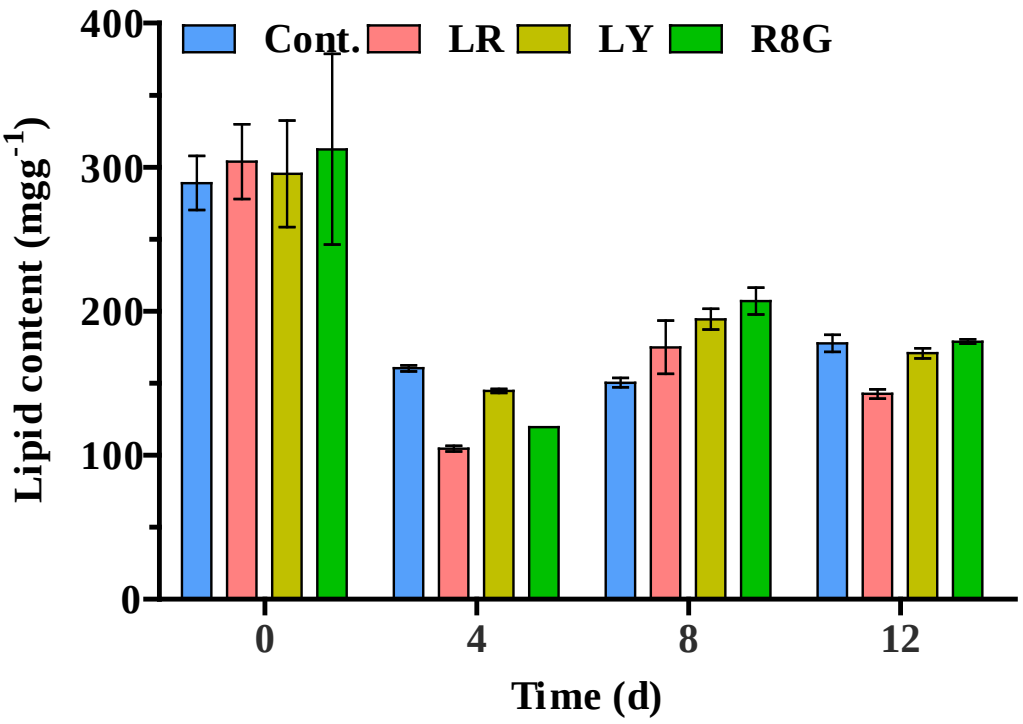

Figure 5.12: Lipid content of *C. reinhardtii* grown under control (Cont.), Lumogen Red (LR), Lumogen Yellow (LY), and Rhodamine 8G (R8G) using 30% UV-*a* and UV-*b* fluorescent tubes. Control reactors were set up where the microalgal cells received light passing through a methanol blank. Data are expressed as a mean ± SD (n = 2).

As the study progressed, growth increased at the expense of lipid production. On day 8 the lipid content ranged between 148 – 152, 162 – 188, 190 – 200, and 200 – 214 mgg^{-1} for the control, LR, LY, and R8G irradiations, respectively ($p < 0.05$). This related to a 3, 14, and 20 *wt.* % significant increase in lipid under LR, LY, and R8G irradiations, respectively. The algae grown under R8G produced slightly higher lipid. The results were similar to the observations of both Ajayan *et al.* (2019) and Vadiveloo *et al.* (2015). Blue light induced a higher lipid content when compared to red light. The researchers suggested that under blue light, the higher lipid content in *C. reinhardtii* and *Nannochloropsis* sp., respectively, were attributed to the enhanced activity of enzymes like carbonic anhydrase and RuBisCo. In algae, these enzymes

play pivotal roles in the carbon cycle regulation and are usually regulated by the blue wavelength. The authors reasoned that the higher enzyme activity stimulated by the low irradiance levels in blue light leads to the higher the accumulation of triglycerides (Vadiveloo *et al.* 2015; Ajayan *et al.* 2019). This observation could also explain the increase in RuBisCo gene expression in R8G (Figure 5.7).

On day 8, lipid content was higher than carbohydrate content. The shift from carbohydrate to lipid biosynthesis occurred due to the alteration of the carbon flux because the energy value of lipid is about 2.25-fold that of carbohydrate (Nwoba *et al.* 2019). Furthermore, when excess light is imposed on microalgal culture, the lipid content provides a large sink for excess carbon and energy (Sung *et al.* 2018; Vuppaladadiyam *et al.* 2018). Similarly, findings by Seo *et al.* (2015) further corroborate the current observations. Under the irradiance of DPA and R101, *C. vulgaris* increased its lipid content (Table 2.4). At a light intensity of 50 Wm^2 (~ 105 μmol photons$\cdot m^{-2} \cdot s^{-1}$), there was a 30 and 23% increase in DPA and R101 irradiated cultures. The finding verified the possibility that light colour affected lipid accumulation, and therefore, the researchers evaluated a mixture containing both dyes. It was found that this mixture improved biomass and enhanced lipid content by 30%. It was concluded that increased lipid resulted from increased dye-mediated PFDs in both the red and blue regions.

Sung *et al.* (2018), found that after 10 days *N. gaditana* increased lipid productivity by 26.9 and 39.4% under DPA and R101 irradiations, respectively (Table 2.4). The authors concluded that the increased lipid content was likely due to the deprivation of nitrogen rather than the specific wavelength irradiation. However, the dye-based approach could still have the potential for stimulating lipid production in systems based on continuous multi-stage processes (Sung *et al.* 2018). In the current study, the triggered physiological synchronisation in the

microalgal cells may have increased lipid formation for the maintenance of cellular redox homeostasis (Chia *et al.* 2015). Similar to the cited studies, in this study, the red and green/blue emissions from LR and R8G increased light availability to *C. reinhardtii*, thereby increasing growth and metabolite content. Interestingly, the increases in the algal growth and metabolite content at specific time points can be tentatively categorised using the PCA.

5. 3. 5. Multivariate analysis

From the PCA data (Figure 5.13), PC1 and PC2 accounted for ~ 89 and 8% of the total variation, respectively. The three PCs represented 100% of the total variance in dye-irradiations (Table 5.2). The PCA considered the trend within the data sets, classifying the microalgae growth patterns into two phases with different characteristics (pre-and post-acclimation). Both phases had different characteristics (Figure 5.13 A), while members within the group had similar trends (*i.e.*, increased/decreased simultaneously). The score plot illustrated the successful clustering of all parameters according to Phase-II and Phase-I (Figure 5.13 B).

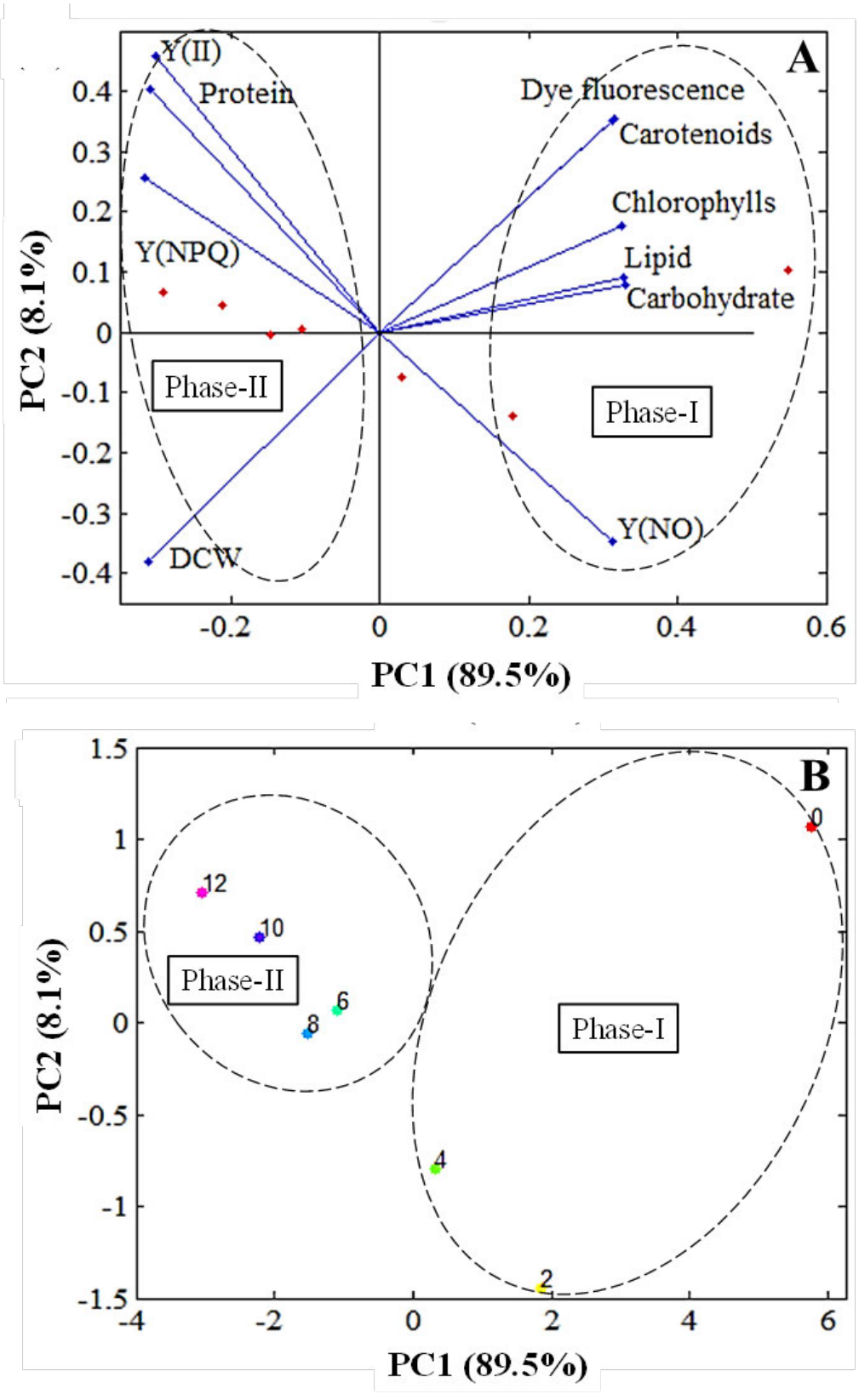

Figure 5.13: PCA describing the correlation among dye characteristics, metabolites, and biomass production within the pre-and post-acclimation phases **(A)** loading plot, and **(B)** score plot.

The highest eigenvalues represented the most dominant PCs of the data set, namely PC1 (8.6) and PC2 (1.1), (Table 5.2). Accordingly, these principal components were used to identify and discuss the correlations among the investigated datasets. The fundamental task of PCA is to express large quantities of observed variables in terms of a smaller number of hypothetical (and non-observed) new variables. This ensures that the maximum variation in the original set of data can be evaluated. Principal component analyses transformed the original data to fit new and orthogonal axes known as principal components (PCs) from which information on the most significant parameters was extracted (Nasr and Zahran 2016; Deepnarain *et al.* 2019; Colina *et al.* 2020).

Table 5.2: Loadings of the principal component analysis of *C. reinhardtii* grown under dye-mediated irradiations.

	PC1	**PC2**	**PC3**
Dye fluorescence	0.31	0.35	0.36
DCW	-0.31	-0.38	0.36
Total carotenoids	0.31	0.35	0.13
Total chlorophyll	0.33	0.18	0.31
Protein	-0.31	0.40	0.18
Carbohydrate	0.33	0.08	-0.03
Lipid	0.33	0.09	-0.42
Y(II)	-0.30	0.46	-0.11
Y(NPQ)	-0.32	0.26	0.40
Y(NO)	0.31	-0.35	0.50
Variance (%)	89.52	8.11	2.37
Cumulative variance (%)	89.52	97.63	100.00
Eigenvalue	8.66	1.10	0.24

The loading plot showed that Phase-I (the initial phase [dye-acclimation]) incorporated contained dye fluorescence, carotenoid, chlorophyll, lipid, carbohydrate, and Y(NO) which

were located in the positive direction of PC1 (horizontal axis) (Figure 5.13 A). Interestingly, Y(NPQ), Y(II), DCW, and protein were distributed on the negative side of PC1. This indicated an opposite trend between these parameters. However, biomass concentrations increased sharply from days 0 to 3. This inconsistency may be due to the increased dye fluorescence which led to increased Y(NO) during Phase-I (Figure 5.13 A), subsequently reducing photon conversion efficiency and restricting biomass production up to day 5. This response was validated by the decreased growth and RuBisCo gene expression in *C. reinhardtii* during the dye-acclimation phase (Figure 5.3 and Figure 5.7). This increased chlorophyll, carotenoid, carbohydrate, and lipid production (Figure 5.3, Figure 5.8, Figure 5.9, Figure 5.11, and Figure 5.12, respectively). Moreover, the PCA showed that parameters in Phase-I decreased simultaneously after day 5. This trend could be associated with autophagy, where essential macromolecules such as proteins are recycled in a cellular degradation process to allow the reallocation of nutrients (Figure 5.10). This pathway has been known to occur under increased irradiance levels (Meagher *et al.* 2021). Consequently, the findings revealed that PC1 potentially gathered variability related to dye-acclimation, thereby affecting microalgal photosynthesis.

Phase-II (second phase [> day 5]) was associated with positive loadings on Y(II), Y(NPQ), and protein while the DCW exhibited a negative loading on PC2 (vertical axis) (Figure 5.13 A). The PC2 was represented by two major correlations, *i.e.*, Y(II) vs Y(NO) and DCW vs Y(NPQ). Decreases in microalgal biomass (DCW) was related to increases in Y(II), Y(NPQ), and protein content (Figure 5.4, Figure 5.5, and Figure 5.10, respectively). Similarly, Y(NO) was distributed on the negative side of PC2, and thus, decreased Y(NO) values were correlated with increased Y(II) and Y(NPQ). This observation demonstrated that the photosynthetic capacity was influenced by the information retained in PC2. Phase-II was

characterised by increases in the DCW, Y(NPQ), protein, and Y(II), and thus, grouped early responses in terms of growth. It is important to note that as experiments were conducted in duplicate, caution should be used for interpretation of the data and when extrapolating the conclusions discussed. Additionally, when performing similar experimentations, approaches other than PCA should be explored as they may be more appropriate and offer more significance to the resulting studies.

The prospect of manipulating the algal metabolite content by spectrally tuning the irradiance or the prediction of the biomass composition as a function of irradiance has the potential to open the way for the exploitation of microalgal biotechnology according to the biorefinery concept (Figure 2.1). This study revealed the promising applicability of the LR and R8G dyes as effective spectral converters of incident irradiation, supporting photosynthetic energy utilisation, and increasing metabolite yields with less input of energy in the algal systems. Hence, the proposed dye-mediated irradiations are useful for microalgae cultivation and production mechanisms, which may potentially contribute toward the SDGs, (Figure 2.2). The extracted algal lipids and carbohydrates (189 $mg \cdot g^{-1}$ and 138 $mg \cdot g^{-1}$, Figure 5.12 and Figure 5.11, respectively), could be potentially applied to the biofuels industries, (Figure 2.1). This advantage could meet GOAL 7 "*Affordable and Clean Energy*". The increased protein fractions under dye-mediated irradiations ($\geq$ 49%, Figure 5.10), suggest promising applications for the production of nutritional and functional food/feed products, upholding GOAL 2 "*Zero Hunger*". The antioxidant pigment fractions (Figure 5.8 and Figure 5.9), may find relevant application in the food and nutraceuticals industries indirectly meeting GOAL 3 "*Good Health and Well-being*" (Ansari *et al.* 2021; Sutherland *et al.* 2021).

5. 4. Conclusion

Overall, the dyes had a positive effect on biomass and metabolite production in *C. reinhardtii*. However, the LY dye, used in this study, should not be considered for spectral conversion applications due to dye photo-degradation. The blue-green and red emitted light from R8G and LR was associated with increased biomass productivity and metabolic contents when compared with the control, respectively. The *Chlamydomonas* early response to the dye-irradiations was to increase growth (day 0 – 4), demonstrating the beneficial effect of the increased dye-mediated irradiance on algal growth. At later stages, dye-mediated irradiance was found to be in excess which resulted in increased protein and carbohydrate production. The RuBisCo gene expression further justified the increased photochemical energy utilisation [Y(II)] and decreased regulated heat dissipation [Y(NPQ)]. Additionally, the PCA results can be used to predict the biomass and/or metabolite content in future applications. Dye emissions were found to be effectively utilised by the algae as evidenced by the increases in metabolite contents.

Chapter 6 : Conclusions and Recommendations

6. 1. Conclusions

The premise of this research was to evaluate organic dyes for their ability to absorb and emit PAR, thereby improving light availability in *C. reinhardtii.* By employing organic dyes as spectral converters, the metabolite production was expected to increase in *C. reinhardtii*. The novel findings from the current research were that:

- From the solvents tested, dyes dissolved in methanol maintained the highest irradiances and, therefore, can be used for dye dissolution.

- With regards to the dyes tested, high dye concentrations (100 mgL^{-1}) lead to dye aggregate formation resulting in self-absorption, thus lower concentrations (10 mgL^{-1}) should be used to maintain the efficacy of the dye.

- The findings indicated that R8G and LR can be applied to microalgal cultivation systems, however, the dyes need adequate UV stimulation to perform the spectral conversion.

- To ensure the high efficiency of organic dyes under long-term incident irradiations, the required design specifications considered should be wide absorption and emission spectra (to limit self-absorption) and high quantum efficiency coupled with the minimisation of photo-degradation.

- Dye emissions improved algal growth in the initial growth stages, while toward the later stages it improved metabolite production. The LR and R8G dyes were able to stimulate the production of pigments and was found to be effectively utilised by the algal cells. Furthermore, the blue-green emissions from R8G were able to penetrate deeper into the culture medium.

6. 2. Recommendations

In the hopes of broadening the scope of microalgae biotechnology, the recommendations for continued academic research and development of commercial dye-mediated spectral conversion systems are:

- Future research in this field should test the DPA and R800 dyes for their potential to be applied to microalgal cultivation systems. Also, lower dye concentrations (1 – 10 mgL^{-1}) need to be evaluated to create reliable measurements of dye excitation and emission maxima. Utilising dyes or dye combinations that are capable of up and down-conversion (UV and IR), will increase the efficacy of spectral conversion systems. Dyes and/or combinations should be chosen to reduce the spectral excitation/emission overlapping.

- Due to the potential for dye aggregation, it is important to take cognisance of dye solubility. Dye aggregates promote emission enhancement or quenching resulting in fluorescence inaccuracies. Consequently, minimisation of these effects could be achieved by the addition of highly ionised hydrophilic groups or the attachment to hydrophilic biopolymers, or the incorporation into supramolecular systems (such as nanoparticles).

- Inevitably, photo-degradation will also have negative implications in the potential commercialisation of the technology. It is fundamental to develop strategies for future upregulation processing of this technology. Therefore, to increase dye photo-stability and intensification of fluorescence, it is recommended that future work consider dye immobilisation on solid media. A variety of host materials should be considered and subjected to reliability and durability (longevity) testing. Additionally, the fabrication of PBRs with immobilised dyes or coating the surfaces of PBRs with fluorescent dye layers can potentially be used to increase dye fluorescence lifetimes.

- To gain a clearer perspective, forthcoming research on dye spectral conversion should be performed outdoors using sunlight to fundamentally determine if UV exposure, temperature, humidity, or a combination of these factors affect dye stability. In this way, real-time conclusions can be drawn on the effectiveness of dye conversions and the effects of dye-mediated PPFDs on microalgal growth.

- When employing this technology, practical implementations should focus primarily on reabsorption and scattering losses, dye fluorescence lifetimes, absorption/emission, tunability *etc*. In addition, time-dependent studies should be conducted to test dye emission efficiencies, and, to save on overall process costs, dye reusability should be assessed.

- Dye spectral conversion should be performed on a wider range of microalgal species to promote the production of similar high-value metabolites in the response to the enhanced spectra. As much as this study relied on closed jacketed bioreactor vessels,

bacterial/fungal contamination should be routinely checked. Such information will be essential for forthcoming research and possibly future scale-up of the technology.

- Dye-mediated spectral conversion could be used as an effective strategy to manipulate the metabolism of multiple metabolites sequentially derived from the same biomass. As an alternative, future research can be done to evaluate multi-stage cultivation as a strategy for the conversion of desired metabolites. For example, the potential regulation of starch biosynthesis and its degradation to obtain higher-value products such as carotenoid and lipid. In this way, dye-based metabolite conversion can be used for sector-specific utilisation.

References

Abou-Kana, M. T. H. 2012. Optical, Photophysical, Stability and Mirrorless Lasing Properties of Novel Fluorescein Derivative Dye in Solution. *Open Journal of Applied Sciences*, 2 (4): 228 - 235.

Abu-Ghosh, S., Fixler, D., Dubinsky, Z. and Iluz, D. 2016. Flashing light in microalgae biotechnology. *Bioresource Technology*, 203: 357 - 363.

Abu-Ghosh, S., Fixler, D., Dubinsky, Z., Solovchenko, A., Zigman, M., Yehoshua, Y. and Iluz, D. 2015. Flashing light enhancement of photosynthesis and growth occurs when photochemistry and photoprotection are balanced in *Dunaliella salina*. *European Journal of Phycology*, 50 (4): 469 - 480.

Ahmed, H., McCormack, S. J. and Doran, J. 2017. Plasmonic luminescent down shifting layers for the enhancement of CdTe mini-modules performance. *Solar Energy*, 141: 242 - 248.

Ajayan, K. V., Anjula, K., Syamasurya, A. P. and Harilal, C. C. 2019. Energy efficient technology for enhanced growth and lipid production in *Chlamydomonas reinhardtii* through additional reflector coated LED photo-bioreactor. *Biochemical Engineering Journal*, 144: 81 - 88.

Al-Aqmar, D. M., Abdelkader, H. I. and Abou Kana, M. T. H. 2015. Spectroscopic properties and amplified spontaneous emission of fluorescein laser dye in ionic liquids as green media. *Optical Materials*, 47: 573 - 581.

Ali, R. A., Abdul-Munem, O. M. and Abd, A. N. 2012. Study the spectroscopic characteristics of Rhodamine B Dye in Ethanol and Methanol mixture and Calculation the Quantum Efficiency. *Baghdad Science Journal*, 9 (2): 352 - 358.

Alishah Aratboni, H., Rafiei, N., Garcia-Granados, R., Alemzadeh, A. and Morones-Ramirez, J. R. 2019. Biomass and lipid induction strategies in microalgae for biofuel production and other applications. *Microbial Cell Factories*, 18 (178): https://doi.org/10.1186/s12934-12019-11228-12934.

Allard, B. and Tazi, A. 1993. Influence of growth status on composition of extra-cellular polysaccharides from two *Chlamydomonas* species. *Phytochemistry*, 32 (1): 41 - 47.

Almeida, A. C., Gomes, T., Langford, K., Thomas, K. V. and Tollefsen, K. E. 2017. Oxidative stress in the algae *Chlamydomonas reinhardtii* exposed to biocides. *Aquatic Toxicology*, 189: 50 - 59.

Altschul, S. F., Madden, T. L., Schäffer, A. A., Zhang, J., Zhang, Z., Miller, W. and Lipman, D. J. 1997. Gapped BLAST and PSI-BLAST: a new generation of protein database search programs. *Nucleic Acids Research*, 25 (17): 3389 - 3402.

Ansari, F. A., Nasr, M., Rawat, I. and Bux, F. 2021. Meeting sustainable development goals (SDGs) through progression of pilot-scale algal system to commercial raceway pond (300,000 L). *Biomass Conversion and Biorefinery*: https://doi.org/10.1007/s13399-13021-01661-13390.

Asuthkar, M., Gunti, Y., S, R. R., Rao, C. S. and Yadavalli, R. 2016. Effect of different wavelengths of light on the growth of *Chlorella pyrenoidosa*. *International Journal of Pharmaceutical Sciences and Research*, 7 (2): 847 - 851.

Baer, S., Heining, M., Schwerna, P., Buchholz, R. and Hübner, H. 2016. Optimization of spectral light quality for growth and product formation in different microalgae using a continuous photobioreactor. *Algal Research*, 14: 109 - 115.

Bafana, A. 2013. Characterization and optimization of production of exopolysaccharide from *Chlamydomonas reinhardtii*. *Carbohydrate Polymers*, 95 (2): 746 - 752.

Beecraft, L., Watson, S. B. and Smith, R. E. H. 2017. Multi-wavelength Pulse Amplitude Modulated fluorometry (Phyto-PAM) reveals differential effects of ultraviolet radiation on the photosynthetic physiology of phytoplankton pigment groups. *Freshwater Biology*, 62 (1): 72 - 86.

Benavente-Valdes, J. R., Aguilar, C., Contreras-Esquivel, J. C., Mendez-Zavala, A. and Montanez, J. 2016. Strategies to enhance the production of photosynthetic pigments and lipids in chlorophycae species. *Biotechnology Reports*, 10: 117 - 125.

Bernaerts, T. M. M., Gheysen, L., Foubert, I., Hendrickx, M. E. and Van Loey, A. M. 2019. The potential of microalgae and their biopolymers as structuring ingredients in food: A review. *Biotechnology Advances*, 37 (8): 107419.

Berteotti, S., Ballottari, M. and Bassi, R. 2016. Increased biomass productivity in green algae by tuning non-photochemical quenching. *Scientific Reports*, 6: 21339.

Boyle, N. R. and Morgan, J. A. 2009. Flux balance analysis of primary metabolism in *Chlamydomonas reinhardtii*. *BMC Systems Biology*, 3 (4): https://doi.org/10.1186/1752-0509-1183-1184.

Boyle, N. R., Sengupta, N. and Morgan, J. A. 2017. Metabolic flux analysis of heterotrophic growth in *Chlamydomonas reinhardtii*. *PLoS One*, 12 (5): e0177292.

Brackmann, U. 2000. *Lambdachrome® Laser Dyes*. 3rd Edition ed. Göttingen, Germany: Lambda Physik AG.

Brody, J. R., Calhoun, E. S., Gallmeier, E., Creavalle, T. D. and Kern, S. E. 2004. Ultra-fast high-resolution agarose electrophoresis of DNA and RNA using low-molarity conductive media. *BioTechniques* 37 (4): 598 - 602.

Burlacot, A., Peltier, G. and Li-Beisson, Y. 2019. Subcellular Energetics and Carbon Storage in *Chlamydomonas*. *Cells*, 8 (10): 1154.

Carbone, I. A., Frawley, K. R. and McCann, M. K. 2019. Flexible, Front-Facing Luminescent Solar Concentrators Fabricated from Lumogen F Red 305 and Polydimethylsiloxane. *International Journal of Photoenergy*, 2019: https://doi.org/10.1155/2019/8680931.

Cecchin, M., Benfatto, S., Griggio, F., Mori, A., Cazzaniga, S., Vitulo, N., Delledonne, M. and Ballottari, M. 2018. Molecular basis of autotrophic vs mixotrophic growth in *Chlorella sorokiniana*. *Scientific Reports*, 8 (1): 6465.

Chandaravithoon, P., Ritchie, R. J. and Runcie, J. W. 2020. Measuring photosynthesis of both oxygenic and anoxygenic photosynthetic organisms using pulse amplitude modulation (PAM) fluorometry in wastewater ponds. *Journal of Applied Phycology*, 32 (4): 2615 - 2629.

Chandra, R., Iqbal, H. M. N., Vishal, G., Lee, H.-S. and Nagra, S. 2019. Algal biorefinery: A sustainable approach to valorize algal-based biomass towards multiple product recovery. *Bioresource Technology*, 278: 346 - 359.

Chia, M. A., Lombardi, A. T., da Graca Gama Melao, M. and Parrish, C. C. 2015. Combined nitrogen limitation and cadmium stress stimulate total carbohydrates, lipids, protein and amino acid accumulation in *Chlorella vulgaris* (Trebouxiophyceae). *Aquatic Toxicology*, 160: 87 - 95.

Chia, S. R., Ong, H. C., Chew, K. W., Show, P. L., Phang, S.-M., Ling, T. C., Nagarajan, D., Lee, D.-J. and Chang, J.-S. 2018. Sustainable approaches for algae utilisation in bioenergy production. *Renewable Energy*, 129: 838 - 852.

Choi, Y. K., Kumaran, R. S., Jeon, H. J., Song, H. J., Yang, Y. H., Lee, S. H., Song, K. G., Kim, K. J., Singh, V. and Kim, H. J. 2015. LED light stress induced biomass and fatty acid

production in microalgal biosystem, *Acutodesmus obliquus*. *Spectrochimica Acta Part A: Molecular and Biomolecular Spectroscopy*, 145: 245 - 253.

Choix, F. J., Ramos-Ibarra, J. R., Mondragon-Cortez, P., Lara-Gonzalez, M. A., Juarez-Carrillo, E., Becerril-Espinosa, A., Ocampo-Alvarez, H. and Torres, J. R. 2021. Mixotrophic growth regime as a strategy to develop microalgal bioprocess from nutrimental composition of tequila vinasses. *Bioprocess and Biosystems Engineering*, 44 (6): 1155 - 1166.

Colina, F., Carbo, M., Meijon, M., Canal, M. J. and Valledor, L. 2020. Low UV-C stress modulates *Chlamydomonas reinhardtii* biomass composition and oxidative stress response through proteomic and metabolomic changes involving novel signalers and effectors. *Biotechnology for Biofuels*, 13 (110): https://doi.org/10.1186/s13068-13020-01750-13068.

Cyprych, K., Kopczyńska, Z., Kajzar, F., Rau, I. and Mysliwiec, J. 2015. Tunable wavelength light emission and amplification in Rhodamine 6G aggregates. *Advanced Device Materials*, 1 (2): 69 - 73.

da Fontoura Prates, D., Duarte, J. H., Vendruscolo, R. G., Wagner, R., Ballus, C. A., da Silva Oliveira, W., Godoy, H. T., Barcia, M. T., de Morais, M. G., Radmann, E. M. and Costa, J. A. V. 2020. Role of light emitting diode (LED) wavelengths on increase of protein productivity and free amino acid profile of *Spirulina* sp. cultures. *Bioresource Technology*, 306: 123184.

da Silva Ferreira, V. and Sant'Anna, C. 2016. Impact of culture conditions on the chlorophyll content of microalgae for biotechnological applications. *World Journal of Microbiology and Biotechnology*, 33 (1): 20.

Danaee, S., Yazdanbakhsh, N., Naghoosi, H. and Sheykhinejad, A. 2018. Assessment of phosphorescent paint effects on microalgae cultivation. *Korean Journal of Chemical Engineering*, 35: 10.1007/s11814-11018-10009-11819.

Darko, E., Heydarizadeh, P., Schoefs, B. and Sabzalian, M. R. 2014. Photosynthesis under artificial light: the shift in primary and secondary metabolism. *Philosophical Transactions of the Royal Society B*, 369 (1640): P20130243.

Davis, M. C., Fiehn, O. and Durnford, D. G. 2013. Metabolic acclimation to excess light intensity in *Chlamydomonas reinhardtii*. *Plant, Cell and Environment*, 36 (7): 1391 - 1405.

de Mooij, T., de Vries, G., Latsos, C., Wijffels, R. H. and Janssen, M. 2016. Impact of light color on photobioreactor productivity. *Algal Research*, 15: 32 - 42.

de Mooij, T., Nejad, Z. R., van Buren, L., Wijffels, R. H. and Janssen, M. 2017. Effect of photoacclimation on microalgae mass culture productivity. *Algal Research*, 22: 56 - 67.

Deepnarain, N., Nasr, M., Kumari, S., Stenström, T. A., Reddy, P., Pillay, K. and Bux, F. 2019. Decision tree for identification and prediction of filamentous bulkingat full-scale activated sludge wastewater treatment plant. *Process Safety and Environmental Protection*, 126 25 - 34.

Delattre, C., Pierre, G., Laroche, C. and Michaud, P. 2016. Production, extraction and characterization of microalgal and cyanobacterial exopolysaccharides. *Biotechnology Advances*, 34 (7): 1159 - 1179.

Delavari Amrei, H., Ranjbar, R., Rastegar, S., Nasernejad, B. and Nejadebrahim, A. 2014. Using fluorescent material for enhancing microalgae growth rate in photobioreactors. *Journal of Applied Phycology*, 27 (1): 67 - 74.

Delgado-Sanchez, J.-M. 2019. Luminescent solar concentrators: Photo-stability analysis and long-term perspectives. *Solar Energy Materials and Solar Cells*, 202: 110134.

Derks, A., Schaven, K. and Bruce, D. 2015. Diverse mechanisms for photoprotection in photosynthesis. Dynamic regulation of photosystem II excitation in response to rapid environmental change. *Biochimica et Biophysica Acta* 1847: 468 - 485.

Dogaris, I., Welch, M., Meiser, A., Walmsley, L. and Philippidis, G. 2015. A novel horizontal photobioreactor for high-density cultivation of microalgae. *Bioresource Technology*, 198: 316 - 324.

Duarte, J. H. and Costa, J. A. V. 2018. Blue light emitting diodes (LEDs) as an energy source in *Chlorella fusca* and *Synechococcus nidulans* cultures. *Bioresource Technology*, 247: 1242 - 1245.

Durairaj, A., Obadiah, A., Ramanathan, S., Johnson, P. M., Bella, A. P. and Vasanthkumar, S. 2017. Synthesis, Characterization and Solvatochromic Studies Using the Solvent Polarity Parameter, ENT on 2-Chloro-3-Ethylamino-1,4-Naphthoquinone. *Journal of Fluorescence*, 27 (4): 1505 - 1512.

Eroglu, E., Eggers, P. K., Winslade, M., Smith, S. M. and Raston, C. L. 2013. Enhanced accumulation of microalgal pigments using metal nanoparticle solutions as light filtering devices. *Green Chemistry*, 15 (11): 3155 - 3159.

Esquivel, M. G., Matos, A. R. and Marques Silva, J. 2017. Rubisco mutants of *Chlamydomonas reinhardtii* display divergent photosynthetic parameters and lipid allocation. *Applied Microbiology and Biotechnology*, 101 (13): 5569 - 5580.

Ferreira, V. S., Pinto, R. F. and Sant'Anna, C. 2016. Low light intensity and nitrogen starvation modulate the chlorophyll content of *Scenedesmus dimorphus*. *Journal of Applied Microbiology*, 120 (3): 661 - 670.

Gao, F., Woolschot, S., Cabanelas, I. T. D., Wijffels, R. H. and Barbosa, M. J. 2021. Light spectra as triggers for sorting improved strains of *Tisochrysis lutea*. *Bioresource Technology*, 321: 124434.

Gao, Z., Hao, Y., Zheng, M. and Chen, Y. 2017. A fluorescent dye with large Stokes shift and high stability: synthesis and application to live cell imaging. *RSC Advances*, 7 (13): 7604 - 7609.

García-Cañedo, J. C., Cristiani-Urbina, E., Flores-Ortiz, C. M., Ponce-Noyola, T., Esparza-García, F. and Cañizares-Villanueva, R. O. 2016. Batch and fed-batch culture of *Scenedesmus incrassatulus*: Effect over biomass, carotenoid profile and concentration, photosynthetic efficiency and non-photochemical quenching. *Algal Research*, 13: 41 - 52.

Gifuni, I., Pollio, A., Marzocchella, A. and Olivieri, G. 2018. New ultra-flat photobioreactor for intensive microalgal production: The effect of light irradiance. *Algal Research*, 34: 134 - 142.

Giridhar Babu, A., Wu, X., Kabra, A. N. and Kim, D.-P. 2017. Cultivation of an indigenous *Chlorella sorokiniana* with phytohormones for biomass and lipid production under N-limitation. *Algal Research*, 23: 178 - 185.

Girolomoni, L., Cazzaniga, S., Pinnola, A., Perozeni, F., Ballottari, M. and Bass, R. 2019. LHCSR3 is a nonphotochemical quencher of both photosystems in *Chlamydomonas reinhardtii*. *PNAS*, 116 (10): 4212 - 4217.

Goff, M. L., Ferrec, E. L., Mayer, C., Mimouni, V., Lagadic-Gossmann, D., Schoefs, B. and Ulmann, L. 2019. Microalgal carotenoids and phytosterols regulate biochemical mechanisms involved in human health and disease prevention. *Biochimie*, 167: 106 - 118.

Gomaa, M. A., Al-Haj, L. and Abed, R. M. 2016. Metabolic engineering of Cyanobacteria and microalgae for enhanced production of biofuels and high-value products. *Journal of Applied Microbiology*, 121 (4): 919 - 931.

Gomes, T., Xie, L., Brede, D., Lind, O.-C., Solhaug, K. A., Salbu, B. and Tollefsen, K. E. 2017. Sensitivity of the green algae *Chlamydomonas reinhardtii* to gamma radiation: Photosynthetic performance and ROS formation. *Aquatic Toxicology*, 183: 1 - 10.

Gomez, J. A., Höffner, K. and Barton, P. I. 2016. From sugars to biodiesel using microalgae and yeast. *Green Chemistry*, 18 (2): 461 - 475.

Goncalves, A. L., Pires, J. C. and Simoes, M. 2016. Biotechnological potential of *Synechocystis salina* co-cultures with selected microalgae and cyanobacteria: Nutrients removal, biomass and lipid production. *Bioresource Technology*, 200: 279 - 286.

Gong, M. and Bassi, A. 2016. Carotenoids from microalgae: A review of recent developments. *Biotechnology Advances*, 34 (8): 1396 - 1412.

Goss, R. and Lepetit, B. 2015. Biodiversity of NPQ. *Journal of Plant Physiology*, 172: 13 - 32.

Grudzinski, W., Krzeminska, I., Luchowski, R., Nosalewicz, A. and Gruszecki, W. I. 2016. Strong-light-induced yellowing of green microalgae *Chlorella*: A study on molecular mechanisms of the acclimation response. *Algal Research*, 16: 245 - 254.

Guha, A. and Basu, A. 2014. Role of rare earth oxide nanoparticles (CeO_2 and La_2O_3) in suppressing the photobleaching of fluorescent organic dyes. *Journal of Fluorescence*, 24 (3): 683 - 687.

Hannan, M. A., Sohag, A. A. M., Dash, R., Haque, M. N., Mohibbullah, M., Oktaviani, D. F., Hossain, M. T., Choi, H. J. and Moon, I. S. 2020. Phytosterols of marine algae: Insights into the potential health benefits and molecular pharmacology. *Phytomedicine*, 69: 153201.

Hashimoto, H., Sugai, Y., Uragami, C., Gardiner, A. T. and Cogdell, R. J. 2015. Natural and artificial light-harvesting systems utilizing the functions of carotenoids. *Journal of Photochemistry and Photobiology C: Photochemistry Reviews*, 25: 46 - 70.

Hassan, A. F., Ali H, A.-H. and Abbas, F. S. 2014. Study the Effect of Concentration on Spectroscopic Properties of Fluorescein Sodium dye in Ethanol. *Journal of Kufa- Physics*, 6 (1): 112 - 118.

He, Q., Yang, H., Wu, L. and Hu, C. 2015. Effect of light intensity on physiological changes, carbon allocation and neutral lipid accumulation in oleaginous microalgae. *Bioresource Technology*, 191: 219 - 228.

Jang, H., Namgoong, J. W., Sung, M.-G., Chang, Y. and Kim, J. P. 2018. Synthesis and characterization of fluorescent dyes and their applications for the enhancement of growth rate of *Chlorella vulgaris*. *Dyes and Pigments*, 158: 142 - 150.

Kang, M., Kim, H., Lee, T. H., Huh, Y. H., Kim, Y. S., Park, S. J., Jin, J.-O., Lee, P. C. W. and Kwak, M. 2019. Highly photostable rylene-encapsulated polymeric nanoparticles for fluorescent labeling in biological system. *Journal of Industrial and Engineering Chemistry*, 80: 239-246.

Katiyar, R., Gurjar, B., Biswas, S., Pruthi, V., Kumar, N. and Kumar, P. 2017. Microalgae: An emerging source of energy based bio-products and a solution for environmental issues. *Renewable & Sustainable Energy Reviews*, 72: 1083 - 1093.

Kendirlioglu, G. and Cetin, A. K. 2017. Effect of Different Wavelengths of Light on Growth, Pigment Content and Protein Amount of *Chlorella vulgaris*. *Fresenius Environmental Bulletin*, 26 (12A/2017): 7974 - 7980.

Khoobkar, Z. and Delavari Amrei, H. 2020. Effect of fluorescent dye positioning and concentration on the growth parameters and lipid content of *Chlorella* sp. in a flat panel photobioreactor. *Biotechnology Letters*, 42 (8): 1397 - 1405.

Kim, D. G., Lee, C., Park, S. M. and Choi, Y. E. 2014. Manipulation of light wavelength at appropriate growth stage to enhance biomass productivity and fatty acid methyl ester yield using *Chlorella vulgaris*. *Bioresource Technology*, 159: 240 - 248.

Kroen, W. K. and Rayburn, W. R. 1984. Influence of growth status and nutrients on extracellular polysaccharide synthesis by the soil alga *Chlamydomonas mexicana* (Chlorophyceae). *Journal of Phycology*, 20 (2): 253 - 257.

Krzeminska, I., Piasecka, A., Nosalewicz, A., Simionato, D. and Wawrzykowski, J. 2015. Alterations of the lipid content and fatty acid profile of *Chlorella protothecoides* under different light intensities. *Bioresource Technology*, 196: 72 - 77.

Kumar, S., Cheng, J., Kubar, A. A., Guo, W., Song, Y., Liu, S., Chen, S. and Tian, J. 2021. Orange light spectra filtered through transparent colored polyvinyl chloride sheet enhanced pigment content and growth of *Arthrospira* cells. *Bioresource Technology*, 319 (124179)

Langhals, H. 2020. Fluorescence and fluorescent dyes. *Physical Sciences Reviews*, 5 (8): 20190100.

Levasseur, W., Perre, P. and Pozzobon, V. 2020. A review of high value-added molecules production by microalgae in light of the classification. *Biotechnology Advances*, 41: 107545.

Li-Beisson, Y., Thelen, J. J., Fedosejevs, E. and Harwood, J. L. 2019. The lipid biochemistry of eukaryotic algae. *Progress in Lipid Research*, 74: 31 - 68.

Li, D., Yuan, Y., Cheng, D. and Zhao, Q. 2019. Effect of light quality on growth rate, carbohydrate accumulation, fatty acid profile and lutein biosynthesis of *Chlorella* sp. AE10. *Bioresource Technology*, 291: 121783.

Li, Y., Li, L., Liu, J. and Qin, R. 2020. Light absorption and growth response of Dunaliella under different light qualities. *Journal of Applied Phycology*, 32 (2): 1041-1052.

Liang, F., Lindberg, P. and Lindblad, P. 2018. Engineering photoautotrophic carbon fixation for enhanced growth and productivity. *Sustainable Energy & Fuels*, 2 (12): 2583 - 2600.

Lichtenthaler, H. K. and Wellburn, A. R. 1983. Determinations of total carotenoids and chlorophylls a and b in leaf extracts in different solvents. *Biochemical Society Transactions*, 11: 591 - 592.

Liu, J., Song, Y. and Qiu, W. 2017. Oleaginous microalgae *Nannochloropsis* as a new model for biofuel production: Review & analysis. *Renewable & Sustainable Energy Reviews*, 72: 154 - 162.

Liu, X., Xu, Z. and Cole, J. M. 2013. Molecular Design of UV–vis Absorption and Emission Properties in Organic Fluorophores: Toward Larger Bathochromic Shifts, Enhanced Molar Extinction Coefficients, and Greater Stokes Shifts. *The Journal of Physical Chemistry C*, 117 (32): 16584 - 16595.

Lub, J., van Hal, P. A., Smits, R., Malassenet, L., Pikkemaat, J. and Hikmet, R. A. M. 2019. On the photo-oxidation of perylene bisimide dyes in alcoholic solutions. *Journal of Luminescence*, 207: 585 - 588.

Lukavenko, O. N., Eltsov, S. V., Grigorovich, A. V. and McHedlov-Petrossyan, N. O. 2009. Solubility and fluorescence lifetime of 2,5-diphenyloxazole and 1,4-bis(5-phenyl-oxazolyl-2)benzene in water–ethanol and water–acetone solvent systems. *Journal of Molecular Liquids*, 145 (3): 167-172.

Ma, R., Zhao, X., Xie, Y., Ho, S. H. and Chen, J. 2019. Enhancing lutein productivity of *Chlamydomonas* sp. via high-intensity light exposure with corresponding carotenogenic genes expression profiles. *Bioresource Technology* 275: 416 - 420.

Maillard, J., Klehs, K., Rumble, C., Vauthey, E., Heilemann, M. and Furstenberg, A. 2020. Universal quenching of common fluorescent probes by water and alcohols. *Chemical Science*, 12 (4): 1352 - 1362.

Malfatti, L., Suzuki, K., Erker, A., Jang, Y. and Innocenzi, P. 2018. Photoluminescence of zinc oxide mesostructured films doped with Rhodamine 6G. *Journal of Photochemistry and Photobiology A: Chemistry*, 357: 30 - 35.

Markou, G. and Nerantzis, E. 2013. Microalgae for high-value compounds and biofuels production: a review with focus on cultivation under stress conditions. *Biotechnology Advances*, 31 (8): 1532 - 1542.

Masojídek, J., Torzillo, G. and Koblížek, M. 2013. Photosynthesis in Microalgae. In: Richmond, A. and Hu, Q. eds. *Handbook of Microalgal Culture: Applied Phycology and Biotechnology*. Second edn. Blackwell Publishing Ltd, 21 - 36. Available: https://onlinelibrary.wiley.com/doi/abs/10.1002/9781118567166.ch2 (Accessed 10/01/2022).

Mattos, E. R., Singh, M., Cabrera, M. L. and Das, K. C. 2015. Enhancement of biomass production in *Scenedesmus bijuga* high-density culture using weakly absorbed green light. *Biomass and Bioenergy*, 81: 473 - 478.

Matuszynska, A., Saadat, N. P. and Ebenhoh, O. 2019. Balancing energy supply during photosynthesis - a theoretical perspective. *Physiologia Plantarum*, 166 (1): 392 - 402.

Meagher, E., Rangsrikitphoti, P., Faridi, B., Zamzam, G. and Durnford, D. G. 2021. Photoacclimation to high-light stress in *Chlamydomonas reinhardtii* during conditional senescence relies on generating pH-dependent, high-quenching centres. *Plant Physiology and Biochemistry*, 158: 136 - 145.

Metsoviti, M. N., Papapolymerou, G., Karapanagiotidis, I. T. and Katsoulas, N. 2019. Effect of Light Intensity and Quality on Growth Rate and Composition of *Chlorella vulgaris*. *Plants (Basel)*, 9 (31): https://doi:10.3390/plants9010031.

Michael, C., del Ninno, M., Gross, M. and Wen, Z. 2015. Use of wavelength-selective optical light filters for enhanced microalgal growth in different algal cultivation systems. *Bioresource Technology*, 179: 473 - 482.

Minagawa, J. and Tokutsu, R. 2015. Dynamic regulation of photosynthesis in *Chlamydomonas reinhardtii*. *The Plant Journal*, 82 (3): 413 - 428.

Moejes, F. W., Matuszynska, A., Adhikari, K., Bassi, R., Cariti, F., Cogne, G., Dikaios, I., Falciatore, A., Finazzi, G., Flori, S., Goldschmidt-Clermont, M., Magni, S., Maguire, J., Le Monnier, A., Muller, K., Poolman, M., Singh, D., Spelberg, S., Stella, G. R., Succurro, A., Taddei, L., Urbain, B., Villanova, V., Zabke, C. and Ebenhoh, O. 2017. A systems-wide understanding of photosynthetic acclimation in algae and higher plants. *Journal of Experimental Botany*, 68 (11): 2667 - 2681.

Mohsenpour, S. F., Richards, B. and Willoughby, N. 2012. Spectral conversion of light for enhanced microalgae growth rates and photosynthetic pigment production. *Bioresource Technology*, 125: 75 - 81.

Nama, S., Madireddi, S. K., Yadav, R. M. and Subramanyam, R. 2018. Non-photochemical quenching-dependent acclimation and thylakoid organization of *Chlamydomonas reinhardtii* to high light stress. *Photosynthesis Research*, 139 (1 - 3): 387 - 400.

Nasr, M. and Zahran, H. F. 2016. Performance evaluation of agricultural drainage water using modeling and statistical approaches. *Egyptian Journal of Aquatic Research*, 42: 141 - 148.

Natali, A. and Croce, R. 2015. Characterization of the major light-harvesting complexes (LHCBM) of the green alga *Chlamydomonas reinhardtii*. *PLoS One*, 10 (2): e0119211.

Nawrocki, W. J., Bailleul, B., Cardol, P., Rappaport, F., Wollman, F. A. and Joliot, P. 2019a. Maximal cyclic electron flow rate is independent of PGRL1 in *Chlamydomonas*. *Biochimica et Biophysica Acta (BBA) - Bioenergetics*, 1860: 425 - 432.

Nawrocki, W. J., Bailleul, B., Picot, D., Cardol, P., Rappaport, F., Wollman, F. A. and Joliot, P. 2019b. The mechanism of cyclic electron flow. *Biochimica et Biophysica Acta (BBA) - Bioenergetics*, 1860 (5): 433 - 438.

Nawrocki, W. J., Liu, X. and Croce, R. 2020. *Chlamydomonas reinhardtii* Exhibits De Facto Constitutive NPQ Capacity in Physiologically Relevant Conditions. *Plant Physiology*, 182 (1): 472 - 479.

Nikolaou, A., Bernardi, A., Meneghesso, A., Bezzo, F., Morosinotto, T. and Chachuat, B. 2015. A model of chlorophyll fluorescence in microalgae integrating photoproduction, photoinhibition and photoregulation. *Journal of Biotechnology*, 194: 91 - 99.

Nowicka, B. 2020. Practical aspects of the measurements of non-photochemical chlorophyll fluorescence quenching in green microalgae *Chlamydomonas reinhardtii* using Open FluorCam. *Physiologia Plantarum*, 168 (3): 617 - 629.

Nwoba, E. G., Parlevliet, D. A., Laird, D. W., Alameh, K. and Moheimani, N. R. 2019. Light management technologies for increasing algal photobioreactor efficiency. *Algal Research*, 39: 101433.

Nzayisenga, J. C., Farge, X., Groll, S. L. and Sellstedt, A. 2020. Effects of light intensity on growth and lipid production in microalgae grown in wastewater. *Biotechnol Biofuels*, 13 (4): https://doi.org/10.1186/s13068-13019-11646-x.

Ooms, M. D., Dinh, C. T., Sargent, E. H. and Sinton, D. 2016. Photon management for augmented photosynthesis. *Nature Communication*, 7: 12699.

Pang, N., Gu, X., Chen, S., Kirchhoff, H., Lei, H. and Roje, S. 2019. Exploiting mixotrophy for improving productivities of biomass and co-products of microalgae. *Renewable and Sustainable Energy Reviews*, 112: 450 - 460.

Park, K. C., Whitney, C. G., Kozera, C., O'Leary, S. J. and McGinn, P. J. 2015. Seasonal isolation of microalgae from municipal wastewater for remediation and biofuel applications. *Journal of Applied Microbiology*, 119 (1): 76 - 87.

Patel, A. K., Joun, J. M., Hong, M. E. and Sim, S. J. 2019. Effect of light conditions on mixotrophic cultivation of green microalgae. *Bioresource Technology*, 282: 245 - 253.

Patelou, M., Infante, C., Dardelle, F., Randewig, D., Kouri, E. D., Udvardi, M. K., Tsiplakou, E., Mantecón, L. and Flemetakis, E. 2020. Transcriptomic and metabolomic adaptation of *Nannochloropsis gaditana* grown under different light regimes. *Algal Research*, 45: 101735.

Pawar, S. 2016. Effectiveness mapping of open raceway pond and tubular photobioreactors for sustainable production of microalgae biofuel. *Renewable & Sustainable Energy Reviews*, 62: 640 - 653.

Pilla, V., Gonçalves, A., Dos Santos, A. and Lodeiro, C. 2018. Lifetime and Fluorescence Quantum Yield of Two Fluorescein-Amino Acid-Based Compounds in Different Organic Solvents and Gold Colloidal Suspensions. *Chemosensors*, 6 (3): 26.

Pruvost, J., Le Gouic, B., Lepine, O., Legrand, J. and Le Borgne, F. 2016. Microalgae culture in building-integrated photobioreactors: Biomass production modelling and energetic analysis. *Chemical Engineering Journal*, 284: 850 - 861.

Quaas, T., Berteotti, S., Ballottari, M., Flieger, K., Bassi, R., Wilhelm, C. and Goss, R. 2015. Non-photochemical quenching and xanthophyll cycle activities in six green algal species suggest mechanistic differences in the process of excess energy dissipation. *Journal of Plant Physiology*, 172: 92 - 103.

Ra, C. H., Kang, C. H., Jung, J. H., Jeong, G. T. and Kim, S. K. 2016. Effects of light-emitting diodes (LEDs) on the accumulation of lipid content using a two-phase culture process with three microalgae. *Bioresource Technology*, 212: 254 - 261.

Raeisossadati, M., Moheimani, N. R. and Parlevliet, D. 2019. Luminescent solar concentrator panels for increasing the efficiency of mass microalgal production. *Renewable and Sustainable Energy Reviews*, 101: 47 - 59.

Ramya, S., Nataraj, D., Krishnan, S., Premkumar, S., Thrupthika, T., Sangeetha, A., Senthilkumar, K. and Thangadurai, T. D. 2020. Aggregation induced emission behavior in oleylamine acetone system and its application to get improved photocurrent from In_2S_3 quantum dots. *Scientific Reports*, 10 (1): 19712.

Randhir, A., Laird, D. W., Maker, G., Trengove, R. and Moheimani, N. R. 2020. Microalgae: A potential sustainable commercial source of sterols. *Algal Research*, 46: 101772.

Rastogi, R. P., Sinha, R. P., Moh, S. H., Lee, T. K., Kottuparambil, S., Kim, Y. J., Rhee, J. S., Choi, E. M., Brown, M. T., Hader, D. P. and Han, T. 2014. Ultraviolet radiation and cyanobacteria. *Journal of Photochemistry and Photobiology B: Biology*, 141: 154 - 169.

Rayati, M., Rajabi Islami, H. and Shamsaie Mehrgan, M. 2020. Light Intensity Improves Growth, Lipid Productivity, and Fatty Acid Profile of *Chlorococcum oleofaciens* (Chlorophyceae) for Biodiesel Production. *BioEnergy Research*, 13 (4): 1235 - 1245.

Reisfeld, R. and Levchenko, V. 2017. The influence of surface plasmons on fluorescence of the dye Lumogen F red 300 in condensed phase. *Optical Materials*, 63: 88 - 94.

Roach, T., Na, C. S., Stoggl, W. and Krieger-Liszkay, A. 2020. The non-photochemical quenching protein LHCSR3 prevents oxygen-dependent photoinhibition in *Chlamydomonas reinhardtii*. *Journal of Experimental Botany*, 71 (9): 2650 - 2660.

Sager, J. C. and McFarlane, C. 1997. Radiation. In: Langhans, R. W. and Tibbitts, T. W. eds. *Plant Growth Chamber Handbook : a manual on maintaining the environment and growing plants in controlled growth facilities.* Ames(Iowa) : Iowa agricultural and home economics experiment station, 1 - 30. Available: https://books.google.co.za/books?id=n0FFAQAAIAAJ (Accessed 10/01/2022).

Sánchez-Saavedra, M. d. P., Sauceda-Carvajal, D., Castro-Ochoa, F. Y. and Molina-Cárdenas, C. A. 2020. The Use of Light Spectra to Improve the Growth and Lipid Content of *Chlorella vulgaris* for Biofuels Production. *BioEnergy Research*, 13 (2): 487 - 498.

Sanchez-Tarre, V. and Kiparissides, A. 2021. The effects of illumination and trophic strategy on gene expression in *Chlamydomonas reinhardtii*. *Algal Research*, 54: 102186.

Sandmann, G. 2021. Diversity and origin of carotenoid biosynthesis: its history of coevolution towards plant photosynthesis. *New Phytologist*, 232 (2): 479 - 493.

Saroussi, S., Karns, D. A. J., Thomas, D. C., Bloszies, C., Fiehn, O., Posewitz, M. C. and Grossman, A. R. 2019. Alternative outlets for sustaining photosynthetic electron transport during dark-to-light transitions. *PNAS,* 116 (23): 11518 - 11527.

Sasso, S., Stibor, H., Mittag, M. and Grossman, A. R. 2018. From molecular manipulation of domesticated *Chlamydomonas reinhardtii* to survival in nature. *Elife,* 7: e39233.

Sathasivam, R., Radhakrishnan, R., Hashem, A. and Abd Allah, E. F. 2019. Microalgae metabolites: A rich source for food and medicine. *Saudi Journal of Biological Sciences*, 26 (4): 709 - 722.

Sekar, N. and Ramasamy, R. P. 2015. Recent advances in photosynthetic energy conversion. *Journal of Photochemistry and Photobiology C: Photochemistry Reviews*, 22: 19 - 33.

Seo, Y. H., Cho, C., Lee, J. Y. and Han, J. I. 2014. Enhancement of growth and lipid production from microalgae using fluorescent paint under the solar radiation. *Bioresource Technology*, 173: 193 - 197.

Seo, Y. H., Lee, Y., Jeon, D. Y. and Han, J. I. 2015. Enhancing the light utilization efficiency of microalgae using organic dyes. *Bioresource Technology,* 181: 355 - 359.

Sforza, E., Calvaruso, C., Meneghesso, A., Morosinotto, T. and Bertucco, A. 2015. Effect of specific light supply rate on photosynthetic efficiency of *Nannochloropsis salina* in a continuous flat plate photobioreactor. *Applied Microbiology and Biotechnology*, 99 (19): 8309 - 8318.

Sforza, E., Simionato, D., Giacometti, G. M., Bertucco, A. and Morosinotto, T. 2012. Adjusted light and dark cycles can optimize photosynthetic efficiency in algae growing in photobioreactors. *PLoS One,* 7 (6): e38975.

Sharma, K. K., Ahmed, F., Schenk, P. M. and Li, Y. 2015. UV-C Mediated Rapid Carotenoid Induction and Settling Performance of *Dunaliella salina* and *Haematococcus pluvialis*. *Biotechnology and Bioengineering*, 112 (10): 2106 - 2114.

Shen, Y., Chen, B. and van Beek, T. A. 2015. Alternative solvents can make preparative liquid chromatography greener. *Green Chemistry*, 17 (7): 4073 - 4081.

Shene, C., Asenjo, J. A. and Chisti, Y. 2018. Metabolic modelling and simulation of the light and dark metabolism of *Chlamydomonas reinhardtii*. *The Plant Journal*, 96 (5): 1076 - 1088.

Sim, S. J., Joun, J., Hong, M. E. and Patel, A. K. 2019. Split mixotrophy: A novel cultivation strategy to enhance the mixotrophic biomass and lipid yields of *Chlorella protothecoides*. *Bioresource Technology*, 291: 121820.

Singh, R., Upadhyay, A. K., Singh, D. V., Singh, J. and Singh, D. 2019. Photosynthetic performance, nutrient status and lipid yield of microalgae *Chlorella vulgaris* and *Chlorococcum humicola* under UV-B exposure *Current Research in Biotechnology*, 1: 65 - 77.

Smith, R. T. and Gilmour, D. J. 2018. The influence of exogenous organic carbon assimilation and photoperiod on the carbon and lipid metabolism of *Chlamydomonas reinhardtii*. *Algal Research*, 31: 122 - 137.

Speight, J. G. 2018. Chapter 7 - Redox Transformations. In: Speight, J. G. ed. *Reaction Mechanisms in Environmental Engineering*. Butterworth-Heinemann, 231 - 267. Available: https://www.sciencedirect.com/science/article/pii/B9780128044223000079 (Accessed 12-01-2022).

Stanley, C., Mojiri, A. and Rosengarten, G. 2016. Spectral light management for solar energy conversion systems. *Nanophotonics*, 5 (1): 161 - 179.

Straka, L. and Rittmann, B. E. 2018. Effect of culture density on biomass production and light utilization efficiency of *Synechocystis* sp. PCC 6803. *Biotechnology and Bioengineering*, 115 (2): 507 - 511.

Sun, H., Zhao, W., Mao, X., Li, Y., Wu, T. and Chen, F. 2018. High-value biomass from microalgae production platforms: strategies and progress based on carbon metabolism and energy conversion. *Biotechnology and Biofuels*, 11 (1): 227.

Sun, Y., Chen, Y., Wei, J., Zhang, X., Zhang, L., Yang, Z. and Huang, Y. 2021. Ultraviolet-B radiation stress alters the competitive outcome of algae: Based on analyzing population dynamics and photosynthesis. *Chemosphere*, 272: 129645.

Sung, M. G., Han, J. I., Lee, B. and Chang, Y. K. 2018. Wavelength shift strategy to enhance lipid productivity of *Nannochloropsis gaditana*. *Biotechnology for Biofuels*, 11 (70): 1 - 12.

Sutherland, D. L., McCauley, J., Labeeuw, L., Ray, P., Kuzhiumparambil, U., Hall, C., Doblin, M., Nguyen, L. N. and Ralph, P. J. 2021. How microalgal biotechnology can assist with the UN Sustainable Development Goals for natural resource management. *Current Research in Environmental Sustainability*, 3: 100050.

Tamura, K., Peterson, D., Peterson, N., Stecher, G., Nei, M. and Kumar, S. 2011. MEGA5: Molecular evolutionary genetics analysis using maximum likelihood, evolutionary distance, and maximum parsimony methods. *Molecular Biology and Evolution*, 28: 2731 - 2739.

Teo, C. L., Atta, M., Bukhari, A., Taisir, M., Yusuf, A. M. and Idris, A. 2014. Enhancing growth and lipid production of marine microalgae for biodiesel production via the use of different LED wavelengths. *Bioresource Technology*, 162: 38 - 44.

Thermo.Fisher.Scientific. 2015. *Fluorophore Selection*. Available: https://www.thermofisher.com/za/en/home/life-science/cell-analysis/fluorophores.html (Accessed

Tibocha-Bonilla, J. D., Zuniga, C., Godoy-Silva, R. D. and Zengler, K. 2018. Advances in metabolic modeling of oleaginous microalgae. *Biotechnology for Biofuels*, 11 (241): https://doi.org/10.1186/s13068-13018-11244-13063.

Torkamani, S., Wani, S. N., Tang, Y. J. and Sureshkumar, R. 2010. Plasmon-enhanced microalgal growth in miniphotobioreactors. *Applied Physics Letters*, 97 (4): 043703.

Tran, N. T. and Kaldenhoff, R. 2020. Achievements and challenges of genetic engineering of the model green alga *Chlamydomonas reinhardtii*. *Algal Research*, 50: 101986.

Vadiveloo, A., Moheimani, N. R., Cosgrove, J. J., Bahri, P. A. and Parlevliet, D. 2015. Effect of different light spectra on the growth and productivity of acclimated *Nannochloropsis* sp. (Eustigmatophyceae). *Algal Research*, 8: 121 - 127.

Varela, J. C., Pereira, H., Vila, M. and Leon, R. 2015. Production of carotenoids by microalgae: achievements and challenges. *Photosynthesis Research*, 125 (3): 423 - 436.

Vuppaladadiyam, A. K., Prinsen, P., Raheem, A., Luque, R. and Zhao, M. 2018. Microalgae cultivation and metabolites production: a comprehensive review. *Biofuels, Bioproducts and Biorefining*, 12 (2): 304 - 324.

Wahidin, S., Idris, A. and Shaleh, S. R. 2013. The influence of light intensity and photoperiod on the growth and lipid content of microalgae *Nannochloropsis* sp. *Bioresource Technology*, 129: 7 - 11.

Wang, S.-K., Stiles, A. R., Guo, C. and Liu, C.-Z. 2014. Microalgae cultivation in photobioreactors: An overview of light characteristics. *Engineering in Life Sciences*, 14 (6): 550 - 559.

Wobbe, L., Bassi, R. and Kruse, O. 2016. Multi-Level Light Capture Control in Plants and Green Algae. *Trends in Plant Science*, 21 (1): 55 - 68.

Woodworth, B. D., Mead, R. L., Nichols, C. N. and Kolling, D. R. J. 2015. Photosynthetic light reactions increase total lipid accumulation in carbon-supplemented batch cultures of *Chlorella vulgaris*. *Bioresource Technology*, 179: 159 - 164.

Xiong, J. 2006. Photosynthesis: what color was its origin? *Genome Biology*, 7 (12): 245, https://doi:210.1186/gb-2006-1187-1112-1245.

Xu, J. and Gao, K. 2016. Photosynthetic contribution of UV-A to carbon fixation by macroalgae. *Phycologia*, 55 (3): 318-322.

Xu, X., Gu, X., Wang, Z., Shatner, W. and Wang, Z. 2019. Progress, challenges and solutions of research on photosynthetic carbon sequestration efficiency of microalgae. *Renewable and Sustainable Energy Reviews*, 110: 65 - 82.

Yadav, R. M., Aslam, S. M., Madireddi, S. K., Chouhan, N. and Subramanyam, R. 2020. Role of cyclic electron transport mutations pgrl1 and pgr5 in acclimation process to high light in *Chlamydomonas reinhardtii*. *Photosynthesis Research*, 146 (1 - 3): 247 - 258.

Yang, Y. and Weathers, P. 2015. Red light and carbon dioxide differentially affect growth, lipid production, and quality in the microalga, *Ettlia oleoabundans*. *Applied Microbiology and Biotechnology*, 99 (1): 489 - 499.

Yarnold, J., Ross, I. L. and Hankamer, B. 2016. Photoacclimation and productivity of *Chlamydomonas reinhardtii* grown in fluctuating light regimes which simulate outdoor algal culture conditions. *Algal Research*, 13: 182 - 194.

Zavrel, T., Szabo, M., Tamburic, B., Evenhuis, C., Kuzhiumparambil, U., Literakova, P., Larkum, A. W. D., Raven, J. A., Cerveny, J. and Ralph, P. J. 2018. Effect of carbon limitation on photosynthetic electron transport in *Nannochloropsis oculata*. *Journal of Photochemistry & Photobiology, B: Biology*, 181: 31 - 43.

Zehentbauer, F. M., Moretto, C., Stephen, R., Thevar, T., Gilchrist, J. R., Pokrajac, D., Richard, K. L. and Kiefer, J. 2014. Fluorescence spectroscopy of Rhodamine 6G: concentration and solvent effects. *Spectrochimica Acta Part A: Molecular and Biomolecular Spectroscopy*, 121: 147 - 151.

Zhang, S. and Bryant, D. A. 2015. Biochemical Validation of the Glyoxylate Cycle in the Cyanobacterium *Chlorogloeopsis fritschii* Strain PCC 9212. *Journal of Biological Chemistry*, 290 (22): 14019 - 14030.

Zhang, X. F., Zhang, J. and Liu, L. 2014. Fluorescence properties of twenty fluorescein derivatives: lifetime, quantum yield, absorption and emission spectra. *Journal of Fluorescence*, 24 (3): 819 - 826.

Zhao, B. and Su, Y. 2014. Process effect of microalgal-carbon dioxide fixation and biomass production: A review. *Renewable and Sustainable Energy Reviews*, 31: 121 - 132.

Zhao, C., Brück, T. and Lercher, J. A. 2013. Catalytic deoxygenation of microalgae oil to green hydrocarbons. *Green Chemistry*, 15 (7): 1697 - 2012.

Zhu, C., Chen, C., Zhao, L., Zhang, Y., Yang, J., Song, L. and Yang, S. 2012. Bioflocculant produced by *Chlamydomonas reinhardtii*. *Journal of Applied Phycology*, 24 (5): 1245 - 1251.

Appendices

Appendix A: Organic dye spectra.

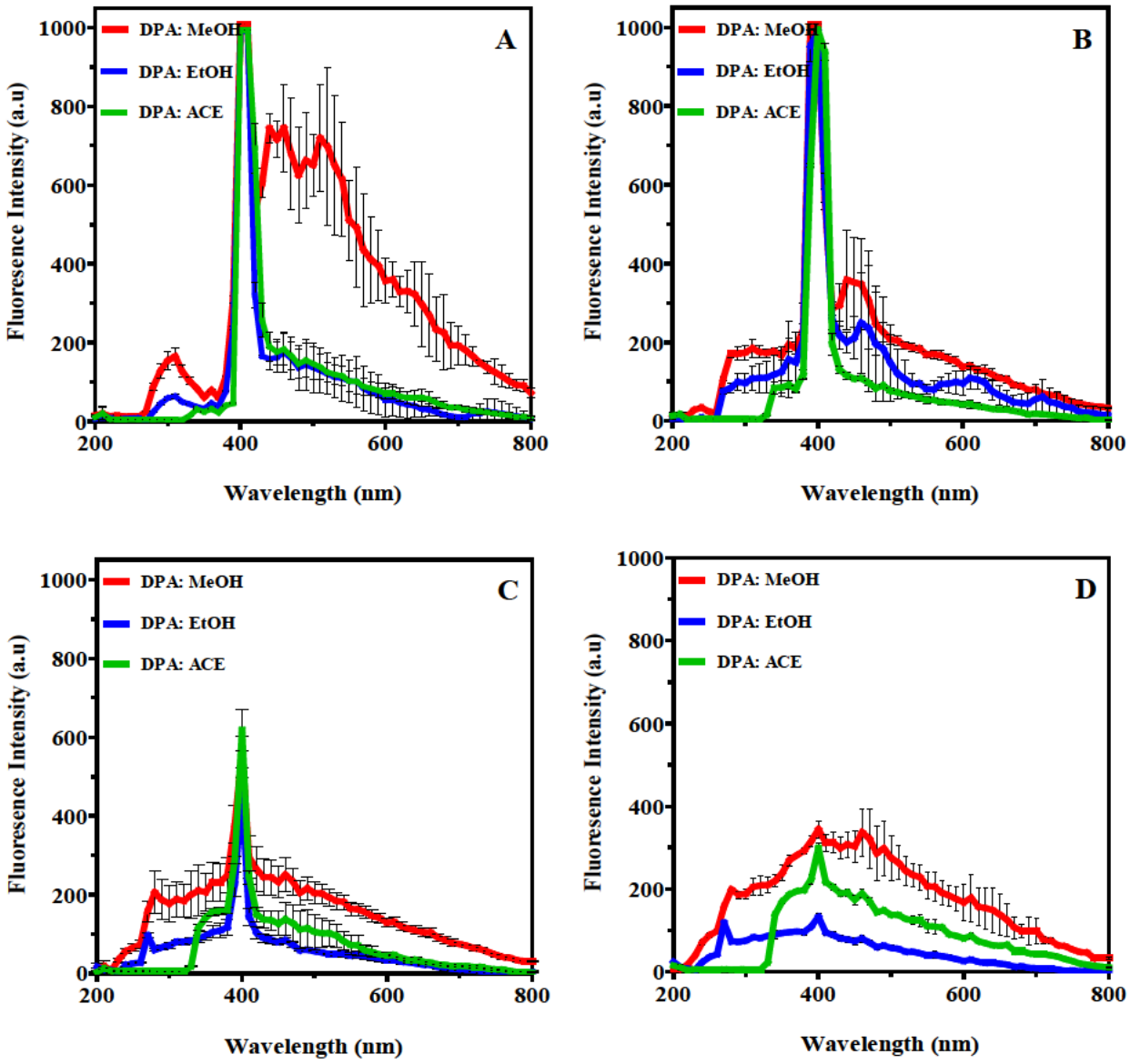

Figure A1: Diphenylanthracene at varying concentrations in methanol (MeOH), ethanol (EtOH), and acetone (ACE). **(A)** 100 mgL^{-1}, **(B)** 10 mgL^{-1}, **(C)** 1 mgL^{-1}, and **(D)** 0.1 mgL^{-1}. Data are expressed as a mean ± SD (n = 3) and plotted every 10 nm.

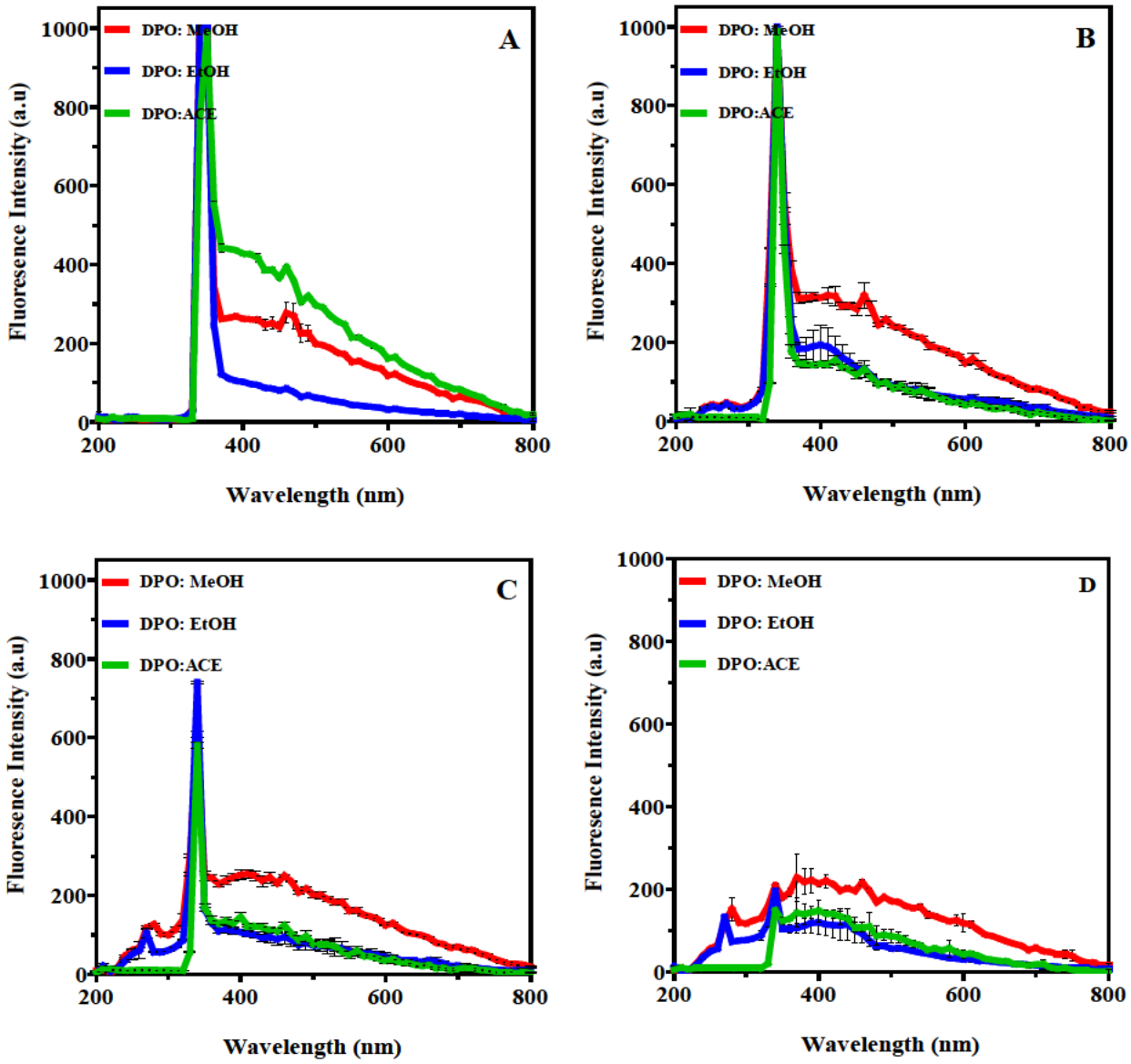

Figure A2: Diphenyloxazole at varying concentrations in methanol (MeOH), ethanol (EtOH), and acetone (ACE). **(A)** 100 mgL^{-1}, **(B)** 10 mgL^{-1}, **(C)** 10 mgL^{-1}, and **(D)** 0.1 mgL^{-1}. Data are expressed as a mean ± SD (n = 3) and plotted every 10 nm.

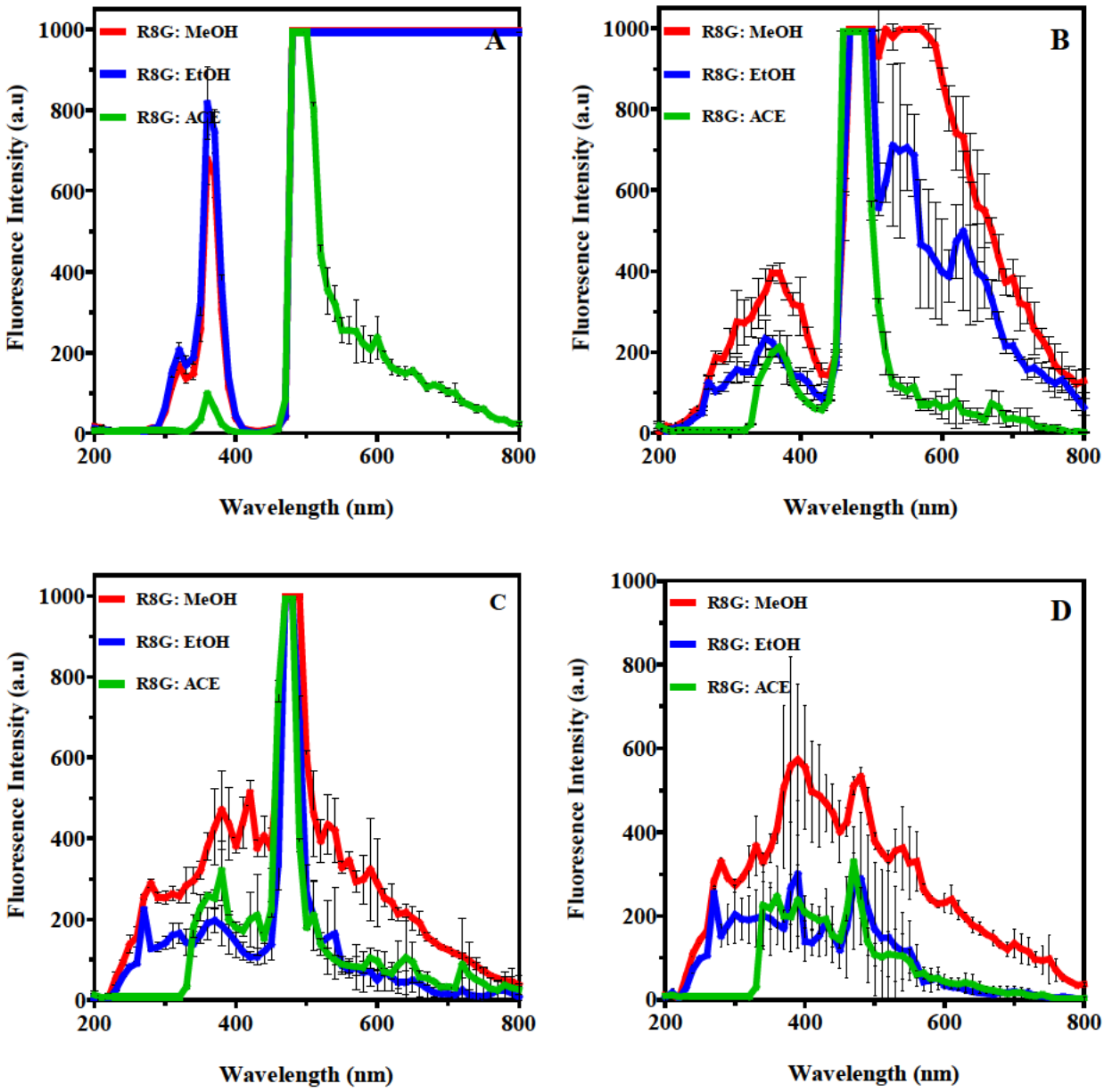

Figure A3: Rhodamine 8G at varying concentrations in methanol (MeOH), ethanol (EtOH), and acetone (ACE). **(A)** 100 mgL^{-1}, **(B)** 10 mgL^{-1}, **(C)** 10 mgL^{-1}, and **(D)** 0.1 mgL^{-1}. Data are expressed as a mean ± SD (n = 3) and plotted every 10 nm.

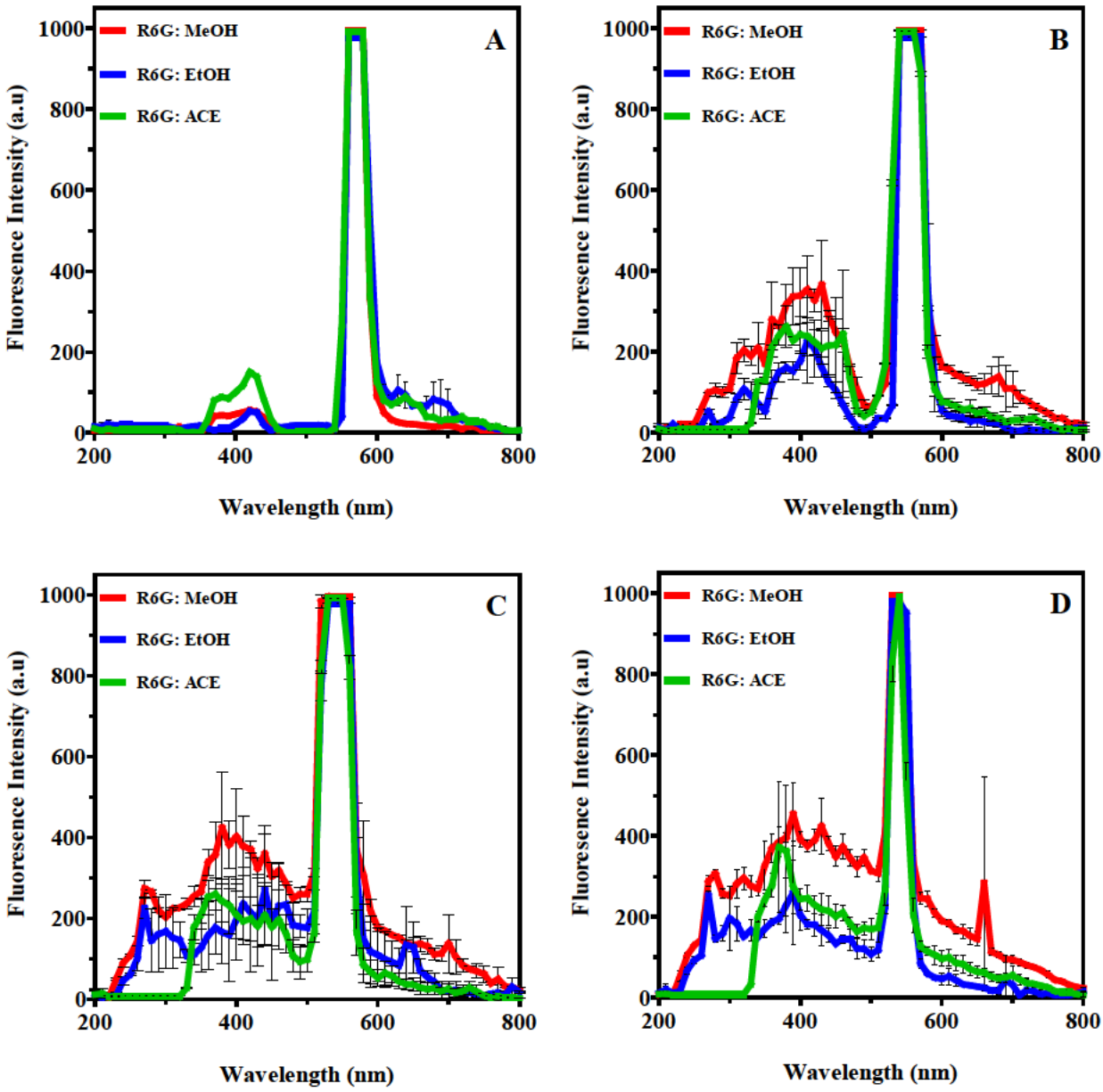

Figure A4: Rhodamine 6G at varying concentrations in methanol (MeOH), ethanol (EtOH), and acetone (ACE). **(A)** 100 mgL^{-1}, **(B)** 10 mgL^{-1}, **(C)** 10 mgL^{-1}, and **(D)** 0.1 mgL^{-1}. Data are expressed as a mean ± SD (n = 3) and plotted every 10 nm.

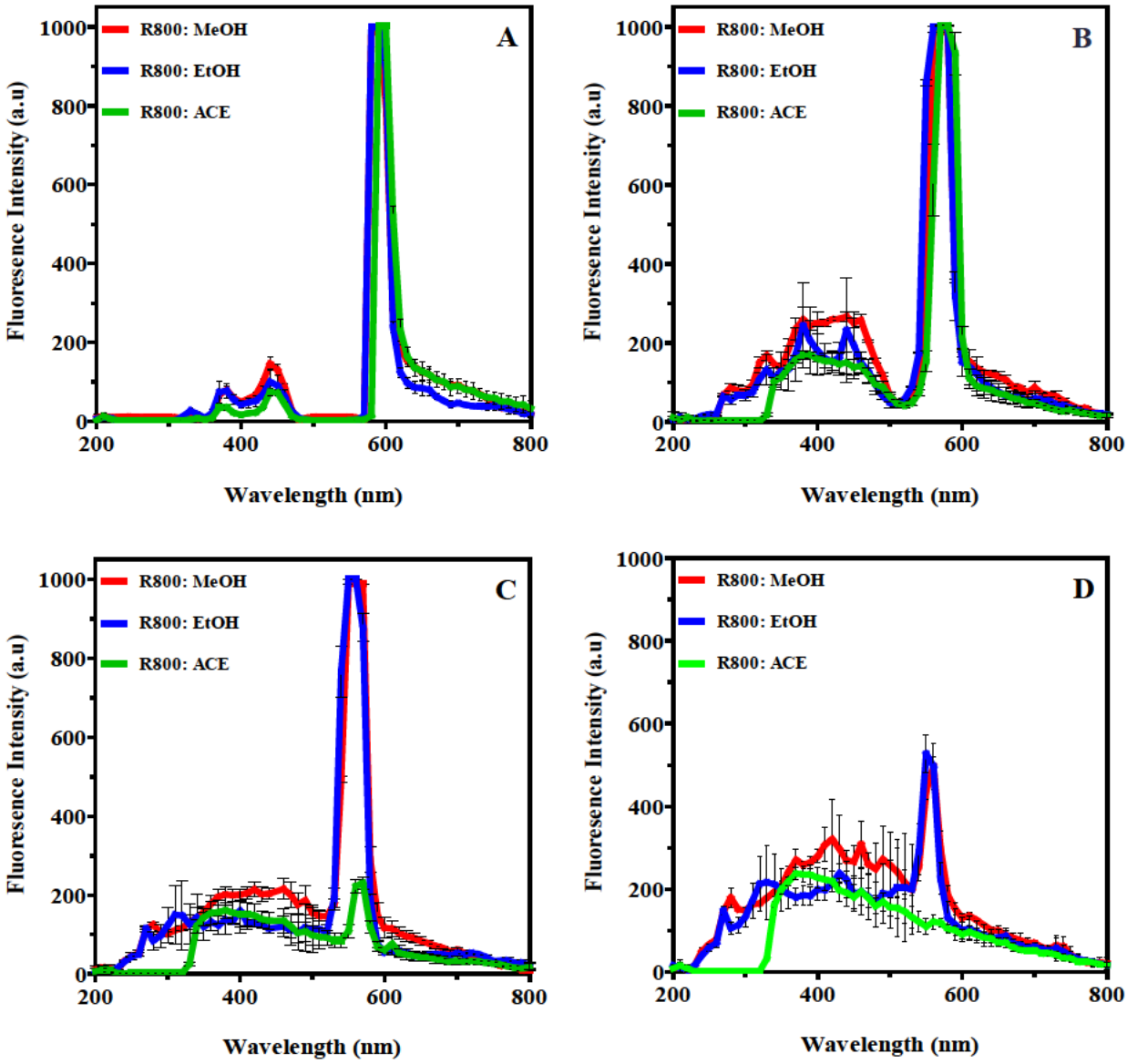

Figure A5: Rhodamine 800 at varying concentrations in methanol (MeOH), ethanol (EtOH), and acetone (ACE). **(A)** 100 mgL^{-1}, **(B)** 10 mgL^{-1}, **(C)** 10 mgL^{-1}, and **(D)** 0.1 mgL^{-1}. Data are expressed as a mean ± SD (n = 3) and plotted every 10 nm.

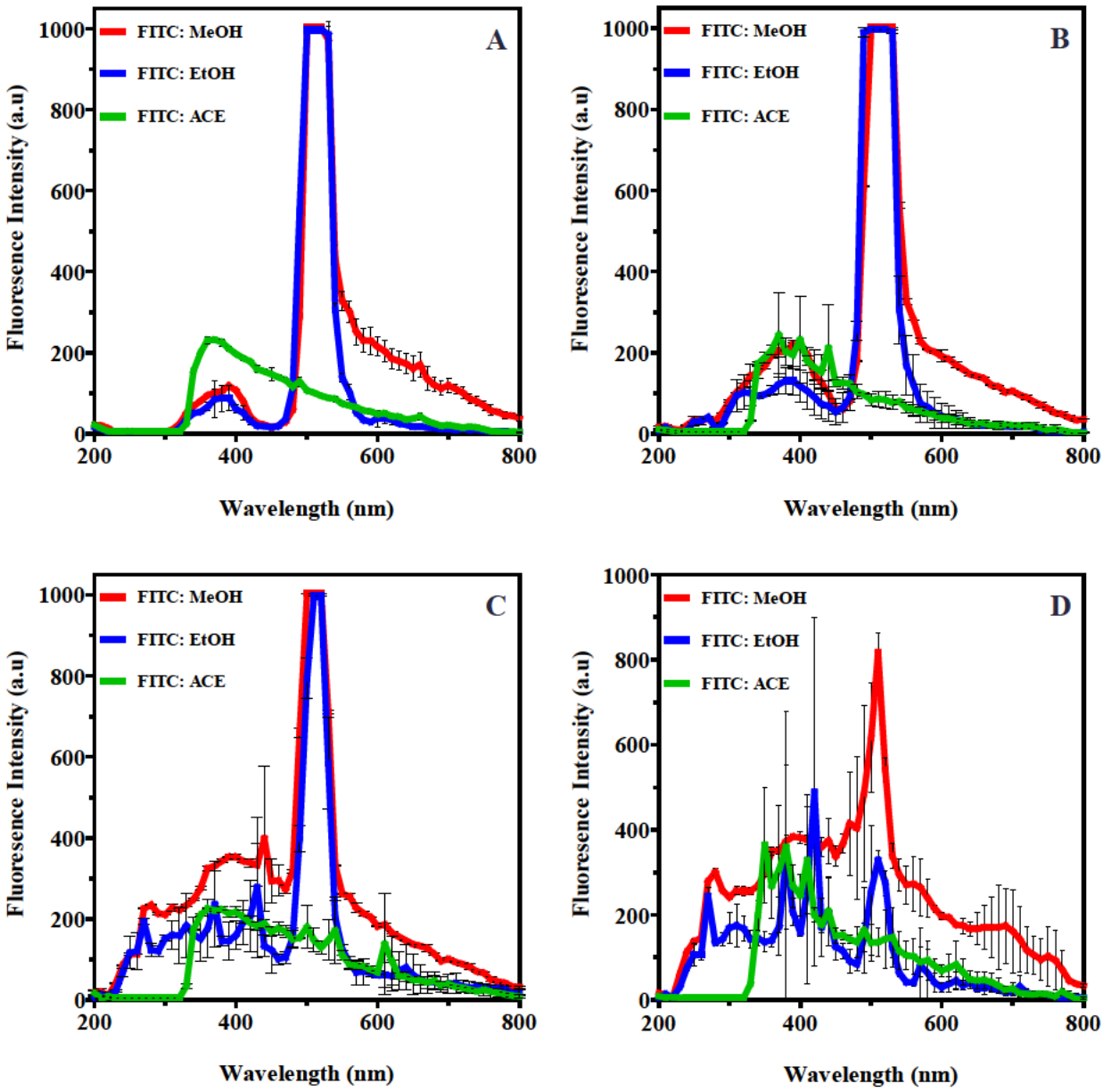

Figure A6: Fluorescein Isothiocyanate at varying concentrations in methanol (MeOH), ethanol (EtOH), and acetone (ACE). **(A)** 100 mgL^{-1}, **(B)** 10 mgL^{-1}, **(C)** 10 mgL^{-1}, and **(D)** 0.1 mgL^{-1}. Data are expressed as a mean ± SD (n = 3) and plotted every 10 nm.

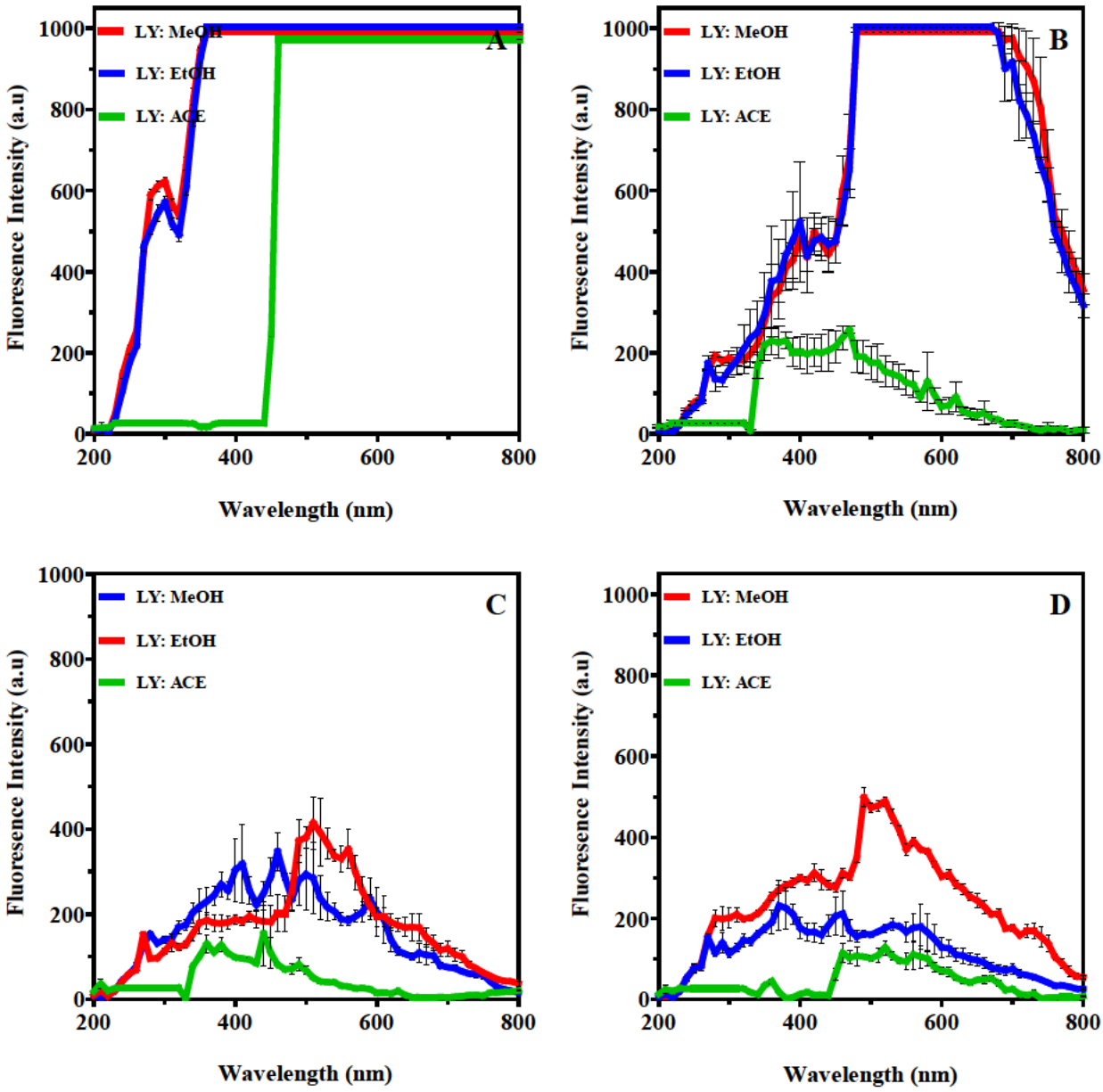

Figure A7: Lumogen yellow at varying concentrations in methanol (MeOH), ethanol (EtOH), and acetone (ACE). **(A)** 100 mgL^{-1}, **(B)** 10 mgL^{-1}, **(C)** 10 mgL^{-1}, and **(D)** 0.1 mgL^{-1}. Data are expressed as a mean ± SD (n = 3) and plotted every 10 nm.

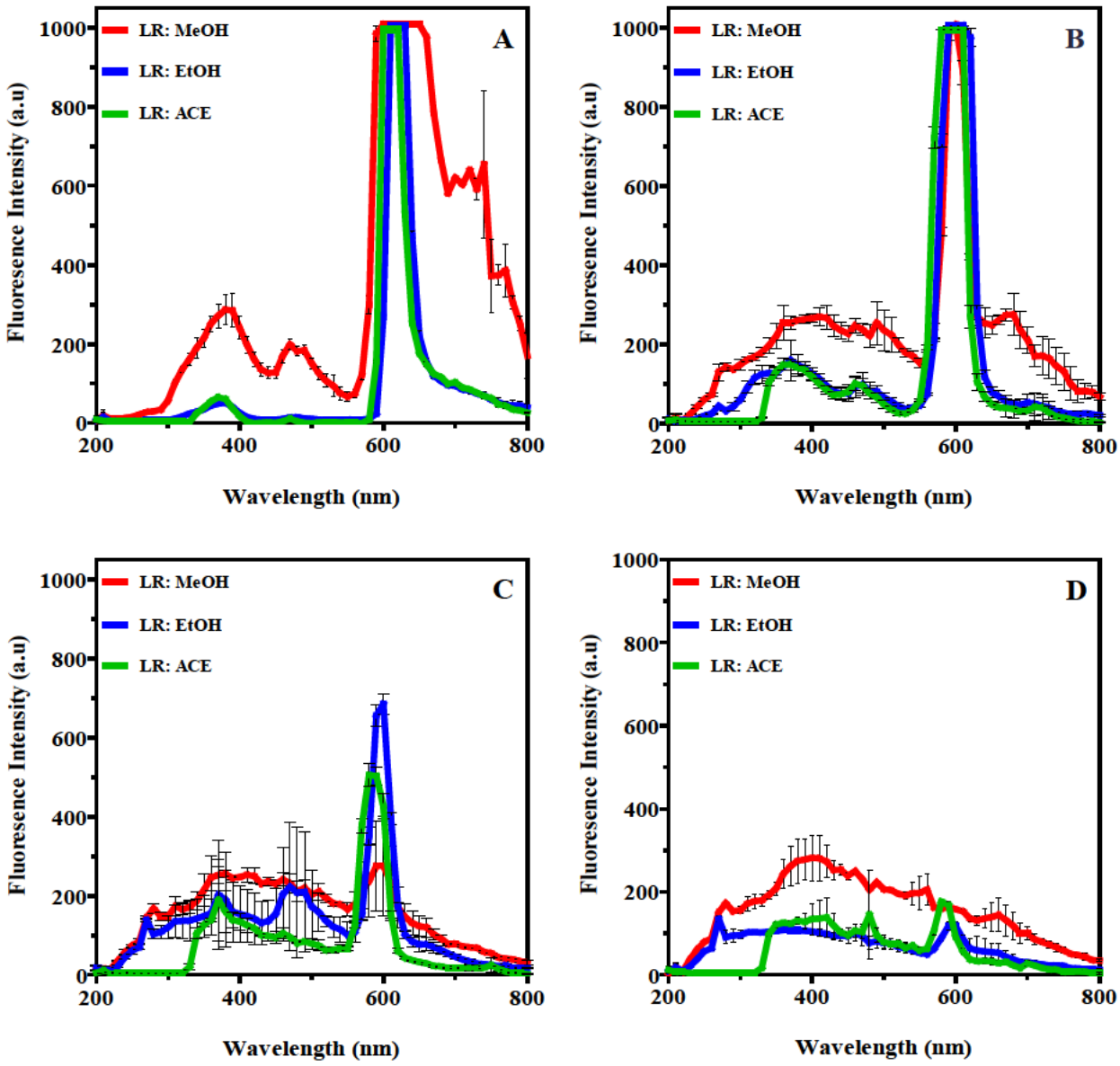

Figure A8: Lumogen red at varying concentrations in methanol (MeOH), ethanol (EtOH), and acetone (ACE). **(A)** 100 mgL^{-1}, **(B)** 10 mgL^{-1}, **(C)** 1 mgL^{-1}, and **(D)** 0.1 mgL^{-1}. Data are expressed as a mean ± SD (n = 3) and plotted every 10 nm.

Appendix B: Photo-bioreactors and incubator

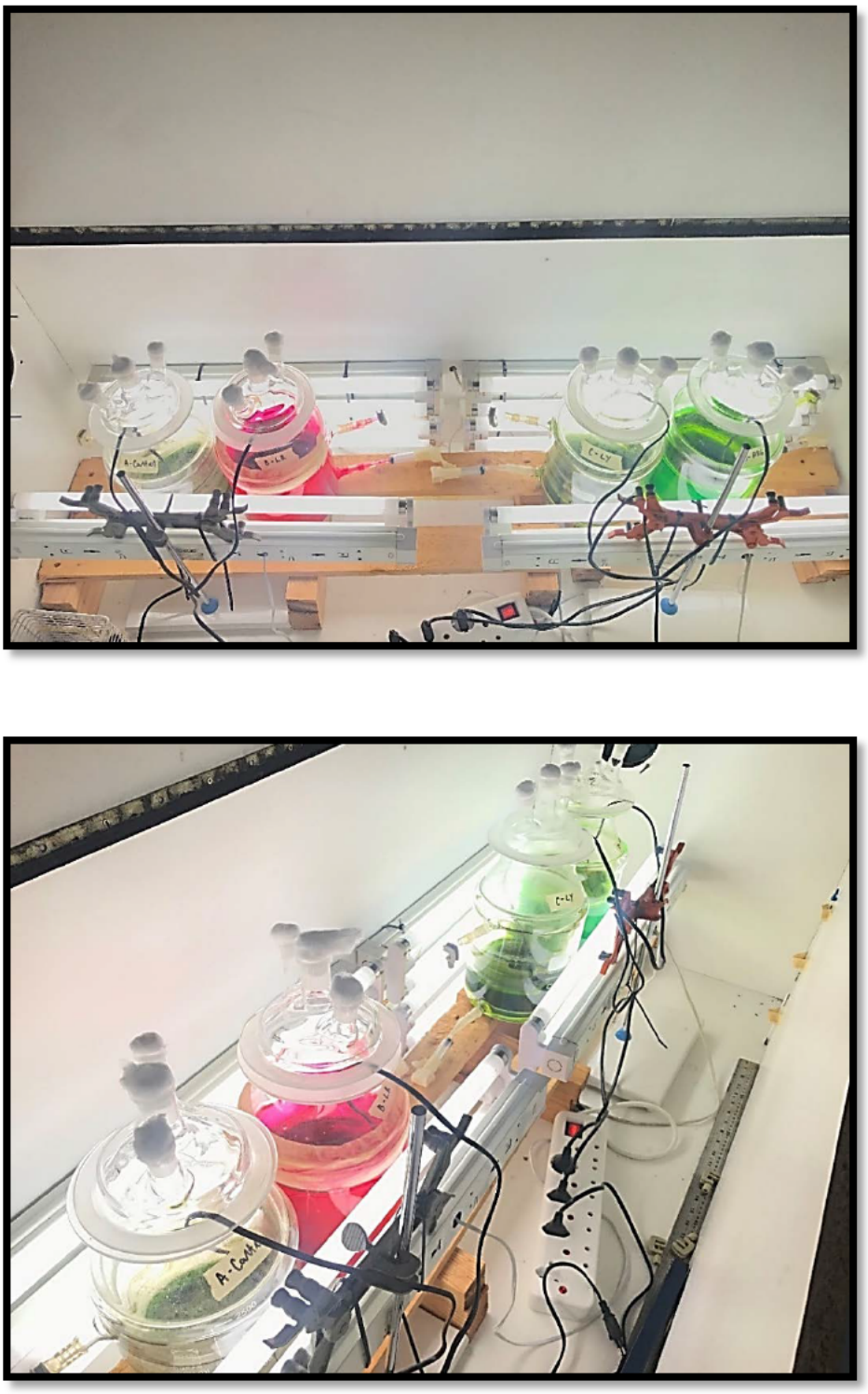

Figure B1 and B2: Photo-bioreactors and incubator. From left to right, PBRs containing the control, LR, LY, and R8G. Due to the light irradiance, the contrast on the images has been adjusted.

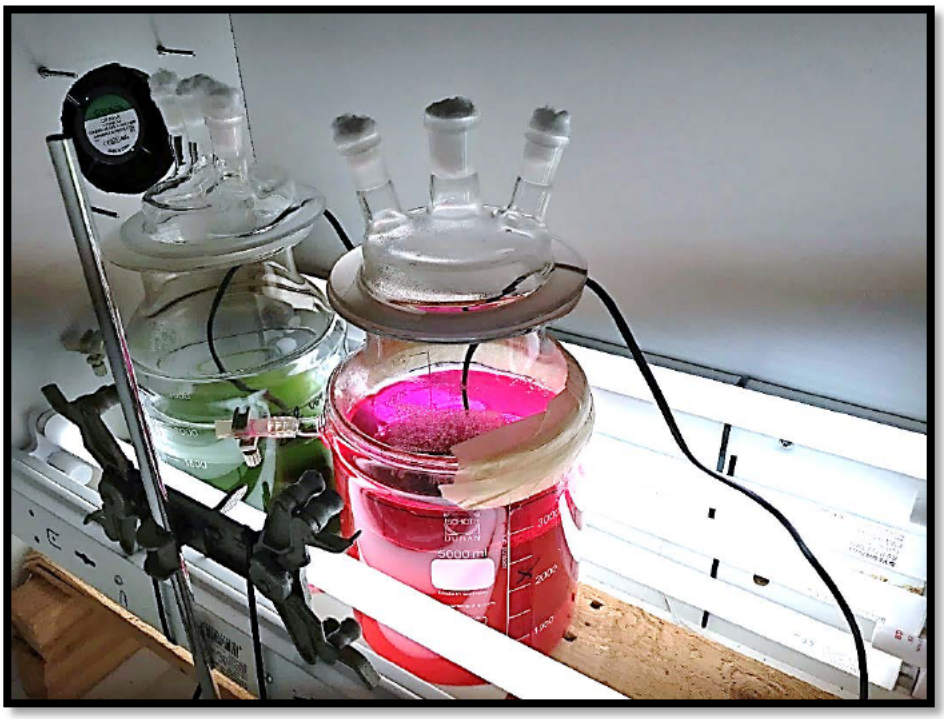

Figure B3: From left to right, PBRs containing the control and LR.

Figure B4: From left to right, PBRs containing LY and R8G. Due to the light irradiance, the contrast on the images has been adjusted.

Appendix C: Tris Acetate Phosphate medium

Table C1: TAP media recipe.

Component	Concentration
Trizma® base	2.42 g
TAP salts	25 mL
Phosphate solution	0.375 mL
Hunter's trace elements	1.0 mL
Glacial acetic acid	1.0 mL

The media components listed below are required to make up 1.0 L of TAP medium (Natali and Croce 2015). The pH ranged between 7.0 and 8.0. The media was autoclaved for 15 min at 121 °C.

Table C2: TAP media components.

Stock Solutions	**gL^{-1}**
TAP salts	
Ammonium chloride (NH_4Cl)	15.0
Magnesium sulphate ($MgSO_4.\ 7H_2O$)	4.0
Calcium chloride ($CaCl_2.\ 2H_2O$)	2.0
Phosphate solution	**g/100 mL**
Dipotassium phosphate (K_2HPO_4)	28.8
Monopotassium phosphate (KH_2PO_4)	14.4
Hunter's trace elements	
Ethylenediaminetetraacetic acid (EDTA) disodium salt	50 g /250 mL
Zinc Sulphate Heptahydrate ($ZnSO_4.\ 7H_2O$)	22 g /100 mL
Boric acid (H_3BO_3)	11.4 g /200 mL
Manganese (II) chloride ($MnCl_2.\ 4H_2O$)	5.06 g /50mL
Cobalt (II) chloride ($CoCl_2.\ 6H_2O$)	1.61 g /50mL
Copper (II) sulphate ($CuSO_4.\ 5H_2O$)	1.57 g /50mL
Ammonium molybdate tetrahydrate [$(NH_4)_6Mo_7O_{24}.\ 4H_2O$]	1.1 g /50mL
Iron (II) sulphate ($FeSO_4.\ 7H_2O$)	4.99 g /50mL

Appendix D: pH and temperature

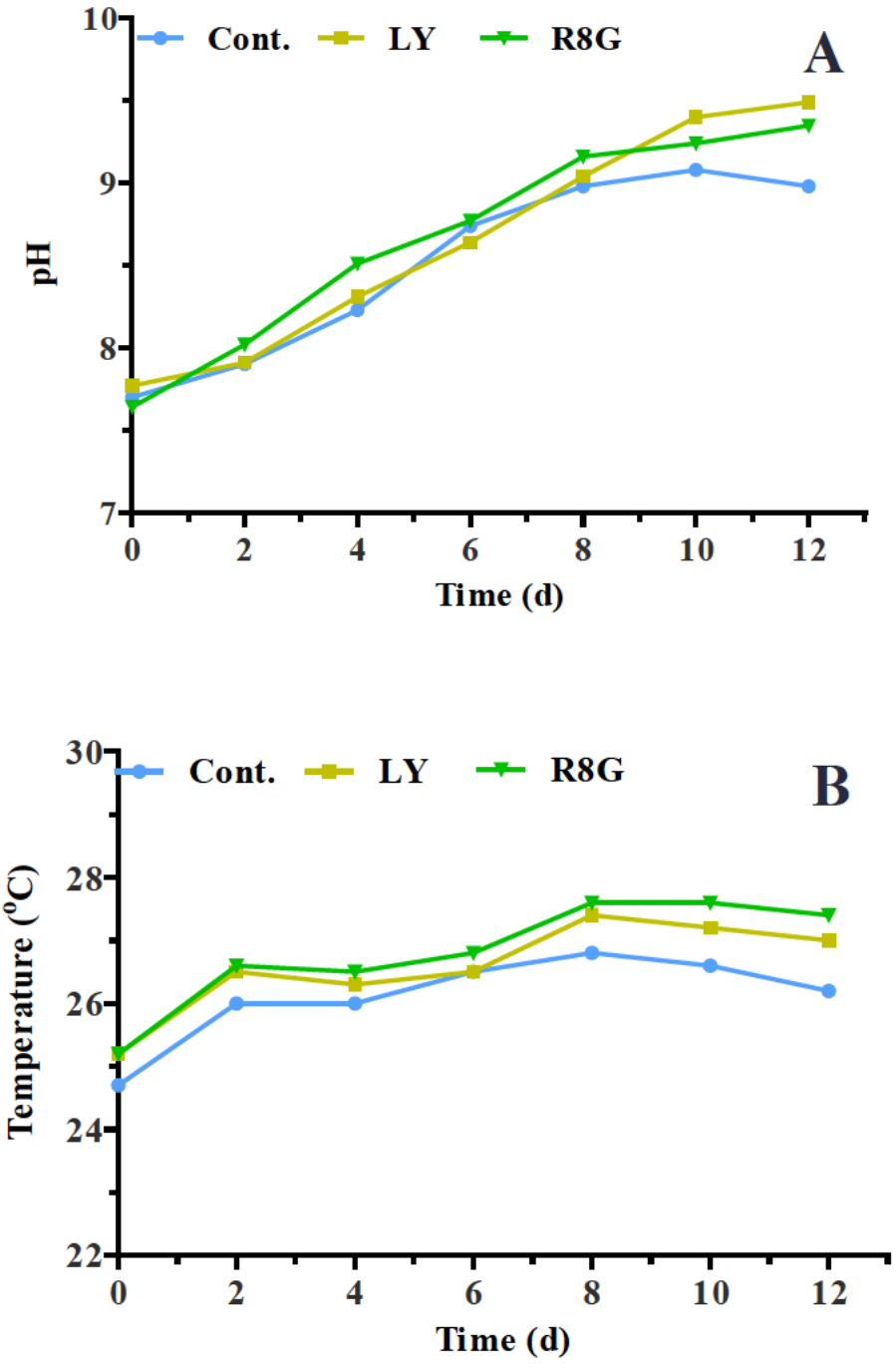

Figure D1: (A) The average pH and **(B)** average temperature values of the cultures grown under control (Cont.), Lumogen Red (LR), Lumogen Yellow (LY), and Rhodamine 8G (R8G) using daylight tubes. Control reactors were set up where the microalgal cells received light passing through a methanol blank. Data are expressed as a mean ± SD (n = 3). The pH was increased from 8 to ~ 9 while temperatures fluctuated between 24 – 26 ºC throughout the study.

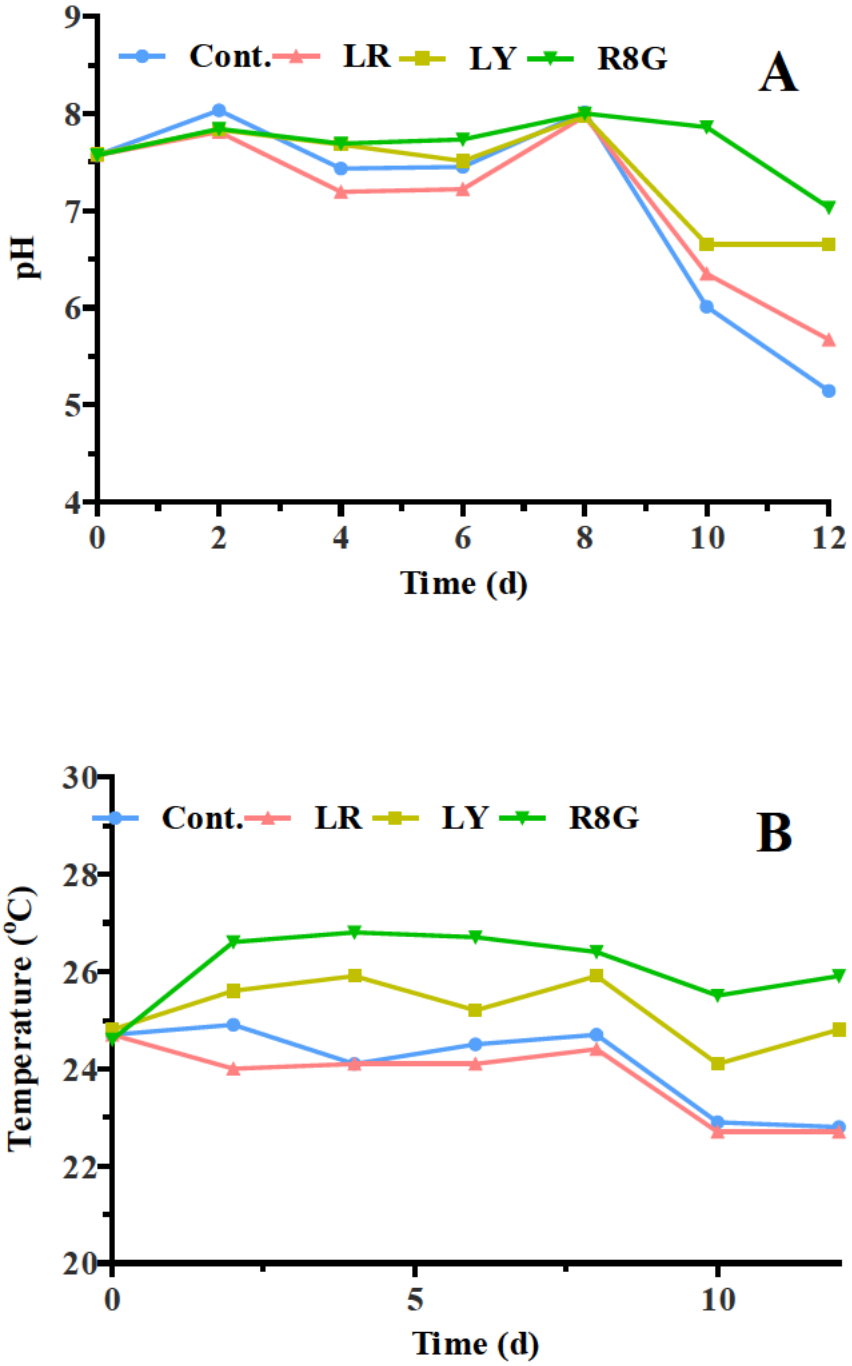

Figure D2: (A) The average pH and **(B)** average temperature cultures grown under control (Cont.), Lumogen Red (LR), Lumogen Yellow (LY), and Rhodamine 8G (R8G) using 30% UV-*a* and UV-*b* fluorescent tubes. Control reactors were set up where the microalgal cells received light passing through a methanol blank. Data are expressed as a mean ± SD (n = 2). The pH ranged between 7 and 8, however unlike the previous findings, after day 8 the pH dropped (< 8). The same effect was seen with the temperature data. Temperatures ranged between 24 – 26 ºC, however, toward the end of the experimentations, temperatures decreased.

Appendix E: Microalgal biomass concentrations (DCW) vs absorbance calibration curve

Table E: The DCW vs absorbance calibration curve values.

DCW gL^{-1}	A 1	A 2	Avg.	SD
0,25	0,546	0,555	0,5505	0,0045
0,8	1,064	1,075	1,0695	0,0055
1,45	1,732	1,792	1,762	0,03
1,75	2,055	2,026	2,0405	0,0145
2,15	2,491	2,479	2,485	0,006

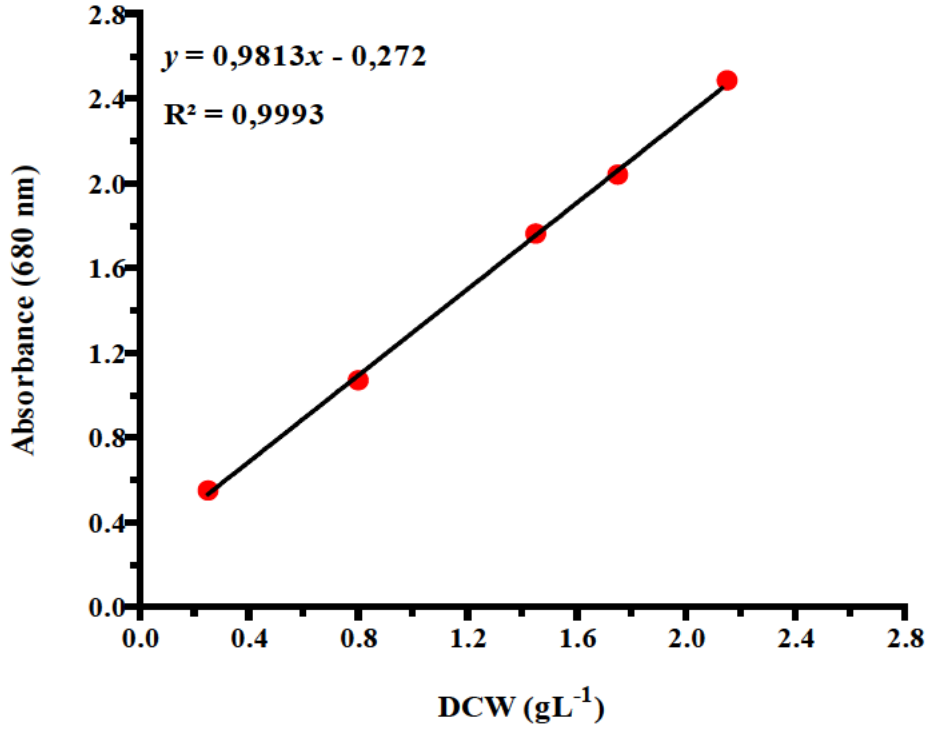

Figure E: The DCW vs absorbance calibration curve.

Appendix F: LAB buffer and gel preparation

Table F: The LAB buffer components.

LAB Buffer	**gL^{-1}**
Lithium acetate dihydrate	1.0
Boric Acid	0.25

Made up to 1.0 L with dH_2O. LAB gels were made by weighing out 1.2 g agarose and adding to 100 mL LAB buffer. This was heated until agarose dissolved. Then, 2.0 µL ethidium bromide was added to the gels before casting. Gels were run at 300 V for 5 min (Brody *et al.* 2004).

Appendix G: PCR amplicon gel verification

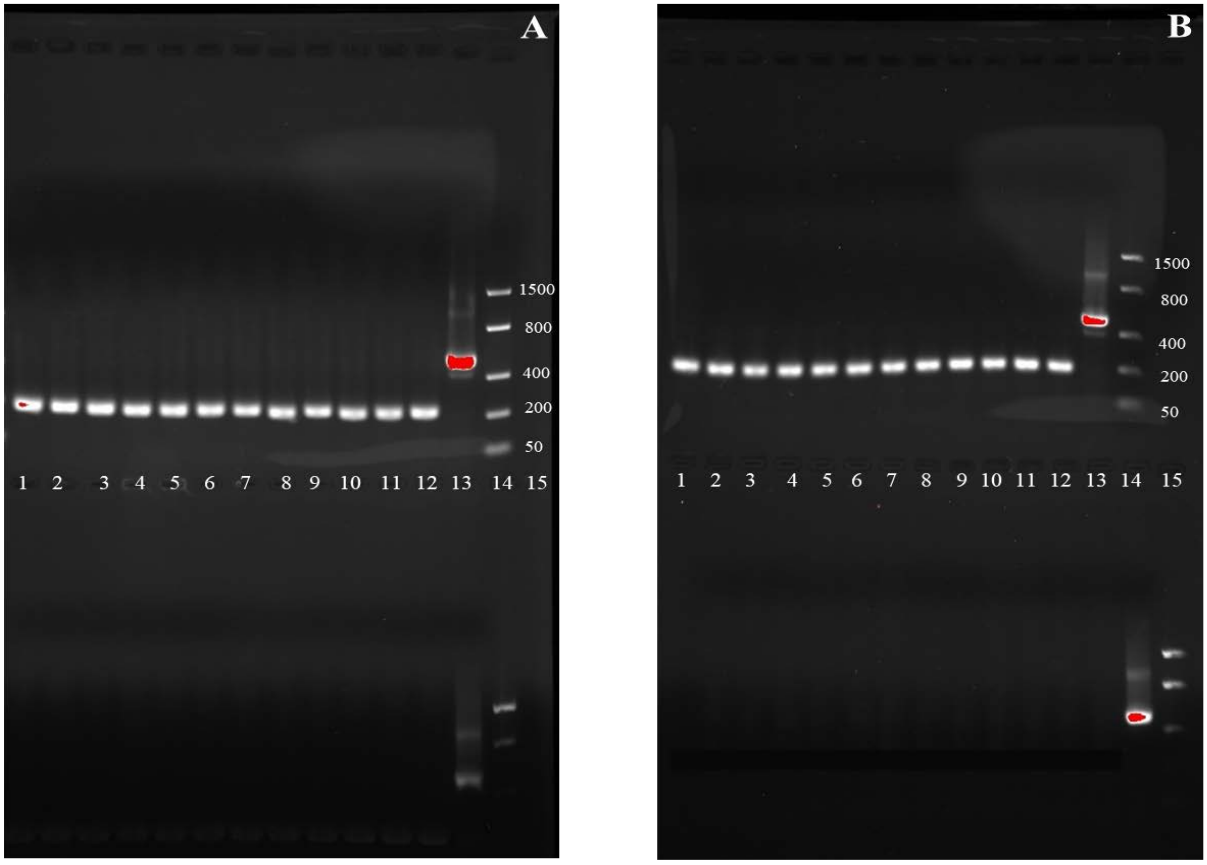

Figure G: (A) rbcL amplicon verification. From left to right: Lane 1 – 12: rbcL amplicons (201 bp); Lane 13: control GAPDH amplicon (496 bp); Lane 14: DNA ladder (low range ≤ 1500 bp). The bottom gel from left to right: Lanes 1 – 6: NTC; Lanes 7 – 12: NRT; lane 13: control GAPDH amplicon (496 bp); Lane 14: DNA ladder (low range ≤ 1500 bp). **(B)** 18S amplicon verification. From left to right: Lanes 1 – 12: 18S amplicons (192 bp); Lane 13: control GAPDH amplicon (496 bp); Lane 14: DNA ladder (low range ≤ 1500 bp). The bottom gel from left to right: Lanes 1 – 6: NTC; Lanes 7-12: NRT; lane 13: control GAPDH amplicon (496 bp); Lane 14: DNA ladder (low range ≤ 1500 bp).

Appendix H: qPCR melt curves and summaries

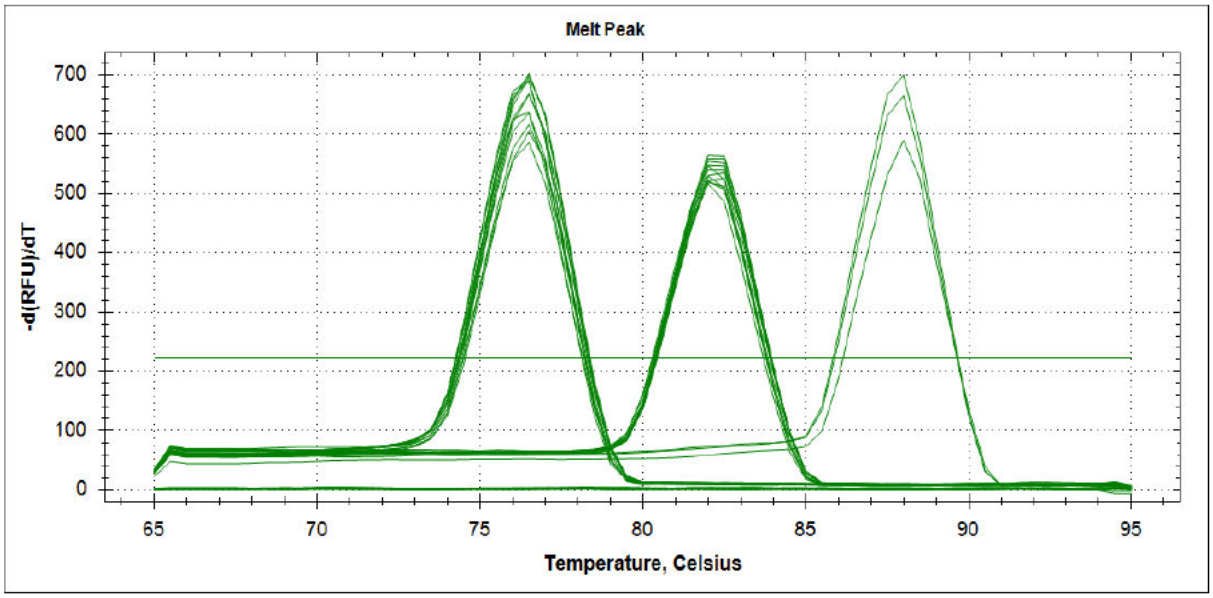

Figure H1: The melt curve data of the generated qPCR amplicons represent the gene expression on day 4 of cultivation under control (Cont.), Lumogen Red (LR), Lumogen Yellow (LY), and Rhodamine 8G (R8G) irradiance. No template control (NTC) and no reverse transcriptase control (NRT) showed no melt temperatures and no additional melt peaks indicated no contamination of samples.

Table H1: Melt curve data on day 4.

	Day 4	
Target	**Sample**	**Melt Temp. °C**
NTC	NTC	None
NTC	NTC	None
NTC	NTC	None
NRT	NRT	None
NRT	NRT	None
NRT	NRT	None
GADPH- RNA	Positive control	88
GADPH- RNA	Positive control	88
GADPH- RNA	Positive control	88
rbcL	Experiment control	76,5
rbcL	Experiment control	76,5
rbcL	Experiment control	76,5

Day 4 continued.		
Target	**Sample**	**Melt Temp**
rbcL	LR	76,5
rbcL	LR	76,5
rbcL	LR	76,5
rbcL	LY	76,5
rbcL	LY	76,5
rbcL	LY	76,5
rbcL	R8G	76,5
rbcL	R8G	76,5
rbcL	R8G	76,5
18S	Experiment control	82,5
18S	Experiment control	82
18S	Experiment control	82
18S	LR	82
18S	LR	82
18S	LR	82
18S	LY	82
18S	LY	82,5
18S	LY	82
18S	R8G	82
18S	R8G	82,5
18S	R8G	82,5

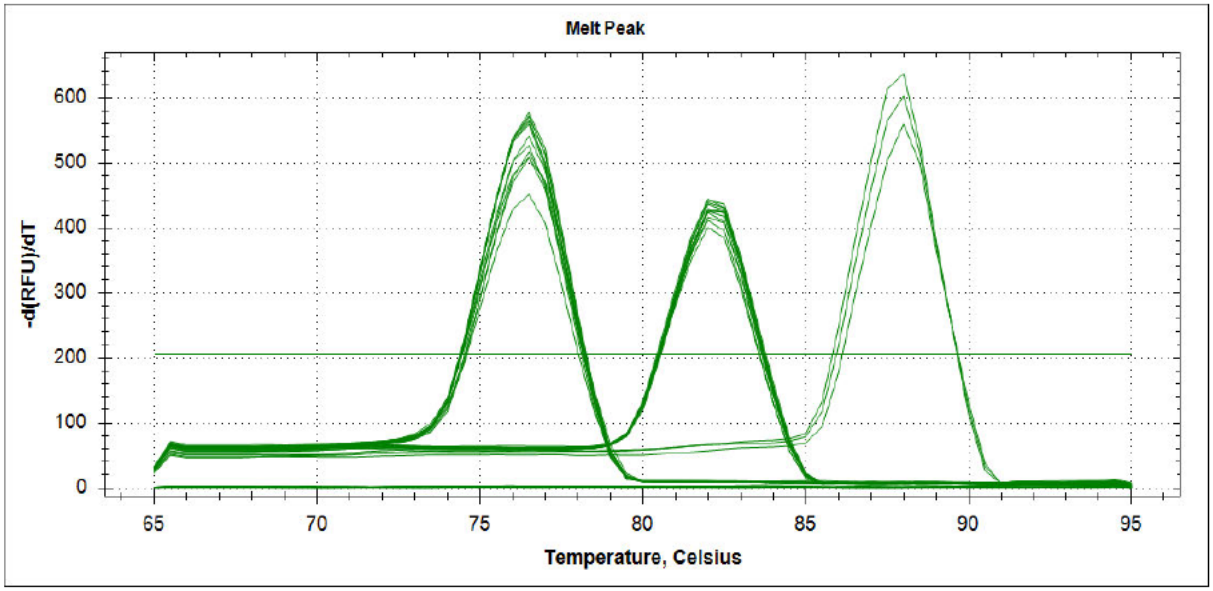

Figure H2: The melt curve data of the generated qPCR amplicons represent the gene expression on day 8 of cultivation under control (Cont.), Lumogen Red (LR), Lumogen Yellow (LY), and Rhodamine 8G (R8G) irradiance.

Table H2: Melt curve data on day 8.

Day 8		
Target	**Sample**	**Melt Temp. °C**
NTC	NTC	None
NTC	NTC	None
NTC	NTC	None
NRT	NRT	None
NRT	NRT	None
NRT	NRT	None
GADPH- RNA	Positive control	88
GADPH- RNA	Positive control	88
GADPH- RNA	Positive control	88
rbcL	Experiment control	76,5
rbcL	Experiment control	76,5
rbcL	Experiment control	76,5
rbcL	LR	76,5
rbcL	LR	76,5
rbcL	LR	76,5
rbcL	LY	76,5
rbcL	LY	76,5
rbcL	LY	76,5
rbcL	R8G	76,5
rbcL	R8G	76,5
rbcL	R8G	76,5
18S	Experiment control	82,5
18S	Experiment control	82
18S	Experiment control	82
18S	LR	82
18S	LR	82
18S	LR	82
18S	LY	82
18S	LY	82
18S	LY	82
18S	R8G	82
18S	R8G	82
18S	R8G	82

Appendix I: Protein calibration curve

Table I: The protein vs absorbance calibration curve values.

Conc. µgmL^{-1}	A 1	A 2	Avg.	SD
10	0,154	0,148	0,151	0,003
20	0,218	0,194	0,206	0,012
40	0,341	0,348	0,3445	0,0035
80	0,599	0,599	0,599	0
160	0,974	0,992	0,983	0,009

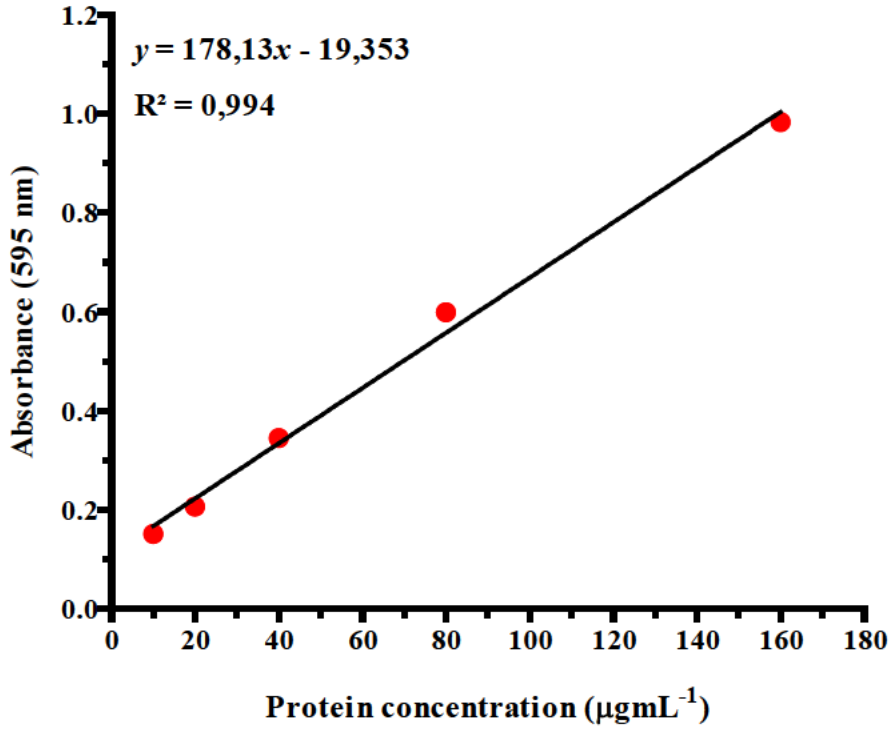

Figure I: The protein vs absorbance calibration curve.

Appendix J: Carbohydrate calibration curve

Table J: The carbohydrate vs absorbance calibration curve values.

Conc. µgmL^{-1}	A 1	A 2	Avg.	SD
10	0,112	0,209	0,1605	0,0485
20	0,174	0,22	0,197	0,023
40	0,468	0,372	0,42	0,048
80	0,796	0,744	0,77	0,026
160	1,607	1,62	1,6135	0,0065

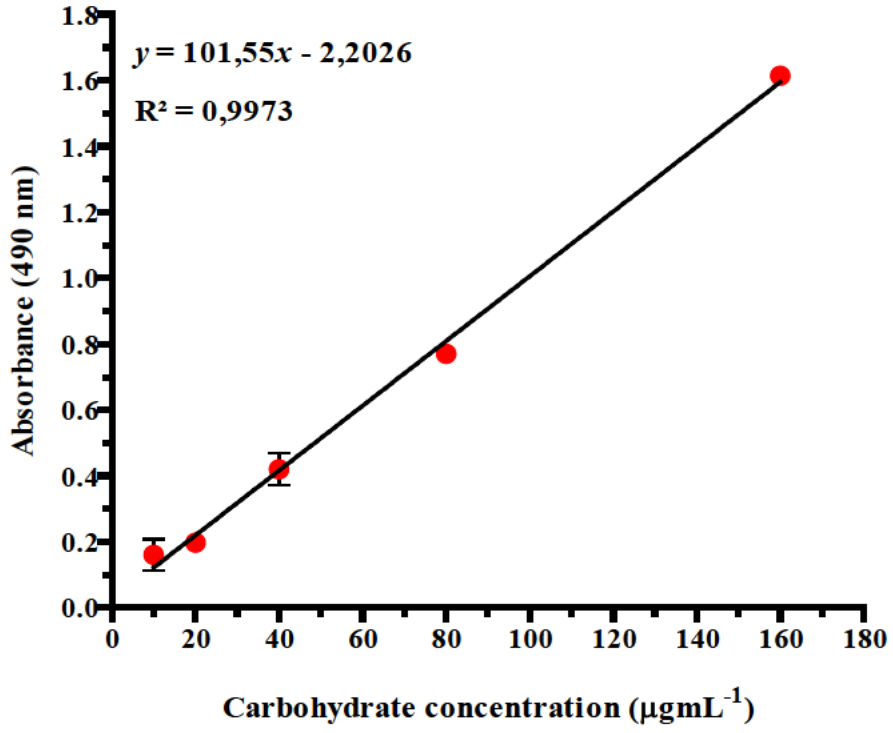

Figure J: The carbohydrate vs absorbance calibration curve.

Appendix K: Estimate of the biomass variability prior to experimentation

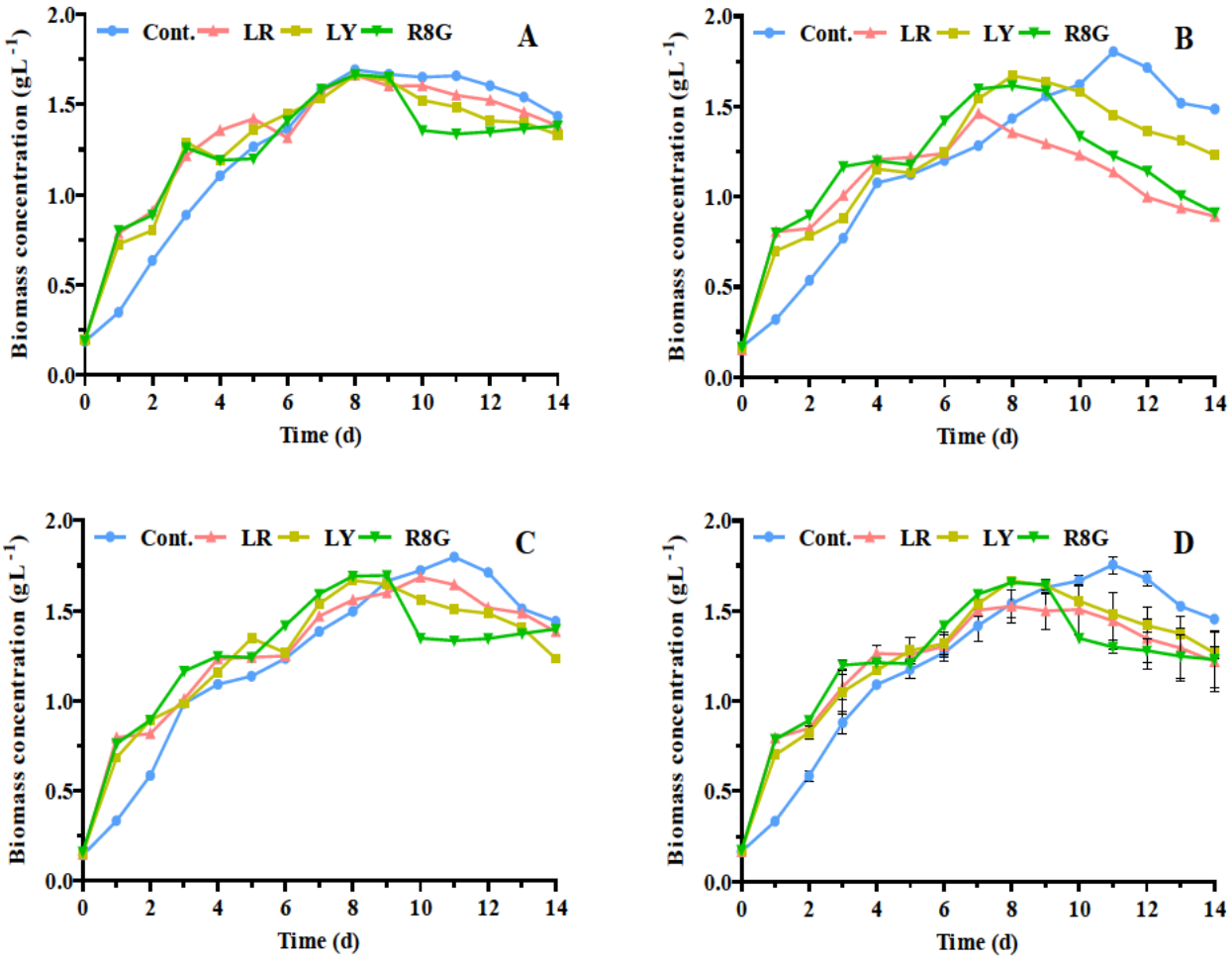

Figure K: Preliminary experimental runs using 30% UV-*a* and UV-*b* fluorescent tubes to demonstrate the lack of sample variability. **(A)** Run 1, **(B)** Run 2, **(C)** Run 3, and **(D)** Combined runs expressed as a mean ± SD (n = 3), ($p > 0.05$).

Appendix L: Publication: A novel organic dye-based approach to increase photon flux density for enhanced microalgal pigment production

Journal of Cleaner Production 198 (2018) 187–194

Contents lists available at ScienceDirect

Journal of Cleaner Production

journal homepage: www.elsevier.com/locate/jclepro

A novel organic dye-based approach to increase photon flux density for enhanced microalgal pigment production

L. Ramanna [a], I. Rawat [a], Djamal Zerrouki [b], F. Bux [a, *]

[a] Institute for Water and Wastewater Technology, Durban University of Technology, P.O. Box 1334, Durban 4000, South Africa
[b] Univ. Ouargla, Fac. des sciences appliquées, Lab. dynamique interaction et réactivités des systèmes, BP 511, Route de Ghardaïa, Ouargla 30000, Algeria

ARTICLE INFO

Article history:
Received 7 February 2018
Received in revised form
8 June 2018
Accepted 3 July 2018
Available online 4 July 2018

Keywords:
Microalgae
Organic dyes: light manipulation
Light wavelength
Pigments

ABSTRACT

Numerous research efforts have channeled toward microalgal cultivation systems due to their potential benefit in several applications. Microalgae utilize specific wavelengths of light for photosynthesis. Manipulation of incident irradiance could increase light availability to algae which could enhance pigment production. This study sought to enhance light availability to *Chlamydomonas reinhardtii* using organic dyes as light converters, thereby improving microalgal pigment production. Diphenylanthracene, Diphenyloxazole, Rhodamine 8G and Lumogen yellow were evaluated at varying concentrations in methanol, ethanol, and acetone. Spectrophotometric analyses revealed that most of the dyes had higher fluorescent intensities in methanol at 10 mgL^{-1}. Lumogen yellow exhibited the highest areal intensity but did not increase biomass production. Rhodamine 8G grown algae increased chlorophyll and carotenoid concentrations by 45 wt% and 36 wt%, respectively. Light stress was observed by increased non-photochemical quenching from approximately 0.05 to above 0.5 and decreased quantum efficiencies of photosystem 2. This novel light manipulation strategy will potentially enable more economical production of high-value microalgal bioproducts using natural sunlight as opposed to artificial light.

1. Introduction

Microalgae are considered to be promising candidates for a broad range of applications ranging from high-value bioproducts (carotenoids, chlorophylls, etc), chemicals, pharmaceuticals and nutraceuticals to next-generation biodiesel (Pérez-López et al., 2014; Piemonte et al., 2016). Immense research efforts are being directed towards the optimization of algal biomass with the intention of increasing the production efficiency of high-value bioproducts (pigments) (Baer et al., 2016; Grudzinski et al., 2016; Ruiz et al., 2016). However, high pigment yields obtained from laboratory investigations are difficult to transfer to industrial scale (Choi et al., 2015). This has been largely limited by biotic, abiotic and operational factors (Baer et al., 2016; Vadiveloo et al., 2015). Light is the main limiting factor influencing the photosynthetic efficiency, carbon fixation capacity, cell growth and biomass production, and cellular metabolism of microalgae (Cuellar-Bermudez et al., 2015; Dal Bo Zanon et al., 2017). Solar radiation is composed of a wide range of wavelengths, most of which are unusable by microalgae (Seo et al., 2014, 2015). Algal photosynthesis only occurs between 400 and 500 nm (blue) and 600–700 nm (red) regions of the light spectrum, known as the photosynthetically active radiation (PAR), whilst green-yellow light (500–600 nm) and far-red (700–800 nm) is mostly transmitted or reflected (Seo et al., 2015; Wang et al., 2017). Converting photons from one wavelength to another can produce a spectrum amenable to increase microalgal growth or metabolite expression (Ooms et al., 2016). Research has been conducted to investigate the possibility of manipulating incident light to increase the amount of PAR as a primary input factor for microalgal systems (Michael et al., 2015; Schulze et al., 2014; Wang et al., 2014).

Organic and inorganic dyes present as promising candidates for converting incident radiation with no photosynthetic potential into PAR (Ooms et al., 2016). The dyes are capable of absorbing light in certain wavelengths and re-emitting this light at other wavelengths (Al-Aqmar et al., 2015; Seo et al., 2015; Zhang et al., 2014). The process begins when incident radiation passes through the organic dye and is absorbed by the luminescent species. These incoming photons excite dye molecules to a higher energy state, one of being ready to emit radiation. Photons are emitted because of molecular decay from an excited state to the ground state. Within this state,

* Corresponding author.
E-mail address: faizalb@dut.ac.za (F. Bux).

https://doi.org/10.1016/j.jclepro.2018.07.016
0959-6526/

Appendix M: Publication: Light enhancement strategies improve microalgal biomass productivity

Renewable and Sustainable Energy Reviews 80 (2017) 765–773

Contents lists available at ScienceDirect

Renewable and Sustainable Energy Reviews

journal homepage: www.elsevier.com/locate/rser

Light enhancement strategies improve microalgal biomass productivity

Luveshan Ramanna, Ismail Rawat, Faizal Bux*

Durban University of Technology, PO Box 1334, Durban 4000, South Africa

ARTICLE INFO

Keywords:
Microalgae
Photosynthesis
Light manipulation
Light wavelength
Light spectrum
Light intensity

ABSTRACT

The rapid increase in global energy demand, global warming and climate change have driven the search for alternative renewable sources of energy with lesser environmental impact. Microalgae have immense potential as renewable energy feedstocks. Microalgal biomass can be used to generate a variety of biofuels including biodiesel, bioethanol, bio-hydrogen, bio-methane and syngas. One of the major hurdles to the commercialization of microalgae-based biofuels and products is limited biomass productivity. Considerable amounts of research have been conducted into enhancing microalgal biomass production due to its potential sustainability and variety of applications. The traditional methods of improving biomass productivity are limited to adaptation of cultivation conditions and more recently genetic engineering. Light is a crucial factor that governs microalgal growth. Research on the adaptation and manipulation of natural light rather than adaptation of microalgae has been very limited. Microalgae utilize only a small fraction of light wavelengths from the wide spectrum of solar radiation for photosynthesis. In order to enhance microalgal biomass, improved photosynthetic efficiency is essential. This can be accomplished by the manipulation of the light spectrum to achieve an optimal balance between photosynthesis and photoprotection. Manipulation of incident irradiance may be viable for increased light harvesting by algae. This not only reduces unused wavelengths but also concentrates the wavelengths in a range utilized by algae. This would allow for a maximum utilization of the light spectrum by microalgae. This review critically analyses different light manipulation techniques that modify the spectrum of light received by the algae to improve biomass productivity.

1. Introduction

The demand for renewable fuels is growing at a considerable rate globally [1–3]. This, along with, global warming and climate change have driven scientists in the search for renewable and sustainable energy sources. Renewable energy offers an environmentally friendly solution to the increasing energy security problems [1,2,4,5]. Renewable energy currently accounts for 13% of the total global energy consumption, of which, bioenergy contributes 10% [6,7]. Bioenergy is energy derived from organic raw materials (biomass) [1,6,8,9]. These may include biogas or syngas (e.g. bio-methane and bio-hydrogen), liquid biofuels (biodiesel and bioethanol), as well as products that produce electricity and heat (e.g. wood chips and pellets) [2,8,10,11]. The exploitation of renewable energy sources is of utmost importance when advancing a strategy for sustainable development [12].

Biofuels are divided into three generations. First generation biofuels are produced from edible crop sources such as corn, soybeans, wheat, barley, maize and sugarcane. The selection of feedstocks depends largely on their availability and cost. European Nations are self-dependent in the production of edible oil and as a result oils like rapeseed are commonly used in European biofuels. Americans favour soybeans while countries such as Malaysia, Indonesia, and Thailand have surplus palm and coconut oils which are used for biodiesel production. In Brazil, soybean, castor, and palm kernel are mostly utilized while Jatropha and Karanja have been reported to be used in India. Almost 50 billion litres of first generation biofuels are produced annually [2,8,10]. Even though vegetable oils are being increasingly utilized to produce biofuels, they are not entirely sustainable. Their usage results in unwanted competition between food, feed and energy, land effect and biodiversity loss debates. Other challenges include low biomass productivity and the prerequisite for excessive amounts of freshwater [10,11,13].

Second-generation biofuels are produced from non-edible lignocellulosic crops such as crop residues, grasses, sawdust and woodchips, and, sludge and livestock manure [14–16]. Cellulosic biomass contains high quantities of carbohydrates which make them more suitable for biofuel production when compared to food crops. Additionally, cellulosic biomass is a relatively cheap and abundant bioavailable material. These feedstocks do not compete with food supply as they make up the majority of the non-food materials available from plants. Therefore,

* Corresponding author.
E-mail addresses: luveshanr@dut.ac.za (L. Ramanna), rawati@dut.ac.za (I. Rawat), faizalb@dut.ac.za (F. Bux).

http://dx.doi.org/10.1016/j.rser.2017.05.202
Received 24 June 2016; Received in revised form 15 May 2017; Accepted 22 May 2017
Available online 01 June 2017

Appendix N: Publication: Photosynthesis and pigment production: elucidation of the interactive effects of nutrients and light on *Chlamydomonas reinhardtii*

Bioprocess and Biosystems Engineering
https://doi.org/10.1007/s00449-021-02651-2

RESEARCH PAPER

Photosynthesis and pigment production: elucidation of the interactive effects of nutrients and light on *Chlamydomonas reinhardtii*

Trisha Mogany[1] · Virthie Bhola[1] · Luveshan Ramanna[1] · Faizal Bux[1]

Received: 2 August 2021 / Accepted: 30 September 2021

Abstract

Chlamydomonas reinhardtii produces a variety of compounds that can be beneficial to human and animal health. Among these compounds, application of photosynthetic pigments, such as chlorophylls and carotenoids, has gained considerable interest in numerous industries. A better understanding on the interactive effects of essential nutrients and light on microalgal physiology and pigment production would be beneficial in improving cultivation strategies. Therefore, this study evaluated biomass, carotenoid and chlorophyll yield and the following fluorescence parameters: quantum yield in PS II [Y (II)] and electron transport rate (ETR) using response surface methodology (RSM). The F_v/F_m, Y(NO) and Y(NPQ) were also monitored; however, no significant relationship was observed. From the investigation it was apparent that nitrogen and carbon, as well as the interactive effects of (nitrogen and carbon) and (carbon and light irradiance) were significant factors. The model predicted the optimum conditions for maximum carotenoids (8.15 ± 0.389 mg g^{-1}) were 0.8.7 mol l^{-1} of nitrogen, 0.2 mol l^{-1} and 50 µmol photon m^{-2} s^{-1} of light irradiance. While maximum chlorophyll (33.6 ± 0.854 mg g^{-1}) required a higher nitrogen (11.21 mol l^{-1}). The photosynthetic parameters [Y(II), ETR] was correlated with the primary pigments and biomass production. Increased photosynthetic activity was associated with high carbon and light. The Y(II)and ETR of PSII under these conditions were 0.2 and ~ 14, respectively. This approach was accurate in developing the model, optimizing factors and analysing interaction effects. This study served to provide a better understanding on the interactions between factors influencing pigment biosynthesis and photosynthetic performance of *Chlamydomonas reinhardtii*.

Keywords Irradiance · Nutrients · Pigments · Photosynthetic parameters · Response surface methodology

Introduction

Microalgae, a group of photosynthetic microorganisms, are ideal sources of natural high value pigments, such as chlorophylls and carotenoids [1, 2]. These pigments are essential for harvesting light and energy transfer during photosynthesis [3]. In recent years, the application of microalgal pigments has increased considerably due to their high biological activity and applications as natural colorants, nutraceuticals and pharmaceuticals [4, 5]. Natural chlorophylls and carotenoids are approved as food additives according to the Food Safety and Standards (Food Products Standards and Food Additives) [6]. Therefore, there is a high market demand for production of these natural pigments.

A report by Value Market Research in 2018 valued chlorophyll extract at USD 279.5 million on the global market. By the year 2025 the global value of chlorophyll extract is expected to reach an astounding USD 463.7 million. This would be a 7.5% compound annual growth rate over the seven years (from 2018 to 2025) [7]. In 2016, the worldwide carotenoid market was valued at USD 1.24 billion and was estimated to reach USD 1.53 billion by the end of 2021. The cost of microalgal-derived carotenoid per kg varies between USD 250 and 7500, while the synthetic equivalent may be half that price. Although most industries rely on the synthetic production of pigments for commercial use as it is cheaper and faster, synthetic pigments are less effective in terms of health-promoting properties [3, 4]. Natural pigments are extremely beneficial to human health owing to their antioxidant and anti-inflammatory properties [8–10].

The model Chlorophyta, *Chlamydomonas reinhardtii*, presents an attractive option to produce high value pigments due to its rapid growth rates, high biomass

✉ Faizal Bux
faizalb@dut.ac.za

[1] Institute for Water and Wastewater Technology, Durban University of Technology, Durban 4001, South Africa

Published online: 20 October 2021